Bioabsorbable materials for use in vena cava filters

Løvdal, Alexandra Liv Vest; Almdal, Kristoffer; Klausen, Kasper

Publication date:
2016

Document Version
Publisher's PDF, also known as Version of record

Bioabsorbable materials for use in vena cava filters

Alexandra Liv Vest Løvdal
PhD Thesis December 2016

DTU Nanotech
Department of Micro- and Nanotechnology

Bioabsorbable Materials for Use in Vena Cava Filters

Alexandra Løvdal

Department of Micro- and Nanotechnology

Technical University of Denmark

A thesis submitted for the degree of

Ph.D.

August 2016

Contents

Abstract

Inferior vena cava (IVC) filters are used to prevent a blood clot from blocking the pulmonary vein causing a pulmonary embolism (PE). The filter is placed in the large vein, vena cava, through a minimally invasive procedure. The filter today are made from various metal alloys. Due to their long-term complications, such as filter fracture, filter migration, caval wall perforation, recurring deep vein thrombosis (DVT) and post-thrombotic syndrome, there is currently a need for an alternative to these IVC filters. A way to overcome the complications is to create a bioabsorbable IVC filter which is the main objective in this project. The aim was to investigate potential bioabsorbable materials for use in a bioabsorbable IVC filter. Certain requirements for the filter were identified, and the aim was to choose and optimize a material which could function in a filter, exhibit adequate radial force to avoid migration while withstanding the constant external force on the vena cava causing it to collapse continuously. Through investigation of the literature and performance of initial experiments on different bioabsorbable polymers, poly(L-lactide) (PLLA) was chosen as a possible material candidate and further investigated. It was hypothesized that PLLA could be optimized through strain-induced crystallization and was extruded into small tubes, which underwent a biaxial strain during an expansion process. The mechanical properties, such as stiffness and strength, were improved through the processing. Several optimal processing parameters, such as high straining temperature, fast axial processing strain and a large degree of strain in the radial direction proved to improve the properties further. The mechanical properties were shown not to be related to the crystal orientation obtained during straining but related to the alignment of amorphous chains. The biaxially strained tubes were laser cut into either appropriate filter designs or the body part of the filter (stent-base) and expanded to 27 mm during a heat

treatment. The effect of processing, heat treatment and sterilization were evaluated under in vitro conditions. The radial force of the stent-base proved to correlate with the circumferential stiffness of the biaxially strained tubes. The fatigue properties of the stent-base were improved when tested under in vitro conditions. Based on these results the stent-bases were implanted in vivo in an ovine model for 2 and 3½ weeks using three sheep. Two stent-bases were implanted per sheep, one cranially and one caudually. After merely 2 weeks the stent-bases showed multiple fractures in the circumferential direction caused by the continuous cyclic compression. The fragments from the caudal device remained in the caval wall, whereas little remained of the cranial device. Histology showed that the PLLA fragments were embedded in neointima to a degree that fragmented pieces did not migrate. It also showed mild fibrosis around the struts caused by the radial force of the stent. It was concluded that PLLA did not exhibit the adequate flexibility in such a filter design to withstand the cyclic compression of the vein over the course of 2 weeks. To achieve the goal of creating a bioabsorbable IVC filter, the stent-base must be made from a different polymer.

Abstract

Bioabsorbabare Materialer til Brug i Vena Cava Filters

Inferior vena cava (IVC) filtre bruges til at forhindre en blodprop i at blokere lungevenen, der forårsage en lungeemboli (PE). Filtrene fremstilles i dag af forskellige metallegeringer og anbringes i den store vene, vena cava, gennem en minimal invasiv procedure. På grund af komplikationer på længere sigt, såsom som filter fraktur, filter migration, perforering af cava væggen, tilbagevendende dyb venetrombose (DVT) og post-thrombotisk syndrom, er der i dag et behov for et alternativ til disse IVC filtre. Dette alternativ kan findes ved at skabe et bioabsorberbart IVC filter, hvilket var det vigtigste formål i dette projekt. Formålet var at undersøge potentielle bioabsorberbare materialer til brug i et bioabsorberbart IVC filter. Visse krav til filteret blev identificeret, og målet var at udvælge og optimere et materiale, som kunne fungere i et filter, udvise tilstrækkelig radial kraft og derved undgå migration, og samtidig modstå den konstante ydre kraft på vena cava, der forårsager venen i at kollapse kontinuerligt. Gennem undersøgelse af litteraturen og resultater fra indledende forsøg på forskellige bioabsorberbare polymerer, blev poly (L-lactid) (PLLA) valgt som en mulig materialekandidat og undersøgt yderligere. Det blev antaget, at PLLA kunne optimeres gennem træk-induceret krystallisation, og PLLA blev ekstruderet i små rør, som undergik et biaksial træk under en ekspansionsproces. De mekaniske egenskaber, såsom stivhed og styrke, blev forbedret ved behandlingen. Flere procesoptimeringsparametre, såsom en høj træktemperatur, et hurtigt proccesseringstræk aksialt og en stor grad af træk i den radiale retning viste sig at forbedre egenskaberne yderligere. De mekaniske egenskaber viste sig ikke at være relateret til krystalorientering opnået under træk, men at være relateret til udstrækning af amorfe kæder. De biaksialt trukkede rør blev laserskåret i enten et passende filterdesign eller basedelen af filteret (stentbasen) og udvidet

til 27 mm under varmebehandling. Effekten af processeringen, varmebehandlingen og sterilisation blev evalueret under in vitro betingelser. Den radiale kraft af stentbasen viste sig at korrelere med stivheden af biaksialt trukkede rør i omkredsen. Udmattelse af stentbasen blev ligeledes forbedret og evalueret under in vitro betingelser. Baseret på disse resultater blev stentbaser implanteret in vivo i en fåremodel i 2 og 3½ uge ved brug af tre får. To stentbaser blev implanteret per får, én kranialt og én kaudualt. Efter blot 2 uger havde stentbaserne multiple brud i omløbsretningen som følge af den kontinuerlige cykliske kompression på venen. Fragmenterne fra det kaudale implantat forblev i cava væggen, mens der var lidt tilbage af den kraniale implantat. Histologien viste, at PLLA fragmenter var blevet dækket af neointima i en sådan grad, at de fragmenterede stykker ikke migrerede. Den viste også mild grad af fibrose omkring stentdelene forårsaget af radialkraft påvirkningen fra stenten. Det blev konkluderet, at PLLA ikke udviste den passende fleksibilitet i det konkrete filterdesign til at modstå den cykliske kompression på venen i løbet af de 2 uger. For at imødekomme målet med at skabe et bioabsorberbart IVC filter, bør stentbasen være fremstillet af en anden polymer.

Acknowledgements

I would foremost like to thank my supervisor Kristoffer Almdal for believing in me as a scientist and his guidance throughout the last 3 years. I would also like to thank Jens Wenzel Andreasen for his expertise in WAXS analysis and pushing to expand my skills beyond the field of biomedical engineering; Karsten Agersted for introducing me to DSC and acting as supervisor for a master student contributing to the project and Lars Pilgaard Mikkelsen for his professional input, curiosity and time.

Kasper Klausen, company supervisor, for his collaboration on this project and guidance on where to take the project next. For helping me to achieve my goals academically, while keeping the company's interest at heart. Steen Aggerholm, Manager of Research at William Cook Europe, for believing in me and giving me the opportunity to achieve my goals. For giving me space and freedom to research and trusting my plans for the project. Christoph Binkert, third-party supervisor, for his passionate support and inputs on the project and animal study.

The non-clinical testing department at Cook Research Inc. for their hospitality and help during the animal study. Especially Mevan L. Siriwardane for his patience and input; Bill Van Alstine, pathologist at Cook Research Inc., for his collaboration and input and Shou Yang, CAE specialist, at Cook Research Inc., for his expertise in FEA modeling. Sarah Calve, Ass. Professor at Purdue University, for her patience and time. I am grateful for the time in her lab and the skills I have obtained.

I would also like to give special thanks to my husband for his support and understanding through this process.

Preface

This Ph.D. thesis is submitted in fulfillment of the Ph.D. degree obtained from the Technical University of Denmark. The duration of the project extended from November 1^{st} 2013 to 1^{st} of August 2016. The Industrial Ph.D. program was partially funded by the Danish Agency for Science, Technology and Innovation and William Cook Europe (Bjæverskov, Denmark). During the time of the Ph.D program, I was employed by William Cook Europe. The program was done in collaboration with the Department of Research, William Cook Europe (Bjæverskov, Denmark) and the Department of Micro- and Nanotechnology, Technical University of Denmark (Kgs. Lyngby, Denmark). Company supervisor, Kasper Klausen, was employed at William Cook Europe in the Department of Research. Prof. Dr. Med. Christoph A. Binkert was third party supervisor and Director of Institute of Radiology and Nuclear Medicine at Kantonsspital Winterthur (Switzerland).

Alexandra Løvdal

Date

Nomenclature

Acronyms

Å	Ångstrom
AT	Adenin and thymin
$BaSO_4$	Barium sulfate
BSA	Bovine serum albumin
BVS	Bioresrobable vascular stent
CAE	Computer-aided engineering
DAPI	4',6-diamidino-2-phenylindole
DES	Drug-eluting stent
DNA	Deoxyribonucleic acid
DSC	Differential scanning calorimetry
DVT	Deep vein thrombosis
EO	Ethylene oxide
FDA	Food and Drug Administration
Fe_3O_4	Iron oxide
FEA	Finite element analysis
GPC	Gel permeation chromatography
H&E	Hematoxylin and eosin stain
Ig	Immunoglobin
Ig	Immunoglobulin
IN	Inner diameter
IVC	Inferior vena cava
MRI	Magnetic resonance imaging
OD	Outer diameter
PBA	Poly(3- or 4-hydroxybutyrate)
PBS	Phosphate buffered saline
PCA	Poly (alkyl cyanoacrylates)
PCL	Polycaprolactone
PDLA	Poly(D-lactic acid) or poly(D-lactide)
PDLLA	Poly(D-L-lactic acid) or poly(D-L-lactide)
PDS	Polydioxanone
PE	Pulmonary embolism
PEA	Poly (ester amide)
PEEK	Polyether ether ketone
PEN	Polyethylene naphthalate
PEO	Polyethylene oxide
PET	Polyethylene terephthalate
PGA	Poly(glycolic acid) or polyglycolide
PHA	Poly(hydroxyalkanoate)
PHO	Poly(3-hydroxyoctanoate)
PLA	Polylactide
PLGA	poly(lactic-co-glycolic acid)
PLLA	Poly(L-lactic acid) or poly(L-lactide)
POE	Polyorthoester
PP	Polyurethanes
PPHO	Polyphosphazenes
PRESERVE	Predicting the safety and effectiveness of inferior vena cava filters
PTFE	Polytetrafluoroethylene
PTMC	Poly(trimethylene carbonate)
PU	Polypropylene
RALLS	Right angle laser light scattering
ROP	Ring-opening polymerization
SAXS	Small angle X-ray scattering
SEQ	Sequential
SIC	Strain-induced crystallization

Nomenclature

SIM	Simultaneous	
THF	Tetrahydrofuran	
TIB	Triiodobenzoic acid	
VTE	Venous thromboembolism	
WAXS	Wide angle X-ray scattering	
WGA	Heat germ agglutinin	
wt/vol	Weight/volume	
wt%	Weight percentage	
XRD	X-ray diffraction	

Greek Symbols

$\dot{\epsilon_p}$	Processing strain rate	1/s
$\dot{\epsilon}$	Strain rate during tensile testing	1/s
ϵ	Strain	
ϵ_a	Axial processing strain	
ϵ_b	Elongation at break	
ϵ_r	Radial processing strain	
Ψ	The angle of the lamella normal to the lamella interface	
σ	Stress	Pa
σ_y	Yield stress	Pa
θ	Bragg's angle	°
(ϵ_a,ϵ_r)	Axial to radial strain ratio	
Φ	Azimuthal angle	°

Roman Symbols

ΔH_m^0	Enthalpy of fusion of a 100% crystalline material	J/g
$\Delta \mathbf{H}_c$	Crystallization enthalpy	J/g
$\Delta \mathbf{H}_m$	Melting enthalpy	J/g
$\Delta \mathbf{L}$	Change in length	
$\Delta \mathbf{R}$	Change in radius	
$\mathbf{A}_0$	Initial cross-sectional area	m^2
$\mathbf{A}_1$	Cross-sectional area after axial strain	m^2
$\mathbf{A}_{exp}$	Degree of total area expansion	%
AP	Anterior-posterior	
$\mathbf{C}_p$	Heat capacity	J/°C
CA	Caudal	
CR	Cranial	
E	Elastic modulus	Pa
Fr	French	
L	Lumbar	
$\mathbf{L}_0$	Initial length	m
$\mathbf{L}_1$	Length after axial strain	m
LAO	Left anterior oblique	
$\mathbf{M}_n$	Number average molecular weight	g/mol
$\mathbf{M}_w$	Weight average molecular weight	g/mol
q	Scattering vector $Å^{-1}$	
$\mathbf{R}_0$	Initial radius	m
$\mathbf{R}_1$	Radius after axial strain	m
$\mathbf{R}_2$	Radius after radial strain	m
RAO	Right anterior oblique	
T	Thoracic	
$\mathbf{t}_a$	Wall thickness after axial strain	m
$\mathbf{T}_{cc}$	Cold crystallization temperature	°C
$\mathbf{T}_c$	Crystallization temperature	°C
$\mathbf{T}_g$	Glass transition temperature	°C
$\mathbf{T}_m$	Melting temperature	°C
$\mathbf{T}_p$	Processing temperature	°C
UTS	Ultimate tensile strength	Pa
$\mathbf{V}_0$	Initial volume	m^3
$\mathbf{V}_1$	Volume after axial strain	m^3
$\mathbf{X}_c$	Degree of crystallinity	%

Other

Embolism Any material including blood clots which are dislodged, from its original site as a thrombus, into the blood stream and blocks the vessel it has traveled to

Embolus Blood clot circulating in the vascular system

Hyperplasia Increase in tissue cells in response to stimulus[1]

Intima Outermost layer facing the lumen[2]

Media Middle layer of the vein [2]

Nitinol Nickel titanium

Percutaneous Performed through the skin

Pulmonary embolism Embolus, which has traveled to the lung and blocked the passage of flow prohibiting oxygenation

Stenosis Occlusion of the vessel

Stent Circumferential scaffold. Primarily used in the vessel to treat stenosis

Thrombosis Formation of a blood clot in a vessel, obstructing blood flow

Thrombus Blood clot

1

Introduction

1.1 Introduction to the project

This thesis describes the research efforts done in the investigation of a bioabsorbable material for use in a bioabsorbable inferior vena cava (IVC) filter. IVC filters are used to prevent blockage of the pulmonary vein caused by free floating blood clots.

Rationale of the project Blood clots formed in the lower extremities (thrombosis) are called deep vein thrombosis (DVT) (Figure 1.1 step 1). When fragmented, it travels upstream through the large vein (vena cava) (Figure 1.1 step 2) to the lungs and creates a blockage, known as a pulmonary embolism (PE)(Figure 1.1 step 3). During the blockage, the oxygenation of blood is prevented, and can be mortal if not treated. It is believed that DVT and PE affect 422 out of a 100,000 people in the United States alone[3]. DVT and the subsequent PE is often prevented by anticoagulants such as heparin and vitamin K antagonists[4]. Additionally 100,000-300,000 Americans die from PE annually[5]. The treatment is often successful, but not suitable for certain patient groups with for example bleeding complications and reoccurring DVTs. As an alternative to anticoagulants, a filtration device is inserted in the IVC, when the need for filtration is short, and anticoagulants are contraindicated [6][3][7]. The mechanism of trapping a blood clot before reaching the lungs is portrayed in Figure 1.2.

Before the filters were invented caval ligation using sutures in the vena cava were performed. It showed a high mortality of 14% and PE still occurred in 6% of patients despite treatment. The mortality was reduced to 2% with the introduction of the Greenfield filter in 1992[4]. It is inserted percutaneously through a small incision in the skin and access to the

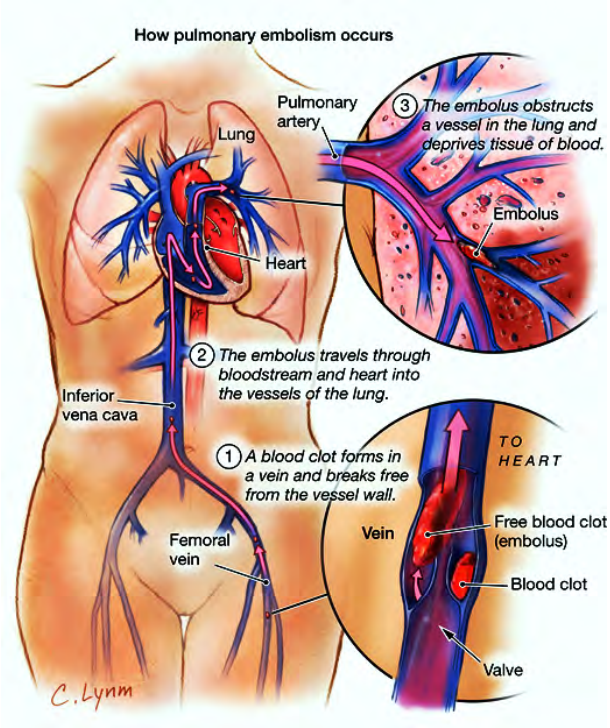

Figure 1.1: Formation of a pulmonary embolism. Used from [8]

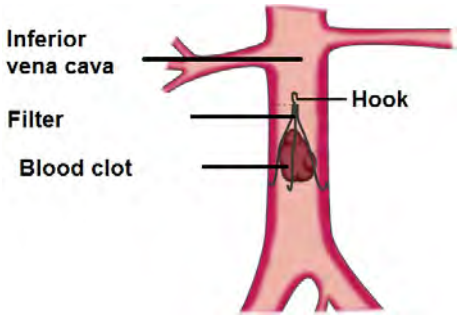

Figure 1.2: Inferior vena cava with filter, which has tapped a blood clot. Used from [9]

vein is obtained and thereby minimally invasive[10]. The filter is usually placed below the renals and mechanically traps the embolus before reaching the lungs.

Several complications are associated with permanent placement of IVC filters in general. Complications include short-term complications during insertion such as insertion site thrombosis (≥28%)[7] and the long-term complications such as filter fracture (≥10%)[3] filter migration (≥69%), dislocation, caval wall perforation (≥29%), rupture, recurring DVT (≥46%) and post-thrombotic syndrome (venous stasis syndrome occurring after a DVT)

(≥59%)[4]. Despite the long-term complications, the vast majority of the placed filters are or become permanent[7] and never retrieved from the body. To reduce the risk of complications the Food and Drug Administration (FDA) issued a statement in both 2010 and 2014, saying that all filters should be retrieved from the patient when the risk of PE has passed. They also require manufacturers to collect clinical data for currently marketed IVC filters in the United States, by either conducting post-market surveillance or participating in the PRESERVE study (Predicting the Safety and Effectiveness of Inferior Vena Cava Filters). The latter examines the use of IVC filters in the prevention of pulmonary embolism. The collected data from both studies will provide safety assessment of the retrievable filters[11].

Whether or not patients benefit from an IVC filter is not conclusive. Patients where anticoagulants are contraindicated, would benefit from the placement of an IVC filter. However reoccurring PE (2-5% with fatal outcome in 0.7%) is seen both with and without placement of a filter. Anticoagulants will in many cases be used in combination with an IVC filter and have a different outcome than just using anticoagulants (in favor of a filter present)[4].

The filter can be permanent or optional with various drawbacks, where the successful prevention of PE is counterbalanced by the excess rate of DVT formation[7] due to the presence of the filter. There is also a difference in the different brands of filters and their benefits and drawbacks [4], which will not be described further in detail in this thesis. A range of filters is portrayed in Chapter 3.

Retrieval of the filter is often done percutaneously by using a snare to 'catch' a part of the filter, for example, a hook as seen for the Cook Medical Celect and Tulip filters. The hook is portrayed in Figure 1.2 at the top of the filter. Low retrieval rate is often due to physician oversight [3] or difficult retrieval of the filter upon retrieval surgery. Over the last 30 years the number of placed IVC filter in the US has increased by a 25-fold. An increase which is partly due to better diagnostic techniques such as computed tomographic pulmonary angiography for PE detection as well as an increase in filter placement for 'prophylactic indication'. The prophylactic indication is based on the risk of thrombosis and PE occurring due to a certain trauma, treatment or procedure. In 2009 the number of placed IVC filter in the US alone was significantly higher than for Europe and the market is today dominated by the US. The higher number is not only due to the large population (309 million) because Europe 'Big 5' countries (France, Germany, Italy, Spain and the United Kingdom) holds just as many (313 millions). The US places 224,700 filters versus the 9,070 filters placed in Europe's

'Big 5'. The number of annual venous thromboembolism (VTE)-related deaths in percentage are the same for the US and the 'Big 5' but it is hard to determine, why the number of filters placed in the US is significantly higher. A few reasons could be the insurance payer status, medico-legal regions and intercontinental differences in financial reimbursement [12]. Additionally, medical tradition can have an impact in the sense that 'we do or operate as we normally do'. Given these substantial numbers, the IVC filter market is large. If filters are banned or advised against in the future, due to long-term complications, the manufacturer, including Cook Medical must act upon this and come up with an alternative treatment strategy. Therefore the next idea on how to eliminate both short-term and long-term complications and eliminate the need for a scheduled filter retrieval surgery lies in the 'true' temporary filter. A filter which consists solely of bioabsorbable materials, which degrade over time, and the waste products are removed by the body when the risk of PE has passed. If a bioabsorbable filter is not marketed, the trend in procedures might switch solely towards the pharmaceutical treatments, which is not suitable for all patients and a poor business case for the IVC filter manufacturers.

1.2 Readers guide on thesis content

This thesis is comprised of 10 parts: Chapter 2 describes the aims and objective of this Ph.D. project. Chapter 3 gives an overview of current IVC filters and the rationale for creating a bioabsorbable IVC filter. Chapter 4 highlights the experimental methods used in this project and the rationale for choosing such. Chapter 5 summarizes the ideas and initial work on the selection of an appropriate material and includes literature findings on the best material candidate applicable. Through this investigation, poly(L-lactide) acid (PLLA) was chosen as a good candidate for such application due to its stiffness and strength. Additionally, it has a slow molecular degradation profile and maintains its strength up to 6 months. Chapter and 5 and 6 both contain the necessary theoretical background shown at the beginning of each chapter followed by the experimental findings of this project. Section 5.2 and 6.2 summarize the work performed with the intent of understanding the mechanical and thermal properties, for identification of how a material could be processed into a bioabsorbable filter. PLLA was investigated as both monofilament in a braided filter, and as a hollow extruded tube, which underwent an expansion process similar to blow molding and subsequently laser cut into a suitable design. More specifically the influence of such process on

the mechanical properties was investigated. The degree of strain, processing temperature and processing strain rate were also studied and discussed in two separate articles 6.2.4.1 and 6.2.7. The first was published in Polymer International, and the latter is under review in the same journal. The expanded tubes were laser cut into a different filter, or partial filter (stent-base) designs portrayed in Chapter 7. They were tested under physiological conditions (in vitro). The results are summarized in Chapter 8. From the in vitro findings, the best design candidate processed at certain parameters was chosen. It was evaluated in vivo in an ovine animal model for determination of the device integrity and tissue response and discussed in Chapter 9 in which the results are summarized in article 9.2, which is currently under revision. Chapter 10 discusses the overall findings in this project and what the future might hold for bioabsorbable filters. A brief conclusion in Chapter 11 sums up the work done during the project period.

Short explanations of less common technical terms can be found under abbreviations and nomenclature.

During the project, I have been co-supervisor on the following three different master projects. With the supervision, their work became beneficial to the overall goal of the this project. For this reason, experimental data and results obtained through their theses are referenced as such

- Maja Madsen 'Thermal and Mechanical Characterization of Bioabsobable Polymers for Implantation use'[13]
- Marco Iwersen 'Investigation of Biosorbable Polymers under Static and Cyclic Stress'[14]
- Tooba Noorzae 'Time Dependent Properties of Medical Implants Made of Poly(L-lactic acid)'[15]

1.2.1 Publications

Within the thesis, there are three publications. Additionally, one US patent application has been submitted.

- Research paper in Polymer International 'Characterization of Biaxial Strain of Poly(L-lactide) Tubes' 15 October 2015
- United States Patent Application 20150367554 'Sequential Biaxial Strain of Semi-crystalline Tubes' December 24, 2015

Under review

- Research paper in Polymer International 'Mechanical Properties of Biaxially Strained of Poly(L-Lactide) Tubes: Strain Rate and Temperature Dependence' version 20 June 2016

Under revision

- Research paper in CardioVascular and Interventional Radiology 'Evaluation of a Bioabsorbable Self-expandable Vein Stent-base Made of Poly(L-lactide) in vitro and in vivo' version 17 June 2016. Currently under revision for resubmission before 15th of September 2016

2

Aims and objectives

The main research objective was to identify the best possible material for creating a bioabsorbable inferior vena cava (IVC) filter. Firstly the material characteristics and properties before and after processing into a filter design were evaluated. Secondly, the mechanical performance upon implantation and over time was identified. The findings in vitro were evaluated in vivo in a suitable animal model. Simultaneously commercial aspects were taken into consideration when choosing material and processing pathways.

2.1 Research objectives: Material

The objective was to obtain the material knowledge needed to design a bioabsorbable IVC filter. Below are the goals for identification of suitable materials

- Conduct a literature review of existing, commercial available bioabsorbable polymer for medical use and choose the best candidate(s)
- Obtain knowledge of mechanical properties initially and the properties of the material over time
- Identify and characterize the parameters within processing and shaping of the device which affect the mechanical behavior of the final device

2.2 Research objective: Validation of material, processing, and design

Prototypes used in this project were based on a convertible temporary filter (explained further in detail in section 3.3.1). From the literature and subsequently experimental material

characterization, the appropriate material was selected and tested under more physiological conditions, in the prediction of its behavior in vivo. Below are the most important considerations and steps during validation of the device in vitro listed.

- Create an in vitro test set-up predicting the outcome in vivo testing
- From the in vitro testing identify the best prototype for an in vivo study. Herein both processing and design are taken into account
- Validate in vitro findings in vivo
- Identify the ingrowth rate of the bioabsorbable material in the vessel wall and the nature of which the tissue will cover the bioabsorbable material with respect to surface of the implant

2.3 Commercial objectives

The material and processing knowledge achieved during the Ph.D. project contributed to the overall end goal; developing a final concept of how a bioabsorbable IVC filter can be created. This includes the following sub-objectives:

- Identify design and materials which provide less late complications than the present design
- Identify certain regulatory setbacks
- Identify processing pathway, which can be held in-house.
- Choice of material(s) must be based on the goal that complete absorption occurs within 2 years
- The filter shall maintain its function as a filter for a period of 60 to 90 days, after which it converts into a non-functional filter and all parts of the filter becomes embedded in tissue to avoid risk of free-floating fragments

3

Background

This chapter includes the indications for placing an inferior vena cava (IVC) Filter and the need for creating a bioabsorbable IVC filter. Furthermore, the requirements of such and the underlying challenges are described. The chapter includes state of the art on bioabsorbable IVC filters and how to proceed from there.

3.1 Indications

In general patients in need of a filter, are people with or in the risk of developing a pulmonary embolism (PE), venous thromboembolism (VTE) and/or deep vein thrombosis (DVT). Below is a list of additional indications where patients could benefit from placement of an IVC filter [4] [16].

- patients with extensive trauma at risk of having VTE
- patients with calf vein thrombosis and upper extremity DVT
- patients with acute and/or reoccurring or chronic symptomatic PE regardless of anticoagulation treatment
- patients with a high risk of PE
- patients with any confirmed VTE with contraindications to anticoagulation or active bleeding
- patients with massive free-floating iliofemoral thrombosis who cannot be treated with anticoagulants
- patients treated with estrogen
- patients with cancer and existing VTE
- patients with limited cardiopulmonary reserve and thereby formation of VTE
- pregnant women with established VTE

3.2 Types of IVC filters

3.2.1 Permanent and optional filters

The filters today as seen in Figure 3.1 and 3.2 are made of metal alloys such as nitinol, strainless steel or conichrome and can be delivery percutaneously either through the jugular or femoral vein through 6-10Fr introducers[10].

A *permanent* filter is placed with the intention of never being retrieved. It becomes endothelialized and incorporated into the caval wall and for that reason, retrieval is not possible[4]. A new generation of filters, the *optional* filter later emerged and had the option of being placed permanently or being retrieved, once the risk of PE has passed. Depending on the design they are not significantly incorporated into the caval wall, which makes retrieval possible[17]. Retrieval is usually done after 12 weeks if the filter is no longer needed. A *convertible* filter on the other hand only allows the filtration component to be removed, while the remaining filter-base remains in the caval wall[17].

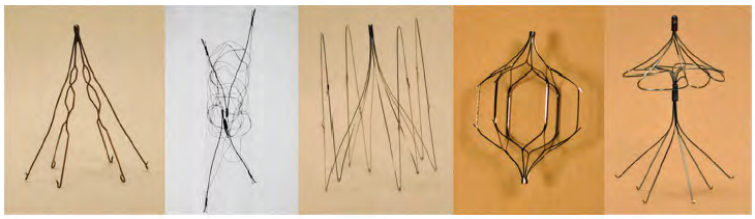

Figure 3.1: Permanent filters. From left to right: Greenfield (Boston Scientific; Natick, MA); Bird's Nest (Cook Medical; Bloomington, IL); Vena Tech LP (B Braun; Bethlehem, PA); Trapease (Cordis Endovascular; Piscataway, NJ); Simon Nitinol (CR Bard; Tempe, AZ.) Used from [17]

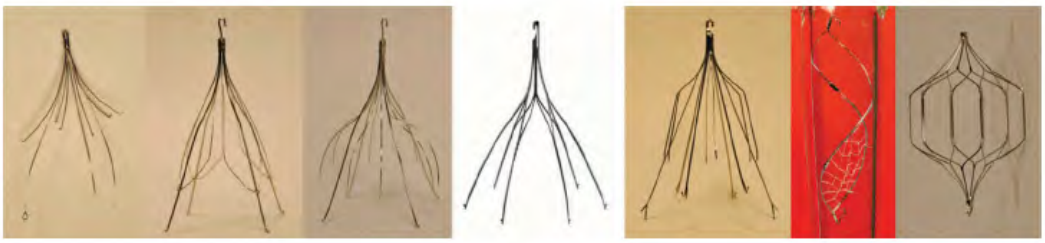

Figure 3.2: Optional filters. From left to right: ALN filter (ALN Implants Chirurgicaux Ghisonaccia, France); Günther-Tulip (Cook Medical; Bloomington, IL); Celect (Cook Medical; Bloomington, IL); Option ELITE (Argon Medical; Athens, TX); Denali (CR Bard; Tempe, AZ); Crux (Volcano Medical Corp; San Diego, CA); OptEase (Cordis Endovascular; Piscataway, NJ) Used from [17]

The first filters were placed in the 1960's and were permanent filters. The first was a Mobin-Uddin umbrella, which filtrated the blood in the IVC, without open surgery. The drawback was disruption of the flow dynamics and caval thrombosis. It was later replaced by a cone filter, the Greenfield IVC filter by Boston Scientific Corporation (Marlborough, MA, USA), which did not disrupt the flow and could hold a large thrombus while autolysis of such occurred. Most of the following filters were then designed as a single cone or a bi-conical filter[17]. Today both permanent (Figure 3.1) and optional filters (Figure 3.2) exist. Long-term studies have been done to evaluate the drawbacks of both permanent and optional filters. The permanent filter reduces the incidence of a PE, but over time there is an increased risk of DVT formation and long-term filter placement is therefore not beneficial. The optional filters eliminate the long-term complication of DVTs and caval stenosis, but retrieval rate is as low as 21% (>5000 patients)[18]. For both filter types, the risk of fracture and perforation still exists. The existing filters still undergo changes to reduce the complications.

3.2.2 Convertible filters

There are currently convertible filters, which transform from a filter into a permanent stent. This hybrid does not solve the late complication as seen with permanent vascular devices, such as metal stents[19][20]. The Sentry filter (Novate Medical, Galway, Ireland) (Figure 3.3) and VenaTech (B. Braun Interventional Systems, Inc, Bethlehem, PA) (Figure 3.4) are examples of convertible filters, which converts from a filter to a non-filter automatically or mechanically. Both have or are undergoing clinical studies, but the results are not known yet. The Sentry filter is a stent-like configuration with a filtration part in the center, which is held together by a bioabsorbable polymeric fragment. As the polymer dissolves the filter opens up and the stent made of non-bioabsorbable metal remains. The VenaTech convertible filter does not convert on its own, but needs a mechanical intervention to remove the apical cap, as seen in Figure 3.4(B) and does not incorporate a bioabsorbable part[21].

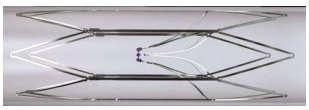

Figure 3.3: Sentry filter. Used from [22]

Additional studies include a non-commercial self-convertible metal filter, which is non-bioabsorbable with an outer diameter (OD) of 25 mm. It consists of three parts: anchoring

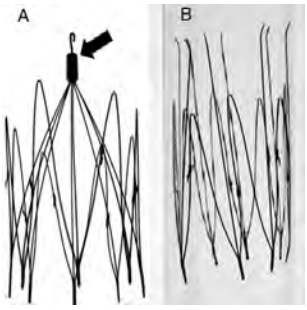

Figure 3.4: VenaTech filter. When implanted the filter in closed and able to filtrate. When no longer needed the apical cap (arrow) is removed with a snare and the filter converts into open state. Modified from [21]

struts, convertible struts and a bioabsorbable switch in the center made of ϵ-polycaprolactone (PCL) and poly(L-lactide) (PLLA) (75/25). As the PCL degrades the filter (Figure 3.5(a)) converts into a stent (Figure 3.5(b)). The filter was tested under clot simulation in vitro with up to 5 mm clots. A serie of clots (n=5) were deployed into the filter, and the success rate of the filter decreased with number of clots. Their in vivo study showed migration as the convertible filter did not have any barbs to hold it in place [23].

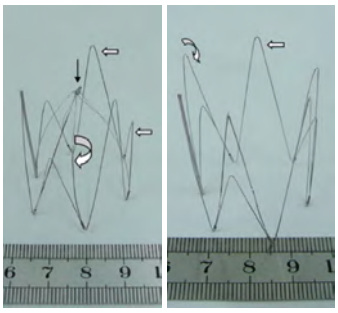

(a) (b)

Figure 3.5: Self-convertible filter before 3.5(a) and 3.5(b) after conversion. Used from [23]

3.3 Bioabsorbable or 'true' temporary filters

The retrieval window of the optional filters depends on the type of filter. In some cases, retrieval is complicated, and the filter is left in situ. A different concept to overcome this and most long-term and some short-term complications is the bioabsorbable filter, which is a

'true' temporary device. In such that no part of the filter is left behind over time, and the retrieval procedure is eliminated. The indications for a 'true' temporary filter are shown by the dotted box in Figure 3.6 and are at first the same as for the permanent and optional filter indications.

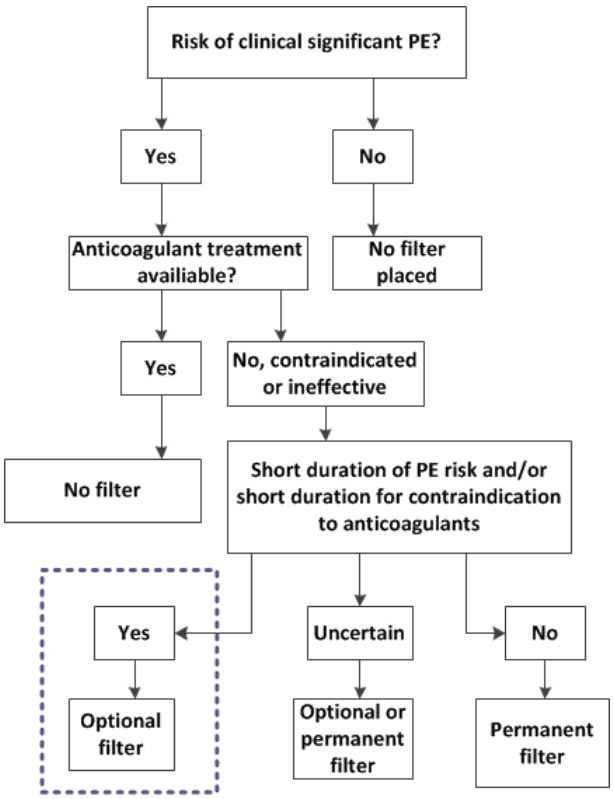

Figure 3.6: Flow chart for choosing correct treatment of PE. Purple dotted box is the market share , where 'true' temporary filters can be used. Modified from [6]

Unlike the bioabsorbable stents, there are currently no commercial available 'true' temporary bioabsorbable filters. The bioabsorbable filter must be made of a material which is engineered to dissolve or degrade by a non-invasive stimulus, whether it is external or from the physiological environment in which it exists. The degradation of the material must be highly predictable so that fragmentation of the material and embolisms, as a result, are eliminated. Nor must a massive embolism be trapped in the filter as it dissolves, which could result in a PE and harm the patient. There are currently a few examples of temporary filters, and some which are 'true' temporary filters, but only at the research and animal testing level as described in further detail in section 3.4.

3.3.1 Bioabsorbable filter concept

There are numerous patents on a bioabsorbable filter, whether 'true' temporary filter or not, but most are on design features. The bioabsorbable filter concept in this project was initially based on a conversion concept design (Patent US2011213404). The filter is a two step bioabsorbable filter design. At stage 1, the filter has one or two active filtration levels (see Figure 3.7(a)). The filtration struts are connected in the center of the device until there is no longer need for blood filtration. At stage 2 the filtration struts flip towards the vessel wall, in order not to limit blood flow or to break off as fragments (see Figure 3.7(b)). Filtration and fixation struts shall be embedded in the tissue and slowly be absorbed over time. The design used in this project is still based on the concept of conversion from a filter to a non-functional filter. The design involves a stent-base and a filtration cone on top of the stent

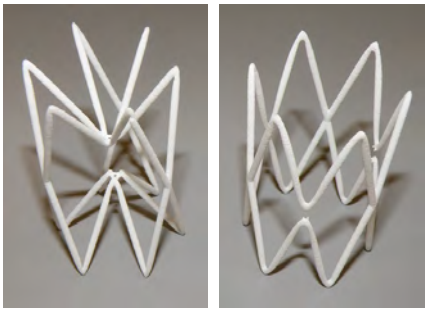

(a) (b)

Figure 3.7: Bioabsorbable filter concept based on patent application US2011213404 by C. Binkert, which has a functioning filtration stage (3.7(a)) and conversion stage (3.7(b))

3.3.2 Functional requirements for a 'true' temporary IVC filter

The material or materials used for the design of a bioabsorbable filter must ensure that the bioabsorbable filter fulfills the functional and the biological criteria as the present filters do so that an appropriate filter function can be achieved.

Initial filter specifications

- 6-8 filtration struts
- Strut diameter in range of 0.4-1 mm
- 30-70 mm in length

- For use in cava sizes in 15-30 mm
- Filtration ability for approximately 1-3months*
- Completely absorbed in 1-2 years
- Applicable for percutaneous placement methods

Additionally

- The material should posses an appropriate degradation profile and mechanical characteristics
- It must be ensured that the degradation process does not lead to adverse effects

*According to Sing et al. [24] 54% of PEs occur seven days after a trauma has occurred. After 28 days the risk of PE is down to 5.5% and a filtration indication time up to 3 months is more than acceptable.

The properties of the final bioabsorbable filter depend on the material properties of which it is made. Based on the type of particular material some properties are an issue, and others are not. The requirements in this projects rely solely on a bioabsorbable filter made from bioabsorbable polymers. An obvious possible adverse effect is the migration of the filter due to shape changes or the release of large filter fragments during the degradation process. If the design is based on the conversion design described in section 3.3.1. Both material and design must, therefore, be susceptible to tissue coverage when placed in the adjacent vessel wall. Material stability and radial force are only needed until sufficient coverage has occurred to avoid device migration.

3.3.3 Commercial requirements

The advantage of a bioabsorbable filter is clear compared to the non-bioabsorbable filters. However, from a cost-benefit analysis point of view, the device price must match the clinical advantages of placing it. If the polymer is commercially available and the processing does not rely on vendors, the price can be kept to a minimum. If processed by a vendor, the processing must be predictable and regulated. The device must be proven to be biocompatible, and preferably clinical data already exist on the material, which makes the regulatory approval of an IVC filter application easier. The procedure must be as easy as the current procedures and the storage of the device up until procedure, must not be complicated. If storage is complicated and the device is not 'on the shelf' the acute procedures might not involve the use of a bioabsorbable filter.

3.3.4 Material requirements and challenges

There are challenges with creating a bioabsorbable filter of bioabsorbable polymers. The considerations and requirements are listed in the following paragraphs.

Radial force Adequate radial force of the filter is crucial. If the force is not adequate, there is a risk of migration of the whole device, both as the IVC compresses the filter continuously and if a large blood clot is trapped inside the filter. It might be possible to create a braided filter from a bioabsorbable monofilament, but there are certain challenges with it. The radial force of a braided stent is expected to be low, depending on the material of which it is braided. The advantage is that it is possible to choose in which direction the stent must have its strength, depending on braiding design. Some current metal non-bioabsorbable filters hold the vein open constantly, but could possibly disturb the blood flow. It is therefore not a requirement that the radial force of a bioabsorbable filter is large enough to keep the vein open. In comparison a bioabsorbable coronary stent made from for example poly(L-lactide) would need a cross-sectional area 240% higher than that of cobalt chromium, to match mechanical strength[25].

Migration Migration is one of the primary concerns for the bioabsorbable filter and filter should be adjacent to the vessel wall. Migration can occur both due to lack of radial force or be time-dependent. The latter is a situation where the initial radial force is adequate, but the device loses integrity over time due to an either permanent set obtained from continuous cyclic compression or stress relaxation of the polymer. The stent-base would then no longer be circumferential and possibly not adhere to the wall, and tissue coverage is no longer possible. Therefore tissue coverage must occur before the permanent set or relaxation. The tissue response of PLLA in veins is poorly investigated.

Fatigue properties The vena cava is a soft vein due to the low pressure of the blood running through it[26]. Because of this, the vein collapses during respiration. If the radial force of a bioabsorbable filter is not large enough to keep the vein open at all times, the filter will be compressed continuously. Advantages of a braided filter with lesser radial force might be that it would be able to deform with the vessel during compression, without the risk of permanent deformation. The fatigue properties are therefore important, and the filter should be able to withstand the continuous cyclic compression during a respiratory cycle 20,000

times a day [27]. It is difficult to find a polymer which both exhibits the adequate stiffness and strength to ensure a high radial force and have adequate flexibility to withstand the cyclic compression. Poor fatigue properties might lead to cracks and fragmented polymeric pieces. The pieces themselves, might be harmful to the patient and cause PE, and the fractured filter could migrate due to the loss in device integrity.

Device profile Devices for the vascular system can either be balloon-expandable, where the device is crimped onto a deflated balloon and expands in the vessel as the balloon is inflated or the device can be self-expandable. A braided filter would in most cases require balloon-expansion where a laser cut tube design could be self-expandable. The advantages for each are listed in Figure 3.8. The self-expandable way is favorable for large vein diameters, such as the vena cava, where the profile of the device itself is large and no need for a balloon upon delivery is preferable. Therefore the filter would from the start have a large profile, regardless of material. During loading into a delivery sheath, a braided filter might risk uneven crimping. Another concern with the balloon expandable is that the inflation during expansion toward the vessel wall must be controlled to avoid device damage. Regardless of the device profile, it might not be possible to create just one filter, which can meet vein diameters ranging from 15-30 mm. It might be more realistic to have two or three set of filters, which covers different vein diameter intervals.

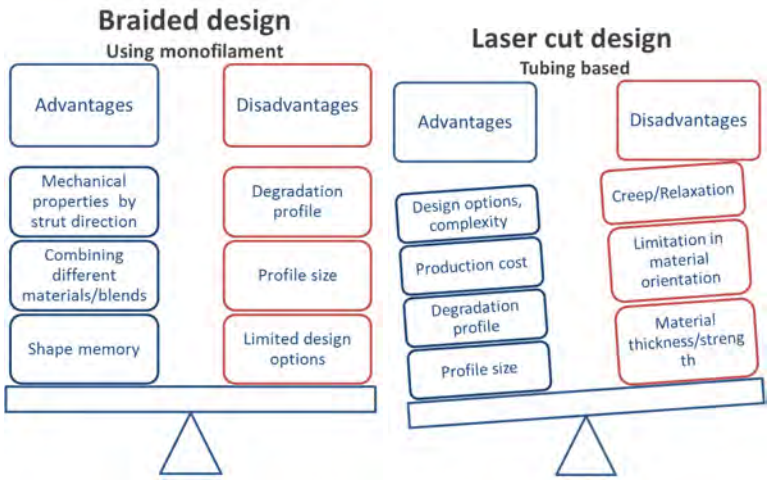

(a) (b)

Figure 3.8: The advantages and disadvantages of using braided monofilament (3.8(a)) or a laser cut tubing (3.8(b)) in an IVC filter

Molecular degradation It is a given that the filter must not degrade and be absorbed before the risk of PE has passed. Some of the more investigated bioabsorbable polymers for medical use are used as internal sutures, which degrades within 1-2 months. It sets a limitation to which polymers are appropriate for the IVC filter application. It should also be noted that as the polymer degrades, the amorphous domain is reduced, leaving the polymer crystalline and highly brittle. The fatigue properties are thereby reduced and the polymer would more easily fracture and fragments can travel to the lungs and cause small PEs[28].

Permanent set The mechanical properties of for example the bioabsorbable polymers are inferior to stainless steel or nickel-titanium and other metal alloys. Due to the permanent deformation of some of the stiffer polymeric devices, difficulties upon crimping and expansion upon delivery arise.

Change in material properties Mechanical degradation or loss of mechanical properties are not linear with in vivo degradation [25]. Mechanical degradation, where no significant molecular cleavage has occurred, may cause a loss of device integrity and parts of the filter to separate and cause PE. From a regulatory point of view, it becomes harder to justify its safety. However if the filter, both the stent and the filtration part are embedded in tissue as described in section 3.3.1, a potential loss of device integrity and fragments thereof are not in direct contact with the blood stream. It is no longer a potential hazard for the patient. The mechanical degradation must, therefore, be highly predictable.

Biocompatibility As for any medical device, biocompatibility is important and the material used should be both non-toxic and biologically inert to prevent late inflammation[25]. The body will have a natural way of covering or encapsulating any surface, which either harms the body or creates disturbances in the blood flow. There is a fine line between the amount of tissue coverage needed to cover the filter to make sure it stays in place and excessive narrowing on the caval wall. The reaction to bioabsorbable materials by the caval wall is unknown, and it is possible that the reaction is different than what reported on the arterial side for these materials.

Regulatory approval Regulatory approval is a challenge for any material, which has not been used in a particular clinical application previously. It is reasonable to look for polymers and copolymers which have been used in similar applications without adverse effects. In general adding particles or additives to the polymer to optimize the properties for a particular application, would make the approval process harder, unless that particular material has been used before. In this project, the scope was to investigate the already approved commercially available polymers. It should be noted that Abbott Vascular has made a Bioresorbable Vascular Scaffold System (BVS) for coronary use, made from highly crystalline PLLA (52%) with a coating of poly(D-lactide) (PDLA), which has been approved by the FDA. The biocompatibility of the material in the vascular system is, therefore, less of a concern, but the tissue response by the caval wall is unknown and must be investigated.

Premise The premise for the filter used in this particular project is a stepwise configuration. First, the device is delivered into the blood stream through a catheter and expanded into the lumen preferably on its own (self-expandable) and over-expands the vessel once it is fully expanded. The over-expansion should help the stent-base stay in place. The filtration part of the filter is comprised as an extension from the stent-base (filtration struts) and during their filtration period are connected with a small bioabsorbable wire or 'glued' together in the center. Once the connection is broken or dissolved the filter no longer has a filtration function and the filtration struts must move towards the vessel wall. The filtration struts must, therefore, have enough shape memory to flip outwards once they are released from the center. A concern is the tissue coverage at the tip of the cranial stent-base end. The tissue might partially cover the filtration struts and prevent them from reaching the vein wall. This concern was not tested in the animal study in this project, as the main objective was to investigate the rate of tissue coverage and the mechanical integrity of the stent.

Radiopacity For precise placement under X-ray, the device must be radiopaque. In general, polymers are not radiopaque[29] and therefore unlike the currently used metallic IVC filters, the polymeric filter would not be detectable by X-ray, when implanted in the body. For this reason, studies have been done to improve the radiopacity of bioabsorbable polymers. Below is a description of some studies on bioabsorbable polymer radiopacity. Previous studies include adding barium sulfate ($BaSO_4$) in a fine layer of powder bound to poly(lactide-co-glycolide) (PLGA) for bone fixation plates. It released 0.5 mg of $BaSO_4$ every

other day and was shown in vitro not to be cytotoxic. The X-ray attenuation coefficient for barium is 2.20 cm^2/g, whereas calcium it is 0.26 cm^2/g and is a good candidate[30]. Barium sulfate (30%) was also added to a PDLA monofilament used to braid stents [31] without significantly reducing the mechanical properties of the fibers in vitro. Nor does the PDLA with barium sulfate (23wt%) induce a greater inflammatory response than a steel stent would in vivo[32]. An alternative X-ray visibility was achieved by mixing iron oxide (Fe_3O_4) into a PLLA composite bone screw and showed no inflammatory response to it. The mechanical properties decrease if the amount is as high as 30% but 20% proved to be less adverse while providing strong radiopacity at least for four weeks. Perhaps a more straight forward approach is incorporating an iodine contrast agent into the polymer, but with the risk of leakage and radiopacity diminishing with time[33]. Normally low molecular weight contrast agents such as gold nanoparticles, heavy metal powders (tantalum), heavy element inorganic salts (barium sulfate, bismuth sulfide), bromide or iodine are used but are in general cleared quickly. They can induce pseudo-allergic reactions or renal toxicity. Bromide and iodine also reduce the strength and toughness[34] of the polymer. It is a challenge to blend the opacifier with the polymer backbone [29]. Therefore other pathways for reaching radiopacity have been investigated[29]. Mixing 2,3,5-triiodobenzoic acid (TIB) can be mixed in a bioabsorbable hydrogel of methoxy poly(ethylene glycol), and PLA showed strong radiopacity in vivo[33]. It can be synthesized with PCL and blended with various polymers to provide strong radiopacity ex vivo[29]. The concerns regarding radiopacity are not a part of this Ph.D. project, and the above methods were not evaluated. Simple methods could be adding gold markers onto the bioabsorbable stent-base as done for the Igaki-Tamai stent or platinum markers for the Bioresorbable Vascular Scaffold (BVS) stent.

3.4 What is currently out there

The literature is mainly focused on the arterial aspect of bioabsorbable vascular devices. Limited literature exists on bioabsorbable filters and as well as bioabsorbable venous devices in general. There is no direct translation between the devices on the venous side and the arterial side and the literature on the arterial aspect of bioabsorbable devices, might differ from the vein aspect. One study implanted Gianturco stents in both the IVC, portal vein and the infrarenal arterial aorta. A faster incorporation, as well as degree of tissue coverage, is seen for the IVC than the aorta [35]. The thickness of the neointima in the IVC

was 249±49μm yet only 137±42μm in the aorta. Also, it was detected that a stent with the same radial force would create an outwards force on the IVC and a hyperplasia of the media, whereas a hyperplasia of the intima would be seen in the aorta[35]. Additionally, the tissue response to a metal and a polymeric stent is the same in the arteries [36]. It is very possible that the reaction to a metal stent in vena cava is the same as for the polymeric stent and that the thickness of neointima is slightly larger for a bioabsorbable polymer in the veins compared to the arteries. This could however not be confirmed by the literature and the tissue response to the stent might solely depend on the radial force exerted on the vein, rather than the cells reacting to the material itself.

3.4.1 Bioabsorbable filter configurations

There are currently two studies, which investigated a 100% bioabsorbable IVC filter, none of which have been clinically evaluated. The most interesting study was done by Eggers et al. [5], who evaluated different sutures, including PDSII made from polydioxanone (PDS), Monocryl made from PCL and Vicryl made from polyglycolide (PGA)[5], on which they chose PDS as material for the filter and assessed it in vivo in a porcine model. The filter was braided into conically shaped filters (OD=20 mm). However, the device was not self-expandable. PDS is a suture which exhibits excellent stiffness and strength for 35 days, according to their study. Their braided filter exhibited no migration and maintained intact for 12 weeks. The filter was also able to withstand simulated thrombus trapping in vivo even at 35 days[37].

Thors and Muck [38] investigated the effect of the IVC filter made from PLGA strands as filtration cone and anchored to a self-expandable non-bioabsorbable nitinol Z-stent (Cook Medical Inc.) (see Figure 3.9). It was evaluated in a porcine model for six weeks, but the functionality of the filter was not modeled. At termination, only the nitinol stent remained in all but one animal, where one PLGA strand remained incorporated into the caval wall and covered in neointima. Device integrity was not high, as half of the devices experienced some rotation in the horizontal plane. Histology showed intense inflammatory response and thickening of the intima and media. The filter from Thors and Muck was not a true temporary filter, yet only an evaluation of the response to PLGA strands as the filtration cone during degradation.

Zhang et al. [39] continued the idea by creating a bioabsorbable filter made from PCL, an elastomer, as a stent-base (OD=18 mm) and PLGA as bioabsorbable filtration cone (Figure

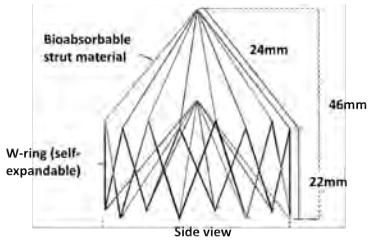

Figure 3.9: IVC filter with a bioabsorbable PLGA filtration cone. Used from [38]

3.10(a)). The filter was evaluated in a canine animal model in an IVC with the diameter of 12 mm for 6 weeks at which mainly the stent-base remained. Migration due to the PCL's poor mechanical strength and stiffness was observed. There was no evidence of PE caused by degradation products from the PLGA filtration struts. The PLGA struts were still present and adhered to the caval wall resulting in an obstruction of the lumen. Inflammation was present to a great extent and where the struts had been.

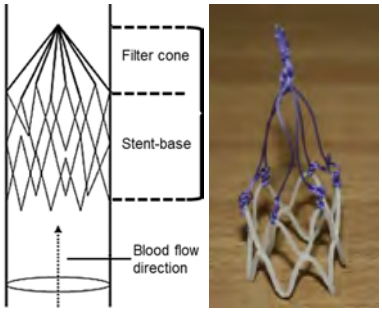

(a) (b)

Figure 3.10: Sketch (3.10(a)) and prototype (3.10(b)) of a bioabsorbable filter made of PCL as the stent-base and PLGA as the filtration cone. Used from [39]

The main concern with the filters using monofilament for filtration struts, regardless of the stent-base, is the risk of debris from degradation products or fragments as degradation occurs causing a PE[39][28].

Xiao-ping et al. [28] focused on the feasibility of a bioabsorbable filter designed along the lines of the permanent TrapEase filter in Figure 3.1. The bioabsorbable version made from PLLA is shown in Figure 3.11. They reported an in vitro study which evaluated the clot trapping ability of PLLA strands cut from film and incorporated in a filter. One drawback was that upon delivery the device deformed to half its initial diameter. Therefore it needed

a center line expansion mechanism to open the device to its original diameter as seen in Figure 3.11 step 1. As it starts to degrade fragments would be released (Figure 3.11(a) step 2) to the system, especially the central line, which could potentially cause PEs.

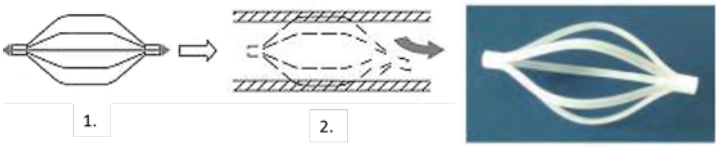

(a) (b)

Figure 3.11: Filter made from PLLA strands as sketched (3.11(a)) and as prototype (3.11(b)). Modified from [28]

3.4.2 Bioabsorbable stent configurations

As previously stated literature on 'true' temporary or bioabsorbable filters is sparse. One should note that there is a great deal of literature on the subject of a bioabsorbable stent for arterial use. Due to the vast literature as well as one already commercially available bioabsorbable stent, it makes sense to apply some, but certainly not all, of the thoughts and challenges to the creation of a bioabsorbable filter. Some of the requirements apply for both metal and polymeric bioabsorbable stents and are good biocompatibility, adequate radiopacity for visualization and sufficient radial strength [40]. In short, a stent is used to treat stenosis or obstructed vascular vessel and used as a scaffold supporting the vessel wall to provide support to an obstructed lumen[41]. They can be divided into two groups (self-expandable or balloon expandable) depending on the application and the dimensions and the way they are meant to be delivered.

Stents are best described as comprised of repeating elements denoted as struts in the circumferential direction. The struts that form a close loop are called cells. The continuous series of struts or cells in the circumferential direction are denoted columns, whereas two adjacent cells or struts in the longitudinal direction are denoted bridges. The junctions of which the struts connect are called connection points. Upon loading, it is required that the stent can be transformed into a compressed state during loading and transformed into the initial shape upon implantation. The design must include an efficient crimp, by folding or packing the cells to a diameter below the maximal diameter for loading.

For balloon expandable stents, there are two key considerations regarding the mechanical behavior. The stent must be ductile enough not to be plastically deformed during expansion in the target vessel. For self-expandable stents, the stent must have enough radial force to open fully up on its own. For both groups, the stent must not creep and remain vessel patency[41] until its surface is covered in tissue. In this project the word *stent* relates solely to a stent functioning as a stent and *stent-base* refers to a construct which resembles the stent, but does not necessarily function as a stent. Stents are typically made of stainless steel, nitinol, cobalt alloys or recently made of polymers. Permanent metal stents have long-term complications such as hyperplasia. To overcome this some of them are drug-eluting, to minimize this hyperplasia. However, when the drug is no longer eluted over time, the hyperplasia becomes an issue[42]. The stents made of nitinol have a significant shape memory effect and superelasticity over the polymeric ones. It also has the advantage over a bioabsorbable polymer, that it is stable at body temperature. Great shape memory is not the case for most of the commercially available bioabsorbable polymers.

As seen in Table A.1 in Appendix A.1, most of the bioabsorbable stents are made from polymers, but the bioabsorbable metal stents are also under development. They comprise primarily of magnesium and iron as pure or in alloys. Today there is only one commercial available stent, the Bioresorbable Vascular Stent (BVS) by Abbott Vascular. A commercial available bioabsorbable stent for arterial use means that approval of using the same type of polymer in the vascular system, but on the vein site of it, becomes easier. Having that said, the mechanical requirements for such as device might not be the same as for arterial stents.

To sum up, more and more IVC filters are placed and primarily due to the long-term complication, FDA has issued a concern regarding the use of IVC filters. There is a present need for a bioabsorbable IVC filter, but the creation of such has many challenges. The bioabsorbable materials today are primarily polymeric and have been widely investigated for several applications, but not approved for a bioabsorbable IVC filter. The materials have their short comings compared to the non-bioabsorbable metals used for IVC filters today. In the selection of a bioabsorbable polymer, the above-mentioned requirements must be fulfilled. An extensive characterization of the initial properties as well as changes over time are described and investigated in Chapter 5.

4

Experimental materials and methods

4.1 Characterization methods

The following section applies to the experimental methods used to characterize the behavior and properties of the materials as a result of processing and are portrayed in Figure 4.1. The methods used to characterize the behavior in vitro are portrayed in Figure 4.2.

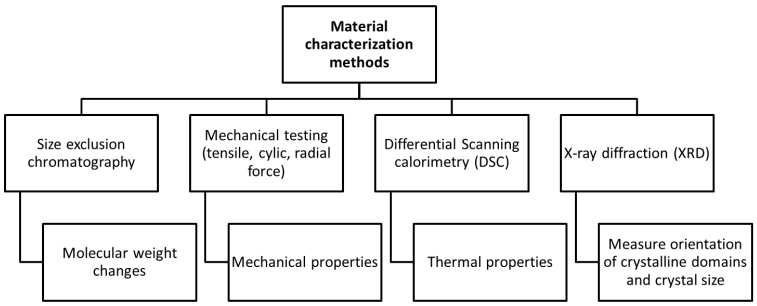

Figure 4.1: Flowchart of methods used for characterization of materials

The most predominant method for characterizing the mechanical properties of the materials was tensile testing. Radial force testing was done to evaluate the force the filter can exert when placed in a vein. Compression testing was done to evaluate fatigue properties of the material over time to simulate when implanted in vivo. The effect of processing was evaluated both regarding mechanical properties and in relation to the changes in crystallinity

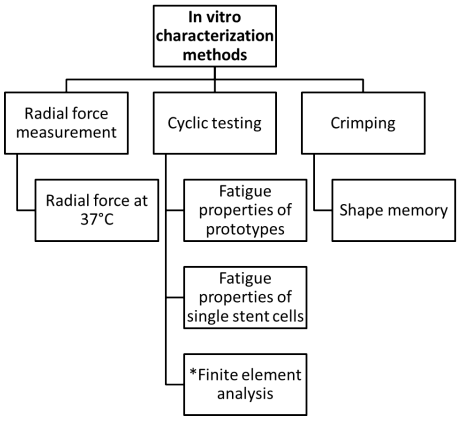

Figure 4.2: Flowchart of methods used for characterization materials in vitro. *Finite element analysis was performed retrospectively

and orientation of the material and characterized by differential scanning calorimetry (DSC) and wide angle X-ray scattering (WAXS), respectively.

4.1.1 Mechanical testing

Tensile testing of monofilament Several types of monofilament were tested to get an overview of the material candidates for a bioabsorbable filter. The raw data was supplied by S. Tanner (Cook Research Inc.) and performed on an Instron 5544 using a 10 N load cell at a testing speed of 25 mm/min and a gauge length of 25.4 mm. Samples were tested until fracture. The monofilaments were also braided into stents (OD 8 mm, length 40 mm) and further evaluated through radial force testing when crimped from 10-2.1 mm. The data analysis was performed using MatLab 2016a.

Tensile test of expanded tubes Specimens for mechanical testing were cut from the tubes both circumferentially and axially along the tube with a width of 5 mm and a length of 18 mm (Figure 4.3). The cross-sectional area was determined as the average thickness times the width of the specimens. Uniaxial tensile testing was performed at a testing speed of 2.7 mm/min on an Instron 5564 using a 500 N load cell and the tubes were pulled to fracture. Stress (σ) is a force over the initial cross-sectional area (A_0), and strain (ϵ) is the difference in length over the initial length. From the stress-strain curves, elastic modulus ($E=\sigma/\epsilon$) was determined in the interval of 20-40 MPa and yield stress (σ_y) was determined as the first local maximum. Data from tensile testing was collected using Bluehill® software V3.25. The

analysis was performed using MatLab 2016a. The definitions of the mechanical properties are shown in Appendix B.1 in Figure B.1. A representative script showing the data analysis for tensile testing (both monofilament and tubes) is found in the Appendix B.2.1.

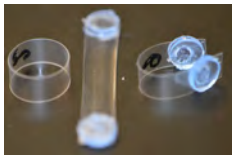

Figure 4.3: Specimens cut from tubing in the axial and circumferential direction. Protective clamps were added to each end

Radial force testing Radial force testing was done to determine the effect of processing and design of a stent-base. It was performed in a compression station, and the stent-base was crimped from 30 mm to 6 mm (0.5 s/min) three times in a controlled dry environment at 37 °C. The compression station measures the crush resistance or said, in other words, the chronic outward force under constant displacement (Figure 4.4). Circumferential crimping down to 6mm does not resemble the physiological compression on the stented vein but gives an idea of resistance to permanent deformation or if the device can to be loaded into a delivery sheath more than once. Data was analyzed using MatLab 2016a. The graph was smoothed with a built-in local regression function and the filter was set to 0.02.

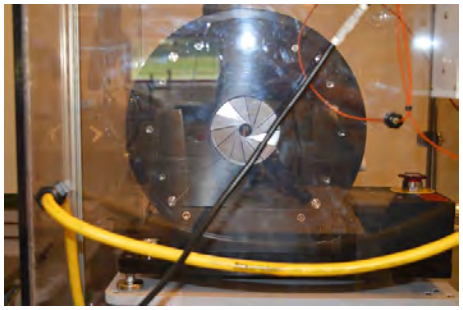

Figure 4.4: Compression station for radial force testing

Cyclic testing The cyclic test was performed on both single stent cells and stent-bases. The former was fixed in an Instron 5942 fixed with custom made grips as seen on Figure 4.5(a) and tested using a 50 N load cell. The cell was compressed to half of their height in a relaxed state with a speed of 200 mm/s for 10-77 cycles. The area underneath the curve after each

cycle was calculated using a built-in 'trapz'-function in Matlab 2016a, which returns the approximate integral of the load. Due to the difference in thickness for each specimen, the areas were normalized between 0 and 1 for better comparison.

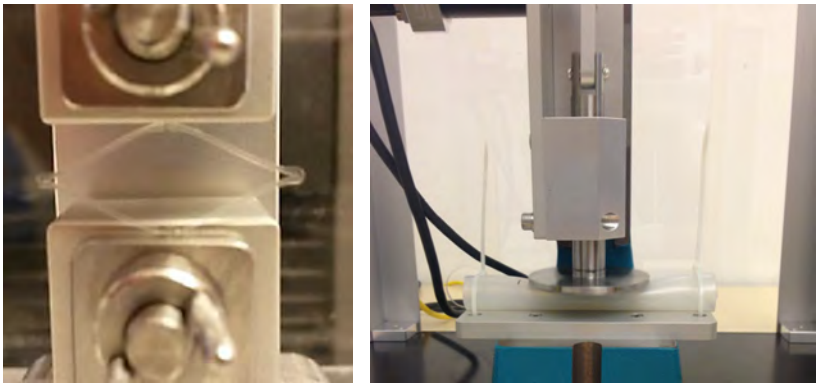

(a) (b)

Figure 4.5: Single stent cell fixed in Instron with customized grip during cyclic compression test 4.5(a) and stent-base fixed in a silicone tube during cyclic compression test under ambient conditions (4.5(b))

Cyclic test of the entire stent was performed on a custom made flat-plate compression station (see Figure 4.5(b)) to evaluate the fatigue properties. The degree of compression is the distance of which the top-flat plate travels towards the bottom flat plate and set to ~30%. The device was placed in a silicon tube to mimic the vein wall and placed between the two flat plates. It gave the option of adding fluids, controlling the temperature and adding flow to the model. The temperature was controlled by a sensor in a small water tank next to the system from which the solution was pumped through the silicone tube between the flat plates. All stents were delivered through a 6 mm sheath, which corresponds to the first crimping in the radial force test. The test would run for 150,000 cycles over the course of 3 days result in a compression speed of approximately 6 mm/s.

4.1.2 Statistical analysis

Statistical analysis was done using a double-sided t-test in MatLab 2016a for comparison of two groups at a significance level of α=0.05%. It was assumed that the distribution of the mean of each test series is normal and that the variance in each test series is similar.

4.1.3 Differential scanning calorimetry

Differential scanning calorimetry (DSC) is a technique which measures the differences in heat flow rate of a sample and a reference during heating or cooling or said in order words, the amount of heat needed to increase the temperature of each. It gives information about the glass transition temperature (T_g), heat capacity (C_p), cold crystallization temperature (T_{cc}) or melting temperature (T_m) and the heat of fusion during constant heating or cooling rate during a DSC scan[43]. It was used to determine the thermal properties of the material before and after processing. DSC scan of the processed materials, can both provide an idea of the degree of crystallinity (X_c) obtained by different processing and the mechanical behavior thereof. It can also provide information about whether or not the material will be affected by the body temperature. Additionally, the changes in the material due to storage, the presence of moisture from sterilization or physiological environment can be detected by changes in the glass transition temperature (T_g) or X_c. Figure 4.6 shows a representative DSC scan for the extruded PLLA used in this project.

DSC was performed either on Netzsch DSC 200 F3 Maia as described in [44] or carried out on TA Instruments DSC Q200. Heat rate was 10°C/min regardless of instrument. The samples (5-10 mg) were heated from ≤20°C to ≥180°C. The T_g was found as the midline between onset and offset before and the transition. The X_c was calculated from the measured enthalpy induced by melting (ΔH_m) minus the measured heat fusion induced by crystallization (ΔH_c) relative to the enthalpy of fusion (ΔH_m^0=93 J/g[45]) of a 100% crystalline PLLA sample (Equation 4.1). Data was analyzed using Netzsch Proteus Analysis software v 6.1.

$$X_c(\%) = \left(\frac{\Delta H_m - \Delta H_c}{\Delta H_m^0}\right) \cdot 100 \tag{4.1}$$

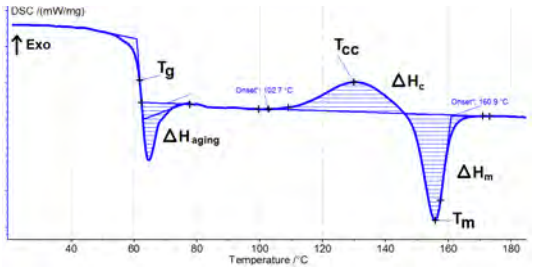

Figure 4.6: Representative DSC scan of extruded PLLA and the determination of T_g, T_{cc} and T_m and the area of crystallization and melting peak

4.1.4 Wide angle X-ray diffraction

Wide angle X-ray scattering (WAXS) was used to determine the textural orientation of the polymer as a result of processing. WAXS gives information on the structure of the crystalline domain, the X_c, crystallite size, and their orientation. The principle behind the technique is placing the sample in front of an X-ray beam. The reflected X-rays at specific angles and intensities are recorded in this case by a diffractometer (Figure 4.7(a)). The structure will produce a unique set of the angular distribution of diffracted intensities. The crystals will give rise to sharp diffractions, whereas the amorphous domains will produce diffuse scattering. The width of the reflections in a specific crystallographic axis corresponds to the size and disorder of the crystallites. The wider the reflection, the smaller the crystals. The orientation is calculated from arc lengths or angular spread of a chosen reflection along the fiber axis[46].

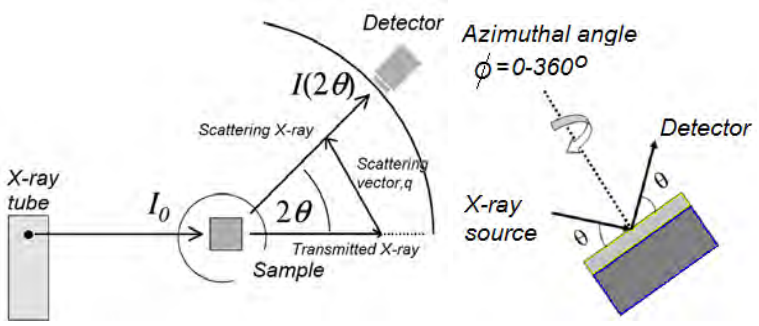

(a) (b)

Figure 4.7: The principle of WAXS, where the X-ray is emitted to the sample and the scattering angle (2θ) at which the projected beam is detected (4.7(a)). The scattering plane defined by the wave vector of incoming and scattered X-ray beam outside the sample, which defines the scattering plane and the scattering vector q between. Modified from [47] and [48]. Figure 4.7(b) show the azimuthal angle (ϕ). Modified from [49]

In this project, a custom-made 2D diffraction setup equipped with a rotating anode Cu Kα X-ray source, monochromatized and focused by 1D multilayer optics was used. It was operated at 50 kV and 200 mA with a 123 mm distance between detector and sample for 30 min. The sample was cut in half and placed with the axial direction vertical and perpendicular to the beam. The crystalline orientation of the lamellae in the stretching direction was determined using Herman's orientation function (Equation 4.2 and 4.3) and a second-order

orientation factor (Equation 4.4)[50]. An orientation factor (F_2) of 1 corresponds to complete orientation. The scattering intensity is integrated as a function of Bragg's angle (2θ) and the azimuthal angle (ϕ). The azimuthal angle, ϕ = 0° is defined at the position of the circumferential direction and the normal direction to the (200/110) plane in the interval of scattering vectors q=1.13-1.24 Å $^{-1}$ between 0-360°.

$$f_H = \frac{3\langle cos^2\phi\rangle - 1}{2} \tag{4.2}$$

where $\langle cos^2\phi\rangle$ is

$$\langle cos^2\phi\rangle = \frac{\int_0^\pi I(\phi) cos^2\phi sin\phi d\phi}{\int_0^\pi I(\phi) sin\phi d\phi} \tag{4.3}$$

$$F_2 = C^{-1} \cdot f_H \tag{4.4}$$

where C is a conversion factor (Equation 4.5) from the orientation of a lamellar normal with respect to the stretching direction[50]

$$C = \frac{3\langle cos^2\Psi\rangle - 1}{2} \tag{4.5}$$

where Ψ is the angle of the lamella normal to the lamella interface and would in this case be Ψ=90° resulting in C=-1/2.

The mean crystal size ($D_{(hkl)}$) (Equation 4.6) was found in both the circumferential direction (scattering vector q=2.2-2.25 Å^{-1}) and axial direction (scattering vector q=1.13-1.24 Å^{-1}) corresponding to the (018) and (110/200) planes, respectively. It uses Scherrer's equation with the shape factor K=0.9[51], the wavelength λ= 1.5418 Å and $\beta_{1/2}$, which is the width at half the maximum of the peak height at the particular Bragg diffraction angle, θ.

$$D_{(hkl)} = \frac{K \cdot \lambda}{\beta_{1/2} \cdot \theta} \tag{4.6}$$

Diffraction patterns were analyzed in Matlab 2016a, using a predefined script (WAXS package version 9.4) written by Dag W. Breiby (2011) (Figure B.2 in Appendix B.3). Further analysis of the intensities and angles, were analyzed in Matlab 2016a.

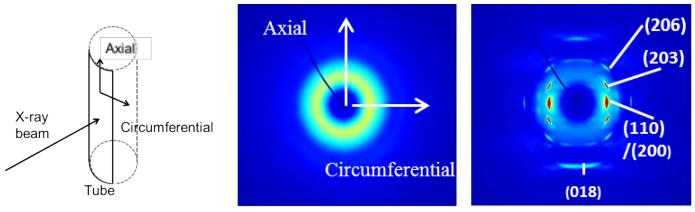

(a) (b)

Figure 4.8: Sketch of WAXS setup (4.8(a)) and WAXS images of an amorphous extruded PLLA tube and semi-crystalline strain-induced PLLA tube (4.8(b)). The most common diffraction crystal planes are shown.

4.1.5 Gel permeation chromatography

Gel permeation chromatography (GPC) were used to determine the average molecular weights using differential refractometer and a right angle laser light scattering (RALLS) detector. The column set consisted of one Waters styragel 10μm HT 6E column and one PLgel 5μm mixed D column. Approximately 2.5 mg/ml PLLA was dissolved in tetrahydrofuran (THF) and filtered by 0.45μm polytetrafluoroethylene (PTFE) filter under constant temperature (22°C) with the flow rate of 0.5 ml/min. From this number average molecular weight (M_n) and weight, average molecular weight (M_w) were determined based on calibration with polystyrene standards using TriSEC software.

4.2 Histology processing

The procedure, interim and follow-up of the in vivo study are described later in Chapter 9. Below are the histology processing described.

4.2.1 Hematoxylin and eosin staining (H&E)

To avoid the tissue from changing and drying out, the explanted tissue was fixated for 48 hours in 10% formalin. The fixated vein was dehydrated with alcohol and embedded in paraffin and cut into slices (5μm thick) using a microtome. The slices were hydrated using Xylene, and stained with first hematoxylin (H) and then eosin (E). Hematoxylin strains purple acidic structures such as DNA in the nucleus. Eosin stains pink but is more non-specific and stains most proteins[52].

4.2.2 Antibody straining and immunochemistry

Two sets of antibodies were used, a primary and a secondary antibody. After staining the tissue was visualized by confocal laser scanning microscopy. The staining can either be done in one or two steps. The one-step method uses antibodies, which are fluorescent, and can bind to directly the tissue and antigen in question. The two-step method uses two antibodies. The primary antibody, which in unlabeled, is raised against an antigen of the cell or tissue for examination and therefore binds to it. Subsequently, a secondary antibody, which is fluorescently labeled, is added and binds to the primary antibody because it has been raised against it. The methods are portrayed in Figure 4.9. In this project, the two-step method was used.

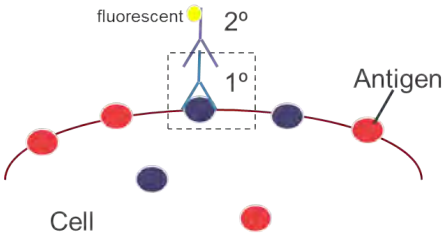

Figure 4.9: Principle of directly labeling of antigen with fluorescent secondary antibody (2°) or indirectly labeling to a primary antibody (1°), which have bonded to the antigen (dashed box)

Primary Antibody (1° AB) The specific targets for visualizing the response to the implant were the precursor for fibrin, fibrinogen, and the inflammatory response regarding the presence of macrophages. The tissue coverage as a result of implantation was expressed by endothelial cells. Anti-Fibrinogen gamma chain antibody (IgG2b) (ab119948 from Abcam)[53] binds to the gamma chain of fibrinogen molecules. Fibrinogen yields monomers to polymerize into fibrin and acts as a cofactor in platelet aggregation. Purified rat anti-mouse CD31 (IgG2a) (MEC 13.3 from BD Biosciences)[54] is an antibody against CD31 and reacts with platelet endothelial cell adhesion molecule-1 expressed on adult and embryonic endothelial cells and many peripheral leukocytes and platelets. Anti-Macrophage antibody (IgG1) (ab22506, MAC 387 from Abcam)[55] binds to an intracytoplasmic antigen expressed by granulocytes, monocytes and by tissue macrophages.

Secondary Antibody (2° AB) Secondary antibodies were used to fluorescently stain the primary antibodies for visualization under a fluorescent microscope. DAPI, wheat germ agglutinin (WGA) and phalloidin were used to counter stain the nuclei, actin-filament and residuals found on the cell membrane surface, respectively.

DAPI (4',6-diamidino-2-phenylindole) (D1306 from ThermoFischer Scientific)[56] (1:500) binds the AT regions within the DNA of the cell and emits blue fluorescence upon at wavelength at 461 nm. WGA (Alexa Fluor 488 (AF488) from ThermoFischer Scientific)[57] (1:500) is an agglutinin which binds to sialic acid and N-acetyl glucosaminyl residues found in the cell membrane and emits green at the wavelength of 519 nm. Phalloidin (Alexa Fluor 488 (AF488) from ThermoFischer Scientific)[58] is a peptide, which binds actin in cells and tissues, and emits green fluorescence at the wavelength of 518 nm. Donkey anti-mouse secondary antibody (IgG), Alexa Flour 555 (AF555) binds to IgG anti-fibrinogen or anti-macrophages and emits red at a wavelength of 556 nm[59]. Chicken anti-rat secondary antibody (IgG), Alexa Flour 647 (AF647) binds to anti-CD31 and emits at a wavelength of 647 nm in the far red spectra[60].

For antibody staining, the fixed tissue was rinsed in phosphate buffered saline (PBS) blocked with 10% donkey serum in 0.2% bovine serum albumin (BSA) and permeabilized with 0.2% TritonX-100 overnight. Tissue was incubated with a primary antibody against fibrinogen (IgG2b 1:100) or macrophages (IgG1 1:100), diluted in 0.2% BSA and PBS, for two days at 4°C and then rinsed three times of 30 min. Samples were next stained with secondary labeling reagents for nuclei (DAPI 1:500), actin filaments (AF488 phalloidin, 1:100), and AF555-conjugated anti-mouse secondary antibody (AF555 1:500) for 2 days at 4°C, then rinsed 3x30 minutes and stored at 4°C until imaged.

4.2.3 Optical clearing

For optimal confocal imaging, the explanted tissue was cleared to ensure greater visibility by incubating the tissue in solutions of gradually increasing fructose concentration. D-(-)-fructose (JT Baker, Center Valley, PA) was dissolved in milliQ water with 0.5% γ-thioglycerol (Sigma-Aldrich St. Louis, MO) at various concentrations (20, 40, 60, 80, 100% wt/vol and 115% wt/wt). The explanted tissues were incubated in each solution for 12-24 hours under gentle rocking.

4.2.4 Confocal imaging

Confocal imaging was used to visualize the newly formed tissue around the connection points without disrupting the tissue. To increase the optical resolution and the contrast of the probe, a spatial pinhole was placed at the confocal plane of the lens to eliminate out-of-focus light. Tissue samples were imaged with an inverted confocal laser microscope (710 LMS, Zeiss, Germany) with laser wavelengths from 405 to 639nm. Images were obtained as 1024x1024 pixels with ZEN 2011 software and taken as the best compromise between overlaid laser wavelengths.

5

Material selection

The following chapter highlights the most common bioabsorbable polymers used in research and commercial devices today. Their advantages and disadvantages are summarized for the sole purpose of choosing the right polymer. The objective was to find the best material candidate for a bioabsorbable filter with processing in mind to improve the performance of the bioabsorbable filter. Based on the screening of materials in the literature review, certain polymers in the form of monofilament were mechanically evaluated, before a choice of material was made.

5.1 Background on bioabsorbable polymers in biomedical applications

There are certain requirements for choosing a biomaterial, including bioabsorbable polymers for a specific application. Not only must it have the appropriate mechanical properties, but it must also be non-toxic and endotoxin-free and thereby biocompatible[61], which is no different than when designing traditional medical devices[62]. As for the bioabsorbable polymers, the degradation products must be non-toxic and be cleared by the body itself. For any given biomaterial, the host-response and tissue response to a polymer depends on the chemical, physical and biological properties of the material[61]. Below are the general requirements for a bioabsorbable IVC filter[61][62]

- biocompatible
- appropriate degradation time
- appropriate mechanical properties

- produce non-toxic degradation product
- processing must be easy

The understanding of the properties become more complex over time as they change, thus resulting in a different host response distinct from the initial[61]. The polymer must also be commercially available and easily processed to tailor its properties. Degradation rate, strength loss, and mass loss must be controlled and fully known and will vary depending on the application. Applications of bioabsorbable polymers in medical devices are numerous and include sutures, orthopedic devices including screws plates, etc., temporary scaffolds for tissue regeneration, drug-eluting cores or strings on nano- or microscale for drug delivery, stents for vascular use and much more.

Bioabsorbable materials have been investigated for decades in different fields including the biomedical field. The predominant reason for this in some applications is the elimination of a second operation to retrieve the device [63] or eliminate long-term complications. Is some applications a retrieval operation is not possible for example with placements of vascular stents. Depending on the application some bioabsorbable polymers has shown greater promise than others. The properties of a bioabsorbable polymer depend on material chemistry, molecular weight, hydrophobicity, surface charge, water absorption, degradation and erosion mechanism[61]. Their main disadvantage is that they are highly time-dependent. As they degrade, they undergo irreversible damage, such as fatigue or creep[64].

5.1.1 Types of polymers: natural or synthetic

There are currently both natural (Table 5.1) and synthetic bioabsorbable polymers (Table 5.2) and both have been investigated extensively[65]. The polymers are often divided into groups, according to their degradation pathway, either enzymatically or hydrolytically[65] as later described in section 5.1.2. A drawback for natural bioabsorbable polymers is that many of them are enzymatic degradable and varies depending on the implant site and availability of enzymes. It is therefore difficult to predict the degradation rate clinically[62][65]. They have the advantages of possessing bioactivity and interacting with the cells, which is some instances, unfortunately, trigger an immunogenic response from the body. This immunogenic response can be avoided by using the synthetically manufactured polymers, where properties are more predictable, and batch to batch variation is low. Keeping the commercial aspect in mind, the natural polymers are therefore not further reviewed in this

thesis. The synthetic ones give us the possibility of tailoring properties to our specific application [62][61]. Synthetic bioabsorbable polymers are often synthesized by either step (condensation) polymerization to make polyanhydrides, poly(ortho esters) and polyurethanes or and addition (chain) polymerization. The latter include ring opening polymerization to make hydrolytic sensitive poly(α-esters) and polyphosphazenes. Degradation rate usually depends on chemical bonds, water diffusion, monomer solubility, device geometry, and size. Depending on the industry, different requirements apply. For example in the packaging industry, the specific degradation time is less significant as some polymers will degrade long after the packaging need has been filled. In the biomedical field, they are used in temporary medical devices, where a function or support is required for a certain period. In a biomedical application, the specifics on strength and mass loss over time is very crucial.

Table 5.1: List of some natural polymers

Natural polymers		
Name	**Degradation type**	**Application**
Proteins and Poly(aminoacids)		
Poly(amino acids)	enzymatic[65]	scaffolds[65]
Albumin	enzymatic[65]	coating[65]
Collagen (protein)	enzymatic[65]	wound dressings and drug delivery[65]
Elastin	enzymatic[65]	scaffolds, coating and drug delivery[65]
Fibrin	enzymatic[65]	drug delivery[65]
Polysaccharides		
Alginate (polysaccharides)	enzymatic[65]	drug delivery and scaffolds[65]
Chitin, chitosan	enzymatic[65]	drug delivery[65]

5.1.2 Degradation pathways

The bioabsorbable polymers can be divided into hydrolytically and enzymatically degradable polymers. Hydrolytic bioabsorbable polymers have hydrolytically labile chemical bonds in their backbone[65] and include polyesters, polyamides, poly(anhydrides), poly(ortho esters), poly(phosphoesters), poly(cyanoacrylates), or poly(phosphazenes)[66][61]. For the production of bioabsorbable biomedical devices hydrolytically degradable polymers can be preferred over the enzymatically, due to minimal site-to-site variation as well as low patient-

to-patient variations[65]. The degradation rate depends on how hydrophilic or hydrophobic the side groups are. The degradation rate decreases when containing the following bonds: ester-, carbonate-, urethane- and amide bonds and in that order[66]. If the polymer is crystalline, the degradation is also slower. The hydrolytically degradable polymers can either degrade by bulk or surface erosion as portrayed in Figure 5.1 or even as a combination of both[61]. In surface erosion (as seen in Figure 5.1(a)) the water diffuse at the surface far exceeds the diffusion into the bulk and the molecular weight stays almost constant, while a fast mass loss occurs. The strength will follow the rate of the mass loss decrease. Bulk erosion (as seen in Figure 5.1(b)) is characterized by a faster water diffusion into the bulk, and mass loss is retained, but a fast molecular weight (M_w) loss is observed. The strength will decrease with decreasing molecular weight (M_w). The degradation pathway must be taken into account when choosing the material for a bioabsorbable IVC filter. Surface erosion is an advantage during drug release in drug delivery systems, but a disadvantage if too quick in a load bearing application. The device would see a more gradual loss in mass than the delayed loss for the bulk degradation (see Figure 5.1). A drawback of bulk degradation is that some polymers such as the carboxylic acid derivatives produce a highly acidic environment during bulk degradation, which can speed up the degradation process from within the bulk[67]. Other polymers such as the polyurethanes are degraded by oxidation controlled by the macrophages, and is therefore not a very controlled degradation pathway and not suitable in all applications[66].

Applications Table 5.1 and 5.2 show the most common polymers used in the biomedical field, each one having suitable properties for a specific application or from a more negative perspective, they all have their shortcomings. To overcome this blends and copolymers and composites have been investigated. Their variety of properties ranges from elastomers to harder polymers, used as a scaffold for tissue engineering or as in orthopedic implants, respectively. PLLA have also been used in studies as a coating on drug-eluting stents (DES), Excel (JW Medical Systems, China), Cura (Orbus Neich, Fort Lauderdale, Florida) and Supralimus (Sahajanand Medical Technologies, India). Polyurethane can also be used as a coating for a controlled DES[72]. Bioabsorbable polymers, such as PLLA has also been used as a biodegradable stent itself as listed in Table A.1 in Appendix A.1. Bioabsorbable polymers in orthopedic devices have an advantage over the traditional metal devices as they can transfer gradually less stress over time to the wounded area as it heals. The non-absorbable

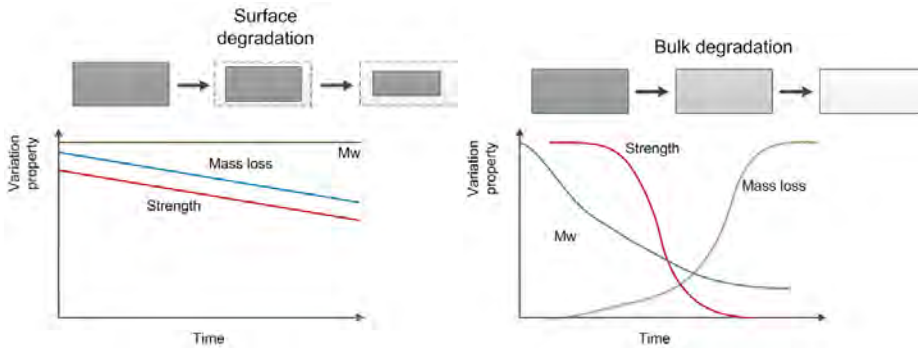

(a) (b)

Figure 5.1: Sketch of surface (5.1(a)) and bulk degradation (5.1(b)) and the changes in molecular weight (M_w), mass and strength loss. During surface erosion the molar mass of the remaining polymer remains constant, but a fast mass loss can be observed. Its strength is dependent on the residual amount of polymer and follows the M_w. In bulk erosion the mass loss is retarded but the molecular weight is reduced faster.

device will not do so, and it is known that regeneration of bone tissue is poorer and break after removal of the device[63]. Some bioabsorbable polymers can also respond to stimuli from the environment. Some are sensitive to pH changes light and temperature. They are known as intelligent or smart polymers, which can be used for drug delivery systems and tissue engineering[72]. However, for a device which must maintain its integrity, it must not be susceptible to environmental changes. The pH value in blood and most tissues are primarily stable at pH 7.4, which is close to the pH of the water. Polymers which are not sensitive to pH changes, water or saline, makes up for an excellent in vitro testing media. There are a great number of polypeptides, which are sensitive to pH [72] for use in drug delivery to tumors, with a lower pH level than blood and normal tissue.

5.1.3 Bioabsorbable polyesters

A large group of bioabsorbable polymers is the aliphatic polyesters, with reactive groups such as carboxyl, hydroxyl, amino, ketal, brom, chloro and carbon-carbon [72]. Depending on the monomeric unit, they can be polymerized via ring opening (most efficient) and condensation polymerization routes[65]. Additionally homopolymer or their copolymers are prepared by homopolymerization or copolymerization of cyclic monomers[72] (see Figure 5.2). The most extensively investigated bioabsorbable polymers are the aliphatic synthetic polyesters e.g. polylactide (PLA), polyglycolide (PGA), polycaprolactone (PCL). Additionally,

Table 5.2: List of some synthetic polymers

Name	Advantages	Disadvantages	Degradation type	Application
Synthetic polymers: α- polyesters				
Poly(L-lactide) PLLA	Highly processable, many commercial vendors[61]	Limited degradation frame, highly acidic degradation products[61]	Bulk, hydrolysis [65]	Orthopedic, oral and maxillofacial surgery[68]
Poly(D,L-lactide) PDLLA			Bulk, hydrolysis[65]	Drug delivery[69], orthopedic, oral and maxillofacial surgery [68]
Poly(glycolide) PGA		T_g close to body temperature	Bulk, hydrolysis [69]	Orthopedic and general surgery, sutures [68]
Poly(lactic-co-glycolic acid) PLGA			Bulk, hydrolysis[65]	Drug delivery[69], sutures, general, periodontal, oral and maxillofacial [68]
Poly(ϵ-caprolactone) PCL	Highly processable, many commercial vendors[61]	Limited degradation frame[61]	Bulk, hydrolysis [65]	Drug delivery, sutures[68]
Poly(p-dioxanone) (PDS)		Loss in strength (1-2 months)[65]	Bulk, hydrolysis [65]	Orthopedic and general surgery, sutures [68]
Poly(trimethylene carbonate) PTMC	Polycarbonate has chemistry-dependent mechanical properties[61]	Polycarbonate has limited degradation and require copolymerization [61]	Enzymatic surface erosion [65]	Soft tissue engineering [70] and drug delivery [65]
Other Synthetic polymers				
Poly (ortho esters) POE	Controlled degradation rate and pH sensitive[61]	Complex synthesis and weak mechanical properties[61]	Surface, hydrolysis [65]	Drug delivery [69]
Polyurethanes PU	Mechanically strong, handle stress well[61]	Limited degradation frame and require copolymerization with other polymers[61]	Hydrolysis [65][71]	Vascular grafts[65]
Pseudo poly (amino acids)	High crystallinity, low degradation rate[61]	Unfavorable mechanical properties, and immunogenicity[61]	Hydrolysis, enzymatic[65]	Load bearing applications, drug delivery[65]
Polyanhydrides	Sign. monomer flexibility, controlled mechanical properties[61]	Low M_w and weak mechanical properties[61]	Surface hydrolysis[65]	Drug delivery [65]and bone tissue engineering[72]
Poly (ester amide) PEA			Bulk hydrolysis	Suture, drug delivery [65]
Polyphosphazenes (PPHOs)[73]	Sign. monomer flexibility, controlled mechanical properties[61]	Complex synthesis[61]	Bulk and surface hydrolysis[74]	Drug delivery [65]
Poly (alkyl cyanoacrylates) (PCA)		Toxic degradation products [65]	Fast bulk hydrolysis	Skin adhesives and glue, drug delivery [65]

polydioxanone (PDS), polyhydroxyalkanoates (PHAs) and polyethylene oxide (PEO), among others have been investigated[64], which can be processed in the same way as most ther-

moplasts. Most bioabsorbable polyesters undergo bulk erosion, but with some exceptions as listed in Table 5.2.

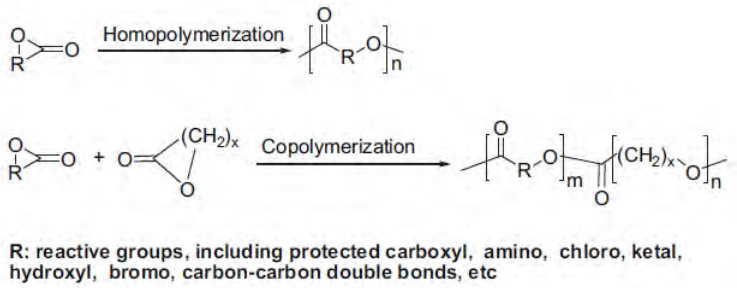

Figure 5.2: Polymerization af aliphatic polymers with reactive group (R). Modified from [72].

Among the polyesters, the most investigated are the aliphatic polyesters such as PLA, PCL, PGA and their co-polymers [65] and have been approved by the FDA for a broad range of medical applications. Research includes the following applications: bone, cartilage, cardiovascular, heart valves, small intestine tissue engineering, and arterial replacement [72]. Their chemical structures are shown in Figure 5.3.

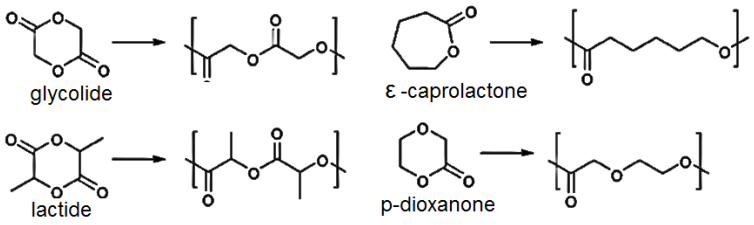

Figure 5.3: Structure of some common bioabsorbable polymers. Modified from [62]

Mechanical and thermal properties In general some α- hydroxy acids are high in crystallinity potential and brittle with a low elongation at break (ϵ_b). To compensate for this, one can produce block copolymers. The properties of such copolymers can be seen in Table 5.3. PGA and PLA and their copolymers have the high molecular weight are typically strong, stiff materials with high modulus and strength[62]. The polymers are sensitive to temperature and when used as a medical device. It has previously been seen that for PLLA the modulus and ultimate tensile stress (UTS) are significantly reduced (by ~ 60 % in modulus, ~ 35% in UTS) as the temperature reaches just above the T_g[77]. The T_g has an impact on how the polymer behaves at body temperature not only regarding mechanical properties but also

Table 5.3: Mechanical and thermal properties of the most common biodegradable thermoplasts and their degradation time

Polymer	T_g°C	T_m°C	X_c(%)	E (GPa)	UTS (MPa)	ϵ (%)	Deg. time (months)	Strength loss (months)
PGA	35-40[a]	200[b]	45-55[b]	~7[a]	70[a]	15 [c]	6-12 [a]	1-2
PLLA	60-65[a]	175[b]	~ 37[b]	2.8-4.2[a]	55-80[a]	2.1 [c]	24	6 [b]
PDLA	59[c]	-	amorph [c]	3.2 [c]	27-50[d]	8.7[c]	12-16[b]	1-2[b]
PDS	-10-0[b]	-	37-55[e]	1.5[b]	139 [d]	62[d]	6-12	1-2
PCL	-60[b]	55-60[b]		0.40[a]	20-35[a]	300[d]	24-36 [d]	-
PCLA 75/25	15-30[f]	130-150[f]		0.3-1.4[a]	~ 8[a]		(50%) 2	~24 [f]
PCLA 50/50	-17[f]	90-120 [f]		0.9[f]	~ 8[a]		(50%) 4-6	6-8 [f]
PCLA 20/80	amorph [b]			0.3-1.4[a]	~ 5[a]		16 [d]	-
PDLGA 50/50	45-50[a]	amorph[a]		1.4-2.8 [a]	45-50[a]	3-10[g]		1-2[a]
PDLGA 75/25	50-55[a]	amorph[a]		1.4-2.8[a]	40-55[a]	3-10		4-5[a]
PDLGA 85/15	50-55[a]	amorph[a]		1.4-2.8[a]	40-55[a]	3-10		5-6[a]
[a] [40], [b] [65], [c] [62], [d] [64], [e] [75], [f] [76], [g] [63]								

how the molecular chains move and position themselves over time. This is described later in section 6.5. PLLA is brittle and a good candidate for load bearing medical devices due to its high modulus and strength and also the slower strength loss over time (6 months) compared to PGA, a more hydrophilic polymer. PGA in general exhibit excellent mechanical properties for load bearing devices with a high modulus and strength, but its T_g is close to body temperature, which means it becomes softer upon implantation. Being a more hydrophilic polymer, it loses it strength more rapidly than PLLA. The polyether ester polydioxanone (PDS) has a lower modulus than the lactides and also loses its strength rapidly (1-2 months) and therefore not ideal for all applications. PCL has an even lower modulus but exhibits an extremely high ϵ_b. Poly(trimethylene carbonate) (PTMC) is an elastomeric polyester, which also exhibits high flexibility and can, therefore, be incorporated into the stiffer polymers to ensure greater elasticity[65].

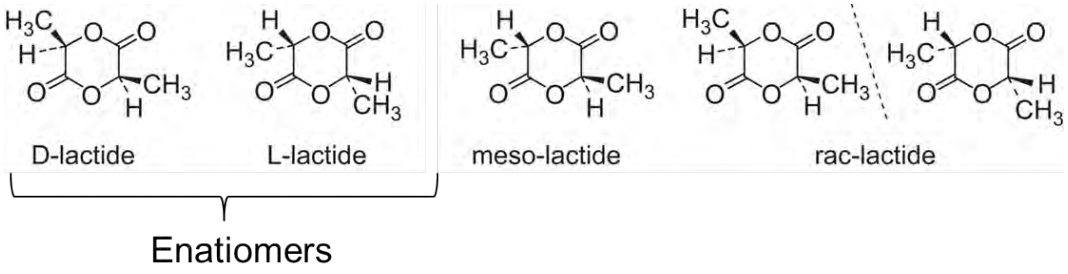

Figure 5.4: Different stereoisomeric configurations for lactic acid

Configuration Apart from the thermal properties of the polymer, the molecular configuration, and their orientation have an impact of the properties of the polymer[75]. An example is the lactic acid, which exists as two stereomers: the enantiomers L-lactide and D-lactide [78][79]. It can also exist as a mixture of the two, the D, L-lactide (meso-lactide). Either enantiomers are commercially available on their own or in form of a racemic mixture (rac-lactide), which consists of an equimolar mixture of D- and L-lactides [78] and portrayed in Figure 5.4.

PLA can exist in blocks of isotactic, syndiotactic and heterotactic and the formation depends on the configuration of the basis lactide molecule[79]. The different tacticities are portrayed in Figure C.1 in Appendix C.1. Ring-opening polymerization (ROP) or the less used condensation of D or L-lactides often leads to isotactic polymers (PLLA or PDLA), primarily consisting of isotactic diads with little meso-lactide. They are both crystalline with a high melting temperature (T_m=180°C)[78]. Syndiotactic diads occur during meso-lactide polymerization [62]. Meso-lactide has lower T_g and T_m due to the different stereotactic configuration [80] than the enantiomers. Poly(D,L-lactide) (PDLLA), when prepared from rac- and meso-lactides with an atactic sequence of D and L units is randomly placed along the chain and thereby becomes amorphous. When polymerized into sequences of both D- and L- lactide units regularly, the polymer becomes crystalline. Stereo-block copolymers (sb-PLA) consists of both isotactic PLLA and PDLA involving block a two-step copolymerization using ROP, which is not described further in detail here. At either end of the PLLA/PDLA ratio in a copolymer, the polymer exhibits lower crystallinity[78]. The methods are preferable because stereo complex crystals (regularly alternating D- and L-lactide packed side by side[81]) can be obtained with low amounts of the more expensive D-lactide.

As seen in Table 5.3 the properties between PLLA and PDLLA differ. Both PLLA and

PDLA are semi-crystalline polymers due to the enantiomeric purity of the monomers and the following stereoregularity. PDLLA is a random copolymer of D- and L-lactide and amorphous due to its irregular structure and therefore have different mechanical properties. It is most used in pharmaceutical applications[80]. It might be a reason that PLLA is much more investigated. PDLA and PLLA have the same thermal properties[80].

Degradation Hydrolytic cleavage of ester bonds occur randomly and attacks the amorphous phase first. It lowers the plastic flow, reduces ductility and toughness[64] and leaves the polymer more crystalline [75]. The polymer then becomes brittle. For PLLA, which is already considered a brittle polymer, this becomes an issue over the course of hydrolysis. The idea is to process a polymeric material, which is not too brittle at first. The PHA is also a class of aliphatic polyesters and covers over a large range of polymers. They give the possibility of creating favorable mechanical properties and degradation times, but they have not been as widely investigated. The information about their physical properties is limited as well as crystallinity, purity, blending composition and processing [64]. PCL is hydrophobic and degrades slowly [64] and therefore retains its strength for a longer period of time. However, its T_g is well below room temperature and behaves like an elastomer. It is very ductile compared to PLLA. When it is used in combination with PLLA in various amounts, the elongation is enhanced. PLLA is, in general, a slow degrading polymer. It swells significantly over time, whereas the pseudo-poly(amino acids) only take up water (5%) towards the end of the degradation stage and then a mass loss is seen. Thereby it is possible to keep the shape and device integrity longer in applications when needed[65]. Auto-catalytic degradation is a concern for some of the polymers such as PLLA, due their acidic degradation products, but not a concern for pseudo-poly(amino acids) such as tyrosine-derived carbonates. In general, the α-polyester are degraded by hydrolytic cleavage of the ester bonds in the polymer backbone. Both PLA and PCL can, however, undergo enzymatic degradation as well [75]. Through hydrolysis, PLA and PGA will be broken down into lactic acid and glycolic acid, respectively. Subsequently, they will be broken down into pyruvic acid and through a metabolic cycle are eliminated as carbon dioxide and water. PCL will turn into hydrohexanoic acid, which is a metabolite [75]. As listed in the Table 5.2, many of the polymers undergo hydrolysis of the bulk, which is only dependent on the water uptake. Such uncontrolled bulk degradation is undesirable for drug delivery [73]. One of the few surface degradation polymers not listed in the table is poly(trimethylene carbonate) (PTMC). It has

relatively poor mechanical performance and even when present as co-polymer is has a low stiffness and degrades within 3-4 months. A drawback is that in vivo degradation is much faster than in vitro degradation most likely due to the enzymatic degradation in vivo[65]. For the hydrolytically degradable polymers, the rate in vivo and in-vitro are much the same and dependent on water absorption.

Co-polymers and blends The configuration of which the polymer is shaped into the device plays a role in the mechanical performance. For example orientation of PGA, fibers increase the stiffness and strength. When used as fibers in a braided suture, they can lose up to 50% of their strength after two weeks, while 100% absorption occurs after 4-6 months[75][63]. Usually, PGA is used in combination with PLLA to increase the degradation rate of PGA[64]. Additionally mixing PGA and PLLA will decrease the melting temperature and reduce the mechanical properties with the amount of L-lactide as seen in Table 5.3 compared to pure PGA. Through copolymerization of glycolide with lactide the T_g can be increased above body temperature (T_g=54°C) compared to pure PGA and therefore more suitable for long-term implantation. PGA can exhibit a high degree of crystallinity (X_c) (40-55%). However, when copolymerized with L-lactide in the ratio of 25/75, it becomes amorphous[62].

Copolymers from ϵ-caprolactone and D, L-lactide yields materials with faster degradation rate. When ϵ-caprolactone is copolymerized with glycolide, the stiffness is reduced compared to pure PDLA.

The degradation rate is higher for PDLA, and the modulus and strength are less than for PLLA. A 50/50 PDLLA has proven to be more resistant to hydrolysis than both pure PLLA and PDLA [82]. PDLLA is amorphous due to the random distribution of L- and D-Lactide units and shows a faster degradation than its crystalline counter units[82]. PLA with 90% or more L-lactide will be crystalline, but when below the PLA tends to be amorphous[82]. PLLA is semi-crystalline and can be quenched into its amorphous state upon processing. As far as crystallinity goes, it consists of both crystalline and amorphous domains with tie-molecules within both domains. Blending L-lactide with D-lactide influences the mechanical properties as well as the thermal properties [83]. In general blending D-lactide will reduce T_g from 58 to 53°C, but increase T_{cc} from 110 to 130°C up to 60% D-lactide. D-lactide of ≥80% will result in an amorphous polymer. The stiffness and strength values decrease with increasing amount of D-lactide. The flexibility or the ϵ_b also decrease with D-lactide content, but only up to a ratio of 50/50 after which the elongation increase [62][83]. Incorporation

of rac-lactide into a dilactide will reduce the crystallinity potential and with just 25% dilactide become amorphous. Co-polymerization between lactide and glycolide, does not make a linear relationship between the copolymers' properties. For example a 50/50 copolymer of D, L-lactide and glycolide degrade faster than either homopolymer (see Table 5.3). The composition can also lead to amorphous polymers due to disruption in the regularity of the polymer backbone[63].

5.1.4 Selection

As stated in requirement (see section 3.3.4), a adequate radial force of filter is needed, and it must withhold its strength until sufficient tissue coverage has occurred. The polymer should be flexible to a degree where permanent deformation is avoided, while still have enough radial force. Significant molecular weight degradation must not occur within the first three months. These requirements might be difficult to meet with the polymers as they are. There is room for improvement. To sum up the above findings, PCL is too soft. PDS, PDLA, and PGA lose their strength too quickly (1-2 months). PGA clearly shows the highest stiffness of the three, but as mentioned previously it has a T_g close to body temperature, and it degrades fast. However, the elongation appears more suitable than PLLA. The copolymer PLGA could be a suitable compromise. PLGA 50/50 raises the T_g, but strength loss still occurs still after 1-2 months. 75/25 PLGA has an even higher T_g and the strength is preserved up to 5 months and is a possible combination. The stiffness is at the lower end of what it would be for PLLA and using PGA as the reinforcement element in the copolymer does not work as intended.

There are several ways to reinforce or manipulate the mechanical properties of polymers. As mentioned the properties of the bioabsorbable polymers could be tailored by copolymerization or blending polymers. Blending polymers does not necessarily have a chemical bond between them (e.g. be miscible or immiscible respectively) and is obtained by mixing the blends. Copolymers have a chemical bond between them and is produced by copolymerization of two or more monomers[84]. Improving the mechanical properties can be done through processing as well. An example is applying a strain to the polymer during processing with the attempt to orient the material and optimize the mechanical properties. Monofilament of different blends and processing were characterized in the following section 5.2.

There are different approaches on how to create a stent-base for a bioabsorbable filter. One possibility is to create the stent-base from monofilament as described in the following section 5.2.

5.2 Results and analysis: Bioabsorbable monofilaments and their properties

The previous section of this chapter highlighted the background on some of the most common polymeric candidates for a bioabsorbable filter. Some polymers are more easily available than others, and some are medical while others are industrial grade. Based on the literature described, some of the most common polyesters were evaluated for further selection of the best bioabsorbable candidate. Mechanical characterization (both tensile and radial force testing) was done on several monofilaments internally at Cook Research Inc., and the raw data was provided to this project.

From a processing perspective testing monofilament for material characterization and selection is favorable as it is readily available in many compositions and sizes and can be braided into simple stents. Monofilaments can be positioned in a braided configuration in a way that the strength of the filament is in the radial direction and for the optimal radial force. Monofilaments of different polymers were purchased from Corbian (previous Purac) under the name Purasorb as a medical grade and the medical grade Absorb from Zeus. All filaments were tested by S. Tanner at Cook Research Inc., and raw data was provided for analysis in this project. The comparison between polymers was used to choose the best possible material candidate for bioabsorbable vascular devices. Based on the literature PLLA and PDLA have the appropriate degradation profile and retain strength over time, but does not have the highest modulus or strength. To optimize these properties, the monofilament were oriented in the extrusion detection and compared with the plain extruded filament. PLLA monofilaments were tested alone as well as in a 50:50 blend with PDLA (PDLA-PLLA). As previously mentioned PGA alone has a low T_g and looses its strength too fast. For that reason, it was tested in combination with PLLA as a random copolymer (PLGA 85:15) and oriented. It was also assumed that the incorporating PGA would increase the ϵ_b compared to pure PLLA. Information of each polymer is listed in Appendix C.2, Figure C.1. For improvement of ϵ_b, PLLA was also tested in combination with PLLA-PCL (70:30) (PLLA-PCL) as a blockly copolymer. For optimal radial force, stiffness and strength were supposedly

optimized by an elongation of the monofilament during extrusion and tested up against the non-elongated. Elongation of the polymer can have the same effect as straining of a polymer and improve its mechanical properties in the straining direction. Orientation or elongation of the polymer can be thought of as fibrous orientation. The monofilament is processed under high axial deformation, leading to the orientation of crystals in the deformation direction and thereby improved stiffness and strength[85].

To evaluate the different types of material and their mechanical behavior small scale stents were braided with a diameter of 8 mm and 40 mm in length from various types of monofilaments (OD 2.5 mm) (Figure 5.5(a)). Tensile testing of the monofilament on its own and the radial force of the whole stent was measured as the stent was crimped.

(a)

(b)

Figure 5.5: Braided stent (OD 8 mm, length 40 mm) of 2.5 mm PLLA 5.5(a) and PLLA-PCL 5.5(b) monofilament after radial force testing *Image provided by Shaun Tanner (Cook Research Inc.)*

It is expected that PLLA would have a larger modulus than extruded PDLA-PLLA, but there is no significant difference between their stiffnesses as seen in Figure 5.6(a). The orientation of the monofilament does not induce an increase in stiffness at it has almost the same stiffness as the extruded PLLA. The elastic modulus is not significantly different for PLLA whether extruded or oriented and the same goes for PDLA-PLLA. However, there is a difference in radial force as seen in Figure 5.6(d). It is, a bit unexpected that the radial force of the corresponding stents differs.

As expected from Table 5.3 from the literature the experimental data are seen in Figure 5.6(a) show that PGA becomes sensitive to the amount of L-lactide as the modulus is reduced from normally 6.0-7.0 GPa as stated by the manufacturer to less than 2 GPa, and exhibits the longest ϵ_b, despite its large variation. Another noticeable polymer is the block-copolymer PLLA-PCL (85/15), which has significantly larger elastic modulus than both elon-

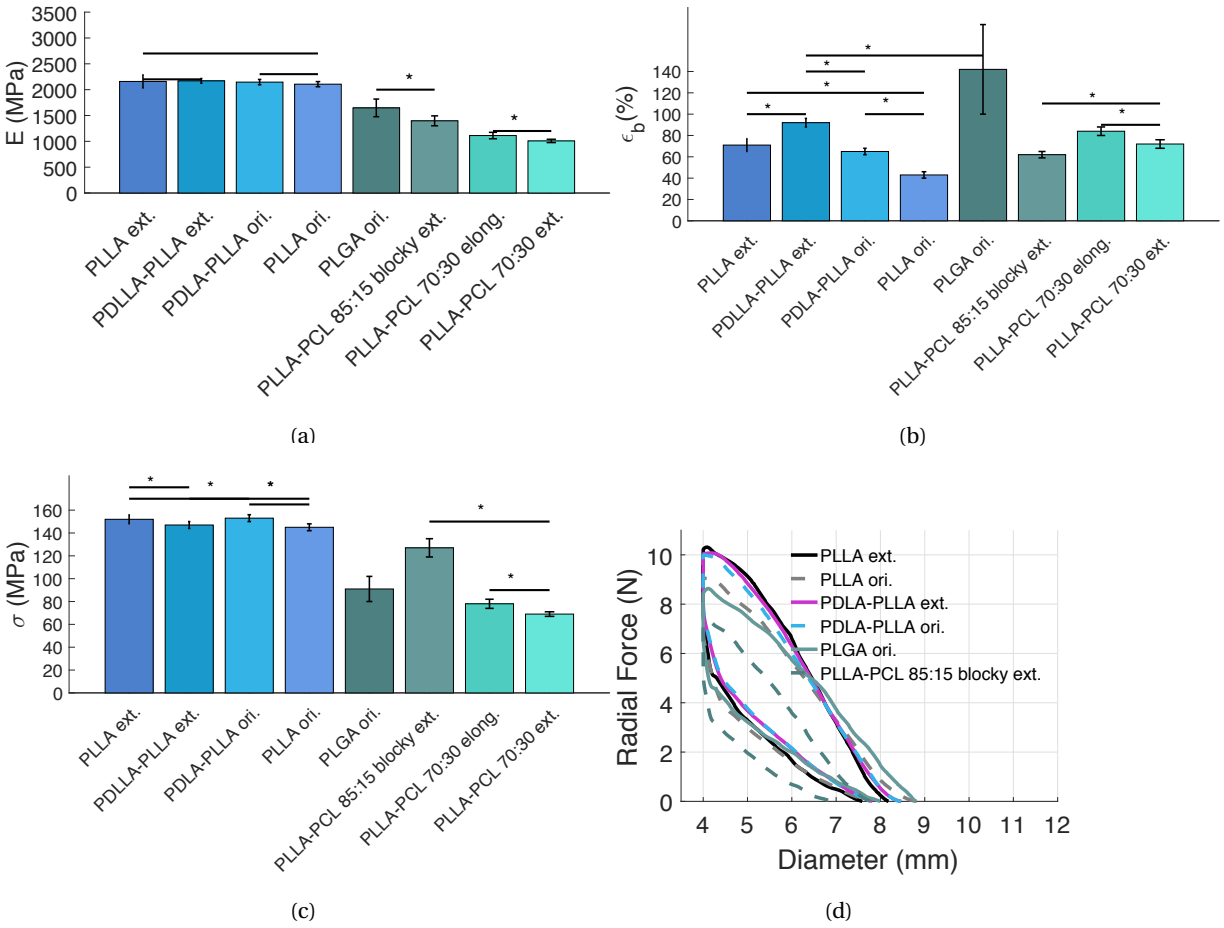

Figure 5.6: Elastic modulus (5.6(a)), ϵ_b (5.6(b)) and σ_y (5.6(c))of materials used for braided stents obtained by tensile testing. Materials are ordered according to the radial force ranking. Radial force of the second cycle (crimped down to 40% of initial OD) on braided stents is shown in 5.6(d). *Experimental data supplied by Shaun Tanner (Cook Research Incorporated)*

gated and extruded copolymer is PLLA-PCL (70/30), due to the higher content of PLLA. The addition of 30% PLLA-PCL to PLLA does not induce a longer ϵ_b, yet only reduces the stiffness and strength. It is therefore hypothesized that a bioabsorbable filter would not benefit from using 70/30 co-polymer. The ϵ_b is higher than expected for all polymers, possibly due to their processing into monofilaments (see Figure 5.6(b)). However, it was not anticipated that PLGA would have an ϵ_b much higher than any of the copolymers containing PLLA-PCL, which has a far superior ϵ_b to any of the other polymers. It is possible that there are micro cracks in the PLLA-PCL, which occurred during processing and ϵ_b is less. This was not

evaluated further.

The stents underwent crimping for two cycles during radial force testing. The first cycle is portrayed in Appendix D.1 Figure D.1 was done to simulate the size of the sheath, which it would be loading into during placement. During the second cycle, the stent is crimped down to the target vessel size. During the second cycle, all braided stents lost a significant amount of radial force. The PLLA-PCL 85:15 blocky showed the greatest difference between the two cycles and a lower radial force and the polymer with the least loss in radial force. It is more susceptible to permanent deformation as seen in Figure 5.7(a) with the largest change in diameter after crimping.

Figure 5.6(d) and 5.6(a) show that there is some correlation between elastic modulus of the monofilament and the radial force of the braided stent. Crimping the stent changed the diameter for all stents (Figure 5.7(a)). PLLA-PCL (70/30) was damaged during crimping or did not crimp evenly and was not included in Figure 5.6(d). Instead, a different composition of PLLA-PCL (85/15) was tried, which showed the highest change in diameter after crimping (Figure 5.7(a)). PLLA as extruded showed little change in diameter as well, but the results were unreliable due to a significant variation. Oriented PLGA showed the least change in diameter as well as the least change in length 5.7(b).

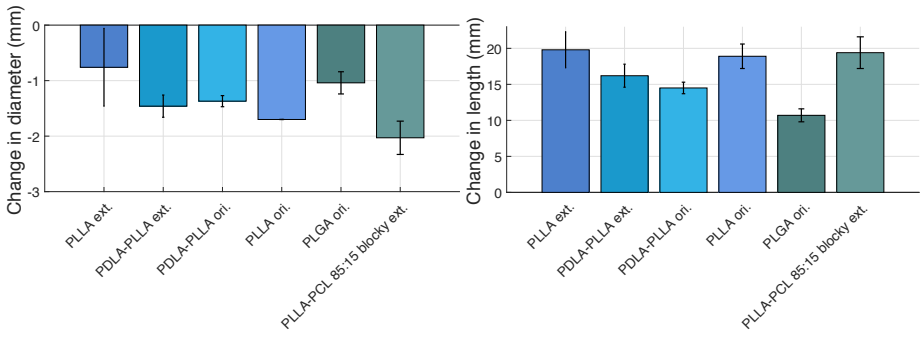

(a) (b)

Figure 5.7: Change in diameter (5.7(a)) and length (5.7(b)) of braided stents (OD 8 mm and length 40 mm) made from different 2.8 mm diameter monofilaments crimping. *Experimental data supplied by Shaun Tanner (Cook Research Inc.)*

From the above study, it was seen that oriented PLLA did not show as promising a radial force as expected, and for that reason, an additional oriented PLLA provided by Zeus was purchased and compared with an extruded non-oriented monofilament. The thermal properties, T_g and T_m, were the same despite (Table 5.4) the orientation of the material and

in accordance with the literature (Table 5.3). How the orientation was obtained is unknown, but WAXS analysis showed a high crystal orientation of 0.8 and DSC showed a crystallinity of 61 %, which is at the top end of reachable crystallinity for PLLA. The non-oriented monofilament had 13% crystallinity (Table 5.4). Automatically the higher crystallinity means that the oriented monofilament has superior stiffness and strength, solely due to the large crystallinity as well as a high degree of crystal orientation. The rationale of crystal orientation and the mechanical properties are described later in section 6.1.4.

The oriented PLLA from Zeus does not have the same mechanical properties (Table 5.5) as oriented PLLA from Corbion. Their orientation process and crystallinity possibly differ along with differences in molecular weight (M_w) distribution. Despite the low X_c of non-oriented PLLA monofilament, the ϵ_b is very poor and it does not undergo strain-hardening above yield stress (σ_y), thus σ_y and UTS becomes the same (see Figure D.2(a) in Appendix D.2). As expected the stiffness and strength of oriented PLLA monofilament from Zeus far exceeds the ones of the non-oriented PLLA from the same supplier.

Table 5.4: Thermal properties of extruded and oriented PLLA monofilament from Zeus

	T_g (°C)	T_m (°C)	X_c%	F_2	D_{ax}	D_{circ}
Monofilament	64	182	13	-	-	-
Monofilament oriented	65	183	63	0.8	90	139
Monofilament oriented annealed 80°15min	-	-	-	0.8	65	145

From Table 5.5 it is seen that the orientation, which improves the stiffness and strength, is lost during annealing even at low temperature (70°C). The stiffness and strength decreased as a function of annealing temperature. An interesting point is that annealing at 80°C for 15 min, induces a higher stiffness and strength, which are not significantly different from when not annealed. Annealing, in general, induces the material with a longer ϵ_b, which means that the molecular chains might have been relaxed upon heating or microcracks have disappeared during heating. Increasing the annealing temperature to above T_{cc} does not change the stiffness or strength, indicating that crystal was not formed at such short annealing times. Annealing the oriented monofilament from Zeus for just 15 min at 80°C does not change the crystal orientation from 0.8. The crystal size differs, and the crystal become narrower and longer as seen in Table 5.4. Stress-strain curves can be found in Appendix D.2

in Figure D.2(b). The fact that the mechanical properties decrease with further annealing is a downside as the monofilament needs to be heat treated after braided into a stent to keep its shape.

Table 5.5: Mechanical properties of extruded and oriented PLLA monofilament from Zeus

	E (MPa)	UTS (MPa)	σ_y (MPa)	ϵ_f (%)
Monofilament	2635±245	80±0	80±0	5±1
Monofilament oriented	5972±124	374±29	134±12	31±2
Monofilament oriented annealed 70°1min	5117±215	353±23	127±4	33±4
Monofilament oriented annealed 80°1min	4856±159	357±31	120±4	33±3
Monofilament oriented annealed 80°15min	5713±154	350±33	128±2	34±1
Monofilament oriented annealed 90°1min	4670±198	338±24	113±2	36±2
Monofilament oriented annealed 110°1min	4535±342	339±17	111±3	36±2

The conclusion made from the above literature review on materials and the initial mechanical testing of monofilaments, whether braided or not, shows that the ideal material for bioabsorbable filters, does not exist, and the choice of material lies in the best compromised between properties. As the risk of migration is a major concern, a high radial force was chosen over the flexibility of the stent-base. Copolymers of PLLA and PLLA-PCL were not used for further investigation. It was determined that PLGA shows the best recoverability after crimping, but as it did not show as a high radial force as PDLLA or PLLA and it was not chosen. PLLA was selected over PDLLA, due to it slower degradation rate and thereby also greater strength retention during implantation. Further experimentation is related to improving the properties of PLLA.

6

Biaxial straining of Poly(L-lactide) tubes

This chapter describes the nature of the raw material used in extruded tubes for later expansion into larger tubing for IVC filter prototypes. It describes the background on thermal properties, crystallization and mechanical properties of the PLLA and the investigation of processing parameters such as strain processing temperature (T_p) and processing strain rate ($\dot{\epsilon_p}$) performed in this project. It also includes the results and findings of the mechanical behavior and thermal properties as a result of strain-inducing PLLA tubing. Furthermore, an investigation was done to evaluate the influence of further processing such as thermal treatment for permanent set into a stent-base configuration and the effect of sterilization. Some observations were performed retrospectively in search for an explanation to the results of the in vivo study. For comparison between the biaxial straining process and other processed tubes, Zeus supplied an oriented and non-orientated PLLA tube. The mechanical and thermal properties are shown in Table in D.1 and Table D.2 in Appendix D.2, respectively, but not discussed further.

6.1 Background on crystallization, thermal properties and strain-inducing of PLLA

PLLA can exhibit 3 different crystal structures, α, β or γ. The two former can easily be obtained at moderate processing conditions (reasonable temperatures and stress). Hot-drawing melt-spun or solution-spun PLLA fibers to a high draw ratio lead to the β-crystal

form with the lattice dimension of its orthorhombic unit cell a=1.031 nm, b=1.821 nm, and c=0.900 nm and a chain conformation with left-handed 3_1 helices. The α-crystal form grows from a melt or cold crystallization at high temperatures[86]. The lattice dimension of its orthorhombic unit cell is as followed, a = 1.066 nm, b = 0.616 nm, c = 2.888 with a left-handed 10_3 helix chain configuration [80]. Additionally, a disordered form, α', with the same space group and lattice dimensions as α-crystals has been detected [87][88][86], which appears at low temperatures, and is characterized by slightly larger lattice dimensions and more disordered. Heating crystalline PLLA containing the α'-form, can alter them into α-form and is seen by the possible appearances of multiple endotherm and exotherm peaks during DSC scans.

6.1.1 Background: Crystal structure of PLLA

When examining strain-induced crystalline samples that contain α or α' with WAXS, the diffraction patterns are very similar. There is a slight difference in position of the diffraction peaks for the α- and α'-crystals. The peaks for the α-crystals appear at (010), (110/200), (203), (204), (015), and (207) planes and their corresponding Bragg angles 2θ=15°, 16.7°, 19.1°, 21°, 22.3° and 27.4°. The α'-crystals shows peaks at (110/200), (018), (203), and (206) planes at their corresponding Bragg angles 2θ=16.4°, 18.7° and 24.5° and 33.1° [88] .

Crystallization at T≥ 145°C only forms the α-crystal. At T≤95 °C only the α'-crystals form. At temperatures in between, 105°C ≤ T_c ≤125°C the two forms co-exists[86]. As the highest T_p was 93°C in this project only α'-crystals are expected to form in the strained tubes. It is said that formation of α'-crystals will ultimately with its disorder and loose chain packaging leads to a lower stiffness and strength[89].

6.1.2 Background: Crystallization

Crystallization can occur after or simultaneous with polymerization[90]. High regularity in the chains are capable of crystallizing, but the conditions must be favorable[85]. In short, the concept of nucleation is related to thermodynamics, where the onset of crystallization occurs when there is a change in thermodynamic (cooling from the melt). The cooled melt fluctuations can overcome Gibb's free energy barrier, and nucleation can take place and transformation to the crystalline domain begins[90]. Crystallization is a process in which

a material is either a heated from an amorphous solid or a cooled liquid amorphous structure to convert into an organized solid crystalline structure[90]. The former has a cold crystallization temperature, T_{cc}, and the latter has a crystallization temperature when cooling from melt T_c. A third possibility is the strain-induced crystallization, which has a crystallization temperature interval as later described in section 6.1.4. Annealed at a given temperature, depending on the thermal properties of the material, is named isothermal crystallization and depends on the thermal history of the material, annealing temperature and time. Quenching of the extruded tube induces crystallinity with thin crystals, but with many defects. If the cooling rate is slower, the crystals are thicker and the dislocations fewer. Usually, cavitation occurs at slower cooling. Isothermal crystallization with slow cooling induces higher crystallinity and thicker crystals, fewer tie molecules in the amorphous domain and a greater degree of cavitations[91].

6.1.3 Background: Thermal properties

The theoretical heat of fusion enthalpy for a 100% crystalline for crystals of infinite size are most commonly reported as ΔH^0_m=93-94J/g[45][80]. The X_c is calculated from the difference in enthalpy for the crystalline (ΔH_c) and the melting (ΔH_m) peaks over the reference melting enthalpy for PLLA (see equation4.1 in section 4) in a DSC experiment.

Typical DSC scans for PLLA and PDLLA are seen in Figure 6.1. The amorphous PDLLA and PLLA quenched into an amorphous state does not have the same enthalpies. As noted previously, their T_g are the same. PLLA is initially amorphous and as temperature rising during a DSC scan with the heat rate of 10°C/min, shows a crystallization peak at T_c=132°C starting at 100°C and a melting peak T_m=182°C (Figure 6.1(a)). The ΔH_c=38J/g and ΔH_m=38J/g and therefore X_c=0%. Amorphous PDLLA can show an aging peak between 65-90°C of up 10 J/g if aged. The longer the aging time or, the closer the aging temperature is to T_g, the more intense the peak is[80]. The phenomenon is described later in section 6.5. PLLA, which has been processed into crystallinity, has a different DSC scan than the amorphous and is portrayed in Figure 6.1(b). Upon the first heat cycle to above T_m, no new crystals are formed, and no crystallization peak occurs. At a second heat cycle, the thermal memory is erased, and the DSC scan resembles the amorphous[80].

All thermal components, T_g,T_{cc},T_m, and their respective enthalpies vary and depend on the M_w of the material. The X_c depends on the on M_w as well and increases with it. Highest X_c reported in [80] was 71% for PLLA, but this is not commonly seen elsewhere in

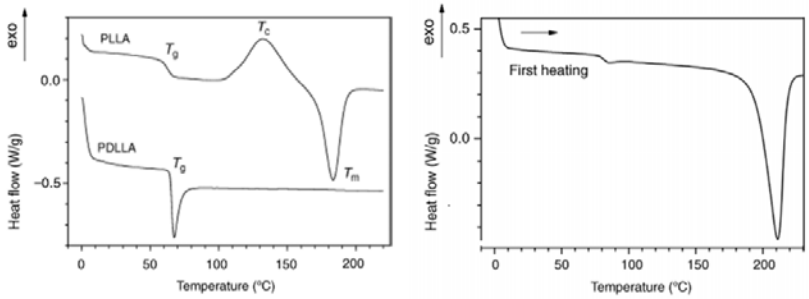

(a) (b)

Figure 6.1: Differential scanning calorimetry scans of amorphous PLLA and PDLLA (6.1(a)) and for crystalline PLLA (6.1(b)) (heating rate 10°C/min). Used from [80].

the literature. When the crystallinity is high for a material the T_g will be higher, because the crystalline domains hinder mobility of the amorphous chains. The X_c increase with annealing time, but also with increasing temperature. A higher annealing temperature will provide a greater mobility and thereby a greater ability to crystallize[80].

6.1.4 Background: Strained semi-crystalline polymers

Semi-crystalline polymers such as PLLA can undergo strain-induced crystallization (SIC), when in a rubbery state between T_g and T_{cc}. Normally slow crystallizing polymers, such as PLLA, are quenched into its glassy state below T_g and subsequently heated into its rubbery state, where the SIC will take place under applied strain. This processing technique has previously been used in the industry, when processing films and can be applied to other polymers such as polyethylene terephthalate (PET), polyethylene naphthalate (PEN), and polyether ether ketone (PEEK). The SIC of films, both include simultaneous and sequential biaxial strain. Ou and Cakmak have described in detail the phenomenon of both simultaneous and sequential biaxial straining of PLLA films and the presence of a bimodal orientation texture upon transverse stretching [92][93].

Selection of straining temperatures highly depends on the thermal properties. To induce crystallinity by straining, the temperature must be above T_g and below T_{cc}[92].

The tube expansion used in this project is similar to film blowing. The material is extruded through an annular die forming a tube. The molten polymer tube is further filled with air and expanded to the desired diameter. This process resembles the simultaneous

and sequential biaxial strain process used for tube expansion in this project. The small tube (OD 3.4 mm) was first extruded and then cooled into an amorphous state, after which it was placed in the tube mold and heated into the rubbery state, and air was injected as described in section 6.2.1.

There are certain restrictions for film blowing of PLLA. It is not desired to have more than 15 wt% meso-lactide and the rest should be L-lactide[94]. Strain-inducing semi-crystalline polymers promote structural changes, which involves both the amorphous and the crystalline domain of the polymer. The mechanical properties are said to primarily depend on the crystalline domain[88]. To optimize the mechanical properties of the tube circumferentially as opposed to axially different pathway of processing were investigated.

6.1.5 Background: The mechanical properties of crystalline PLLA

Crystallinity has an impact on how the polymer performs mechanically. The force in which the molecules are held into the crystalline lattice restricts the mobility of the polymer chains. Both the X_c and the crystal sizes influences the mechanical properties. Both the E, σ_y, and impact strength increases with crystallinity. The UTS is more complex, as in some cases it increases with crystallinity, but in others the UTS decrease as a result of stress-concentration and brittle failure. The ϵ_b decreases with crystallinity as a result of limited mobility. Amorphous PLLA (grade 4060, ~10% D-isomer) from NatureWorks has an E of 2.5 GPa, tensile strength (TS) of 44 MPa and ϵ_b of 7%, where the semi-crystalline PLLA (grade 4032, ~1.5% D-isomer) has E of 2.6 GPa, UTS of 54 MPa and ϵ_b of 9%. One thing should be noted that most commercial PLA is copolymerized L-Lactide with small amounts of meso-lactide, to lower crystallinity and ultimately brittleness. Increasing the M_w reduces the variation in properties. For PDLLA increasing the M_w will increase σ_y, E, UTS and flexural modulus, but the ϵ_b diminishes. [95]. Despite PLLA having a T_g above body temperature, it does not mean that the mechanical properties remain unaffected during implantation. When storing quenched amorphous PLLA at body temperature, the flexural strength is reduced by 23%, ϵ_b by 4% and elastic modulus by 5%. The reduction is more dramatic for a crystalline PLLA (X_c=52%), where the flexural strength was reduced by 27%, ϵ_b by 10% and E by 13%, ultimately ending up with similar properties. Heating further near T_g, which is not relevant for implant use, the amorphous PDLLA is down to 0.4% of it initial flexural strength, 1% of the E and increase in ϵ_b by nearly 200%. The flexural strength and E for the crystalline PLLA are down to 24% and 22%, respectively and the ϵ_b increased 156%[95]. Crystalline PLLA is

less influenced by the body temperature, and this should be taken into account during in vitro testing of the material or device. Furthermore, it proves that processing, annealing, orientation and crystal nucleation is useful for the final properties of the device.

Strain-induced crystallinity The mechanical properties of PLA can be improved by straining and orientation. In principle when the polymer chains are stretched, the chains are no longer is their most probable conformation, which leads to a decrease in conformational entropy. The tendency to crystallize is greatly enhanced, hence less conformational entropy is needed to transform from amorph to the crystalline state[85]. In strain-induced PLLA, crystallization and subsequent melting temperatures are moved to higher temperatures during a DSC scan, meaning that a strain-induced polymer can not as easily be crystallized. At the same time, the deformation increases the crystallization rate greatly. Without the presence of deformation, the crystalline texture is obtained by merely cooling, which results in a random distribution of crystals next to each other. Also, the strain-induced crystalline chains are oriented parallel to the stretching direction, and the extent of orientation depends on the degree of strain, temperature, and rate. The strain-induced oriented crystallites have a higher modulus than the amorphous chains. Additionally, the crystallites act as physical cross-links and gives the polymer as a whole an increased modulus. At a larger degree of strain, the amorphous chains are aligned and oriented [85]. There are three conditions which must be met to obtain strain-induce crystallinity in semi-crystalline polymers. For one the temperature must be above T_g and below T_{cc} to ensure chain mobility. Secondly, the strain rate must be adequate and thirdly the degree of strain must be sufficient to achieve adequate alignment of the chains to form crystals[92]. During SIC the molecular chains are oriented along the stretching direction, and when a certain level of orientation is achieved, the formation of highly oriented crystals occurs. The polymer chains are randomly bundled and amorphous as seen in Figure 6.2a. Upon strain they remain in the amorphous structure but become more ordered (Figure 6.2b) until a certain degree of strain is achieved, before becoming more ordered and crystalline (Figure 6.2c). With further extension both the crystalline and the amorphous domain are further aligned as seen in Figure 6.2[92].

During simultaneous biaxial strain, the axial and transverse strain occur simultaneously and orients the polymer chains in the plane of which they are stretched, creating in-plan isotropy. The crystalline orientation is not very high as some of the chains are randomly oriented and tend not to crystallize because they are unable to find chains in their orientation

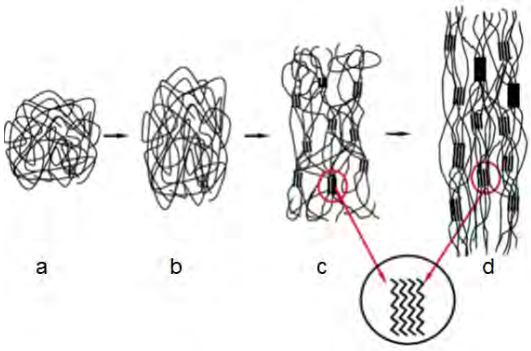

Figure 6.2: Structural mode during axial stretching. Modified from [92]

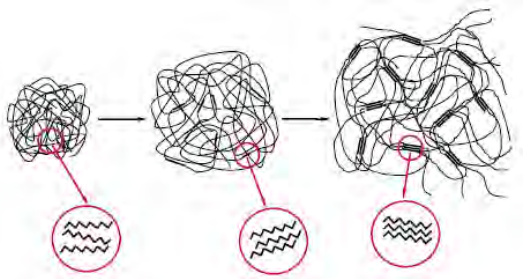

Figure 6.3: Structural mode during simultaneous biaxial stretching. Modified from [92]

to crystallize with. This is especially an issue if they are formed at low strains, but crystallization increases with increased deformation (Figure 6.3). Applied transverse stretching to crystals formed in the axial stretched material with a weak crystalline domain, reduces orientation in the axial direction as seen for the sequential biaxial strain, (Figure 6.4). High degree of transverse stretching would lead to crystallite destruction formed during axial strain, while new crystals are formed in the transverse direction, resulting in a bimodal texture, with a better structural order than seen in the axial direction.

A similar structure is seen initially when applying transverse stretch to an axially stretched material with a strong crystalline domain. As the transverse stretch continues, the strain transmits forces deep into the polymer using the pre-existing axial crystals and physical cross-linking points and axial orientation is destroyed. A new poorly orientation crystal domain occurs in the transverse direction (Figure 6.5)[92].

In general semi-crystalline polymers are comprised of a complicated structure, both the crystalline lamella domain and the amorphous domain and formation of spherulite structure. Upon deformation both in tension and compression, the spherulitic structure is transformed into a fibrillar structure. When applying a force, the material first undergoes elastic deformation, which quickly changes as yield point is reached into the permanent plastic deformation if further force is applied. Plastic deformation first occurs in the softer amorphous domain and later the stiffer crystalline domain. As for the crystalline structure, deformation furthermore occurs, without the polymer fracturing. This state is known as twinning or chain slip, which occurs only in the crystalline plane and in two ways. One is a continuous deformation of the lamellar structure, and the other is sectioning into crystalline blocks.

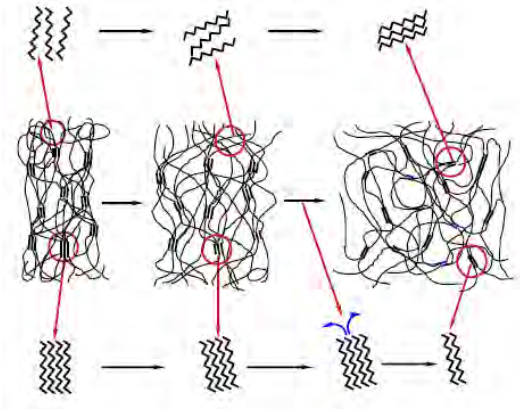

Figure 6.4: Structural mode during sequential biaxial stretching with a weak crystalline domain after axial strain. Modified from [92]

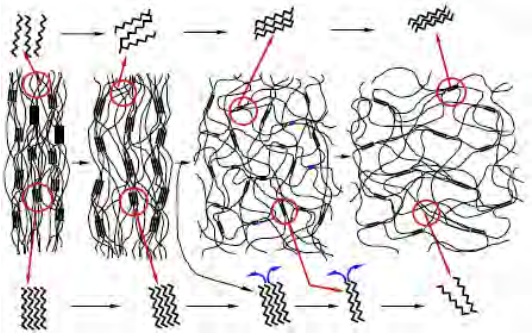

Figure 6.5: Structural mode during sequential biaxial stretching with a strong crystalline domain after axial strain. Modified from [92]

The chain slip will most likely occur in the places of screw dislocation among the crystals under the influence of a shear force. With a further degree of deformation, new dislocations form from which the crystal chains can slip. As opposed to compression disentanglement of the amorphous chains can happen during tensile deformation[91]. It is possible that this phenomenon is seen during expansion and straining of tubes. On a macroscopic level localized deformation will occur at the site with the smallest cross-sectional area, from which necking propagates. When the deformations paths as described above are exhausted the polymer will undergo strain-hardening, until the final break. It should be noted that crystallization induces the material with embrittlement, and the material has a reduced fracture toughness.

Deformation of crystals Any fracture of the expanded tubes can be related to the processing and possible formation of crazes and cavitations before or after processing. Plastic deformation is easily obtained in the amorphous polymer under T_g, which can either contribute to microscopic shear processes within the material or create crazes and depend on strain rate and temperature. The crazes consist of elongated voids with oriented microfibrils. Their presence will allow the crazes to transfer shear stresses adding to the total deformation. For semi-crystalline polymers, this phenomenon can also occur at higher temperatures than T_g[91]. The PLLA can fracture from crazes. They increase in size with the degree of deformation and are elongated in the direction of deformation. The deformation

is understood as a combined mechanism of cavitation and fibrillated shear. Upon deformation, polymeric chains are extended, and the craze spans. The crazing results in the polymer being brittle in tensile and impact testing. The crack propagation is also different when annealed or quenched. For the annealed PLLA, the craze propagation is through spherulites and along the spherulite boundaries with few or no crazes formed from the main crack, whereas the quenched sample show various crazes in at vicinity of the crack tip. [95]. Once crystallized the E, tensile and flexural strength and impact resistance increase and the ϵ_b is reduced. This is however only true up to 65% deformation, afterward, material embrittlement is an issue[95]. The greater the crystallinity of the polymer after processing, the more ordered and tightly bound a structure resides, where slippage between adjacent polymer chains is limited. The tightly bound structure leads to superior mechanical properties [75]. The resistance to slippage is time dependent under constant load, due to the viscoelastic behavior[96]. However, the greater the crystallinity, the less ductile the polymer would behave. In an application where is it exposed to multiple compression cycles it is important that polymer still exhibits some flexibility. Therefore the crystallinity must be controlled to reasonable levels to ensure great strength and stiffness while allowing some slippage between polymer chains.

6.2 Results and analysis: Biaxially strained PLLA

As previously seen the radial force of a stent is somewhat related to the stiffness of the material of which it is made, if the orientation is placed in the circumferential direction (section 5.2). The idea was to orient the material circumferentially by straining the material and create a high radial force to avoid migration during implantation. For this biaxial strain was applied to a hollow extruded PLLA tubing (an expansion process), from which the stent-base would be laser cut. Below are the investigations of strain degree and strain temperatures during processing. The investigation was performed on non-medical PLLA tubing, unlike the investigation of monofilament is section 5.2. The reasoning why is described in section 6.2.3.

6.2.1 Raw material for tube extrusion

PLLA 2003D pellets were purchased from NatureWorks LLC (Minnetonka, MN, USA) (~4.1 % D-isomer; molecular weight (M_w), 1.85kg/mol), heated to 194°C and extruded into tubes

with outer diameters and inner diameters (ID) as listed in Table 6.1 or into 10.5 mm tubes, with 0.2 mm wall thickness. After extrusion, the tubes were quenched well below T_g in a cooling medium at 15.5°C/s for 14.5 s, leaving the tube with a low crystallinity (~1%), as determined by DSC. Figure 6.6 show the different extruded tubes used in this study. The wall thickness of the raw material proved to be nonsignificant as seen in Figure 6.7(a).

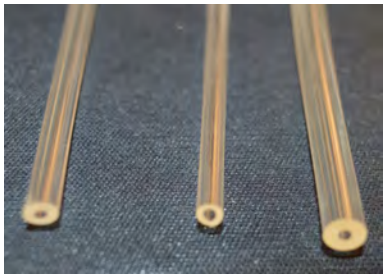

Figure 6.6: Extruded tubes with the outer diameters 13.2Fr, 10.2Fr and 16.5Fr

Table 6.1: Extruded tubes size available in this study and their outer and inner diameter

French size	OD (mm)	ID (mm)
10.2 Fr	3.4	1.7
11.7 Fr	3.9	1.7
13.2 Fr	4.4	1.7
16.5 Fr	5.5	1.7
30Fr	10.5	9.2

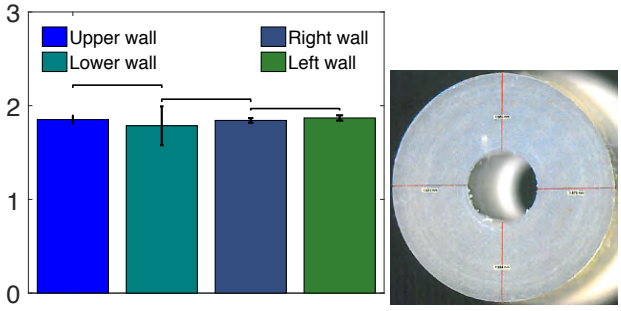

(a) (b)

Figure 6.7: Wall thickness of an extruded tube measured at six different cross sections over the a distance of 150 cm. No * means that samples are not significantly different at the level of p≤0.05 (6.7(a)). The cross-section of the extruded tube is seen in 6.7(b)

According to NatureWorks an extruded sheet processed at 190°C from the same raw material has an E of 3.5 GPa, ϵ_b of 6 % and a σ_y of 60 MPa. Tensile testing of the extruded 10 mm tubes showed an axial E of 3292±403 MPa and a σ_y, which was also the UTS, of 50 ±4 MPa. The samples were very brittle, despite no crystallinity or crystal orientation (see Figure 6.8(a)) and showed a short ϵ_b below 4% (see Figure 6.8(b)). Circumferentially the samples showed a smaller modulus of 1628±61 and a σ_y of 55±2 MPa. The ϵ_b was longer circumferentially (see 6.8(b)). This proves that the extrusion creates an orientation axially, but it is not related to any crystal orientation as seen in Figure 6.8(a), which only shows amorphous scattering. Due to the lesser stiffness and strength circumferentially, extrusion of the larger tube, was not chosen as an optimal processing way for creating optimal circumferential stiffness and strength. Instead, the smaller extruded tubes were used and expanded to a larger diameter. The process is described in section 6.2.2.

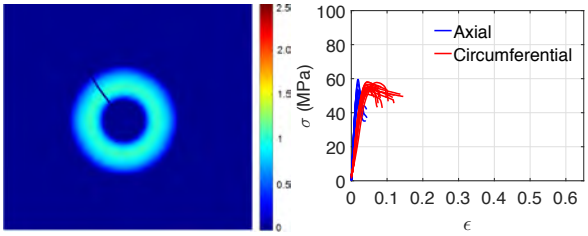

(a) (b)

Figure 6.8: WAXS image of a 10.5 mm extruded tube (6.8(a)). Stress-strain curves for extruded PLLA (OD 10.5 mm and thickness 0.22 mm) in both axial and circumferential direction6.8(b)

6.2.2 Straining of extruded PLLA tubes

Table 6.1 shows the extruded tube sizes available in this study. To achieve the appropriate size of the stent-base device, 16.5Fr (OD 5.5 mm) tubes were used, but for mechanical evaluation, the 10.2Fr (OD 3.4 mm) tubes were tested as they were easier to handle. As opposed to the extruded 10 mm tubes, expanded tubes were believed to have a higher mechanical strength circumferential and preferable for a stent in need of a high radial force. Tubes for mechanical evaluation were made of 10.2Fr (OD 3.4 mm) or 11.7Fr (OD 3.9 mm) and a wall thickness of 1.7 mm and expanded into tubes, 50 mm in length. Tubes with the outer diameter of 5.5 mm and an initial wall thickness of 2.7 mm were placed in a mold of 100 mm in length. The tube were heated to the desired temperature. For sequential biaxial strain,

an external force was used to axially strain the tubes after heating. To ensure completion of an axial strain, the tubes were heated for additional 3 s before a pressure (air injection) from one end of the lumen was applied resulting in the tubes to expand to 8.5, 9.5 or 10.5 mm in diameter. Figure 6.9 portrays a sketch of the extruded tube, after axial elongation and radial expansion and Figure 6.10 shows the expanded tube. To achieve simultaneous biaxial strain, pressure was applied before the axial strain. After expansion is finished the tube is quenched below T_g within 35 s.

The degree of axial strain during processing (ϵ_a) is given for each specimen as the change in length (ΔL) over the original length (L_0) (Equation 6.1). The radial strain (ϵ_r) is given as the change in diameter (ΔR) over the diameter prior to axial strain (R_0) minus the reduction in thickness due to the axial strain (t_a)(Equation 6.2).

$$\epsilon_a = \frac{\Delta L}{L_0} \tag{6.1}$$

$$\epsilon_r = \frac{\Delta R}{R_0 - t_a} \tag{6.2}$$

Total area expansion (A_{exp}), or the degree of expansion, is the relation between the radius after any axial strain and the radius after expansion (R_2) (Equation 6.3). The radius after axial (R_1) strain is calculated with the assumption that the volume of the material (V) is the same before (V_0) and after axial strain (V_1). V is calculated as the cross-sectional area before (A_0) and after (A_1) the axial strain times the length before (L_0) and after (L_1) the axial strain. The R_0 is the radius after the axial strain and seen in Equation 6.4.

$$A_{exp} = \frac{R_2}{R_1} \tag{6.3}$$

$$V_1 = V_0 \Rightarrow A_1 \cdot L_1 = A_0 \cdot L_0 \Rightarrow \pi \cdot R_1^2 \cdot L_1 = \pi \cdot R_0^2 \cdot L_0 \Rightarrow R_1 = \sqrt{\frac{R_0^2 \cdot L_0}{L_0 + \Delta L}} \tag{6.4}$$

6.2.3 Industrial vs. medical grade

Creating a medical device made from bioabsorbable polymers entails specifics of the purity and degradation profile of it. Loosely the polymers can be divided into 'industrial' and 'medical' grade. Previous studies were conducted on the industrial grades and some also on PLLA purchased from NatureWorks [97][87][92][93][98][88]. Often a wider M_w is to be

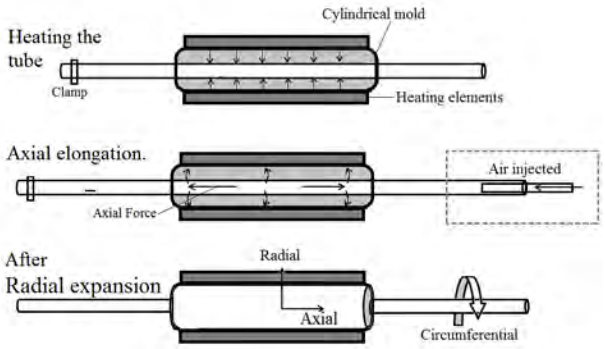

Figure 6.9: Sketch of biaxial straining. The extruded tube is placed in a cylindrical mold of a given diameter with heating elements surrounding the mold. During the simultaneous biaxial strain, the pressure (air injection) was applied before the axial strain. During the sequential biaxial strain, the pressure was applied after the axial strain. Used from [44]

Figure 6.10: Biaxially strained 16.5Fr tubes to 10.5mm diameter

expected for the industrial grade. Both industrial and medical grade PLLA pellets were extruded into tubes and after straining tested for differences in mechanical properties. The difference within the properties of the two grades can also be related to differences in crystallization rate during expansion. In a comparison of the two grades, mechanical testing of tubes with a total area expansion equal to ~300% showed a significantly higher modulus and σ_y for the medical tubes provided by Zeus than the industrial tubes. The medical grade in Figure 6.11(a) show a significantly higher E and σ_y and a longer ϵ_b. The variation appears the same for the two groups. In general, medical grade pellets have a higher price. When processing in-house the industrial tubes have a price of 0.40 USD/pc. Moreover, 16.10 USD/pc. for the medical grade. Special handling of the medical grade is believed to raise the price further by 2-4USD. The up-scaling cost is not an issue at the development stage, but the processing of medical grade is less convenient during handling. Purchasing already extruded medical tubes from a supplier is highly expensive with a cost close to 150 USD for 50 cm of tubing (usually 25-30 cm are used for 5 cm tubes as tested in this study). For this reason, test specimens and prototypes were made from the industrial grade. Ideally, further testing should be done for a medical grade, as the degradation properties might differ from the industrial grade. The profile must be very predictable in a bioabsorbable device.

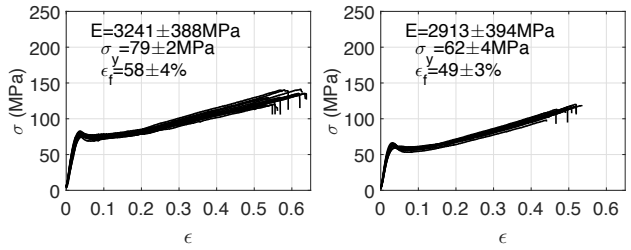

(a) (b)

Figure 6.11: Stress-strain curves for biaxially strained PLLA tubes in the circumferential direction after an A_{exp}=~300%. Both medical (6.11(a)) and industrial (6.11(b)) grade PLLA were tested

6.2.4 Degree of strain

In general, the shape of the stress-strain curve of the tubes in each direction depends on the degree of strain in each direction. The influence of the degree of strain as a whole is the total area expansion (A_{exp}) as portrayed in section 6.2.4.1 regardless of simultaneous or sequential biaxial strain. In summary, an increase in the degree of strain in both directions results in isotropy at high strains, but only for the sequential biaxially strained tubes. This was not detected for simultaneous biaxially strained tubes. At the same time, it was seen that crystal orientation was diminished at high strains for sequential biaxially strained tubes, compared to the simultaneous biaxially strained. There is no direct method to quantify the amorphous strength. It was therefore hypothesized that any strength not related to crystal orientation was related to amorphous orientation. One can assume that the entangled amorphous chains act as in a solid frozen melt and when disentangled act as in a melt state. The strength of the melt acts as a negative pressure formed during spherulite crystallization. The pressure is built up within the material as it is being stretched and leads to cavitations. Theoretically, this deformation pressure, p, is -1/3 of the tensile stress[91], but not described further here in detail. For biaxially strained PLLA tubes the crystallinity was no more than 32% for any strain or process, and it was thereby concluded that the improved stiffness and strength properties were not in relation to crystallization and more likely related to the strength or deformation pressure of the amorphous domains.

6.2.4.1 Article: Characterization of biaxial strain of poly(L-lactide) tubes

The influence of the degree of strain is described in detail in the following article 'Characterization of biaxial strain of poly(L-lactide) tubes' by Løvdal et al. [44]. There is a mistake in the references, where reference 30 in Table 3 should be 31. Additionally, there is a typo in Figure 7 and Table 3, where (1.0;4.3) should be (1.0;3.3) and (0.2;4.3) should be (0.2;2.3) instead.

For full manuscript follow the
Link: http://orbit.dtu.dk/files/117353557/Characterization_Of_Biaxial_Strain.pdf

6.2.4.2 The influence of total area expansion

It was seen that for both axial or radial processing strains (ϵ_a and ϵ_r, respectively), the A_{exp} is the main contributor to the increased stiffness and strength. It is not solely dependent on the degree of A_{exp}, but also the degree of ϵ_a versus ϵ_r. The shape of the stress-strain curves is similar for (0.2;2.0) and (0.5;2.4) in both directions (Figure 6.12), but there is a significant difference in stiffness, σ_y, UTS and the ϵ_b for the axial samples. The same can not be said for the circumferential samples. There is a significant difference between the stiffness and σ_y, but the UTS and ϵ_b are not significantly different. To obtain the highest stiffness and strength in the circumferential direction, a larger strain both axially and radially strain would be preferred. It was not possible to determine the influence of the extrusion direction on the orientation. However as previously seen in Figure 6.8, an extruded tube, which have not been expanded further, would have superior properties in the axial direction. It is therefore believed that the extrusion direction will have some effect on developing orientation in the axial direction. Perhaps it is amplified during straining and had it not been extruded prior, the effect of axial strain could be less.

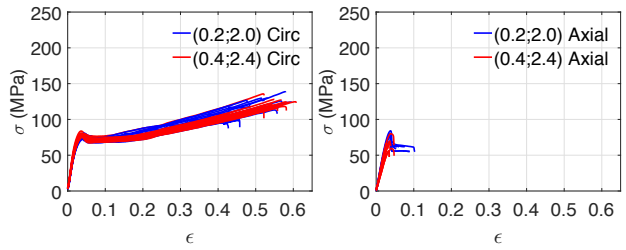

(a) (b)

Figure 6.12: Stress-strain curves for simultaneous biaxially strained PLLA tubes in both circumferential (circ) (6.12(a)) and axial direction (6.12(b))

As seen in Table 6.2, the degree of strain is much larger in the circumferential than the axial direction and for this reason, the circumferential mechanical properties are greater. The stent-base used in this project was made from a diamond-shaped stent with cells and cut at an angle of 40° to the axial direction. The properties would be between the axial and circumferential properties.

It is the ratio between ϵ_a and ϵ_r, which determines the degree of orientation of the amorphous chain and thereby the mechanical properties. The A_{exp} can in some instances be the same, while the ratio (ϵ_a;ϵ_r) is different. As seen in Table 6.2 a larger axial strain ϵ_a=0.4 does

Table 6.2: Mechanical properties of simultaneous biaxial strained PLLA tubes at different axial strains and thereby different A_{exp}.

	E_{axial} (MPa)	$\sigma_{y,ax}$ (MPa)	UTS_{ax} (MPa)	$\epsilon_{f,ax}$ (%)	E_{circ} (MPa)	$\sigma_{y,circ}$ (MPa)	UTS_{circ} (MPa)	$\epsilon_{f,circ}$ (%)	X_c (%)
(0.2;2.0) A_{exp}=269%	2614±219	75±6	75±6	6±2	3274±198	76±2	119±10	53±5	30
(0.4;2.4) A_{exp}=300%	2320±273	78±3	66±7	4±1	3456±195	79±2	119±8	54±3	30

Table 6.3: Mechanical properties of sequential biaxial strained PLLA tubes in axial, circumferential and 40° direction at different axial and radial strains but same A_{exp}. Data was provided by T. Noorzae

	E_{axial} (MPa)	UTS_{ax} (MPa)	$\sigma_{y,ax}$ (MPa)	$\epsilon_{f,ax}$ (%)	E_{circ} (MPa)	$\sigma_{y,circ}$ (MPa)	UTS_{circ} (MPa)	$\epsilon_{f,circ}$ (%)	X_c (%)
(0.2;2.3) A_{exp}=333%	2418±258	68±5	68±5	40±28	3748±323	86±5	119±10	37±3	30±2
(0.2;2.3) A_{exp}=333% , 40°	2263±270	63±4	63±4	39±7	-	-	-	-	-
(0.8;2.3) A_{exp}=333%	3020±335	82±7	82±7	48±9	3154±220	69±4	95±8	54±4	33±1
(0.8;2.3) A_{exp}=333%, 40°	2647±298	70±6	70±6	50±14	-	-	-	-	-

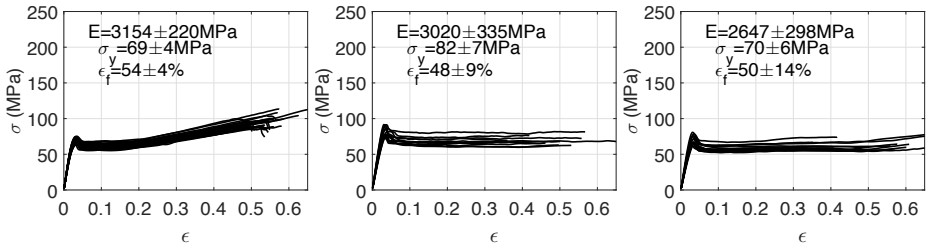

(a) (b) (c)

Figure 6.13: Stress-strain curves for sequential biaxially strained PLLA tubes (0.2;2.3, A_{exp}=332%) obtained in the circumferential 6.13(a), axial 6.13(b) and diagonal6.13(c) direction. Raw data supplied by T. Noorzae.

not mean that the axial stiffness and strength are greater than seen for ϵ_a=0.2. Because the ϵ_r is greater in the latter instance (2.4) the A_{exp} is larger for (0.4;2.4). To achieve a larger axial stiffness and strength, one must keep the ϵ_a high and/or the ϵ_r low. Specimens cut in the axial direction in this particular setup did not undergo necking and fractured much sooner that the circumferential, which resulted in a shortening of ϵ_b than normally seen.

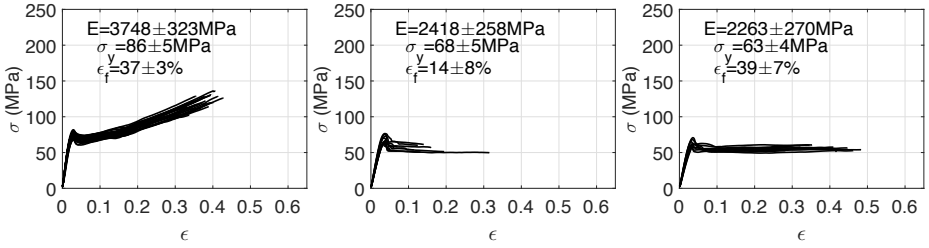

Figure 6.14: Stress-strain curves for sequential biaxially strained PLLA tubes (0.8;2.3, A_{exp}=332%) obtained in the circumferential 6.14(a), axial 6.14(b) and 40° 6.14(c) direction. Raw data supplied by T. Noorzae.

The stent-base design is usually cut at about 40° angle from the axial direction. It is therefore hypothesized that the properties will be between the axial and circumferential properties for an isotropic material. The question is, what happens if the material is anisotropic as a result of different ϵ_a and ϵ_r. It is seen that the stress-strain curves for the 40° samples after sequential biaxial strain (Figure 6.13(c) and 6.14(c)) resemble the shape of the curve in the axial direction (Figure (6.13(b) and 6.14(b))) more than in the circumferential direction (Figure 6.13(a) and 6.14(a)). Regardless of axial strain degree, the properties at a 40° angle are not in between the axial and circumferential properties, but inferior to the axial properties (Table 6.3). This is by the hypothesis that the molecules are stretched in the axial direction first and then in the circumferential direction during the expansion. Because the radial strain is much larger than the axial, it appears that all molecules are aligned circumferentially and some in the axial direction, depending on the degree of radial strain and not so much in 40° direction. Despite the same A_{exp} the mechanical properties in each direction (axial and circumferential) is dependent on the degree of strain in each direction. Therefore a large axial strain (0.8) results in a larger axial stiffness and strength (as given in Table 6.3), possibly due to a more profound alignment of the molecular chains in the axial direction than if the axial strain is less (0.2). Less axial strain (0.2) results in less molecu-

lar chain alignment and allows a greater alignment in the circumferential direction during the radial strain. At the same time, a large initial axial strain allows for a greater ϵ_b in the circumferential direction, yet with a large variation. Why this occurs is unknown. In conclusion, it appears that the properties at an angle of 40° therefore, does not benefit from radial expansion, but from the degree of axial strain.

6.2.5 Investigation of thermal properties of strained PLLA tubes

It was previously seen that the quicker the heating rate, the higher the T_g as well as T_{cc} [13]. The T_m remains constant. It is important that all measurements must be run at the same heating rate. Several phenomena during a DSC scan occur for different extruded PLLA tubes. One shows the traditional glass transition, with an endothermic peak followed by a cold crystallization and subsequently melting peak (Figure 6.15 turquoise curve). Another is the double melting peak as seen in Figure 6.15 (blue curve). The double exothermic peak has been investigated before and is attributed to recrystallization [99]. The first endothermic peak is the melting of the formed crystals, then an exothermic peak representing recrystallization and the last endothermic peak is the melting of the recrystallization. In general, the double peak occurs when the heating rate is low [99] or in certain combinations of the cooling rates and sequent heating rates during the DSC scan[100]. The first was confirmed in previous DSC measurements of the same material using a heating rate of 2°C/min [13].

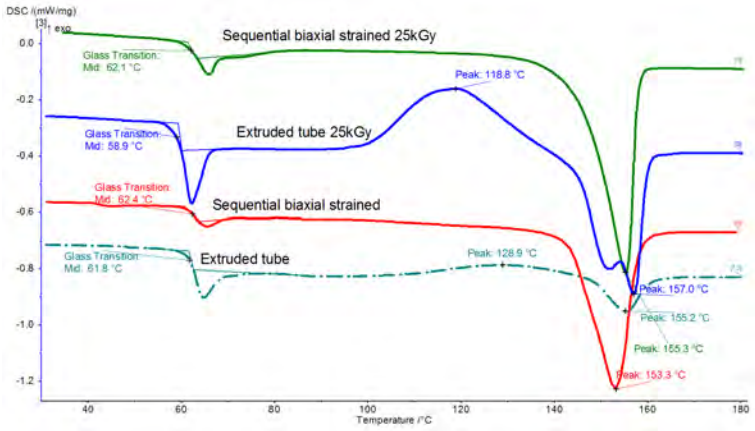

Figure 6.15: DSC scan for axially strain and sequential biaxially strained tubes strained at 73°C, and sterilized at 25kGy using γ-radiation along with the scan for an extruded tube

In Figure 6.15 only one of the DSC curves (γ-sterilized) shows this double peak despite

the same heating rate (10°C/min). This phenomenon is later analyzed in section 6.4.2.1. If the sequential biaxially strained tube is γ-sterilized (Figure6.15 green curve), the double melting peak is not present and resembles the curve the sequential biaxially strained tubes (Figure6.15 red curve), where no cold crystallization peak occurs. It is later shown that further crystallization is possible, but not at the rate of which the DSC scan is running.

The untreated extruded tube, shows a cold crystallization peak at 129°C and a melting peak at 156°C and remains amorphous (<1%) (Figure 6.16). When the extruded tube is strained between T_g and 73°C at a ϵ_a below 100% the thermal analysis shows that T_{cc} has shifted to the right at 107°C, whereas the T_m remains constant. Even lower degrees of axial strain (68%) will move the T_{cc} peak to 88 °C. This means that when the polymer has been strained the energy needed to form crystals is less. A low ϵ_a of 68% very little crystallinity is seen(3%). Increasing the strain to 88% induces a X_c of 8% (Figure 6.16). The double melting peak occurs just as the chains are stretched enough (38%) to form crystals. Only at strain degree close to 100%, the amorphous chains are so alignment that little energy in the form of heat is needed to form crystals and the crystallinity increases to 35-36%.

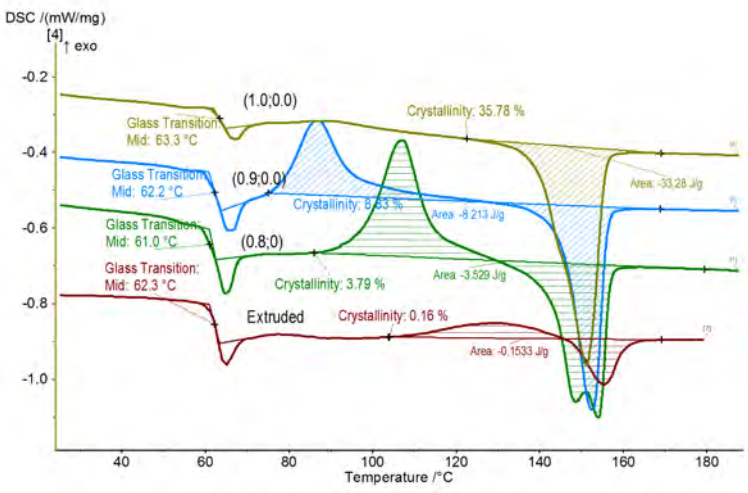

Figure 6.16: DSC scan for axially strained tubes at different ϵ_a along with the an untreated extruded tube

Figure 6.17 shows that the processing strain temperature (T_p) may be as low at 65°C to induce crystals, with a X_C between 24 and 29% as long as the degree of strain is close to 100%. Straining at 65 or 70°C shows an unexpected crystallization peak around 85°C. Normally crystallization from the cold would indicate the onset of the crystallization peak

to be about 100°C and 129°C at the peak. Increasing the T_p to 73°C shifts the T_g higher to 63°C as opposed to 59°C. At this T_p, the crystallization peak is non-existent resulting in a higher crystallinity of 35-36%. Increasing the temperature further will not induce crystals. Increasing the straining temperature will increase the T_{cc} from 85°C to 118°C at 90°C. This means that more energy is needed to further crystallize. It is hypothesized that the chains at high T_p relax due to a high degree of mobility and are therefore not able to crystallize. The phenomenon is further described in section 6.2.7.

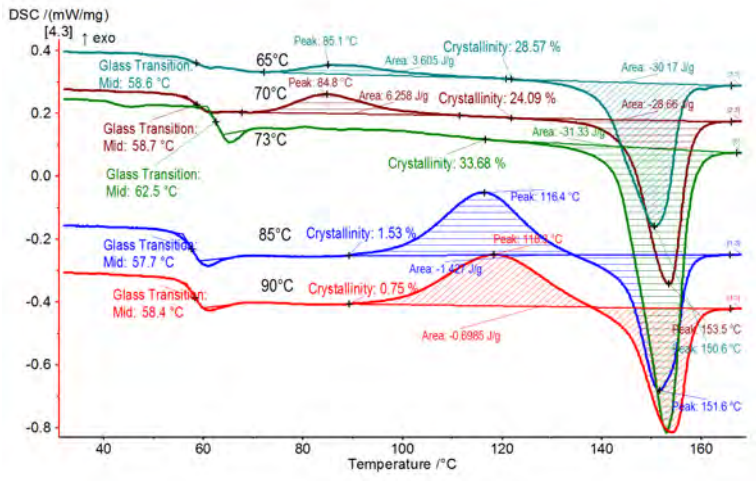

Figure 6.17: DSC scan for axially strained tubes (0.8;0) at different T_p

Table 6.4: Thermal properties of axially strained tubes at different ϵ_a along with the an untreated extruded tube

	T_g (°C)	T_{cc}(°C)	T_m(°C)	X_c%
Raw material	58±-	128 ±-	154±0	1±-
(0;0)	61±0	129 ±-	156±0	0±-
(0.8;0)	62±0	107 ±0	154±0	3±1
(0.9;0)	63±0	88 ±1	153±0	8±1
(1.0;0)	63±0	- ±-	151±0	36±0

At T_p close to the onset of T_{cc}, the material would be soft. Experimental work at a high T_p showed that after the axial strain the tube becomes soft and relax from its normal shape. It starts to bend in the mold leading to a considerable variation in thickness after expansion. To avoid the bending, a metal rod was placed inside the tube, and it was possible to strain

the tube at a maximum temperature of 93°C. At lower temperatures, this was not an issue.

The tubes would be thicker toward the ends of the mold. However, it was confirmed that it had no significant influence on the thermal characteristics of the tube and the crystallinity, T_g and T_m remained constant throughout the entire length of the tube [13]. Thickness variation along the tube did not correlate with any variances in mechanical properties for specimens taken along the tube, and it is hypothesized that the amorphous chains are stretched somewhat uniformly along the tube at least for straining of 10.2Fr and 13.2Fr tubes.

6.2.6 Processing strain rate and temperature

In investigation of axial processing strain rate ($\dot{\epsilon_p}$) and processing temperature (T_p) the degree of axial processing strain ϵ_a was kept constant at nearly 100% and the A_{exp}=432% as done in section 6.2.4.1. The ($\dot{\epsilon_p}$) was set to 0.1, 0.2 or 2.1 s^{-1}. In summery it was seen that crystals form during an axial strain (ϵ_a), only occurs when then $\dot{\epsilon_p}$ is above 0.2 s^{-1} and at T_p<85°. Both $\dot{\epsilon_p}$ of 0.1 and 0.2 s^{-1} are too slow for the crystals to form during strain and the chains either does not become oriented in the first place or the chains have enough time to relax from oriented to non-oriented state and crystals are not formed. The faster the deformation, the less chance for the polymer chains to relax, which is seen by an increase in UTS and σ_y of the material. According to Pawlak et al. [91] the improvement of properties is related to the crystal strength and not the amorphous chains. When the polymer is not as soft, cavitations during high strain rates are more likely. This should be seen by a shortening in ϵ_b and is only seen vaguely for sequential biaxial strained PLLA tubes in this study with increasing $\dot{\epsilon_p}$. At higher T_p the plastic deformation degree is smaller, and the ϵ_b is improved, and therefore cavities are not formed during deformation. This is seen by the degree of ϵ_b for tubes strained at T_p=93°C. Overall cavities are expected when the chain mobility is insufficient for lamellar deformation through crystal plan slip and the amorphous deformation occurs[91]. Therefore a minimum T_p=68°C has previously been identified to avoid the cavities and shortening of ϵ_b and discussed later in section 6.2.9. Zhang et al. [87] showed that increasing the strain temperature for PLLA (2002D) specimens from 70 to 90°C eliminates the formation of cavities as the PLLA is deformed. At higher T_p, the PLLA can be strained further before cavities occur compared to lower T_p. This is also seen for sequential biaxially strained PLLA tubes, as the ϵ_b increases with increasing T_p.

One thing that should be noted is that the higher the T_p, the more mobility within the material. The final tube upon expansion is much thinner than at lower strain temperatures.

It is possible that the distribution of the material is more uniform at higher T_p. Despite the improved mechanical properties, the thinner tubes are not preferable when creating the filter. Again it must be remembered that there is a limit to how thin the wall thickness of a filter can be to exert to appropriate radial force on the vessel wall. Therefore the optimal filter would be made of material, which showed excellent strength and stiffness while being as thin as possible. It is most likely be a compromise between adequate radial force and wall thickness.

6.2.7 Article: Mechanical Properties of Biaxially Strained of Poly(L-lactide) Tubes: Strain Rate and Temperature Dependence

The influence of ϵ_p and T_p are clarified in the following submitted article.
The manuscript is currently under review.

6.2.8 Opaque nature of strained PLLA tubes

Based on literature it is known, that to induce the PLLA with crystallinity upon strain, the T_p must be above the T_g. The T_g for the extruded tube is 63°C. Temperatures below 73°C but above T_g made the material milky-white as opposed to transparent. It became apparent that low T_p created opaque tubes (Figure 6.18(a)) compared to the transparent tubes processed at higher temperature (Figure 6.18(b)).The opaque nature might be related to stresses built up within the polymer or due to microvoids created during straining. It was not possible to release the stresses through heat treatment. The cooling rate at which the tubes are exposed appears to create microvoids, which are not possible to remove through heat treatment. It is thus important to both select a T_p as well as a degree of strain to limit the presence of microvoids or stresses.

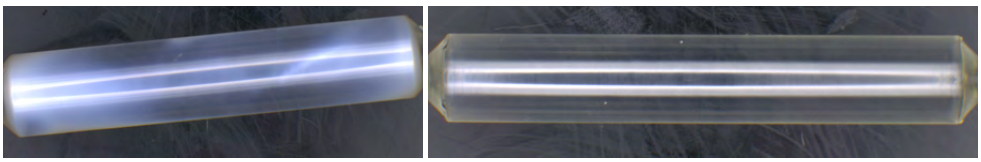

(a) (b)

Figure 6.18: Sequential biaxially strained tubes which is of opaque nature 6.18(a) and of transparent nature 6.18(b)

Small angle X-ray diffraction (SAXS) will show that for PP the cavitations and the whitening of the material occur at yield point and that the voids are formed perpendicular to the deformation direction[91]. SAXS was used in the attempt to determine a higher degree of cavitation within the material in this project. Two tubes which processed the same way, but one of the tubes appeared white, where the other appeared transparent. The SAXS signal was too weak for the biaxially strained PLLA tubes to confirm differences between the two tubes. It is a possibility that the lower the T_p, the higher the risk of inducing stresses within the material leaving it white. Supposedly the polymer can become opaque when crystals form from the un-nucleated state due to the formation of larger spherulites, but WAXS did not show larger individual crystals. Both incidences showed radial crystal sizes of 56 and 60 Å and axial crystal sizes of 142 Å. It is a possibility that the white represents clusters of crystals of the same size, creating a different light refractive index. The tubes were processed in the same fashion, and the orientation factor for (200/100) plane is the same, despite the

white tube shows more amorphous scattering overall (Figure 6.19(b)). It can therefore not be concluded that the opaque nature of the expanded PLLA tubes is related to crystals.

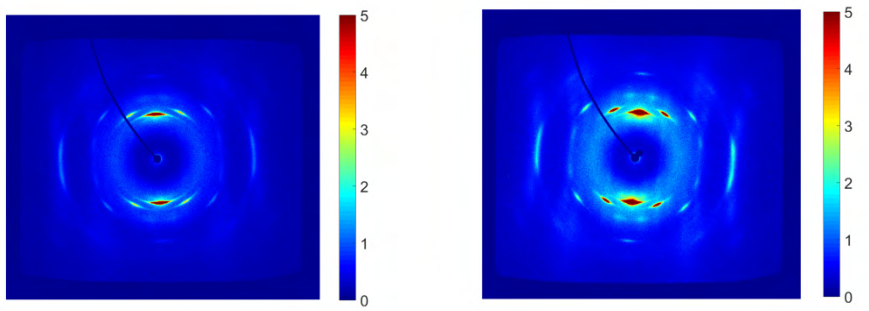

(a) (b)

Figure 6.19: WAXS images of transparent (6.19(a)) and opaque tubes after expansion (6.19(b))

Additionally, the Bragg's angles showed that the packing of crystals was the same (Figure 6.20). Small differences in the extruded tube, despite the same processing parameters, lead to slightly different tubes. An investigation of the expansion machine was not done, and tubes which were optically not processed correctly were discarded for further investigations.

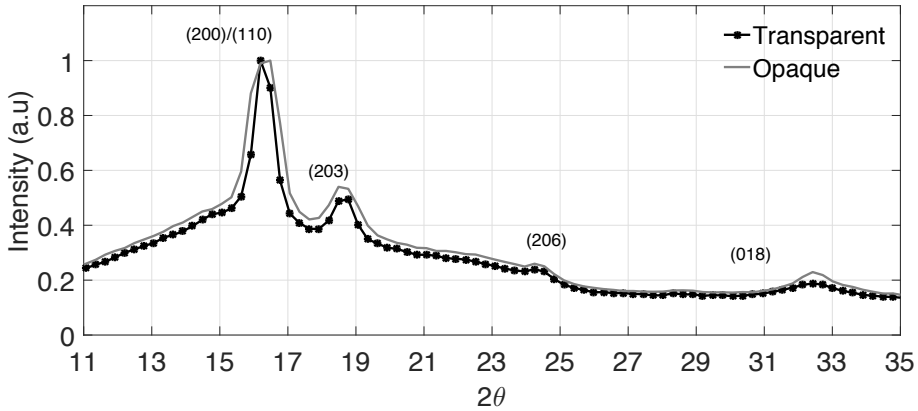

Figure 6.20: Intensity as a function of Bragg's angle (2θ). The figure shows both the intensity for transparent and opaque tube after expansion. The most common peak for the α' crystals for PLLA are denoted

6.2.9 Cooling during processing

Experimental data show that cooling the mold follow a linear cooling function of the tube itself (Figure 6.21). Cooling the mold for 14 s before axial strain would reduce the outer temperature of the tube from 73 to 68 °C. At this temperature, the inside of the tube is usually 60 °C. The tubes are opaque rather than transparent at this stage. From Figure 6.22(a) it is then seen that a lower straining temperature will cause a shortening in ϵ_b presumably caused by microvoids or cavities formed during the strain.

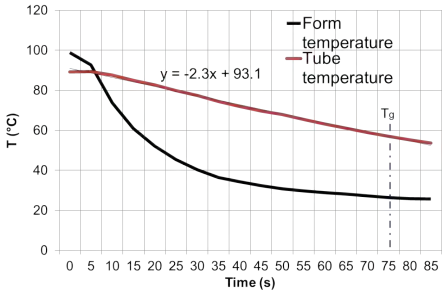

Figure 6.21: Cooling of mold from 100°C to room temperature and the tube temperature during cooling

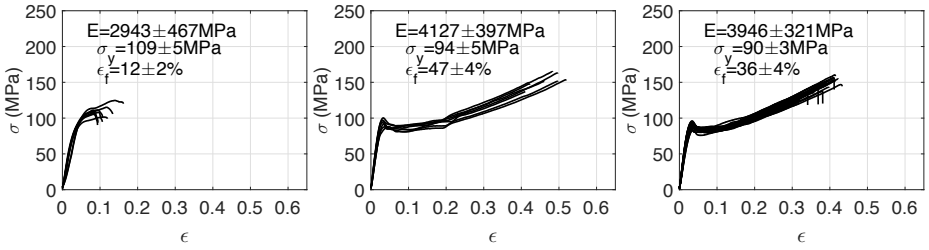

(a) (b) (c)

Figure 6.22: Strain-stress curves for tubes testing in the circumferential direction. The tubes have been cooled to 60°C before expansion (6.22(a)) or heated in the mold after expansion for 2 s (6.22(b)) or 10 s (6.22(c))

6.2.10 Tube thickness variation

In general, the biaxially strained tubes were thicker in the proximal than the distal end (to the pressure air injection) and thinnest in the middle. Overall sequential biaxial appears to show the least thickness variation going from distal to proximal. Additionally, it was seen

that a larger degree of axial strain, would automatically reduce the thickness variation. From Figure 6.23 and 6.24 it was seen that 0.3 axial strain as opposed to 0.5 strain, results in the thicker wall at both ends of the tube over 100 mm and more variation along the length. Therefore when possible prototypes were made, laser cutting was done in the middle of the tube. Unfortunately, in retrospect, the prototypes from tubes used in the animal study showed a larger variation from one end to another. The proximal end had a much larger thickness (0.80 mm), and the distal end had a thickness of 0.45 mm (see Table 9.1 in section 9.1.1). A possible explanation for this could be that the tubes were not completely straight but bend upwards (3.1°) when received from the supplier (see Figure 6.25). The tubes for the animal study were processed in the same way as previously despite the large thickness variation along the tube. It is possible that an uneven heating of the material occurred, and some part of the material would be softer and thinner after axial strain from which point the expansion would develop. The uneven heating of the material might be due to the disturbance in the heating element of the mold or due to the material bending and parts of it were closer to the heated mold and thereby became soft and the weakest point.

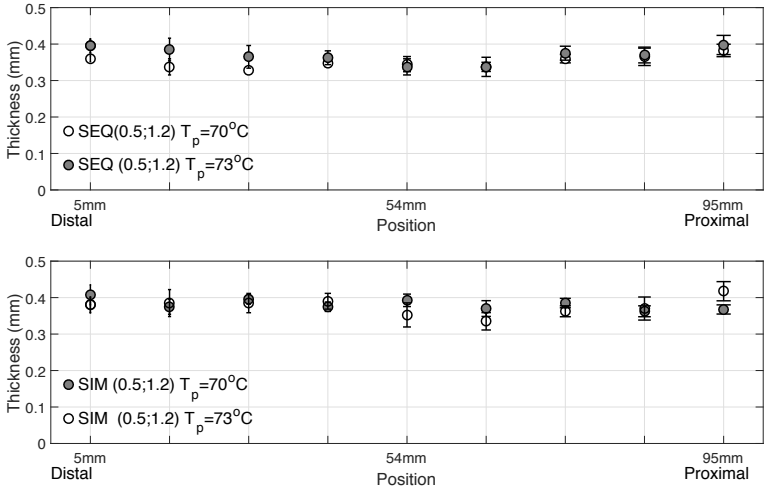

Figure 6.23: Simultaneous (SIM) and sequential (SEQ) biaxially strained tubes (OD 5.5 mm). Strain temperature was either 70 or 73°C

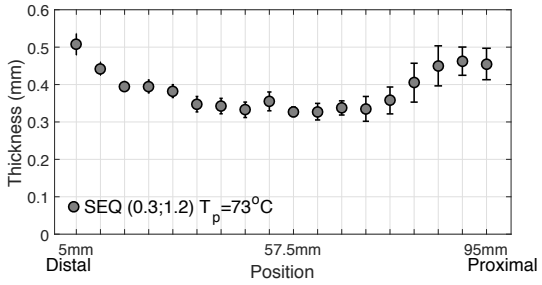

Figure 6.24: Sequential biaxial strain of OD 5.5mm tubes. Strain temperature was 73°C

Figure 6.25: Extruded PLLA tube (16.5Fr)

6.3 Annealing and loss of orientation

6.3.1 Annealing

As previously stated mechanical properties depend on crystallinity. Regarding annealing, isothermal crystallization of the extruded tube occurs at 80°C and above but depend on the annealing time. At 80°C a X_c of 28% could be obtained after 3 hours, whereas heating the temperature at 90°C induces a X_c of 30% after only 1 hour. Heating the temperature further to 100°C and above induces a X_c of 38% after just 30min and 41% at 130°C. A maximum X_c of 44% was achieved at 140°C [13]. As crystallinity increases as a function of temperature the mean crystal size for the three isothermal rings portrayed by WAXS (see Figure 6.26), increased from 131, 118 and 186 Å to 190, 165 and 193 Å. It should be noted that the crystals do not grow in any specific orientation plane as seen for biaxially strained PLLA tubes. Annealing the raw material leads to double melting peaks at 90 and 100°C next to each other [13].

When annealing the strained material the double melting peak occurs only at 120°C (Figure D.4 in Appendix D.3). Below this temperature the two melting peaks are further apart. The T_g is more difficult to determine, as it come is two different transitions due to a noisy signal. For annealing at 130°C the first is at 60°C and the second is 67°C. An increase in annealing temperature increases the X_c to 41±0%. From Table 6.5 and 6.6 it is seen that crystallization increase as a function of temperature despite the already strain-induced

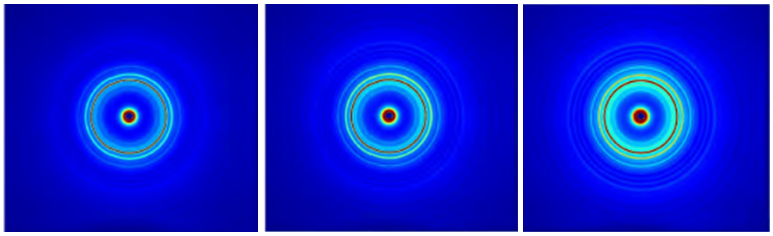

(a) (b) (c)

Figure 6.26: WAXS images of annealed extruded tube at 100°C (6.26(a)), 120° (6.26(b)) and 140° (6.26(c)) for 30 min

Table 6.5: Isothermal annealing of the extruded tube [13]

	T_g	1^{st} T_m	2^{nd} T_m	X_c
(0;0) 100°C, 30 min	60	149	156	38
(0;0) 110°C, 30 min	61	-	156	40
(0;0) 120°C, 30 min	59	-	155	41
(0;0) 130°C, 30 min	60	-	157	41
(0;0) 140°C, 30 min	58	-	160	44

crystallinity. However it is also seen that the temperature must be above 90°C to induce further crystallinity in strained tubes, whereas crystallinity during isothermal annealing can occur, but takes longer.

Table 6.6: Isothermal annealing of sequential biaxially strained tubes

	1^{st} T_g	2^{nd} T_g	1^{st} T_m	2^{nd} T_m	X_c
(0.2;2.3) 90°C, 60 min	-	65	-	152	30
(0.2;2.3) 100°C,30 min	60±0	66±1	108±0	153±0	31±0
(0.2;2.3) 110°C, 30 min	60±0	67±0	117±0	152±0	34±2
(0.2;2.3) 120°C, 30 min	59±1	70±1	128±0	152±0	37±1
(0.2;2.3) 130°C, 30 min	60±1	71±1	137±0	152±0	41±1

The crystallization rate differ between strained tubes and the extruded tube as seen on Figure 6.27, where the crystallization rate of strained tubes is approximately linear. The crystallization rate is quicker for the extruded tube, and its function is not linear, though the X_c is the same at 130°C for both materials. It means that more energy is required to the system to crystallize already strained samples further.

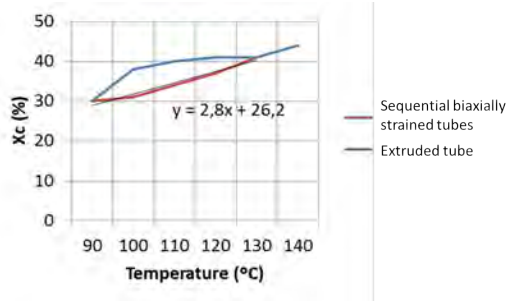

Figure 6.27: Crystallinity as a function of annealing temperature during 30min annealing for sequetial biaxially strained or extruded tubes

As shown above, annealing does not only influence the amorphous samples but also already crystalline samples. The process is referred to post-annealing and is an isothermal heat treatment of the samples. It was previously shown that the orientation of amorphous chains is sensitive to the expansion temperature (section 6.2.4.1). The orientation of an axially strained tube is reduced from 0.7 to 0.3 with post annealing for merely 20s at 120°C, leaving the tube nearly 80°C inside (Figure6.28). The change in crystallinity from 34 to 36%, is likely due to the experimental equipment error and is not considered significant. The same tendency is seen for sequentially biaxially strained tubes, where the orientation factor is reduced from 0.3 to 0.1 when annealed up to 80°. Upon annealing if the tube is first cooled to room temperature at the speed of 0.4°C/s, then subsequently annealed to 80°C, the orientation maintained for that particular plane. At the same time, the stiffness of the material remains unchanged as seen in Figure 6.29 regardless of the annealing pathway. This is by the fact that crystal orientation is diminished upon heating and that the amorphous orientation remains at 80°C. There is a change in the σ_y, which is significantly lower when annealed than when cooled before annealing compared to the sequential biaxially strained tube in Figure 6.29(c). Another interesting point is the crystal sizes after annealing. Upon annealing the crystals for the (110/200) plane grow in the axial direction from 134 to 145 Å, regardless of the cooling and annealing pathway. Annealing of only axial strain makes the crystals diminish in in the circumferential direction from 183 Å to 160 Å but grow in the axial direction from 62 to 126 Å.

Annealing for 60 min at 90°C eliminated any orientation obtained through straining and the modulus and σ_y comes closer to molded PLLA specimens, without straining. At the same time, the crystallinity was reduced from 31-32 % to 28-30 %. This was described in

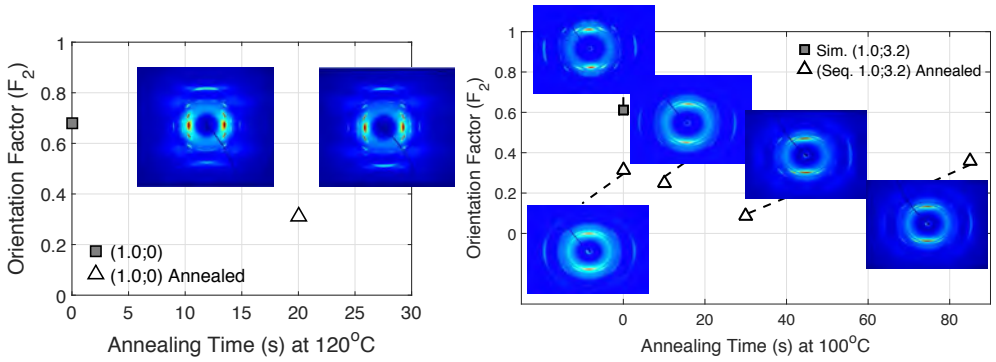

(a) (b)

Figure 6.28: WAXS images of post-annealed axial strained tubes 6.28(a) and post-annealed biaxially strained tubes 6.28(b)

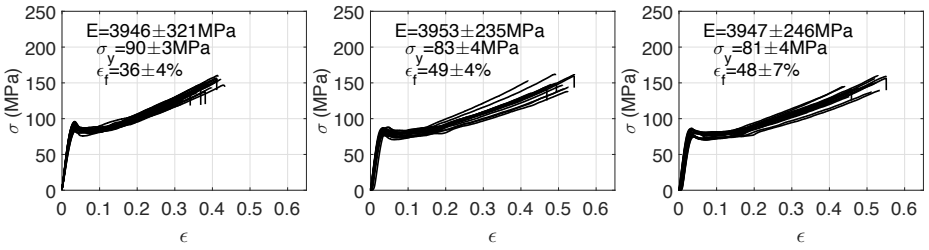

(a) (b) (c)

Figure 6.29: Sequential biaxially strained tubes strained at 73°C (6.29(a)), cooled and annealed for 85s at 100°C (6.29(b)), or expanded at 73°C and annealed for 30 s (6.29(c)). Tubes were tested in the circumferential direction

further detail in section 6.2.4.1 [44]. It is therefore believed that strain-induced crystallinity is not well preserved during annealing and is a concern in further processing of the tubes.

6.3.2 Pre-annealing

Annealing in an oven was done before straining for 1, 3 or 5 min at 80 or 90°C after which they were slowly cooled at room temperature. Based on the previous measurement it is unlikely that the pre-annealing induced any crystallinity. Sequential biaxial straining was done at 73°C subsequently. Annealing at 80°C leads to a modulus and σ_y significantly lower than the non-pre-annealed tubes (Figure 6.30). Annealing at 90°C leads to a modulus and σ_y which were not significantly different from the non-pre-annealed tubes, but the properties

were different at 80°C. It could not be explained why that is, and since the properties were not significantly improved, the idea of beneficial pre-annealing was not pursued.

Preferably the X_c should be moderate after the expansion process, heat treatment (before or after) and sterilization to avoid complications during loading of the device into the delivery system and to avoid fractures during cyclic compression in the vein. For comparison, the already commercially available BVS stent from Abbott Vascular was analyzed and showed a high crystallinity of 52%, while having a low orientation factor of 0.02 (see Table D.2 in Appendix D.2). The stent was very brittle as a result of the high X_c. It is not likely that the stent would not be suitable for the larger diameters under cyclic compression.

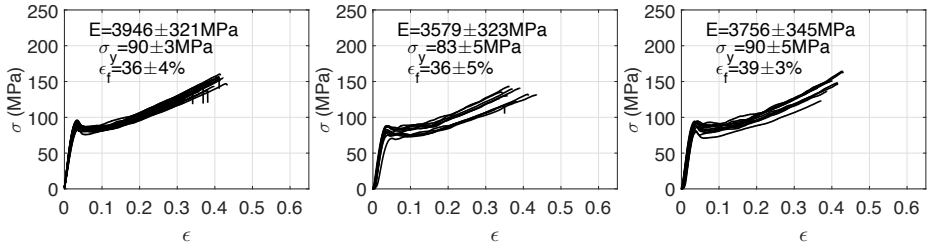

Figure 6.30: Sequential biaxially strained tubes expanded at 73°C (6.30(a)), pre-annealed for 5min (6.30(b)) at 80°C or 90 °C (6.30(c)). The tubes were tested in the circumferential direction

6.4 Sterilization

6.4.1 Background on sterilization

Sterilization, in general, will have an impact on most polymers whether bioabsorbable or not. The most common sterilization methods are dry heat, ethylene oxide (EO) gas and γ-radiation[101]. The sterilization can potentially impact the mechanical performance, such as stiffness and elasticity but also the viscoelastic properties of the polymer [41]. During EO sterilization the molecular weight can be reduced for PLLA [41]. Because bioabsorbable polymer is sensitive to both temperature and moisture, sterilization can become a challenge. Exposure to high temperatures and moisture will result in severe degradation and hydrolysis, with a reduction in molecular weight (M_w) of 11% after a short sterilization cycle of 70 min at 45°C [41]. If the reduced M_w is acceptable, EO still becomes of interest. EO sterilization at 53°C at 75% humidity is acceptable in terms of residual microbes. The key is to

evaluate whether a long expose time to moisture at low temperatures is less harmful than at higher temperature. PLLA microspheres showed that a cool EO sterilization cycle well below T_g will reduce the T_g, whereas warm EO sterilization cycle closer to the T_g, will increase the T_g. In general the T_g can change by storage at elevated temperatures and hydration. Water can act as a plasticizer and lower the T_g and make the polymer soft[64]. Also after a warm EO sterilization cycle, a cold crystallization peak will not be detected during DSC [101], where it remains at 85.5 °C after a cold cycle. A cold crystallinity temperature was detected for a cold EO sterilization cycle. The warn EO sterilization cycle induces a greater crystallinity as opposed to the cold cycle, which only induces a slight increase in crystallinity. This results in a greater chain mobility in the amorphous domain during the warm cycle [101]. At lower sterilization temperature there is not enough mobility among the chains to create crystalline domains. Radiation has the advantage of being performed at room temperature and without the need of moisture as a carrier for sterilization to occur. However, it is also known to reduce molecular weight, by cleaving the molecular chains ultimately altering the degradation profile of the polymer. EO has the advantage over γ-radiation of not reducing molecular weight and from a manufacturing perspective of being cheaper. Sterilization at 25kGy using γ radiation does not change the modulus or σ_y significantly. Radiation of 50kGy significantly increases the modulus and well as the σ_y. The crystallinity increase at 25kGy, but the dose is increased to 50kGy, the crystallinity is reduced[102].

6.4.2 Results on sterilization of biaxially strained tubes

6.4.2.1 γ - sterilization

In this project, no real difference in modulus was detected after a single 25kGy radiation or two times 25kGy (e.g. 50kGy). However, in both instances, the ϵ_b is reduced. Specifically for PLLA it is expected that the major effect of radiation is chain scission of the backbone and through hydrogen abstraction, resulting in a reduction of M_w [103]. As predicted radiation sterilization in this study (2x 25kGy), the M_w was reduced to 67,000g/mol from the preexisting 185,000g/mol (see Table D.3 in Appendix D.4). A small increase in crystallinity (37-38%) was detected upon γ-radiation, which correlates well with the fact that stiffness increase significantly as a result hereof (Figure 6.31(c). The σ_y increases from 83±3MPa to 94±8MPa and the reduced ϵ_b, indicates that oriented amorphous chains have changed, or cavitations have formed. From the literature, it has previously been pointed out that the mechanical

strength (section 5.1.2) is reduced with molecular weight (M_w) reduction. Radiation of the extruded tube does not change the thermal properties or the crystallization, and the tubes remain amorphous. It means amorphous chains cannot form crystals upon radiation if they were not induced previously during extrusion.

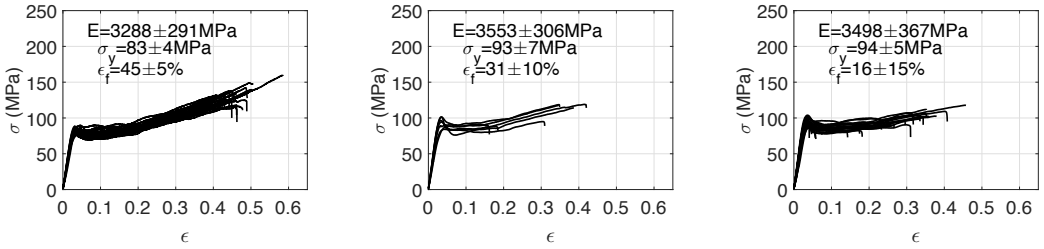

(a) Non-radiated (b) 25kGy (c) 50kGy

Figure 6.31: Stress-strain curves for sequential biaxially strained PLLA tubes sterilized with γ-radiation at 25kGY 6.31(b) and 50kGy 6.31(c). 6.31(a) shows non-radiated PLLA as a reference. All tubes were tested in the circumferential direction

Table 6.7: Mechanical properties of sequential biaxially strained PLLA tubes before and after γ- or EO sterilization

	E (MPa)	σ_y (MPa)	σ_{max}(MPa)	ϵ_f%
Unsterilized	3288±291	83±4	128±13	45±5
25kGy	3553±306	93±7	106±14	31±10
50kGy	3498±367	94±5	99±8	16±15

Table 6.8: Thermal properties of sequential biaxially strained PLLA tubes before and after γ-sterilization. DSC scans can found be in Appendix D.3 Figure D.5

	T_g (°C)	T_{cc}(°C)	T_m(°C)	X_c%	Aging area (J)
Unsterilized biaxially strained	64±1	-	150±1	33±1	-
Unsterilized extruded tube	61±1	119±1	157±1	1±0	3±0
25kGy extruded	62±0	129±1	156±0	1±1	2±0
50kGy extruded	60±0	122±2	158±1	1±1	4±1
25kGy biaxially strained	62±0	-	154±0	38±2	4±1
50kGy biaxially strained	64±0	127±2	156±2	36±0	-

6.4.2.2 Heat treatment and EO sterilization of PLLA

The prototypes in this project were thermally set above T_g and below the T_{cc} to scaled to an appropriate IVC filter diameter. The first heating temperature was 63°C for 5 min. The second temperature was 93°C at which the laser cut tube could be further expanded to 27 mm and a stent cell height of 12 mm. The T_g increased from 63°C to 67°C upon heat treatment, while decreasing the X_c from 32-33% to 26-27% (Table 6.9), if cooled fast. At this temperature, no further crystallization takes place during subsequent sterilization or annealing, regardless of fast cooling or slow cooling. However, the mechanical properties were greatly influenced by the thermal treatment.

Table 6.9: Thermal properties of sequential biaxially strained PLLA tubes before and after EO sterilization in combination with or without heat treatment. DSC scans can be found in Appendix D.3 Figure D.6

	T_g (°C)	T_{cc}(°C)	T_m(°C)	X_c%
Unsterilized	64±1	-	150±1	33±1
63°C, 93°C, rapid cooling	66±1	-	153±0	27±1
63°C, 93°C, slow cooling	67±0	-	152±0	30±1
63°C, 93°C, 53°C 8h	68±1	118±3	153±0	27±2
53°C 8h	67±0	-	152±0	30±3
EO 38°C	66±0	-	152±-	31±2
EO 53°C	69±0	-	152±-	32±1
EO 53°C, 63°C, 93°C	67±0	-	153±0	29±0
EO 38°C, (63°C, 93°C)	67±1	110±1	152±-	26±0

From Figure 6.32 it can be seen that both the σ_y and the elastic modulus are significantly reduced. Subsequently annealing the material at a temperature below T_g for 8 hours, restores the properties, but still to a value lower than prior to annealing. The regain is not related to an increase in crystallinity nor changes in T_g. It appears that the higher the temperature, the more rearrangement of the molecular chains and higher modulus and σ_y. Adding moisture, as occurred during EO sterilization does not change the properties significantly. Heating the material reduces crystallinity and at the same time, the ϵ_b increases at 40°C. Increasing the temperature and adding moisture reduces the elongation. From Figure 6.33 is it clear that sterilization at a low temperature for 8 hours does not change the modulus or σ_y significantly, but the ϵ_b is increased significantly. Heat treatment up to 93°C first allows the

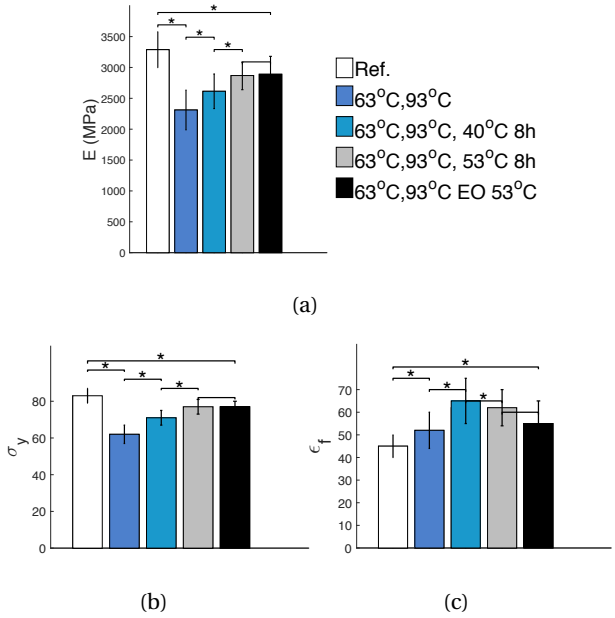

Figure 6.32: Elastic modulus, σ_y and ϵ_b for sequential biaxially strained tubes, which have undergone heat treatment and annealing for 8h at either 40 or 53°C or sterilized by EO at 53°C. *p≤0.05 and signifies if their means are significant different. No * means that they are non significantly different

molecular chains to relax from the strained position during biaxial straining. Some memory of the strained position might be expressed as the polymer is annealed and the properties slowly return to the level before sterilization, heat treatment or annealing. The presence of moisture at this temperature has no effect on the recovery of the chain alignment. If the heat treatment has not been applied, the annealing does not change the position of the chains, and the mechanical stiffness and strength remain unchanged. It can, therefore, be said that the moisture and annealing at low temperature can only change the position of the molecular chains if they have been previously thermally treated and lost their orientation. The sequential biaxial straining, therefore, locks the molecular chains in an aligned position, which can only be relaxed when annealing above T_g. It is expected that upon EO sterilization the both the σ_y and the elastic modulus are reduced ([102]). There is a significant increase in modulus and σ_y when increasing the sterilization temperature. There is no significant difference in modulus or ϵ_b when adding moisture as a part of the sterilization process, a significant difference in σ_y.

Prior to sterilization the expanded tubes (1.0;3.2) showed a crystallinity of 33% and that

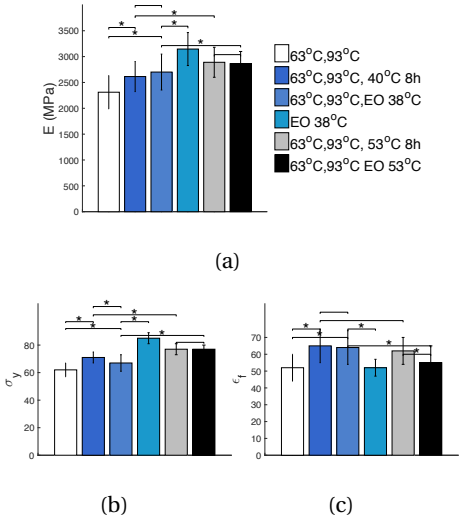

Figure 6.33: Elastic modulus, σ_y and ϵ_b for sequential biaxially strained tubes, which have undergone heat treatment and annealing for 8h at either 40 or 53°C or sterilized by EO at 38°C. and *p≤0.05 signifies if their means are significant different. No * means that they are non significantly different

after heat treatment was lowered to 27%. When exposed to cold sterilization at 38°C the crystallinity remained constant (26%). The T_g went from 64°C to 68°C and after sterilization was to 67-69°C depending on temperature and the presence of humidity. Heating the material appears to reduce the crystalline domain and the energy to achieve chain mobility is more. It was unexpected that the low sterilization temperature caused lower crystallinity.

Both heat treating and sterilization at 53°C increase the T_g, whether it occurs with rapid cooling or slow cooling. To reduce the crystallinity when quenching below T_g the spray cooling was used. There is still a slight increase in T_g and T_m, but the X_c differs. It appears that thermal treatment brings the polymer to a disordered state or melts the smaller crystals so that the X_c is reduced to 30%. Rapid cooling was done with the freeze spray, which is a mixture of flourocarbons (80-95% Norfluran and 5-10% dimethylether)[104] (Kema FS-35A, ITW Spraytec Nordic), which cools small objects down to -35°C and evaporate completely and is not miscible to the PLLA[105]. The rapid cooling done with freeze spray has more of an impact on X_c which is reduced to 27%. It is a possibility that heat treatment melts the smaller crystals, and if cooled slowly, some crystals are formed again. From the thermal characterization of sequential biaxially strained tubes in section 6.3 it is known that annealing 100°C and below does not change the crystallinity, and it is not likely that new crystals

are formed during heat treatment. Cooling after heat treatment also has an effect on the mechanical properties as well. As with annealing, heat treating the material for a shorter period (5 min at 93°C) reduces the values of the mechanical properties by a 1/3. Cooling at room temperature proved to sustain the stiffness and strength better than rapid cooling with freeze spray. Upon cooling at room temperature (slow cooling) the axial elastic modulus is reduced by 11%, the σ_y by 14%, the UTS by 15%, while the ϵ_b increased by 6%. The circumferential elastic modulus is reduced by 6%, the σ_y by 9%, the UTS by 13%, while the ϵ_b increased by 42%. Rapid cooling resulted in a reduction of an axial elastic modulus, σ_y and UTS by 10-11%, but the ϵ_b increased by 3%. The circumferential elastic modulus is reduced by 16%, the σ_y by 19%, the UTS by 13%, but the ϵ_b increase by 25%. The rapid cooling reduced the elastic modulus, and σ_y circumferentially by 22-24% and increased the ϵ_b by 50%. Thermal properties did not change regardless of cooling method. Regardless of cooling rate, the ϵ_b increased after heat treatment.

Annealing the polymer for 8 hours (equivalent time frame to sterilization) close to T_g increase T_g slightly, but reduces the overall crystallinity. It is possible that relaxation or aging occurs during this time frame. EO sterilization close to T_g, increases the T_g of the polymer even further, but the crystallinity remains constant. If EO sterilization temperature is lowered, the effect of the moisture from the process is less predominant. EO sterilization alone did not change the crystallinity of the polymer.

Thickness after EO sterilization Heat treatment of the laser cut stents at 63 and 93 ° for 5 min, increases the thickness from 10.5±0.6 to 12.4±0.7 mm (see Appendix D.5 Figure D.8). Heat treating the specimens at 53°C for 8 hours, reduced the thickness of the tubes to 8.4±1.1 mm. After sterilization, the thickness was 12.0±0.4 mm. The heat and the sterilization will thereby make the specimens shrink in the axial direction and leaving the specimens thicker circumferentially. As for the rings cut from tubes, the laser cut stent also increased in wall thickness after sterilization (Figure 6.34). Furthermore, the increased thickness showed more variation along the tube after sterilization than before. It is possible that the strained tube did not have a uniformly distribution of stretched chains and therefore some shrink more than others. The variation seems higher for prototypes made from a tube with a low degree of axial strain (0.3;2.2) than (0.6;2.4).

The biaxially strained tubes are very sensitive to temperatures above 90°C in the sense that both the mechanical properties and the thermal properties change with temperature.

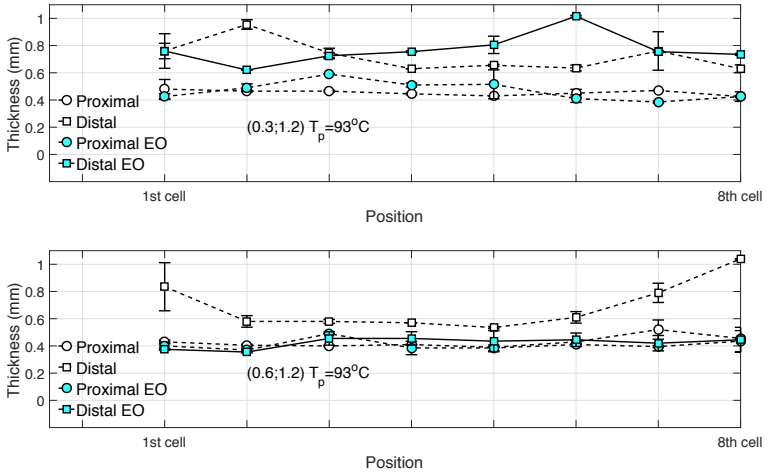

Figure 6.34: Wall thickness of stent cells circumferential measured at the most distal and proximal end of a laser cut stent-base before and after sterilization

Exposure to both humidity and higher temperature, whether it is body temperature or close to T_g, it being short term (8 hours) or over an extended period (2 weeks), the conditions are favorable enough for the molecular chains to move. The chain which was ordered as crystals, become less ordered and reduce the crystallinity.

6.5 Storage and physical aging

Physical aging is both relevant during storage of the extruded tubes, the sequential biaxially strained tubes and the final sterilized device. It also becomes relevant when implanted in the body. During processing the polymer is quenched below T_g and molecular mobility slows down and is unable to reach equilibrium. Storage or implantation close to T_g will cause the polymer to move toward an equilibrium state, which as described below influences the properties of the material. It is unknown if and how the amorphous chains, which have undergone biaxial strain, would behave during aging. Therefore during storage of sequential biaxially strained tubes were kept under vacuum in air under ambient conditions, at 37°C in air, water or bovine serum. Below is a short description of the aging phenomenon and the expected changes as described in section6.5.1. Further down in section 6.5.3 are the results from this project shown and discussed. In comparison, the results on the aging of the extruded PLLA is shown and discussed in section 6.5.2.

6.5.1 Background on physical aging

Physical aging is a phenomenon which can occur when PLLA is quenched from the melt and the polymer chains are in a non-equilibrium glassy state, where mobility is low. Despite the short distance in which the molecules can move in this state, they rearrange to a degree which drives toward a thermodynamic equilibrium. The closer to the T_g the faster the aging or relaxation or put in another way, the greater the ability is to eliminate excess free volume [95]. Aging causes rearrangement of the polymer chains, which affects the mechanical properties[106]. The rate of relaxation and rearrangement of the polymer chains are therefore dependent on how close the aging temperature is to T_g.

In terms of mechanical properties, the elongation of annealed, yet unaged PLLA has been reported to undergo necking during tensile testing. Ductility and flexibility increased the ϵ_b 300% of its original length. The ϵ_b is significantly reduced as a result of aging, yet an increase in stiffness and strength is observed[106].

When PLLA is quenched from rubber state above T_g the polymer chains become 'frozen' and segmental mobility is greatly reduced along with a reduction in the free volume (the space in which the polymer chains can move freely). The T_g is, therefore, dependent on the free volume of the system. Due to the reduced segmental mobility, the system requires more energy to finish morphological rearrangement occurring during glass transition and as a result of the T_g increase. During aging the slow mobility over time, causes chain relaxation and reduction in free volume. Furthermore aged PLLA during DSC scan will show a smaller enthalpy and potential energy and more energy is required for the T_g as seen by the increase of the area of endothermic peak [106]. It has previously been shown that the longer the aging, the larger the endothermic peak will occur on a DSC scan as well as the area during T_g . Any small peak at the end of the endothermic peak is possibly due to energy consumed by a crystalline domain developed during quenching[106].

When the polymer chains are oriented, as in tensile deformation, the free volume, and potential energy increase. The potential energy is related to the required energy to ensure yielding upon deformation. In unaged, nearly amorphous PLLA, there is a larger free volume and strain is more easily transferred through the disordered arranged polymer chains during tensile deformation. The material is more flexible and tough[106]. It is expected that for any of the aged samples, the ϵ_b and stiffness increase. As most of the experiments in this study are done on sequential biaxially strained tubes, where the polymer chains are thought to

be oriented, and not the quenched amorphous PLLA, it is unsure if the same apply during aging of such.

6.5.2 Results on storage of extruded tubes

The extruded tube in itself appears to have undergone some aging as seen previously in Figure 4.6.

During initial stages of the project, an interesting observation regarding tube expansion was made. The expansion process becomes difficult if the tube has been kept in a moist environment in advance. The normal procedure for expansion of for example polyethylene tube for balloon expansion is kept in a moist environment. Straining of extruded PLLA tubes previously kept in a moist environment, using the same processing parameters as on dry tubes, the tubes are punctured when air pressure is applied. It is possible that the tubes experienced some form of aging. It was previously reported that when the extruded tubes were kept in a moist environment between 13 and 97 % humidity at room temperature, the T_g is reduced from 63 to 59°C whereas it increased to 67°C when raising the temperature to 37°C. Additionally, the endothermic peak was shifted to higher temperatures as well as an increase in its area. Despite that fact that aging most likely is only related to the amorphous domains, the T_{cc} and its onset is reduced to 122°C from 129 °C, when exposed to moisture[13]. The temperature window for inducing crystallinity is bigger for samples with moisture content. The effect is less apparent on tubes kept at room temperature in a moist environment. The storage is important before straining PLLA.

6.5.3 Results on storage of sequential biaxially strained tubes

The sequential biaxially strained tubes were kept in a dry environment with and without the presence of moisture and in water or bovine serum (Statens Serum Institut, Denmark) at 37°C. From Table 6.10 it appears that moisture and temperature have little effect on the endothermal aging peak during glass transition. Instead, it appears that it is the temperature, which causes the increase in T_g. Diffusion and water uptake occur instantly and not only start the degradation by hydrolysis but can also lead to recrystallization. As previously mentioned water acts as a plasticizer and lowers the T_g. However keeping the tubes in water or bovine serum at 37°C increases the T_g (Table 6.10) and keeps the crystallinity constant. This is in accordance with the fact that a polymer with a high X_c reduces the affect of plasticizers, as it is not able to separate the molecules in the crystalline structure. The diffusion

of water molecules to the bulk are limited to the amorphous domain and is restricted by the crystalline domain. Permeability depends on the solubility and diffusion, which are both reduced by the crystallinity[90].

It has previously been shown that over the course of nearly 2 weeks the presence of water at 37 °C changes the mass about 1% for the extruded tube, with a small reduction is M_w from 1.85 to 1.74kg/mol[13]. It was reported that the T_g for the extruded tube aged for 2 weeks in water, increased by 2°C. For the sequential biaxially strained tube in this project, the increase was as large as 6°C . In both instances, the water does not act as a plasticizer. Interestingly it has previously been reported that in water at ambient temperature, the T_g is reduced and the water acts a plasticizer[13], but this is not seen for sequential biaxially strained tubes. Increasing the temperature increases the T_g further, which was unexpected compared to the results of the extruded tubes. It is unlikely that increasing the temperature restricts the chance for water molecules to get in between the polymer chains. However, the higher temperature might enhance chain mobility and order them in a fashion that does not allow the water molecules to separate the chains. In terms of mechanical properties, the only significant increase in stiffness and strength and reduction in ϵ_b was observed after two weeks at 37°C, regardless of the presence of fluids. This could not be explained by an increase in crystallinity, which remained constant regardless of conditions. Aging close to T_g would change the density of the amorphous chains and ultimately reduce the T_g. If aging is defined by an increase in enthalpy release during DSC scan, aging could not be detected at ambient conditions.

Table 6.10: Thermal properties of sequential biaxially strained PLLA tubes stored in water at 37° and vacuum at ambient temperature and in air at ambient conditions for 2 weeks. All tubes were sequential biaxially strained (1.0;3.2). The DSC scans are summarized in Figure D.7 in Appendix D.3. Raw data collected from [15]

	T_g (°C)	T_{cc}(°C)	T_m(°C)	X_c(%)	ΔH_{aged}
Reference tube	64±0	-	152±0	32±2	
In air (1.0;3.2)	65±0	-	152±0	30±3	1±0.1
In vacuum (1.0;3.2)	65±0	-	152±0	28±1	0.3±0.1
In 37°C (1.0;3.2)	68±1	-	152±0	31±1	1.1±0.1
In 37°C water (1.0;3.2)	69±0	-	152±0	30±2	1.1±0.3
In 37°C serum (1.0;3.2)	68±1	-	152±0	30±1	1.1±0.1

It was previously seen that there is no significant difference in stiffness between samples kept in a dry environment and in serum at 37°C for two weeks. There was a significant difference in σ_y both at body temperature and additionally when kept in serum (see Table 6.11). The UTS was unaffected by the fluids, and the significance lies within raising the temperature to 37°C. This is in agreement with the constant X_c. There is no significance in endothermic enthalpy during the glass transition (see Table6.10), except for tubes kept in vacuum, which is significantly lower than for the rest of the tubes. Whether it is due to an error, or the vacuum prevents the aging from happening is unknown. Had the material become more brittle as a result of changes in crystallinity over the course of two weeks, the specimens would have been more likely to fracture.

Table 6.11: Mechanical properties of simultaneous biaxially strained PLLA tubes at aged in at 37°*C* in serum or under dry conditions. All tubes were strained to (1.0;3.2) at 73°C

	E_{axial} (MPa)	$\sigma_{y,ax}$ (MPa)	UTS_{ax} (MPa)	$\epsilon_{f,ax}$ (%)	E_{circ} (MPa)	$\sigma_{y,circ}$ (MPa)	UTS_{circ} (MPa)	$\epsilon_{f,circ}$ (%)
(1.0;3.2)	3021±355	80±5	80±5	39±28	3578±332	74±7	117±15	50±8
(1.0;3.2) 37°C	3226±131	87±4	87±4	33±21	3714±375	79±7	109±12	48±6
(1.0;3.2) Serum 37°C	3111±229	87±6	87±6	34±24	3650±285	81±6	104±10	45±4

Aging was taken one step further as sequential biaxially strained tubes, were stored in vacuum for 8 and 18 months. The crystallinity was reduced as a function of aging, whereas the aging caused the T_g to increase. The area of the endothermic glass transition peak was three times higher than after sequential biaxial straining. Unfortunately, the mechanical properties after aging were not evaluated. In conclusion storage at ambient conditions in a vacuum is not enough to slow down the aging of the material and the rate of which it occurs seems to be related to the aging temperature. Therefore it is possible that the device must be stored at lower temperatures to avoid the aging. Figure 6.35 showed that the T_g of strained induced tubes increased over the course of 8-18 months. The thermal properties are summarized in Table 6.12. The crystallinity remained constant and showed that the amorphous chains were not subjected to degradation, and it is expected that the storage of sequential biaxially strained tubes was sufficient under vacuum. The sequential biaxially strained

tubes underwent aging over the course of the first 8 months, by an increase in endothermic enthalpy from the system (see Figure 6.35), which increase by a 3-4 fold. The aging is then suppressed, and no further change is detected after 18 months. It is a concern that the amorphous chains possible relax during this period and no longer are the primary source of stiffness and strength to the system. Changes in the mechanical properties, including the radial force of an aged stent-base, was not confirmed.

Table 6.12: Thermal properties of aged sequential biaxially strained 16.5Fr tubes stored under vacuum at ambient temperature for 8 and 18 months. All tubes were strained to (0.2;1.2) at 73°C

	T_g	1^{st} T_m	2^{nd} T_m	X_c	ΔH_{aged}
Extruded reference	59±0	110±1	153±0	29±1	-0.4±0
Aged for 8 months in vacuum	63±2	117±2	152±1	27±1	-1.7±0
Aged for 18 months in vacuum	63±0	111±2	152±1	28±3	-1.7±0.4

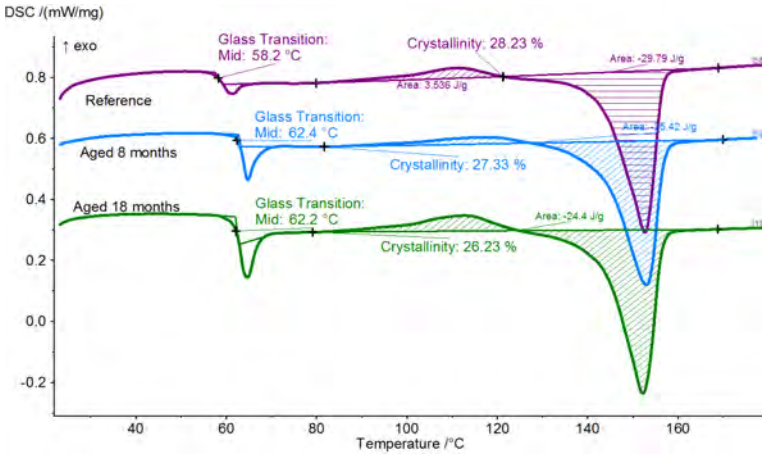

Figure 6.35: DSC scan for 16.5Fr tubes which have been aged at ambient temperature under vacuum for 0, 8 and 18 months. All tubes were strained to (0.2;1.2) at 73°C

It appears that laser cutting and heat treatment reduced the crystallinity, which was not seen to such extend for heat treated tubes in section 6.4.2.2. Furthermore, the crystallinity was reduced after two weeks implantation to merely 15%. The effect of aging is very slow at ambient temperature, compared to body temperature. The T_g increased by 4-5°C after 2 weeks, regardless of being explanted prototypes or under physiological conditions in vitro for two weeks (see Figure 6.36).

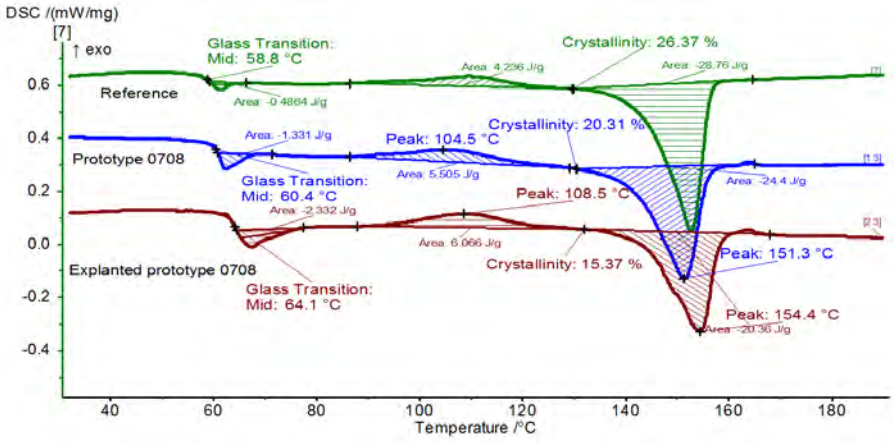

Figure 6.36: DSC scans for sequential biaxially strained tubes (0.2;1.2) at T_p=73°C, as tubes and filter prototype 0708 before and after implantation for 2 weeks

7

Analysis: Prototypes

This chapter includes the main prototypes made from expanded PLLA tubes which have been tested before reaching the final prototype used in the in vivo study. Below is an overview of the concepts relevant in this project.

7.1 Laser cutting

The laser cutting was performed at MeKo (Germany), but the type of laser used in this case is unknown and kept confidential by the vendor. It is expected that laser cutting increases the molecular weight (M_w) by 8%, which was seen when using a CO_2 -laser[41]. Additionally, laser cutting could potentially change the crystallinity locally in some polymers, but it is not expected to change the crystallinity for PLLA[41]. The tubes used in this study whether 10.2Fr or 16.5Fr have on an average between different lots a M_w =1.95±4kg/mol between different lots after extrusion. Laser cutting and heat treatment first at 63°C and secondly at 93°C for 5 min, respectively, did not affect the M_w significantly (see Appendix D.4 Table D.3).

7.2 Concepts

Ideas on the filter or stent-base concepts were not a part of the scope of the project, but evaluation of them was and is described in section 8.

7.2.1 Concept03

The filter concept was cut from a biaxially strained tube with 9.5 mm in diameter in a parallel z-stent configuration (Figure 7.2). It was primarily used to investigate flipping of filtra-

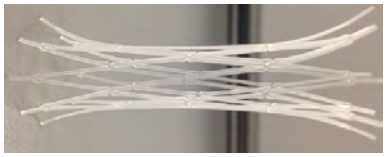

Figure 7.1: An example of a laser cut stent-base design after the initial heat treatment at 63°C

tion struts after heat-treatment of the material (80°C for 5 min). Two different versions of the concept were made, one with 0.25 mm strut cut from a tube (0.2;1.6) with A_{exp}=233%. Another with a 0.75 mm strut was cut from a tube (0.5;1.9) with A_{exp}=263% and was heat treated and scaled up to 15.5 mm in diameter. The stability of the stents was poor in both concept configurations, but primarily the one with 0.25 mm strut, despite it having a thickness of 0.23 mm as opposed to the 0.75 mm struts, which had a thickness of 0.14 mm. The main reason for the instability is the end (apices) of the stents, which are free of the z-stent in parallel. The low wall thickness in relation to strut width of these filters contributed to instability. Usually, stability would be obtained by an appropriate relationship between strut width and thickness.

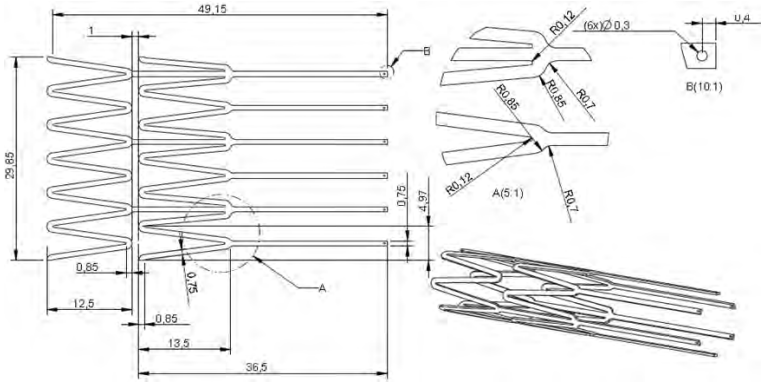

Figure 7.2: Drawing of Concept03 with a 0.75 mm strut width

7.2.2 Concept05

To ensure more stability Concept05 was developed as a diamond shape stent-base configuration and up-scaled to 25 mm during heat treatment. Additionally, three filtration struts were placed at the end of the stent-base, and the remaining three free diamond ends were cut in a Y-fork (zone B on Figure 7.3). In the Y-fork, it is then possible to mount different co-polymers for example PCL together with PLLA to create more elastic filtration struts with

a better shape memory. The stent-base proved to be fragile and fractured in zone C in Figure 7.3. It was seen that first heat treating the stent-base just above T_g for 5-10 min would release stresses within the material causing the apices to point outwards (see Figure 7.4(a)) and additional heating to 95 °C reduced the stresses further. The apices pointing outward could facilitate the flipability of the struts.

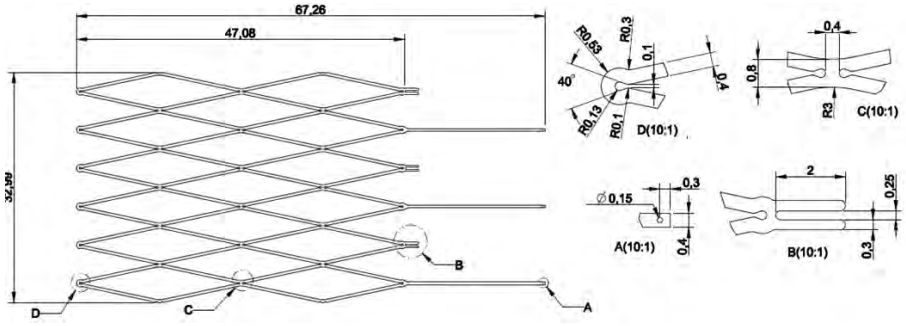

Figure 7.3: Drawing of Concept05

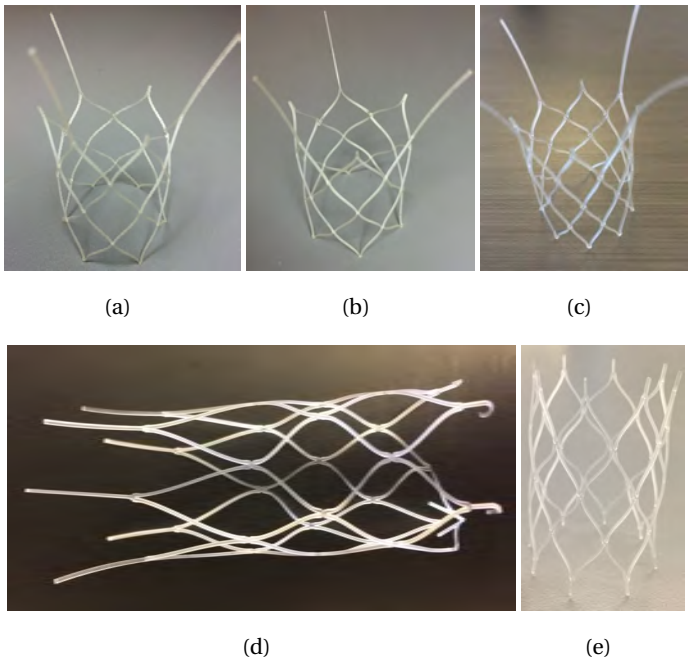

Figure 7.4: Concept05 (see 7.4(a)), Concept0606 (see 7.4(b)) with 6, Concept0608 with 8 cells (see 7.4(c)), Concept0706 (see 7.4(d)) and Concept0708 (see 7.4(e))

7.2.3 Concept0606 and Concept0608

Concept0606 was made to improve stability and integrity of the stent-base further. The apices still had a 40° angle, while the C zone also called the connection point between two cells was widened horizontally and narrowed longitudinally. It was done to ensure a more stress-free opening of the cells. The filtration struts were shortened to make a parabolic shape of the filtration struts when connected as opposed to a sharp conical shape. The concept was made with both 6 circumferential cells (Concept 0606) or 8 circumferential cells (Concept 0608)(see Figure 7.5). When cut from the same tube and heat treated to the same diameter the 8 cell concept would have a smaller cell height.

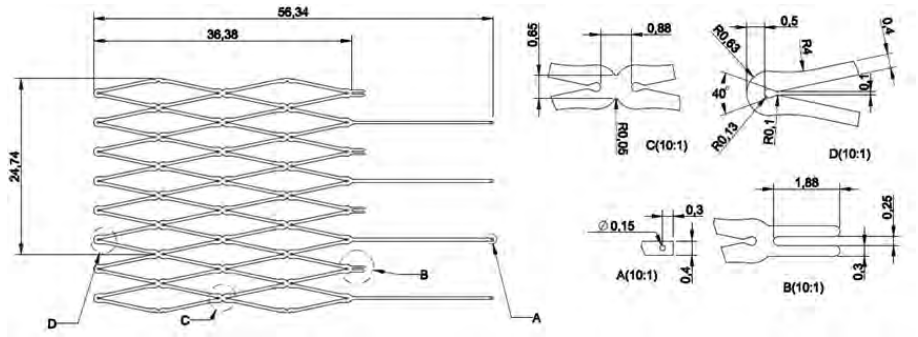

Figure 7.5: Drawing of Concept0608 with 8 cells

7.2.4 Concept0708

Concept 0706 (Figure 7.6(a)) was developed with a wider cell and 6 cells circumferential to ensure asymmetric circumferential cells in the filtering section. Less spacing was made between the 6 struts and point inwards as opposed to outwards. Hooks and filtration struts were added. During implantation, the main concern was risk of migration and therefore the cells were scaled to the equivalent size with 8 cells circumferentially to ensure better radial force in Concept0708 (Figure 7.6(b)). The results of the two concepts are shown in section 8. After heat treatment, the filtration struts pointed outwards, which would help reduce the risk of migration. The hooks and filtration struts were removed for simplicity, and the apices were elongated 4 mm forming smaller end struts. These struts were then cut at an angle to sharpen them with the intend of anchoring the vessel wall and reduced risk of migration. The filter with 6 cells, in general, showed less radial force what with 8 cells. To ensure radiopacity two gold markers were shown onto the prototypes with suture.

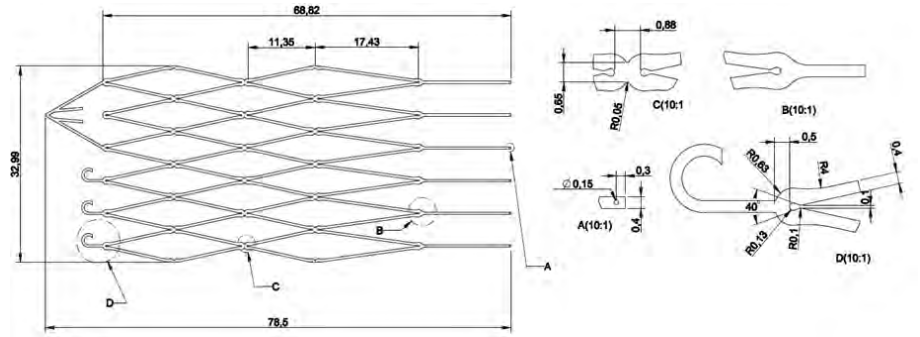

(a)

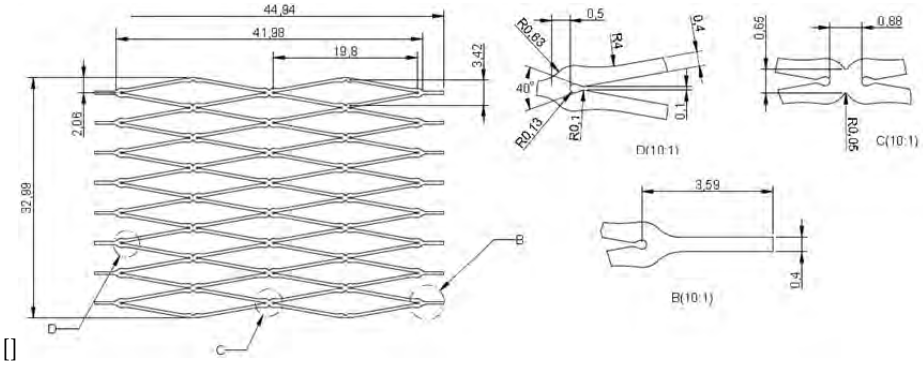

[]

Figure 7.6: Drawing of Concept0706 with either 6 (see 7.6(a)) and Concept0708 with 8 cells scaled (see 7.6(b))

8

In vitro results

This chapter reflects on the in vitro investigations done prior to the in vivo study in Chapter 9. It includes both design based on monofilaments and the expanded PLLA tubes and reflections on the best possible design and process parameters found most favorable in vitro. It was seen that it is possible to create a filter based on oriented PLLA monofilament, but the idea of a self-expandable stent-base made from a strained tube was more favorable. Therefore the following section mostly describes the in vitro finding of filters and stent-bases made from tubing. From the previous findings on choice of processing parameters, such as processing strain rate ($\dot{\epsilon_p}$), total area expansion (A_{exp}), axial and radial processing strain degrees (ϵ_a and ϵ_r) and processing stain temperature (T_p), a few were selected and tried in different designs in vitro.

8.1 Flipability

The concept behind the bioabsorbable filter in this project was based on a conversion from a fully-functional filter, which opens up and converts into a stent-base. The filtration struts and stent-base are then most likely embedded in tissue along the caval wall after which they will degrade. This conversion must not occur before the risk of thromboembolism has passed. The time frame of which the filter is functional depends on the mechanism holding the filtration struts centered in place. Initial steps in investigating if PLLA the ability to convert from a filter to a stent-base lies in the resistance to permanent deformation over time and the likelihood of returning to its original shape after heat treatment. The Concept03, as shown in Figure 7.2 works as a filter, when the filter struts were pinned together by suture.

Before pinning the distance between the struts was 15 mm. The in vitro test of the two filters with different strut diameter (0.25 and 0.75 mm) and thickness (0.23 and 0.14 mm), showed the ability of the filtration struts to move towards its original position in the course of 7 days. The filtration struts were bonded together with a thin piece of monofilament and kept in a tube with phosphate buffered solution (PBS) (see Figure 8.1(a)) for first 14 days at ambient temperature after which the monofilament was cut open. At release, the thinner strut filter opened up 27% and opened up further to 53% of its original diameter at day 24. The same was seen for the filter with thicker struts. However the result was less promising. The filter opened up 13% upon release and 20% after day 24.

(a) (b) (c) (d)

Figure 8.1: Concept03 with a 0.25mm strut cut 8.1(a) and a 0.75mm strut 8.1(b) before immersion in PBS. Figure 8.1(c) show concept at 14 days in PBS after which the conversion mechanism was triggered and Figure 8.1(d) show the concept after further 14 days

Despite these initial results, the strut flipping ability could be diminished by relaxation over a longer period of time, inadequate shape memory, proteins attachment or neointima cell coverage at the transition between filtration strut and the stent-base. It is unknown which forces apply to the stented vein in vivo as well as the tissue response to the PLLA device in veins. The latter was examined in the animal study described in section 9.

8.2 Crimping and delivery options

From a procedural perspective, there are limitations on the size of delivery sheath during implantation. A modified 16Fr Flexor Introducer Sheath (Cook Medical) was used. As the stent-base was loaded into the sheath, it was crimped down to just below 6 mm. Figure 8.2

loading of the stent-base into the sheath. To mimic the result of such delivery on the integrity of the device, the stent-base was crimped to 6 mm multiple times in a compression station (Figure 8.3). It is clear from Figure 8.4(a) shows that the first crimp reduces the diameter from the pre-set diameter of 27 mm to 24 mm. The stent-base should therefore not be used in IVC with a diameter close to 27 mm. It should be noted that the deviation is very low between the two samples. As the crimping continues the diameter change reaches a plateau and additional crimping does not reduce the diameter further, and the stent-base should not be used in a vein of diameters above this plateau. The safeness of the stent-base was only evaluated in vivo in veins up to 19 mm in diameter. The stent-base was able to regain its initial expanded diameter of 27 mm when heated to 93°C after crimping. It shows that heat treatment provided the stent-base with shape memory at 93°C. As seen from Figure 8.4(a) the first step of the heat treatment at 63°C was not enough to make the stent-base unfold. This subsequent treatment experiment was not repeated for multiple stent-bases and is only an indication of the shape memory created at heat treatment, but not further investigated.

Figure 8.2: Loading of stent-base in delivery sheath

(a) (b)

Figure 8.3: Crimping of stent-base in compression station

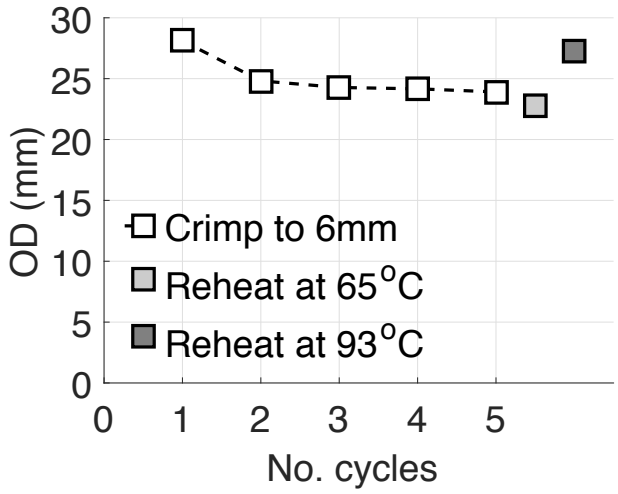

(a)

Figure 8.4: Outer diameter (OD) of the stent-base after 5 times of crimping (n=2). Subsequently the stent-base was then first heated to 63°C for 5 min and then at 93°C for 5 min

8.3 Radial force of stent-bases

8.3.1 Braided filter from oriented PLLA

A filter was braided from the oriented PLLA monofilament (OD 0.36mm) from Zeus (see Figure 8.5) with the diameter of 28mm, stent-base with 40 mm in length (A) and filter cone with the length (B) 28 mm. The filter was heat treated at 85°C for 20 min. After radial force measurement, the filter was permanently elongated to A=96 mm and 25 mm in diameter. After slowly reheating the filter showed a tendency to retract to its original length and diameter. The first cycle of the radial force test (Figure 8.6), showed uneven crimping of the stent-base, but an even crimping at the second and third cycle. There is little difference between the second and the third cycle. The monofilament would after heating between 80 and 90°C exhibit a modulus (4.9-5.7 GPa) and UTS (338-350 MPa) far beyond what has been obtained for a sequential biaxially strained PLLA tubes (4 GPa). The maximal radial force of the braided stent when crimped down to 6 mm was less than 9 N and in a 15 mm vein, the filter would exert a radial force of 1.0 N. In comparison the Concept0708 PLLA stent-base of straine PLLA implanted in the animal study exerted a radial force of 2.3 N when crimped to 15 mm (discussed later in Figure 8.8(b)).

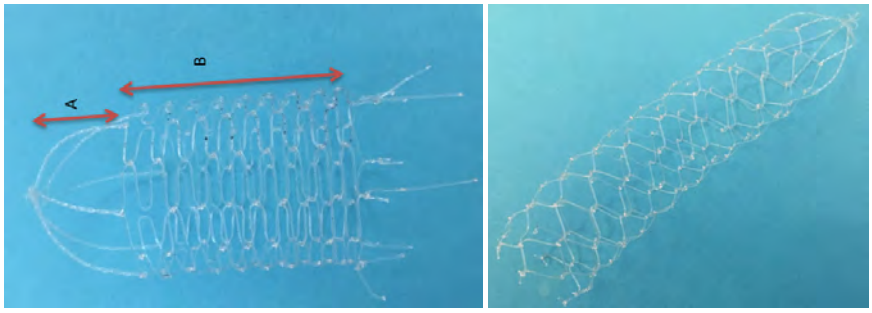

(a) (b)

Figure 8.5: Braided filter made from oriented PLLA (Zeus) before and after crimping to 6 mm

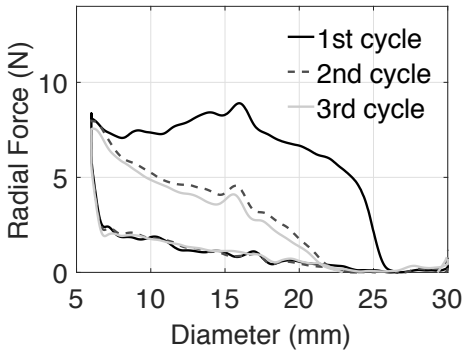

Figure 8.6: Radial force of braided filter from PLLA oriented (Zeus) crimped from 30 mm to 6 mm

8.3.2 Radial force of stent-bases from strained tubes

8.3.2.1 The influence of number circumferential cells

The Concept0606 showed less radial force (Figure 8.7(a)) than Concept0608 (Figure 8.7(b)). Concept0606 showed an even lower radial force at maximal crimping (6 mm) than the braided PLLA sent (Figure 8.6). Both Concept0606 and 0608 showed a radial force in a 15 mm diameter vein of nearly 2 N and therefore perform somewhat better than the braided stent. The initial diameters for Concept0606 and 0608 were 25.3 and 25.5 mm and after three cycles of crimping were down to 20.5 and 22.3 mm. Therefore such devices, should not be used in IVC with diameters above that. The concept with 8 cells provided a larger radial force at each crimp, but the radial force a stent-base exerts on the wall (the bottom part of a cyclic curve during the unloading), is no different than for a stent-base with 6 cells. In general, the stent-bases cut from strained tubes, showed a greater radial force as they open up upon

uncrimping. Their ability to stay in place in the vein could be greater during compression and un-compression by the vein.

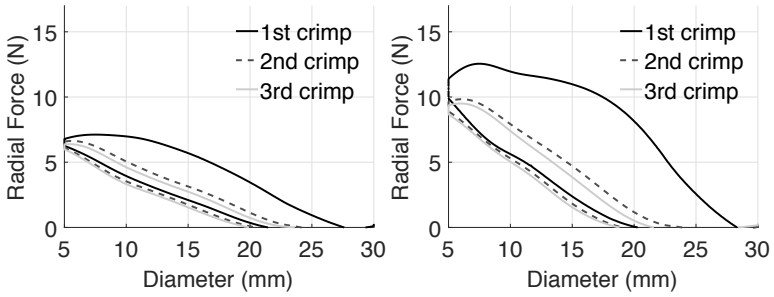

(a) (b)

Figure 8.7: Radial force of Concept0606 (8.7(a)) and Concept 0608 (8.7(b)) when crimped from original OD to 6 mm

8.3.2.2 The influence of processing temperature and strain degree

The mechanical properties for tubes tensile tested circumferentially improved as a function of T_p. This phenomenon is also seen for the final stent-base device, which showed a higher radial force at the first time of crimping at T_p=93°C than T_p=73 °C. It was also seen that the larger the axial strain during processing, the more permanent deformation is detected at the second cycle. From the radial force measurement, it is shown that stents made from tubes (0.3;1.2) strained at T_p=93 °C recover after 3 crimping cycles (Figure 8.8). During the first step of heat treatment (T=63°C) the (0.6;1.4, T_p=93 °C) stent-base coiled up (Figure 8.9(a)). It appears as if the stress build up during the axial strain is released. Despite the additional heat treatment at 93°C the shape remained so. The loss in integrity causes an uneven crimping of the stent-base, which is unfavorable during loading of the device. As for the (0.3;1.2,T_p=93 °C) more integrity of the device is kept during heat treatment, but integrity is best kept for the (0.3;1.2, T_p = 73 °C) stent-base. The tubing used for (0.6;1.4, T_p=93 °C) came out slightly thinner, and the resultant radial force would, therefore, be less.

8.3.2.3 EO sterilized stent-bases

Figure 8.10 shows that for both (0.3;1.2) strained at 73 and 93 °C, EO sterilization at 53 °C for 8 hours increase the radial force of the material. This corresponds well to that fact that the elastic modulus as well as σ_y increased after sterilization for the sequential biaxially

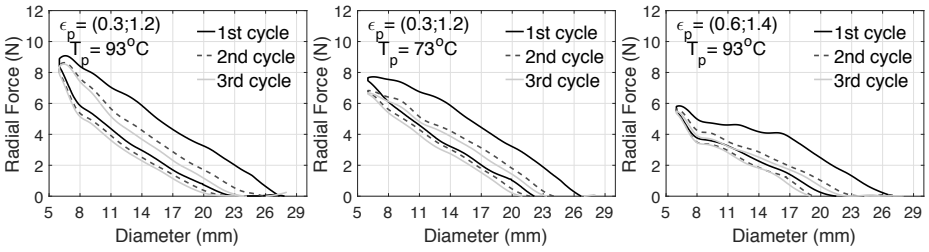

(a) (b) (c)

Figure 8.8: Radial force of Concept0708 from sequential biaxially strained tubes at two different T_p and at (ϵ_a;ϵ_r)

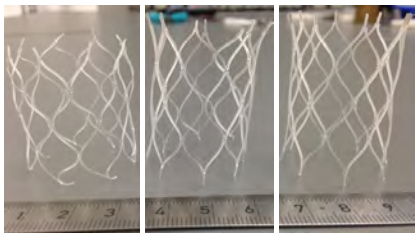

(a) (b) (c)

Figure 8.9: Concept 0708 processed at different T_p and (ϵ_a,ϵ_r) after which they were heat sat at 93 °C. 8.9(a) and 8.9(b) were strained at 93°C with a (ϵ_a,ϵ_r) of (0.6;1.4) and (0.3;1.2) respectively. 8.9(c) was strained at 73°C with a (ϵ_a,ϵ_r) of (0.6;1.4)

strained tubes. It is a rather small increase for T_p at 73°C. Tubes with a larger axial strain (0.6;1.2) strained at 93 °C showed a greater radial force (Figure 8.10(b)) than its counter part with a smaller axial strain (Figure 8.10(c)). Sterilization of tubes with a larger axial strain showed a greater radial force before sterilization. Sterilization did not induce a greater radial force as seen for tubes with an initial smaller axial strain. The axial strain determines if the chains can gain mobility and become ordered during 8 hours of sterilization. For this reason (0.6;1.4), were not used for further animal testing.

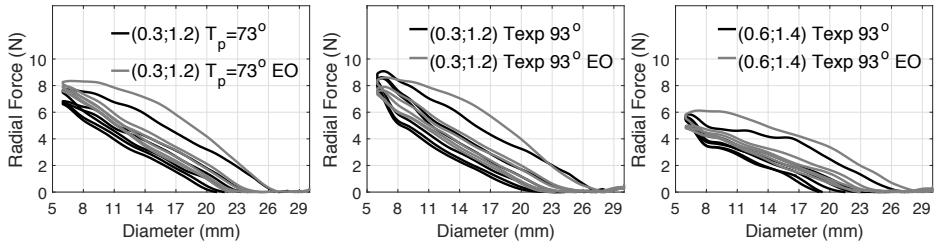

(a) (b) (c)

Figure 8.10: Radial force of Concept0708 from sequential biaxially strained tubes at two different T_p and at (ϵ_a;ϵ_r) before and after EO-sterilization.

8.4 Fatigue properties

The diameter of an IVC is influenced by the respiratory cycle, and the external stresses applied onto the vein by organs. Some IVC filters placed today, does not allow the collapse of the IVC, whereas others do, depending on their radial force. A polymeric IVC filter will have inferior properties compared to metals and will most likely not prevent the vein from collapsing. It will be compressed with the vein, which appears more natural than keeping the IVC open at all times. A device which is under continuous cyclic loading will, therefore, need excellent fatigue properties to withstand the cyclic loading. An investigation of fatigue properties were modeled by finite element analysis as described in section 8.4.1 for Concept 0708 stent-base made from strained PLLA with a wall thickness of both 0.8 and 0.4 mm and evaluated by cyclic flat-plate compression as described in section 8.4.3.

8.4.1 Finite element analysis (FEA)

Finite element analysis (FEA) was done in order to identify at which point of interest the stent-base was most likely to fracture. The analysis was supplied from Cook Research Inc. by Shuo Yang (CAE analyst).

FEA was used to investigate stress distributions under compression throughout the geometry of the stent-base and their displacement, and where fractures were likely to occur. The UTS was set to 100 MPa and wall thickness to 0.4 or 0.8 mm. Under normal conditions, the collapse index (CI) or compression degree on the vena cava has been reported between 20-35% [27]. CI is defined by the diameter upon expiration minus the minimal diameter on inspiration divided by the diameter on expiration. For the calculation, a vena cava diameter

of 15 mm was assumed with a compression to 9.8 mm and CI was set to 35%. The compression model was a flat-plate station, representing an open and compressed state of the stented vein (Figure 8.11(a)). There was no real difference between the model for the difference in wall thickness. The analysis showed that the stent-base is most likely to fracture in the middle of the device indicated by the red zones and near the connection points (Figure 8.11(b)).

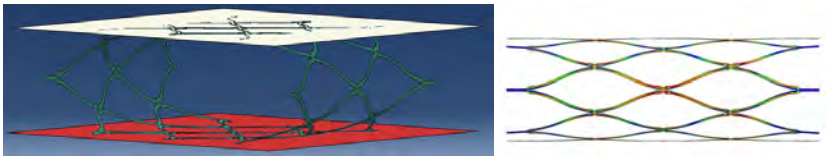

(a) (b)

Figure 8.11: Finite element analysis (FEA) of Concept0708 in a flat-plate compression model. Figure 8.11(a) shows the stent-base compressed between the plates representing the collapsed state. Figure 8.11(b) shows the side of the stent-base not in contact with the plates and where, the most stressed zones (red) are presented.

8.4.2 Cyclic testing of single-cells

Test specimens consisting of a single stent cell were laser cut from the same tube as their corresponding filter design, Concept0608 and 0708.

8.4.2.1 The influence of post-processing parameters and sterilization

After the first initial 10-15 cycles, the area underneath the load-extension curve increased for some specimens, showing a large degree of noise. Figure 8.12(a) showed that the lager cell width in Concept0708 ensures that the material is relaxed slightly quicker than in Concept0608 and energy to compress the cell is reduced with the first five cycles. More variation is seen for Concept0608 but on average preforms better than Concept0708. Heat treatment for the permanent set should not be done at temperatures too close to T_{cc}, but seemed to be beneficial for up to 15 min (Figure 8.12(b)). The influence of EO sterilization at 53°C proved to reduce the resistance to compression slightly faster than the non-sterilized specimens (Figures 8.12(c)), which was not in accordance with the radial force of stent-bases after EO sterilization. It also showed slightly more influence on the specimens which were made from sequential biaxially strained tubes at higher axial strains. The limitation of the

method is the large variation between test specimens. In retrospect, the stent-base could benefit from the Concept0608, which both showed a higher radial force than Concept0708 and proved to resist permanent deformation slightly better on single cell testing.

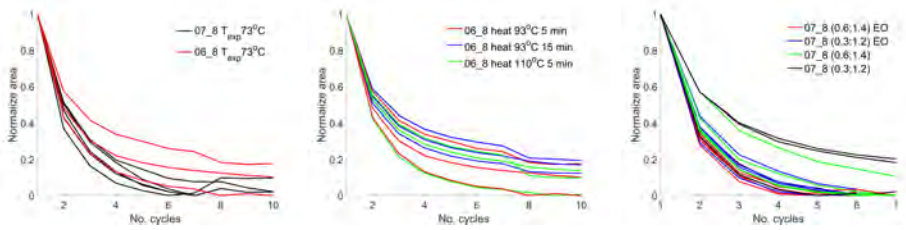

(a) (b) (c)

Figure 8.12: The are underneath the load-extension curve for single-cell specimens under cyclic compression to 50% their initial height. The influence of a wider cell (8.12(a)), where 0708 has the widest. The influence of heat treatment temperature and duration for low and high T_p (8.12(b)). The influence of EO sterilization (8.12(c)) on tubes with a high or low degree of axial strain during sequential biaxial strain at T_p 93 °. An example of teh load extension curve can be found in Appendix D.6 in Figure D.9

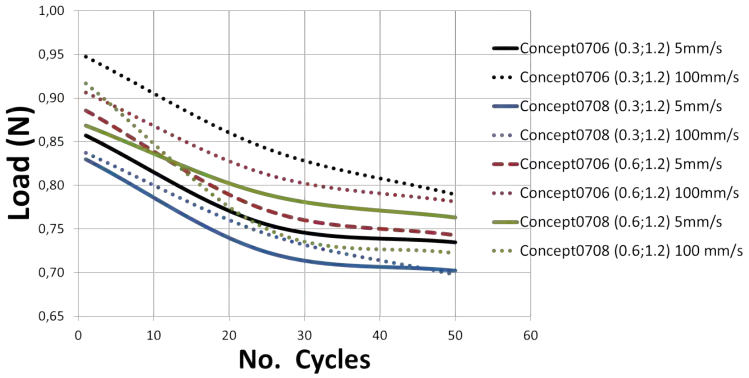

Figure 8.13: Cyclic compression of single stent cells processed at different $\dot{\epsilon_p}$, ether 5 mm/s or 100 mm/s and different (ϵ_a;ϵ_r). Raw data provided by [14]

The width of single stent cells, the degree of axial strain (ϵ_a) and the axial processing strain rate ($\dot{\epsilon_p}$) was previously investigated using the same material and expansion technique[14]. The test was performed on single stent cells from Concept 0706 with a cell width of 24 mm, whereas Concept0708 had a width of 21 mm and were compressed 50% of its original cell height for 50 cycles. The greatest compressional force is seen for the wider cell width at high

axial processing strain rate $\dot{\epsilon_p}$ (Figure 8.13). The trend is less apparent for the shorter cell width, and the investigation would have benefited from several samples in stead of just one, as portrayed in [14]. The ϵ_a has more affect on the wider cell width regardless of$\dot{\epsilon_p}$. The results were in alignment with what was seen in this project, where the circumferential tensile stiffness and strength (Table 6.3) and for the radial force of stent-bases (Figure 8.8) benefits from lesser ϵ_a as well as a high $\dot{\epsilon_p}$.

It has previously been shown that single stent cells made from the same tubing and processing parameters fracture in the same regions (connection points) as the stent-base[15] at ambient and physiological conditions. For that reason, one could argue that single stent cell is a good model for the whole stent-base (see Figure 8.14). During a static compression setup in water, the single stent cells would deform and fracture sooner than in ambient conditions[15]. The result was unexpected as the stent-base which in one instance showed fractures at ambient conditions at the connection point, but it never fractured under physiological conditions (described in section 8.4.3). The presence of water is therefore not optimal unless at body temperature.

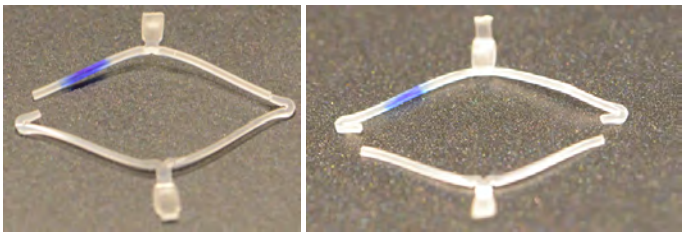

(a) (b)

Figure 8.14: Fractured single stent cell after cyclic testing for ≥4000 cycles under ambient and physiological conditions. Used from [15]

8.4.3 Cyclic testing of stent-bases

Concept06 Concept0606 with 6 cell was the first device to be tested in a hard silicone tube (3.7 mm thickness) which fractured after less than 150.000 compressions of 30% of initial OD (see Figure 8.15(a)). For this reason, the concept was made with 08 cells instead, which also showed a higher radial force.

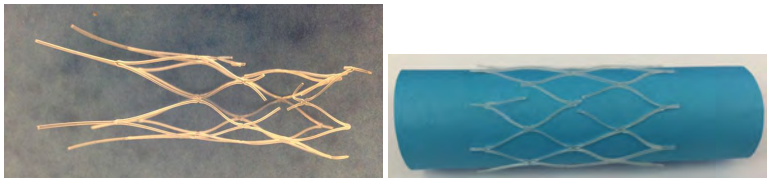

(a) (b)

Figure 8.15: Fractured Concept0606 and Concept0708 after cyclic compression in dry conditions.

Concept0708 The diameter after delivering the stent-base using a 6 mm sheath went from 27.2 mm to 24.2 mm (see Figure 8.16(a)). Cyclic compression 150.000 times in water at 37 °C in a soft silicon tube (OD=19 mm, t=0.45 mm) the stent-base was slightly elliptical with a diameter of 19.2 and 23.2 mm (see Figure 8.16(b)). When testing under ambient conditions, the stent-base fractured in multiple places (see Figure 8.15(b)) and therefore the water and rise in temperature softens the material. This was in disagreement with single stent cells tested under the same conditions[15].

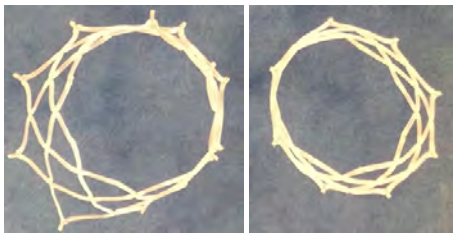

(a) (b)

Figure 8.16: Concept0708 with 8 cells before (8.16(a)) and after (8.16(b)) cyclic compression 150.000 times. Both stent-base were compressed previously in a 6 mm sheath.

Stents cut from tubes at different strain ratio (ϵ_a;ϵ_r) not only influenced the radial force, but also the permanent set under cyclic testing as seen in Figure 8.17. The (0.3;1.2, T_p=93 °C) stent-base had an initial OD of 21.8 mm after radial force testing, after which it underwent 150,000 times compression (30%) resulting in an elliptical form (Figure 8.17(c)) and the final OD was 23.3 and 19.63 mm. The (0.3;1.2, T_p=93°C) had similar initial OD of 21.1 mm, which was transformed into 24.1 and 18.5 mm and therefore slightly more susceptible to permanent set (Figure 8.17(b)). This is in correlation with its poorer radial force as well. (0.3;1.2 T_p=73°C had a slightly larger OD initially (23.6 mm) after radial force testing, but

behaved similar to (0.3;1.2, T_p=93°C) with a final OD of 24.1 and 18.7 mm.

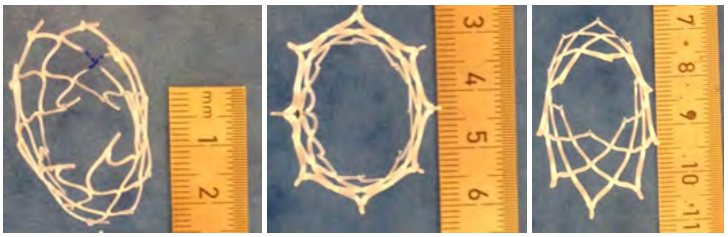

(a) (b) (c)

Figure 8.17: Concept07 with 8 cell after cyclic compression 150.000 times in water. Figure 8.17(c) was sequential biaxially strained at T_p=73 °C at the strain ratio of (0.3;1.2). Figure 8.17(b) and 8.17(a) T_p= 93 °C at the strain ratio of (0.3;1.2) and (0.6;1.4) respectively.

8.5 Implantation ex vivo

Figure 8.18: Concept0708 placed in swine IVC ex vivo.

To determine the risk of migration during implantation, the stent-bases were delivered in swine cavas ex vivo. The swine cavae diameter ranged between range 18-23 mm and therefore in the range, where this particular stent-base after sterilization is possible to use. The stent-base was successfully deployed, and it was not possible to push or pull the stent-base from the deployment site. From Figure 8.18 it was seen that the stent-base over-expands the vessel limiting the risk of migration.

From the above findings, it was seen that Concept0608 and Concept0708 were possible designs to continue with in the in vivo study. In terms of processing, a high ϵ_a was not preferable, as tension was built up in the material and heat treatment made the stent-base

coil up. It also appeared that the $\dot{\epsilon_p}$ must be high in order to obtain the highest compression resistance and in coherence with section 6.2.7, wherein it was seen that the higher the $\dot{\epsilon_p}$ the greater the stiffness and strength. Additionally, the highest radial force would be seen at T_p closer to T_g instead of close to T_{cc}. Sterilization was shown not to have a negative effect on the radial force of the stent-base.

9

In vivo

In the attempt to evaluate the selected material and prototype as well as the fabrication methods an animal study on three sheep was performed July-August 2015 at the Veterinarian School of Purdue University (West Lafayette, Indiana, USA) in collaboration with Cook Research Inc.

Objective Firstly, the main objective was to characterize the tissue response to a PLLA stent-base in the veins. Secondly, the goal was to determine how long such a device must hold radial force and withstand permanent deformation under cyclic stress before loosing its strength. Thirdly the goal was to evaluate device integrity after implantation.

9.1 Summery of animal study and protocol

The study was set up to run over the course of 8 weeks, with termination points after 2, 4 and 8 weeks. The study was terminated earlier than expected due to loss of device integrity (multiple fractures of the stent-base). Therefore the investigation of the mechanical performance of a diamond shaped self-expandable bioabsorbable PLLA stent-based in vivo was evaluated after 2 and 3½ weeks. The sequential biaxially strained PLLA tube (0.3;1.2) was obtained using the parameter shown in Table E.1 in Appendix E. The tube was laser cut as Concept0708 and thermally expanded to 27 mm to accommodate larger vessel sizes. After sterilization and loading, the stent had an OD of 24 mm. During the procedure, radiography was used to identify device location at implantation, interim and termination points, whereas venogram was used to evaluate vessel patency after implantation and at termination points. Venograms were only used at implantation and before termination to protect

the animal from overexposure to contrast media. Histology of explants was conducted at 2 and 3½ weeks to evaluate tissue response using hematoxylin and eosin stain (H&E) staining as well as fluorescent antibody staining.

(a) (b)

Figure 9.1: Crimping of stent-base before (9.1(a)) and after (9.1(b))with stent crimper (Qualcrimp) from Edwards Lifesciences

9.1.1 Implantation

To load the stent into the delivery sheath, a portable stent crimper was used rather than loading it by hand. Despite successful loading and implantation during the proof of concept two months prior in two sheep and in vitro, unexpectedly loading appeared difficult at the time of the animal study. Table 9.1 show that the stent-bases used for this study, unfortunately, showed a much larger thickness variation from top to bottom than previously seen for 16.5Fr tubes (see Figure 6.34). It was not possible to determine why the batch of tubes strained for the animal study showed a larger variation. During loading of the first three devices, fractures occurred during loading with a stent crimper, which was unable to crimp the whole stent at a time. Due to this uneven loading and the variation in thickness along the stent-base, it fractured at the place of most stress near a connection point. None of the fractured stent-bases were used in the animal study. To prevent the remaining stent-bases from fracturing, they were heated in 37°C saline prior to loading after which no fractures occurred. This also corresponds to what was seen with the in vitro cyclic compression where water and rise in temperature prevented it from fracturing. It is however not ideal that the material is that sensitive to temperature. To minimize the risk of fracture during uneven loading into the sheath the stent was slowly crimped using a crimping station (Figure9.1) and loaded into the sheath with the thickest end first.

Prior to implantation the diameters of the vena cava were measured in right and left anterior oblique, RAO and LAO, and anterior-posterior projection (AP) for determination of implantation site. The vein sizes before and after implantation, where the stents were approximately placed are listed in Table 9.1. Three adult sheep at the ages of 1-3 years were used for the study. Anesthesia was applied using isoflurane (1-5%) by intubation and 100-300 IU/kg of heparin was administered intravenously to avoid clotting. Vein access was obtained by a cut-down of the jugular vein, and a 16F sheath was introduced. One stent was placed above, and one stent was placed below the renal veins in the IVC of each animal. After implantation position and vessel diameter was confirmed by radiography (see Table 9.1).

9.2 Article: Evaluation of a bioabsorbable self-expandable vein stent-base made of Poly(L-lactide) in vitro and in vivo

An overall evaluation of the outcome of the animal study is written in article 'Evaluation of a bioabsorbable self-expandable vein stent-base made of Poly(L-lactide) in vitro and in vivo' in this section (9.2). It does not contain all results based on the animal study. Further details on implantation and follow-up and tissue response by H&E and confocal imaging are found in section 9.1.1, 9.2.2 and histology 9.3 below.

The Figures and Tables are listed towards the end of the article starting with Figure 1 and Table 1.

For full manuscript follow the Link:

Title: Evaluation of a bioabsorbable self-expandable vein stent-base made of Poly(L-lactide) in vitro and in vivo

Authors: Alexandra Liv Vest Løvdal[a], Sarah Calve[b], Shuo Yang[c], William Van Alstine[c], Christoph A. Binkert[d], Kasper Klausen[e]

[a] Technical University of Denmark, Department of Micro- and Nanotechnology. Ørsteds Plads, 345E, 2800 Kongens Lyngby, Denmark

[b] Purdue University, Weldon School of Biomedical Engineering, 206 S. Martin Jischke Drive, West Lafayette, IN 47907-2032, USA

[c] Cook Research Incorporated. 1 Geddes Way, West Lafayette, IN 47906, USA.

[d] Kantonsspital Winterthur, Institut für Radiologie, Brauerstrasse 15, 8401 Winterthur, Schweiz

[e] William Cook Europe, Sandet 6, 4632 Bjæverskov, Denmark

Corresponding author:

Alexandra Liv Vest Løvdal, *Technical University of Denmark, Department of Micro- and Nanotechnology. Ørsteds Plads, 345E, 2800 Kongens Lyngby, Denmark, email: alvlo@nanotech.dtu.dk. Mobile: +45 21246043*

Manuscript type: Laboratory Investigation

Funding: This study was funded by the Ministry of Higher Education and Science

Main text: 2395 words (max 2400)

Abstract

Purpose: This study was designed to evaluate performance and tissue response to a mechanically improved self-expandable bioabsorbable stent-base in vitro and in vivo.

Methods: A diamond-shaped stent-base (OD=24mm, L=50mm) was cut from a sequential biaxial strained poly(L-lactide) (PLLA) tube for optimized performance. The performance of the stent-base was evaluated in a finite element analysis and attempted validated in vitro through a cyclic flat-plate compression and radial force measurement. The performance of the stent-base was tested in vivo using 3 sheep with 2 implants each for 2 and 3½ weeks.

Results: In vitro the stent-base showed an elliptical deformation but no fractures. In vivo the stent-base showed adequate radial force and no migration. All implanted stent-bases showed multiple fractures not only at the predicted stress zones but at all connecting points. Fragments of the caudal stayed in the vein wall indicating sufficient tissue coverage to avoid embolization of the fractured stent pieces, whereas fragments from the cranial device were few. Neointima formation was confirmed on histology at 2 and 3½ weeks.

Conclusion: A bioabsorbable self-expandable stent-base made from PLLA for large veins seems feasible however over time the PLLA used in this study appears too stiff and lacks the sufficient flexibility to move with the vena cava causing multiple fractures.

Keywords: self-expandable, IVC filter, bioabsorbable, PLLA, poly-(L-lactide)

Introduction

Permanent metal devices, such as the inferior vena cava (IVC) filter, have been implanted on numerous occasions in the prevention of pulmonary embolism [1-3]. Long-term complications such as vena cava are perforation, migration and reoccurring deep vein thrombosis (DVT) [1] can be avoided using an IVC temporary filter. Retrieval rates of implanted filters can be as low as 21% [4]. To overcome the complications related to the retrieval procedure, the need for a fully bioabsorbable IVC filter becomes of interest. The previous attempt to create a bioabsorbable filter include using the bioabsorbable polycaprolactone (PCL), an elastomer, as a stent-base with an outer diameter (OD) of 18mm for an IVC filter base and poly(L-lactide-co-glycolide) as bioabsorbable filter cone, however their device resulted in migration[5]. Another IVC filter was made of polydiaxone (OD=20mm), a suture which exhibits good mechanical properties for 35 days without migration; however, the device was not self-expandable [6].

Previous work on bioabsorbable stents focused on balloon-expandable designs with a diameter (OD = 3-10mm) [7-14]. These were only for arterial indications and therefore not applicable for large size veins [15]. Poly(L-lactide) (PLLA) is prominent bioabsorbable polymer, which has been widely investigated in medical applications and as a candidate for a bioabsorbable IVC filter [16,17]. It has also been used in the BVS vascular stent (Abbott Vascular, Santa Clara, CA) and the Igaki-Tamai stent (Igaki Medical Planning Company, Kyoto, Japan, [12,18].

Self-expanding stents require an adequate radial force (RF) to maintain its position in the lumen with no migration and must have resistance to permanent deformation [7]. Stents made from PLLA have inferior mechanical properties to those of metals and both radial force and resistance to a permanent deformation is low. PLLA can however be induced to have a greater stiffness, and provide greater resistance towards permanent deformation by straining the polymer above its glass temperature and thereby aligning its molecular chains [19-21]. The scope of this study was to evaluate the performance of PLLA used as a self-expandable PLLA stent-base (outer diameter = 24mm) in an IVC filter in vitro and in vivo.

Materials and methods:

Stent material and design

A PLLA stent was made from sequential biaxial straining (SEQ) previously described [22] using PLLA 2003D tubes (NatureWorks LLC, Minnetonka, MN) and expanded from 5.5 to 10.5mm. The tube was laser cut in a diamond-shape pattern (8 cells circumferentially) (Fig. 1) and thermally expanded to 27mm and sterilized with ethylene oxide. To ensure visibility under x-ray gold markers were sutured on the stent.

Cyclic compression and radial force (RF)

Finite element analysis (FEA) was used to investigate stress distributions under a parallel flat-plate compression mimicking load from organs and the diaphragm on the vena cava. Ultimate tensile stress (UTS) was set to 100MPa [23] and wall thickness to 0.8mm. Under normal conditions, the collapse index (CI) or compression degree on the vena cava has been reported between 20-35% [24]. CI is defined by the diameter upon expiration minus the minimal diameter on inspiration divided by the diameter on expiration. For the calculation, a vena cava diameter of 15.0mm was assumed with a compression to 9.8 mm and CI was set to 35%.

For in-vivo testing the stent was placed into a silicone tube (OD=19mm, 0.46mm wall thickness) in water at 37°C and compressed (30%) using a moving flat-plate for 150,000 cycles, corresponding to 21,600-28,800 breaths per day [25]. The RF measurement was done in air at 37°C using an automated radial force tester from an expanded state to 6mm at a rate of 0.5mm/sec three times.

Animal study

Three adult sheep (1-3 years of age) were used as the animal model. Intubation anesthesia was applied using isoflurane (1-5%)(ca 1.5−2.5 L/min). A cut-down on the jugular vein was used for access and a 16F sheath was introduced into which 100-300 IU/kg of heparin was administered. One stent above and one stent below the renal veins were implanted into the IVC of each animal. Diameters of the vena cava were measured in right anterior (RAO) and left anterior (LAO) projection before and after stent implantation and listed in Table 1. Accurate placement and vein patency were confirmed by venography. Additional venography was performed 2 weeks after implant.

At 1 week and 2 weeks post implant, interim radiography without contrast was performed to evaluate the stent position. One animal was sacrificed after 2 weeks and 2 animals after 3½ week. The vena cava was perfusion fixated using buffered 10% formalin solution before harvesting. The fixed specimens were then examined with MRI to evaluate the integrity of the stents.

Tissue examination:

Half of each explant with the stented vein was embedded in paraffin using routine techniques, cut at 5µm, and stained with haematoxylin and eosin (H&E). The other half was used for confocal imaging. For optimal confocal imaging the explanted tissue was cleared to ensure greater visibility by incubating the tissue in solutions of gradually increasing fructose concentration [26]. D-(-)-fructose (JT Baker, Center Valley, PA) was dissolved in milliQ water with 0.5% α-thioglycerol (Sigma-Aldrich St. Louis, MO) at various concentrations (20, 40, 60, 80, 100% wt/vol and 115% wt/wt) as described previously [27], where explanted tissues were incubated in each solution for 12-24 hours under gentle rocking.

For antibody staining, the fixed tissue was rinsed in phosphate buffered saline (PBS) blocked with 10% donkey serum in 0.2% bovine serum albumin (BSA) and permeabilized with 0.2% TritonX-100 overnight. Tissue was incubated with a primary antibody against fibrinogen (1:100, Abcam, ab 119948), diluted in 0.2% BSA and PBS, for 2 days at 4°C then rinsed 3x30min. Samples were next stained with secondary labeling reagents for nuclei (DAPI, 1:500, LifeTechnologies), actin filaments (AF488 conjugated phalloidin, 1:100 LifeTechnologies), and AF555-conjugated anti-mouse secondary antibody (1:500, LifeTechnologies) for 2 days at 4^{o}C, then rinsed 3x30 minutes and stored at 4^{o}C until imaged.

To increase the optical resolution and the contrast of the probe, a spatial pinhole was placed at the confocal plane of the lens to eliminate out-of-focus light. Tissue samples were imaged with an inverted confocal laser microscope (710 LMS, Zeiss, Germany) with laser wavelengths from 405 to 639nm. Images were obtained as 1024x1024 pixels with ZEN 2011 software and taken as a best compromise between overlaid laser wavelengths.

Results:

Radial force and fatigue testing

The RF was highest after the first crimp and reduced slightly during the second and third crimp (Fig. 3). The stent in the physiological procedure would be crimped into the loading sheath (16Fr) and self-expand into the vessel of a given size. In the in vivo study, the average diameter was approximately 15-16mm and the stent would, therefore, exert an RF of approx. 2.8N on the vessel.

The fatigue performance of the stent was evaluated by a flat-plate crush analysis, both theoretically by finite element analysis (FEA) and in vitro. The FEA results (Fig.2) show that the critical fatigue locations are found at the connection-points on the side of the stent during compression. The critical fatigue locations in the red zone would be expected to fracture first, if physiological loading exceeds the capabilities of the newly-deployed stent. Neither crimping nor flat-plate compression in vitro demonstrated a fracture of the stent.

During crimping the stent was permanently deformed from 28 to 24mm after being circumferentially compressed into a 16Fr sheath while maintaining its circular shape (Table 2). During compression, the stent deformed permanently from circular to elliptical. This is due to the fact that water or physiological fluids acts as a plasticizer and ultimately makes the polymer stent softer and more susceptible to a permanent set [28].

Imaging

The gold markers were at the same location in all animals after implantation, at 1 week and after 2 weeks. The position of the gold markers confirmed a stable position of the stent without migration. Venogram confirmed patency after 2 weeks (1 animal). The vena cava diameter was smaller than before implantation and was likely due to different positioning of the animal and could not be used to determine the integrity of the device. MRI images of explants after 2 weeks illustrated numerous fractures which were visually confirmed by light microscopy. A representative section of the vein had 13 fractures (see Fig. 4a) after 2 weeks and similar section had 18 fractures (see Fig. 4b) after 3½ weeks. The fractures occurred at the connection-points and between cells adherent to each other. The cranial devices at both time points were minimally intact and only a few pieces remained at the site of implantation, whereas the fractured caudal devices remained in the vessel.

Histology

After 2 and 3½ weeks the struts were closely apposed to the lumen surface and were covered by neointima with a thickness of 20-100μm and 100-300μm, respectively (Fig. 5). The neointima was composed of loosely-arranged spindle-shaped cells and fibrovascular tissue with some fibrin. At 2 weeks some struts were covered with a single cell layer of endothelium, and after 3½ weeks most struts were covered with neointima and endothelium. At both time points, inflammation was minimal and composed of a few macrophages immediately adjacent the struts and few lymphocytes in the adjacent neointima. At the attachment sites between struts, vein wall smooth muscle cells were minimally vacuolated, suggesting mild focal pressure change.

Confocal imaging

Confocal imaging was used to visualize the newly formed tissue around the connection-points without disrupting the tissue. It has the advantages of visualizing both the strut surface facing the lumen and the sides of the strut covered with neointima. The images showed cellular ingrowth around and in the connection-points by either neointima nuclei (blue) or actin-filament (green) (Fig. 6). Fibrinogen (red) covers both the struts in (Fig. 6a and b) and connection-points (Fig. 6c). The neointima around a strut that has fractured at the connection-point measured between 70 μm (top of the strut) and 120μm (on the right side) (Fig. 6a). The actin-filaments occur only in the top cell layer (40-66μm) on the sides and are aligned along the strut. At the fracture tip of the strut, the actin-filaments are randomly oriented.

Discussion

One of the major concerns regarding a bioabsorbable polymeric IVC filter is the risk of migration, which has been detected previously [5]. It was hypothesized that a stent-base for an IVC filter can be made from PLLA tubing, which has undergone an SEQ process above glass transition. It would exhibit enough strength to prevent migration, yet flexible enough to withstand continuous cyclic compression from the vein. The stent-base was successfully crimped and delivered to vena cava with no migration upon implantation. Over the course of 3½ weeks, the RF was found adequate to prevent device migration. In vitro test findings predicted that the stent-base would become soft in vivo due to cyclic compression at the physiological conditions and become permanently deformed. Due to lack of device integrity, it was not confirmed if the stent-base was elliptical in vivo instead of circular.

The overall inflammation response to the PLLA stent was minimal. Both H&E and confocal imaging showed fewer smooth muscle cells in the vein wall under the stent suggesting a mild focal fibrosis due to the oversized stent and resultant focal compression. Confocal imaging made it possible to visualize the tissue coverage around and in the

connection-points, which was not possible to determine by H&E. The vessel diameter ranged at implantation from 14-19mm and therefore some stents were stressed more than others. However, the number of fractures within a stent did not correlate to the vessel diameter pre-implantation and post-implantation. Caudal devices were best more intact in the smaller vessel than the cranial devices.

Though in vitro tests did not reveal any fracture of the stent-base, MRI and light microscopy confirmed that multiple fractures occurred at those sites where FEA predicted to be critical. Without the device being intact, it would not be as stressed in the same nature as the FEA prediction and no additional fractures were expected. Additionally, the device continued to fracture circumferentially at every connection-point. The fractures of the caudal device likely occurred after tissue coverage adequately covered the stent.

PLLA is a brittle polymer and this particular stent-base is not flexible enough to move with the vena when the connection-points are covered in tissue, leading to multiple device fractures. For a stent to successfully survive cyclic compression it would have to be made more flexible, but still induce enough radial force to avoid migration.

Conclusion

A bioabsorbable self-expandable stent-base made from PLLA tube was successfully delivered in an ovine vena cava. The tissue response and radial force were found adequate to prevent device migration. However after two weeks, the explants had multiple circumferential fractures in the specific locations predicted by the FEA. The tissue response did not cause vessel narrowing and was sufficient to lock the stent in place. This particular PLLA stent-base did not have the flexibility to move with the vessel after tissue coverage. The locked circumferential stent cells fractured resulting in stent failure.

Ethical approval: All applicable international, national, and/or institutional guidelines for the care and use of animals were followed.

Conflict of interest: Studied sponsored by William Cook Europe as a part of the Industrial PhD Program.

References

[1] Imberti D, Ageno W. Dentali F, Donadini M, Mandredini R, Gallerani M. J Thromb Thrombolysis 2012;33: 258-266

[2] Keeling AN, Kinney TB, Lee MJ. Eur Radiol. 2008; 18: 1556-1568

[3] Fox M, Kahn SR. J Vasc Inverv Radial. 2008; 19: 981-985

[4] Antevil JL, Sise MJ, Sack DI, Sasadeusz KJ, Swanson SM, Rivera L, Lome BR, Weingarten SSK, J Trauma Injury Infect Crit Care J. 2006; 60:35– 40

[5] Zhang F, Hailei L, Liang G, Zhang H. Asian J Surgery. 2015; xx: 1-5

[6] Eggers MD, McArthurt MJ, Figueira TA, Abdelsalam ME, Dixon KP, Pageon LR, Wallace MJ, Huang SY. J Vasc Surg Venous Lymphat Disord. 2015;3:409-420.

[7] Nuutinen J, Clerc C, Törmälä P. J Biomater Sci Polymer Edn. 2003;14: 667-687

[8] Hayman D, Bergsson C, Miller S, Moreno M, Moore JE. J Biomech Eng. 2014; 136: 1-9

[9] Wlech TR, Eberhart RC, Reisch J, Chuong C. Cardiovasc Eng Technol. 2014; 5: 270-280

[10] Vaazjanen A, Nuutinen J, Isotalo T, Törmälä P, Tammela TLJ, Talja M. J Urol. 2003; 169: 1171-1174

[11] Wu Y, Shen L, Wang Q, Ge L, Xie J, Hu X. A Sun, j Qian, J Ge. J Biomed Biotechnol. 2012; 1-8

[12] Ormiston JA, Serruys PW. Circ Cardiovasc Intervent. 2009; 2: 255-260

[13] Ginsberg G, Shah J, Carty A, Kaufmann C, Nuutinen J, Törmäla P. Gastrointest Endosc. 2003; 58:777-784

[14] Mario CD, Borgia F. EuroIntervention Supp. 2009; 5: 103-108

[15] Thomas SD, Ofri A, Tang T, Englund R. Int J Surg Case Rep. 2014; 5: 59–62

[16] Lasprilla AJR, Martinez GAR, Lunelli BH, Jardini AL, Filho RM. Biotechnol. Adv. 2012; 30:321-328

[17] Nair LS, Laurencin CT. Prog Polym Sci. 2007; 32: 762-798

[18] Van Ditzhuijzen NS, Karanosos A, Van der Sijde JN, Van Soest G, Regar E. Bioabsorbable stent. In: Jang I,

[19] Ou X, Cakmak M. Polym. 2010; 51: 783–792

[20] Tsai C, Wu R, Cheng H, Li S, Siao Y, Kong D, Jang G. Polym Degrb Stab. 2010; 95: 1292-1298

[21] Wu J, Yen M, Wu C, Li C and Kuo MC. J Polym Environ. 2013; 21: 303-311

[22] Løvdal A , Andreasen JW, Mikkelsen LP, Agersted K, Almdal K. Polym Int. 2016; 65: 133–141

[23] K. Lingaiah, "Machine Design Data Handbook", McGraw-Hill, 1994.

[24] Wallace DJ, Allision M, Stone MB. Acad Emerg Med. 2010; 17: 96–99

[25] Maddox S, Measuring vital in signs. In: Baillie L, editor. Developing practical adult nursing skills. USA: CRC press Taylor & Francis; 2009. pp. 116-518.

[26] Ke MT, Fujimoto S, Imai T. Nat Neurosci. 2013; 16: 1154–1161.

[27] Calve S, Ready A, Huppenbauer C, Main R, Neu CP. PLoS ONE. 2015; 10: 1-14

[28] Vieira AC, Guedes RM, Tita V. J Polym Eng. 2013; 33; 292-302

Fig. 1 Lasercut PLLA stent

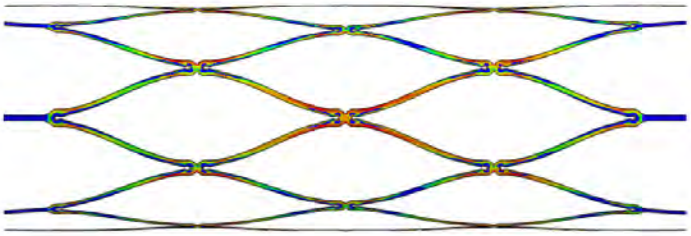

Fig. 2 Fatigue safety factor contour plot during a flat-plate compression of diamond shape stent design based on FEA. Red is the most stressed areas of the stent

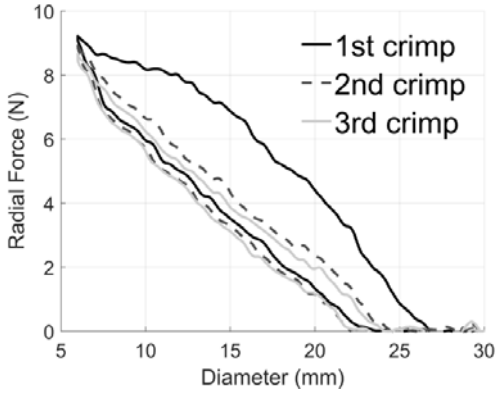

Fig. 3 RF testing at 37°C dry. Crimped from 30mm to 6 mm at of 0.5s/mm. n=1 is the number of stent-bases tested.

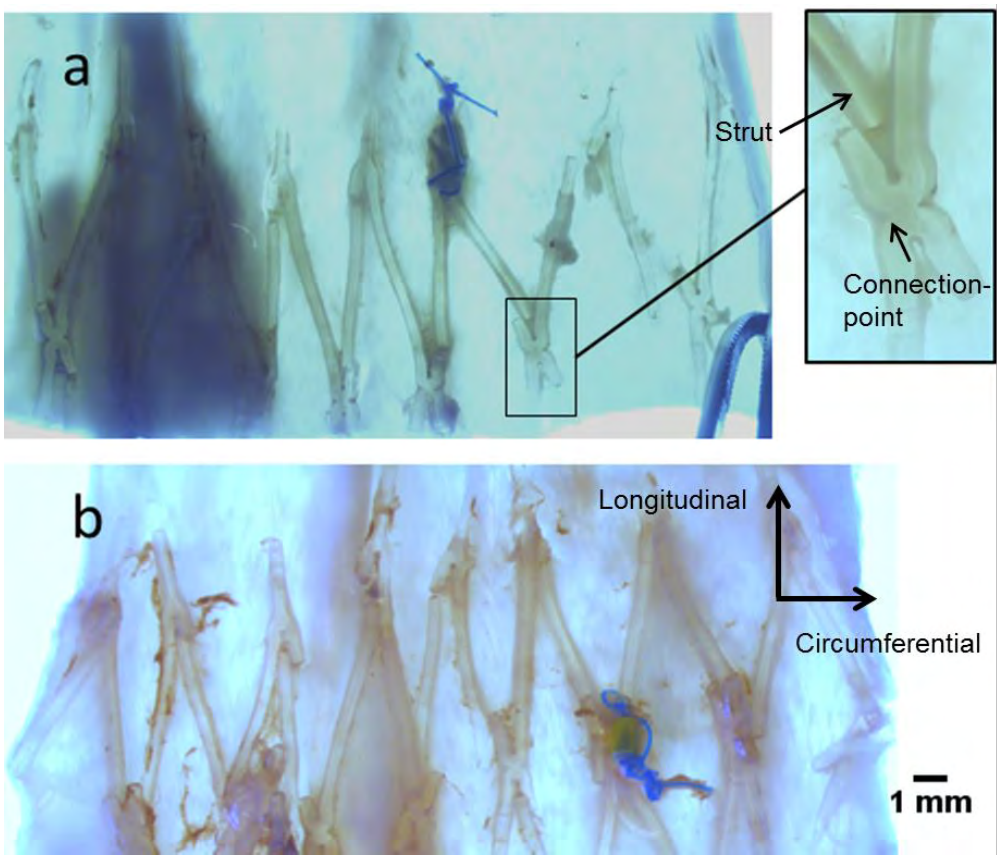

Fig 4. Representative light microscopy (0.75x) of explanted caudal stent-bases and vein after 2 weeks and 3½ weeks. The box on the outside is zoomed in (3.2x)

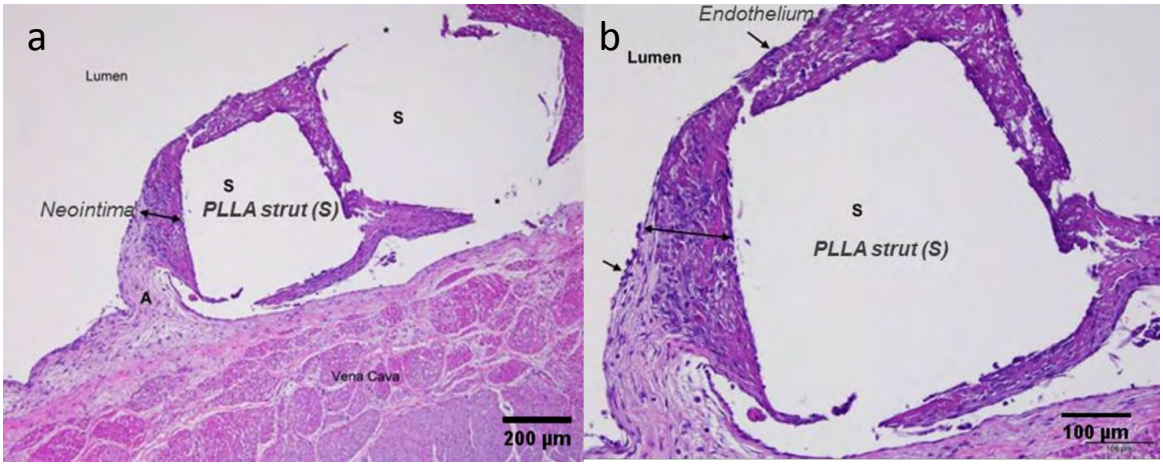

Fig. 5 Representative images of H&E stain of PLLA stent-base (S is the PLLA strut) in vena cava after 2 weeks. Struts are surrounded by loosely arranged fibrovascular tissue (neointima ↔) that contained small amounts of fibrin and a few inflammatory cells (macrophages and lymphocytes). Furthermore the struts are partially covered by endothelium. Smooth muscle cells in the adjacent vena cava wall are minimally vascoulated.

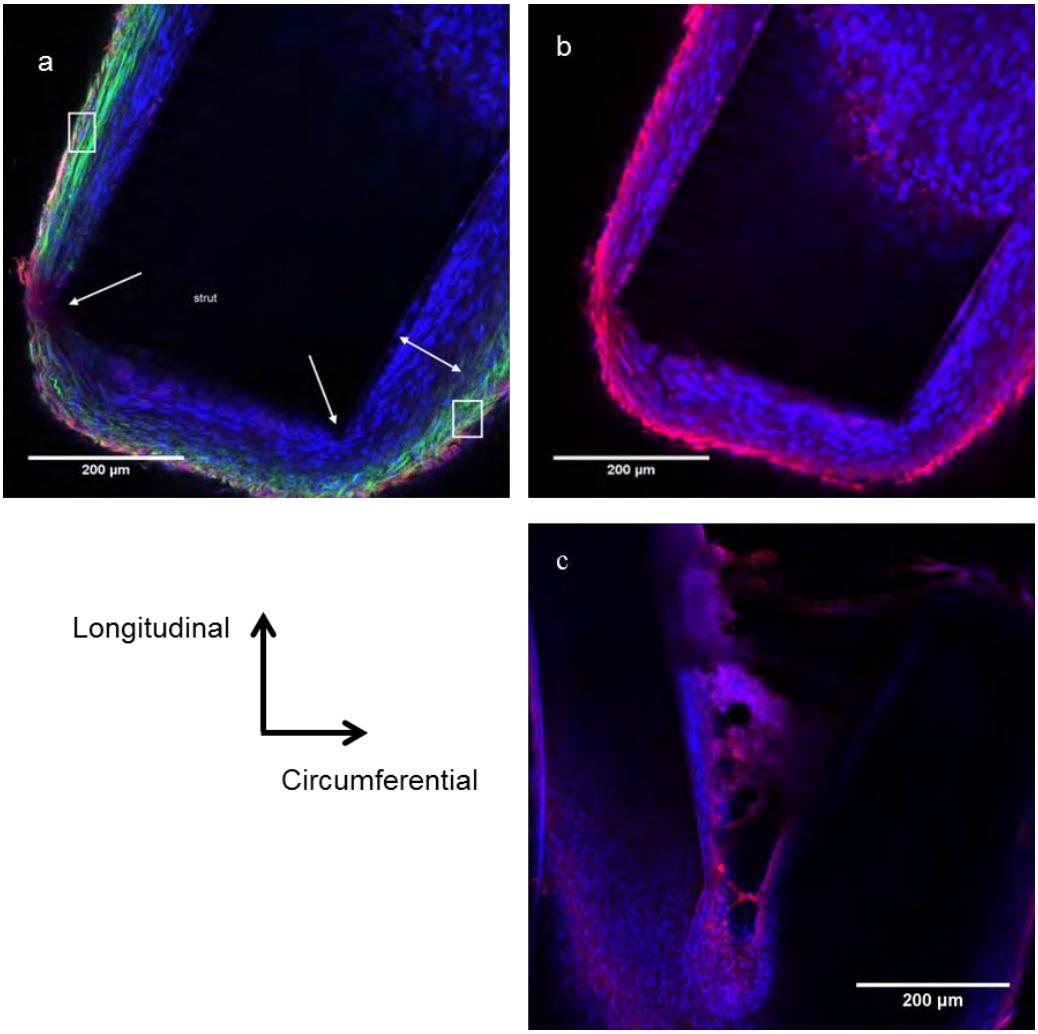

Fig. 6 Representative confocal images of optically cleared specimens after 3½ weeks, where the normal vector to the plan (longitudinal-circumferential) is luminal. (a) and (b) show surface of a fractured strut. (c) show a connection-point covered in nuclei and fibrinogen (10x). Nuclei are represented by blue, actin-filaments by green and fibrinogen by red. The single headed arrows show sides with fewer nucleuses at the corners of the strut. The double headed arrow show the neointema. The box show the muscle/adventitial layer.

Animal	Device	Pre-diameter RAO/LAO (mm)	Post-diameter RAO/LAO (mm)
2 week	Cranial	15.9/13.8	17.3/18.0
	Caudal	18.3/19.2	15.8/16.6
3½ week (1st)	Cranial	16.8/12.5	16.3/15.7
	Caudal	19.3/18.2	17.9/18.3
3½ week (2nd)	Cranial	14.6/15.4	14.4/16.3
	Caudal	16.0/16.5	16.1/19.1

Table 1 Placement and position, diameter pre- and post-implantation from right anterior (RAO) and left anterior (LAO) position

Compression method		OD(mm) before	Upon release OD_{top} (mm)	Upon release OD_{side} (mm)	Shape after
1. Circumferential crimping	Delivery sheath *n=2*	28.1±0.6	24.6±0.4	24.6±0.4	Circular
2. Flat-plate compression	Wet at 37°C *n=1*	24.2	20.4	27.2	Elliptical

Table 2 Diameter before loading into delivery sheath and after release from loading (1). Additionally diameter before stent base was delivered into a silicon tube and after cyclic flat-plate compression under physiological conditions at 37°C (2). n is the number stent-bases tested. OD_{top} is the distance from top to bottom which was in contact with the flat-plate, and OD_{side} is the distance from one side to another not in contact with the flat-plate

Table 9.1: Animal ID, prototypes number, placement in animal, the IVC diameter before and after placement from RAO and LAO view and the average thickness t_{av} of the prototypes at each end used in animal study

Animal no.	**Prototype no.**	**Placement**	IVC dia. LAO (mm)	IVC dia. RAO (mm)	Post IVC dia. LAO (mm)	Post IVC dia. RAO (mm)	$t_{av.}$ (top / bottom) (mm)
0089	07_8#7	CR (T11/12)	15.9	13.8	17.3	18.0	79±4/46±7
0089	07_8#6	CA (L4/5)	18.3	19.2	15.8	16.6	75±2/54±5
0122	07_8#5	CR (L5)	16.8	12.5	16.3	15.7	74±5/51±2
0122	07_8#4	CA (T12/L1)	19.3	18.2	17.9	18.3	75±8/47±7
0350	07_8#2	CR (L5)	14.6	15.4	14.4	16.3	72±5/50±8
0350	07_8#3	CA (L1/L2)	16.9	16.5	16.1	19.1	69±5/52±9

9.2.1 Interim: Device migration and venography

From Figure 9.2 it is seen that one animal (ID 0089) showed displacement of the cranial device is within 4-5 mm after 1 and 2 weeks and the caudal device showed a displacement of 10 mm, none of which are considered as an actual migration of the device. Displacements are often due to the fact that identical positioning of the implant is difficult at two different time points. The second animal (ID 0122) did not show any displacement for either cranial or caudal device. It is therefore concluded that for the duration of 2 weeks, the radial force was adequate and risk of migration limited. When placing a device in the veins, there is a risk of narrowing of the vessel wall, due to an excessive inflammatory response and tissue coverage of the device. Venography confirms vein patency after 2 weeks, and it was concluded that tissue covering did not cause narrowing on the vessel wall. The distance between the gold markers varied over time because they were able to slide along the strut, where they were attached. The radial force was adequate until sufficient tissue coverage occurred in the sense that no device migration was detected within the 3½ weeks.

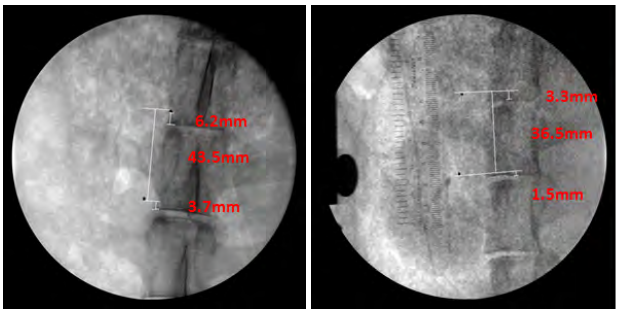

(a) Implant cranial (b) Follow-up cranial

Figure 9.2: Radiograph of cranial device at implant, interim and follow-up in AP-view after 2 weeks (9.2(a)) and (9.2(b)), respectively

9.2.2 Follow-up

One animal was euthanized after 2 weeks and due to a loss in device integrity, the remaining two animals were terminated after 3½ week. Figure 9.3 shows the IVC before harvesting. Before harvesting the vena cava was perfusion fixated using buffered 10% formalin solution for 15 min to avoid contraction of the vein, once removed from the animal as seen during the proof of concept. After harvesting the stent was kept in buffered 10% formalin solution. The

explanted vein with the stent was collapsed after harvesting and nearly flat as seen on Figure 9.4(a). After 24 hours the explants were imaged with MRI (Figure9.5) to estimate integrity of the device.

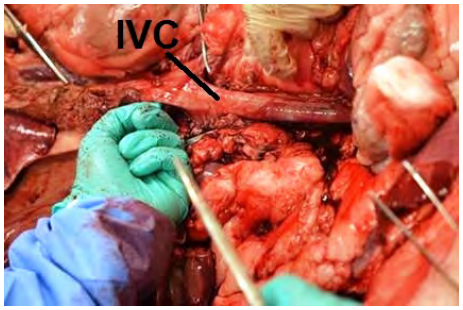

Figure 9.3: Stented IVC before harvesting

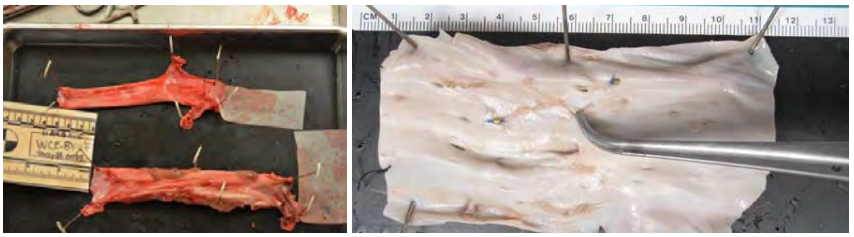

(a) Explanted cranial (top) and caudal (bottom) device

(b) Explant of cranial device

Figure 9.4: Explants after 2 weeks

MRI showed multiple fractures of the stent (Figure 9.5(a)) and an uneven distribution of struts from a cross-sectional point of view (Figure 9.5(b)).

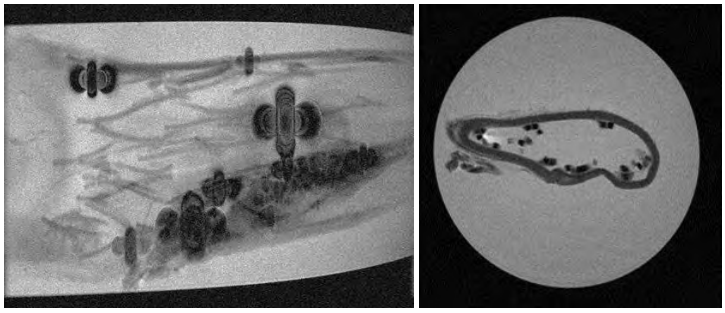

(a) (b)

Figure 9.5: MRI scan of the caudal explanted device after 2 weeks implantation

9.3 Histology

9.3.1 Hematoxylin and eosin straining

After 48 hours the explants was embedded in paraffin for sectioning after which they were stained with H&E. After 2 weeks most of the struts of the caudal device adhered to a surface and was covered in neointima (20-100μm) ($\leftrightarrow$ in Figure 9.6(a)) and was composed of loosely-arranged spindle-shaped cells representing fibrovascular tissue with some fibrin present. Some of the neointima over the strut (S) is covered with a single cell layer endothelium ($\rightarrow$) (Figure 9.6(b)).

Mature connective tissue was seen at attachment site (A) between the strut (S) and vena cava (Figure 9.6(a)). Minimal inflammation was detected as only a few macrophages around the struts and few lymphocytes in the adjacent neointima were present (Figure 9.6(d)). At sites of attachment between struts and vein wall, low numbers of smooth muscle cells in the vena cava were vascoulated, suggesting mild focal pressure change. After 3½ weeks still most of the struts were adhered to the surface and were covered by a thicker neointima (100-300 μm). It was composed of mature neointima and fibrovascular tissue (9.6(c)), but disruption of the tissue occurred due to a processing artifact. At 3½ weeks, most struts were now fully covered with endothelium, and the presence of fibrin was still rare. Inflammation after 3½ weeks was also minimal and composed of a few multinucleated macrophages around the struts and a few lymphocytes in the neointima. As for 2 weeks, the attachment site between struts and vein wall consisted of smooth muscle cells (low in number) and minimally vascuolated.

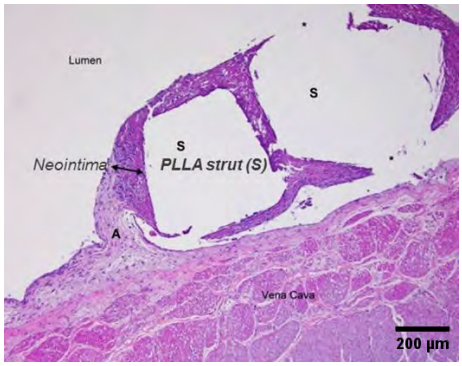

(a) Cranial device 2 weeks 100x

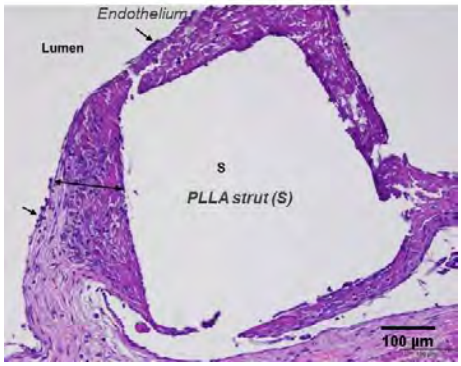

(b) Cranial device 2 weeks 200x

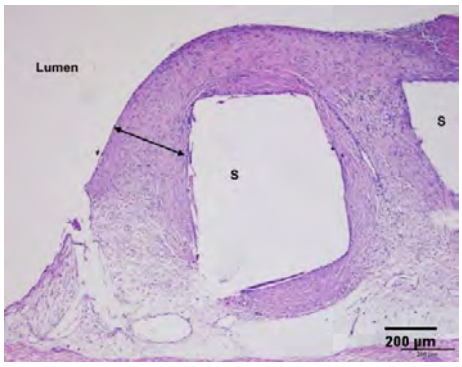

(c) Cranial device 3 ½ weeks 100x

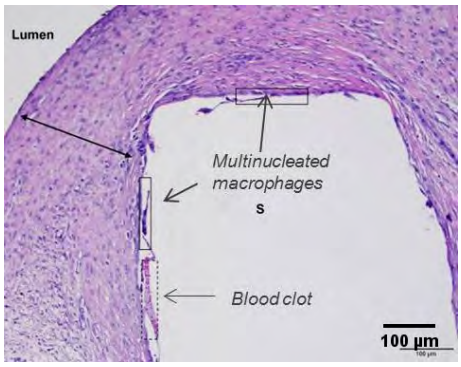

(d) Cranial device 3 ½ weeks 200x

Figure 9.6: Cross-sections from H&E stained IVC with PLLA struts from 2 weeks and $3\frac{1}{2}$.

9.3.2 Clearing and confocal imaging

Goal The overall goals was to stain the vein tissue with antibodies to visualize tissue growth and inflammatory response. The attempt was to identify the suitable antibodies for this. It was done as an alternative way to examine the tissue without disruption of the tissue and device as seen for the paraffin slicing of cross-sections. With slicing, it was seen that the struts were mechanically pulled from the tissue during slicing. The clearing was evaluated as a method to enhance the visibility of the tissue.

As seen in Figure 9.7, clearing gives a much better visibility of the PLLA stent-base and the tissue through light microscopy. It was possible to visualize the fractures of the stent-base more clearly.

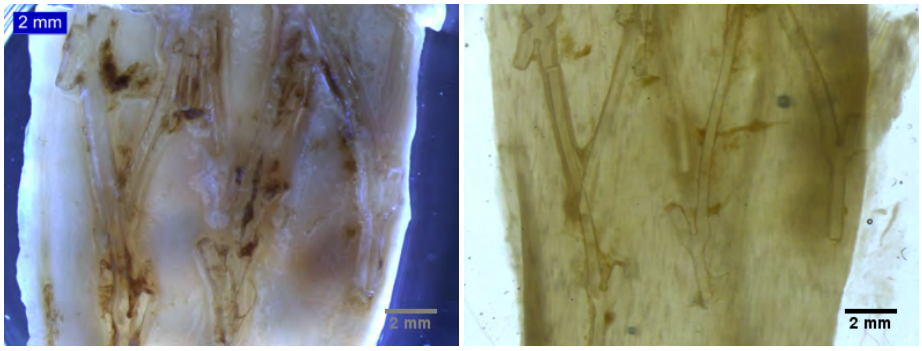

(a) (b)

Figure 9.7: Explants after 3½ weeks, where 9.7(b) was optically cleared.

9.3.2.1 Evaluation of antibody selection

At each time point, two different staining protocols were used. One tissue sample was stained with DAPI, phalloidin, CD31 antibody (IgG2a) and anti-fibrinogen gamma chain antibody (IgG2b). Another piece of tissue was stained with DAPI, WGA and anti-macrophage antibody (IgG1). In Figure 9.8(e) a small residual of the antibodies are seen when taken images for all channels separately. Also, CD-31 antibody appears to stain in the same way as the fibrinogen and the signal for each are overlapping. For this reason, CD-31 antibody was not suitable for this particular tissue and study.

The reference tissue which had not been exposed to PLLA, showed no presence of macrophages (Figure 9.9(c)) and the antibody appeared to stain equally with antibody for WGA (Figure9.9(b)). DAPI staining showed a little degree of residuals in the left corner (Figure 9.9(a)), whereas antibody for macrophages, showed a large degree of residuals. Due to the nature of the fluorescent signal, it is unlikely that Figure 9.9(c) represent macrophages, and the antibody is not a plausible way to evaluate the presence of an inflammatory response. From the H&E staining macrophages were few and the overall inflammatory response to the PLLA was non-existent. It was concluded that the antibody for macrophages was not necessary for this evaluation. For the remaining tissue samples staining with macrophage antibody, the channel for red fluorescent light was not used in the images.

From Figure 9.10 it is seen that visibility is not good without clearing. It was not possible to focus on the tissue in depth. The image showed poor depth resolution and only an outline of the PLLA struts were visible. It is difficult to get close enough to the tissue due to the

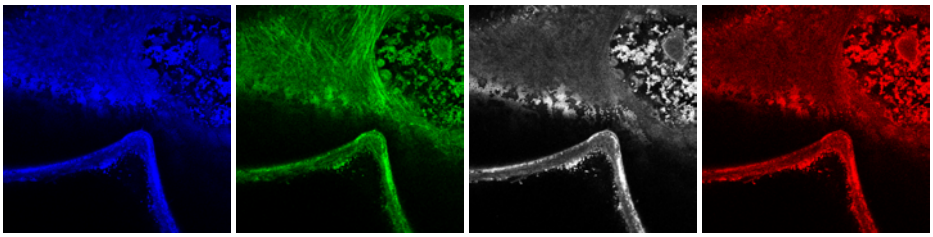

(a) (b) (c) (d)

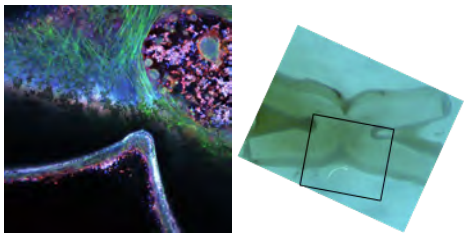

(e) (f)

Figure 9.8: Explants after 2 weeks were optically cleared and stained for nuclei9.8(a), actin-filaments9.8(b), CD31 9.8(c) and fibrinogen 9.8(d) were stained. All channels together are portrayed in 9.8(e). 9.8(f) show where on the stent-base the image is taken.

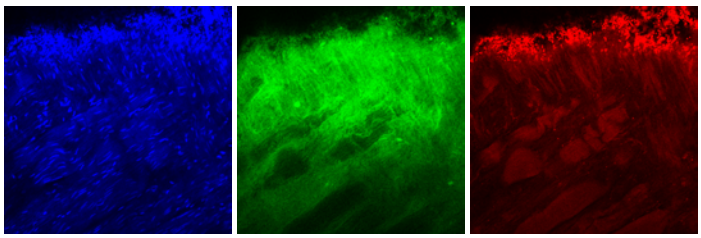

(a) (b) (c)

Figure 9.9: Un-stented reference tissue after 2 weeks were optically cleared and stained for nuclei9.9(a), cell membrane surface9.9(b), and macrophages 9.9(c)

thickness of the PLLA struts. Clearing the samples would induce much greater focus and resolution at 300 μm depth (Figure 9.11). Figure 9.12 shows when the slices at each depth are compiled into a 3D structure and visualization of the connection point is far better than for the paraffin cross-sections. From Figure 9.11 the actin-filament and their direction is very clear. Fibrinogen covers the outer most of the tissue. It shows how the tissue is growing on top of the stent-base connections points and going further into the tissue it also grows along the sides of the connections points.

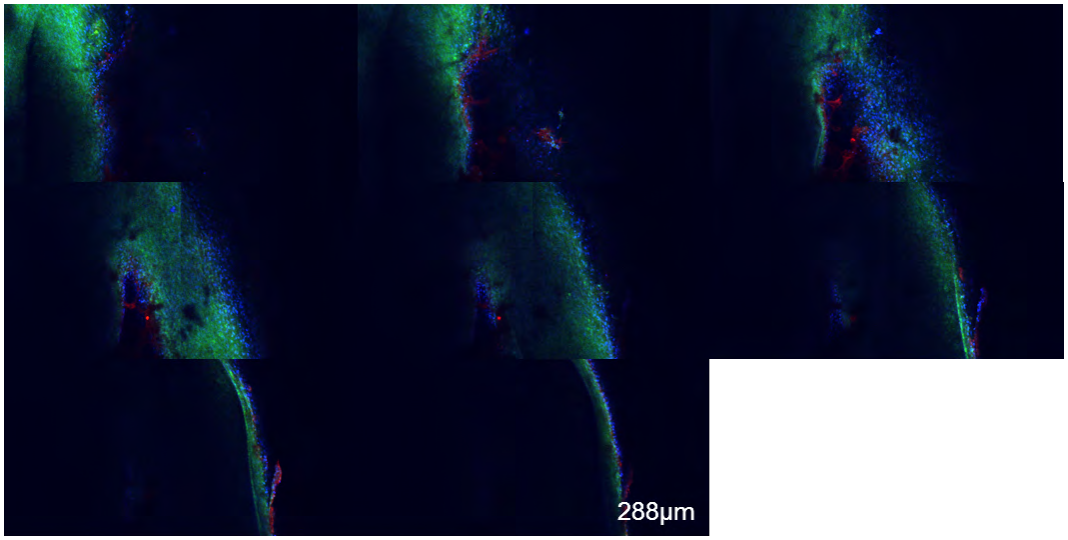

Figure 9.10: Uncleared samples after 3½ weeks from top of the tissue and 288 μm into the tissue. Each slide is 35 μm into the tissue.

The images in Figure 9.13 confirm tissue coverage around and in the connection points by either nuclei (blue) and actin-filament found in the extracellular matrix (green) (Figure 9.13a). Additionally, deposits of what was meant to be fibrinogen, the precursor for fibrin appears red and covers the both struts and connection points on top of the cell layer as seen on Figure 9.13(b). Fibrinogen was also deposited in the connection points in Figure 9.13c and without being part of the cell layer. Fibrinogen is also detected at most peripheral on neointima as Figure 9.13(b) and seems to align with fibrous connective tissue typically represented at the peripheral edges of the stretched vessel. Figure 9.13(a) shows a neointima between 70 (end of the strut) and 120 μm (on the right side of a strut) that has fractured at the connection point. The neointima after two weeks was enough to lock the stent cells as it covers the connections points and as a result, the stent-base is unable to 'move' with the

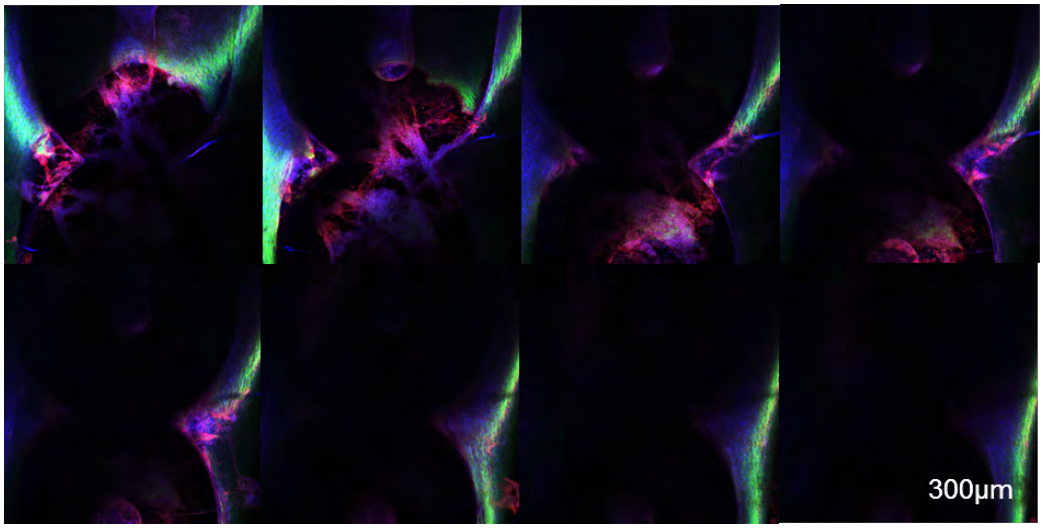

Figure 9.11: Cleared samples after 3½ weeks from top of the tissue and 300 μm into the tissue. Each slide is 27 μm into the tissue.

vessel during compression and release resulting in the multiple fractures. Confocal images showed the presence of smooth muscle cells in low number suggesting a mild focal change in relation to the radial force by the oversized stent.

The actin-filaments (Figure 9.13(a)) occur only in the top cell layer (40-66 μm) on the sides and are aligned along the strut. At the tip of the strut, the actin-filaments are randomly deposited. Moving away from the connection points showed less tissue covering. The box in Figure 9.13a show the muscle layer and their fibers in the smooth muscle cells. The thicker green fibers in this area resemble elastin or, more likely, smooth muscle cells with actin. At the corners of the strut, the tissue appears thinner (single-headed arrow) and represents a compressed vessel. Also, the decreased number of nuclei in this area suggests compression resulting in tissue atrophy and, likely, fibrosis. The increased red at the arrow shows the neointima.

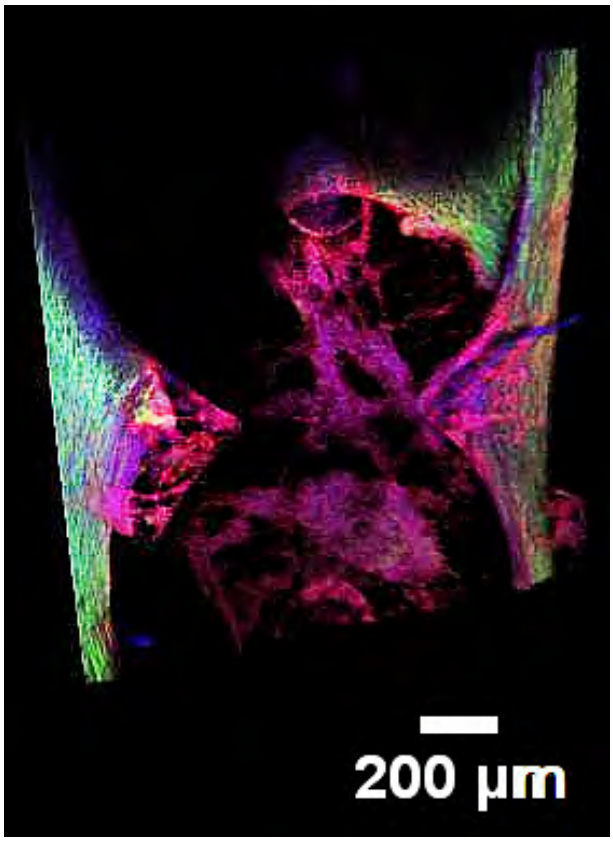

Figure 9.12: Cleared samples after 3½ weeks compiled

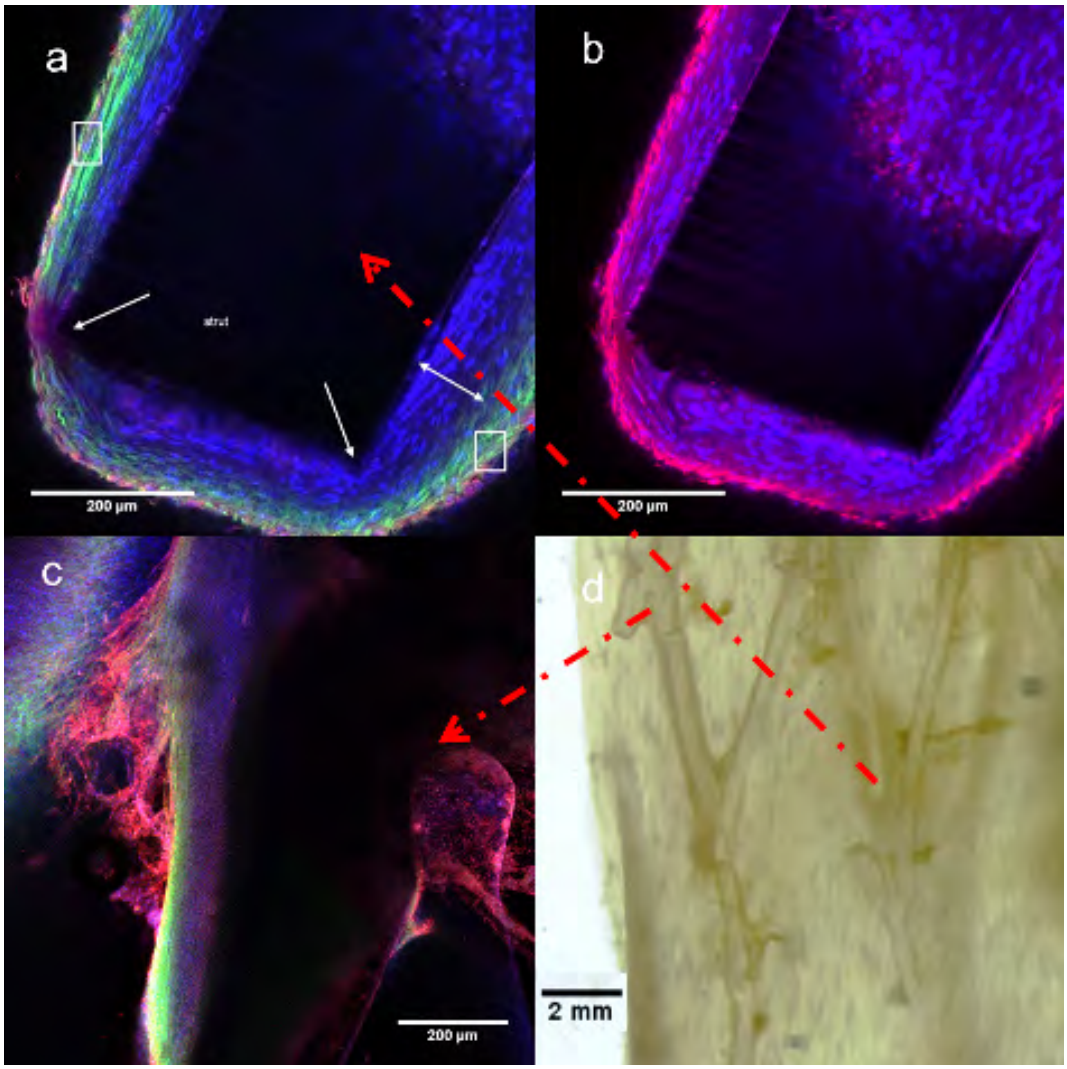

Figure 9.13: Cleared samples after 3½ weeks. (a) Shows a fractured strut for all channels showing actin-filament (green), fibrinogen (red) and nuclei (blue), whereas (b) shows only the red and blue channel for fibrinogen and nuclei, respectively. The double headed arrow in (a) show the neointima, the side headed arrow shows sites with fewer nuclei and the boxes show the muscle/adventitial layer and with fibers. The single headed arrow also represents the tissue at the corners of the strut. (c) shows tissue coverage in a connection point and (d) shows where the strut and connection point are positioned on the explant

10

Discussion in summary

This chapter includes an overall critical assessment of the work is this project and how to proceed.

10.1 Hypothesis

Within the field of PE preventive treatment, a 'true' temporary filter is of great interest. State of the art hypothesized that the 'true' temporary filter could consist of one or more bioabsorbable materials. The filter must withhold its filtering capability until the risk of PE has passed. Furthermore, it was hypothesized that the 'true' temporary filter can be achieved by a convertible filter platform and that it must be fully absorbed with no risk of fragmentation or migration.

The literature review showed that several polymeric bioabsorbable materials exist, and some have been used in carrying out a convertible filter (including PLLA, PLGA, and PCL). There are different ways to interpret the profile of a filter after conversion of it and no longer is capable of filtration. None of the convertible filters with one or more bioabsorbable components address the risk of fragments from the filtration part of the filter. The braided bioabsorbable filter by Eggers et al. [37] was not based on such convertible concept and fragments occur. There is a risk of fragments traveling in the bloodstream as the filter degrades. It would be a difficult process to ensure that no fragment do so and that the fragments which did travel, are of no harm to the patient. The remaining two attempts by Zhang et al. [39] and Thor and Muck [38] were based on the convertible filter. Both filtration parts were made of Vicryl (3-0, Ethicon Inc, Somerville, New Jersey), a PLGA suture, which undergo hydrolytic

bulk degradation and fragment during degradation. The key to avoiding this is either by using a polymer with a controlled surface degradation of struts with narrowing width from wall to center. The filtration struts become thinner and shortens starting at the tip (center of the cone) and more towards the caval wall. That way the fragmentation does not occur. As previously shown the choices of surface hydrolytic polymers are limited. PHA has the disadvantage of being too weak for the application and PCA has a too fast degradation for this application. Polycarbonate is used in the bioabsorbable REVA coronary stent, which exhibits good tensile strength [107], but embrittlement focal mechanical failure occurs as it degrades[108][109]. An alternative is to create the filter, as described in the patent application (US 20110213404 A1) by C. Binkert, based on a convertible filter. It opens up after the risk of PE has passed and the filtration struts move towards the caval wall after which they are embedded in tissue over time. When embedded the risk of fragments traveling to the blood stream is eliminated. The fragmentation will most likely still occur, but the fragments are secured by the tissue.

Monofilament and braided stent-bases In this study, it was possible to create a braided stent-base. A braided stent-base made from oriented PLLA and thereby mechanically improved PLLA. It showed a similar radial force, but lower than stent-bases laser cut from strained PLLA tubing. Despite oriented PLLA having far superior properties to the strained tubing, the radial force is not superior. It was proven that certain processing parameters lead to improved stiffness and strength. The improved stiffness and strength correlate with an increase in radial force during crimping. In retrospect, PLLA tubing appeared to have to appropriate radial force to avoid migration. Unfortunately, the design suffered from poor fatigue properties. If the polymer had been more flexible, it might not have fractured to the same degree in vivo. Other studies used PDS and PCL, which did not fracture when implanted in vivo [37][39]. Both exhibit much better ϵ_b than PLLA. The drawback of PCL is the low stiffness and thereby also a low radial force, while PDS has a better radial force, but the strength of lost too quickly in vivo.

10.2 Overall discussion on strain PLLA tubing

To reduce the risk of migration, processing was used to optimize the mechanical properties. The overall findings are discussed in the following section.

Degree of strain Biaxially straining of extruded PLLA tubes alters the mechanical properties of the polymer. Overall the stiffness, σ_y, UTS and ϵ_b of biaxially strained tubes, increase with the degree of strain (e.g. total area expansion (A_{exp})). It was seen that regardless of (ϵ_a;ϵ_r), the higher the A_{exp}, the greater stiffness, and strength. An interesting observation was that the material could exhibit different behavior in the axial and radial direction. This was regardless of the simultaneous or sequential biaxial strain, and the mechanical changes are due to modification of the amorphous domain. For biaxially strained PLLA tubes the crystallinity remains constant, though the stiffness and strength will increase with increasing strain. The properties are therefore not related to the crystalline domain of the polymer.

Strain-induced crystallinity is only achieved, when several requirements are fulfilled such as the adequate degree of strain the processing strain rate and temperature[110][111]. This study showed that axial processing strains (ϵ_a) between 80-90% the amorphous chains are stretched enough that the relatively low crystallization temperature of 65°C, just a few degrees above T_g, induces crystals. Axial processing strains between 90-100% cause the crystallization to grow as the final degree of crystallinity (X_c) increased from 8-36%. The greater the strain, the lower the cold crystallization temperature is (T_{cc}). Once the ϵ_a=100%, no further crystallization seems possible and the cold crystallization peak is diminished. The behavior is interesting regarding further processing of the filter after the straining process. A crystallinity of 36% is far from maximum achievable crystallinity for PLLA. The same is seen for sequential biaxially strained tubes, where the crystallization peak is diminished (1.0;3.2) (T_p=73°C) with a X_c=30%. It was able to crystallize significantly at a temperature above 110°C, regardless of indications from the DSC scan.

Processing strain rate and temperature Biaxially strained tubes below T_g turn milky-white on the inner part of the tube, compared to the transparent nature seen when raising the temperature. If strain occurs below T_g there is a risk of plastic deformation of the amorphous PLLA, and there is a risk of craze formation. This was not possible to quantify for the strained tubes by SAXS. In instances where a tube was processed under the same condition, one could be white and another transparent. It was confirmed that the crystallinity and orientation between the two were the same. Further more the displacement between crystals was identical, and their size was the same (58Å circumferentially and 142 Å). The light refractive index is different when the tube appears white. It is possibly due to clustering

of crystals of the same size. Individual crystals of the same size distributed evenly throughout the tube would possibly create a transparent material. The tubes were processed at the same temperature and subsequently cooled in the same manner. Despite this, some tubes were more white. Small inhomogeneities in the extruded tube might cause the difference in refractive index. Whether it is crystal clusters or not, their mechanical behavior was the same and no difference in ϵ_b was observed. Successful strain temperature (T_p) was identified as low as 60°C. At T_p above 73°C crystallinity was not induced during the axial strain possibly due to an increase in chain mobility, which prevents sufficient alignment for crystal formation. Despite this, the mechanical properties both circumferentially and axially improve with T_p.

The influence of axial strain and radial stent force It was hypothesized that the larger the circumferential and axial stiffness and strength of a tube, the larger the radial force of the stent made from such tube will be. Overall the design of the stent-bases used in this project was diamond shaped cell stents. It is expected that the radial force lies in the resistance to compress these cells and due to the design of the diamond shaped cells, not dominated by the circumferential properties, but the properties at a 40° angle. It was seen that these diagonal properties are dependent on the degree of axial strain before the radial strain is applied. The axial stiffness and strength, as well as the 'diagonal' (40° to the axial direction) properties, improve if the initial axial strain is high. As a result, the larger the axial strain, the more alignment in that direction is achieved, and the subsequential alignment during the radial strain is thereby smaller and as well the circumferential properties. It is possible to use sequential biaxial straining at large strains and create a material, which exhibits isotropic mechanical properties. It would be beneficial to take advantage of this when using the diamond shape stent design, and potentially better radial force is achieved. In practice, the degree of strain in each direction is a compromise between the best possible mechanical properties and the thickness of the strained tube. In this project, the aim was to create a tube with a wall thickness below 0.4 mm. This fact limits the axial strain to be below 30%.

Orientation of PLLA During straining or stretching the chains in the amorphous domain are stretched and ultimately the amorphous fraction is reduced with increasing degree of strain. While the crystalline fraction remains constant with increasing degree of strain, the reduction in the amorphous domain is taken over by a transitional domain between the two,

before transitioning into the crystalline domain. Axial strain alone is expected to induce less amorphous scattering and result in higher crystallinity. Once the sequential radial strain is applied some of the alignment achieved during the axial strain is lost. The larger the axial strain, the less orientation of the crystals are achieved. During simultaneous biaxial strain, the chains would be stretched in the 2D plan in which they are stretched, creating in-plane isotropy [92]. Orientation, therefore, would be low as a result of randomly oriented chains, at low strains. It appears in this project that the crystal orientation is independent of the axial strain as the crystal orientation remains constant as a function of A_{exp} and radial strain. A sequential biaxial strain will eliminate the crystal orientation in the axial direction and create new crystals in the transverse direction. The efficiency of the transverse strain is dependent on the degree of strain in the axial direction and if the crystalline domain is fully formed (strong crystalline domain). For this reason, there is a difference in crystal orientation between (0.2;2.3) and (1.0;3.3). The former has a weak crystalline domain, and the latter has a strong crystalline domain before the transverse strain is applied leading to a crystal orientation of 0.5 and 0.3, respectively. It was concluded that to achieve a high order of crystalline orientation, the initial axial strain must be low.

The mechanical properties appear to be indifferent of crystal orientation during sequential biaxial strain, but upon annealing the crystal orientation factor is reduced to 0.1 and the mechanical properties are compromised upon annealing. This is the only time, where the change in orientation factor corresponds to a change in directional mechanical properties, regardless of simultaneous or sequential biaxial strain. As for oriented PLLA monofilament from Zeus, the orientation factor before annealing was similar to the axially strained PLLA tubes (0.7), only higher (0.8). The orientation of biaxially strained tubes was reduced to less than half upon annealing below crystallization temperature. It appears that the mechanical properties are compromised upon annealing. It is unknown if it is due to the relaxation of the amorphous domain or due to the lack of oriented crystals. Raman spectroscopy had been investigated to see if there was a difference between the amorphous and crystalline domains. Either the method was not sufficient to establish such, or the difference in orientation between sequential and simultaneous biaxial strain was not enough. The method would need further investigation.

It appears that orientation and X_c are not the main contributors to the mechanical performance of PLLA. The increase in crystallinity will result in an increase in stiffness and σ_y. It is not preferable to create a material that is high in crystallinity and thereby brittle and not

very flexible. Flexibility is needed if the device is to withstand compression repeatedly and move with the vessel during implantation. Biaxially strained tubes with a moderate crystallinity, should be beneficial in this matter. If the tubes are merely extruded into the appropriate size, the stiffness, σ_y and ϵ_b are much less than for the strained tubes. As expected the major strength and stiffness lies in the axial direction, the extrusion direction, where the chains are aligned. The elongation is greater for the direction transverse to extrusion. The extruded tube has been cooled at a rate that prevents the material from crystallizing. It should be noted that the axial properties are in accordance with values reported by the vendor.

The BVS stent from Abbott Vascular, which is composed of most likely a laser-cut PLLA tubing was investigated in this study. It showed a low degree of crystal orientation but exhibits a high crystallinity compared to the sequential biaxially strained PLLA tubes. At the same time, oriented tubing from Zeus exhibited an orientation factor similar to the simultaneous biaxially strained PLLA tubes and a high degree of crystallinity. As simultaneous and sequential biaxial straining evokes mechanical properties in the same range, but not the same degree of crystal orientation, the improved mechanical properties are not related to the crystal orientation itself. It should be noted that despite the higher orientation degree in PLLA tubing from Zeus, the mechanical properties are inferior. It is unknown if the raw material differs slightly. It cannot be ruled out that one of the materials have a narrower molecular weight (M_w) distribution and therefore better stiffness and strength. The tube from Zeus exhibit higher stiffness and σ_y and ϵ_b in the circumferential direction as oppose to their axial direction, indicates it has been biaxially strained as opposed to simple extrusion of the tube. If the straining is sequential, the orientation factor would have been lower, but similar if a simultaneous method used. It is more likely that when manufacturers claim the existence of an oriented tubing and improved mechanical properties thereof, it is important to identify where these properties originate from. It is more likely the degree of crystallinity which caused the improvement of properties. The oriented PLLA tubing from Zeus and the BVS stent from Abbott have a crystallinity close to the maximum crystallinity of PLLA, which is not preferable for the IVC application.

Crystal size Post-annealing reduces the axial crystal size slightly, but it enlarges the radial crystal size significantly. It is expected that during annealing the crystals grow in size either in the plan or depth or both. Crystal sizes in each direction are indifferent to simultaneous

or sequential biaxial strain. It could be expected that the crystals grow in the direction of strain and their sizes likewise. The crystals formed during the axial strain are elliptical and largest in the circumferential direction. Once annealed above crystallization temperature, they become more circular in shape, where the circumferential size is reduced the axial direction is elongated. Perhaps this is a perfect crystal and a natural shape for the crystal to be in. The biaxial strain, regardless of simultaneous or sequential, also shows elliptically shaped crystals, that are largest in the axial direction. Annealing does not change the shape of the crystal below crystallization temperature, which is not very surprising as the crystallinity does not increase. In fact, it was reduced and possibly due to the melting of smaller imperfect crystals.

Crystal structure In all cases of the biaxially stained tubes and axially strained tubes, the α'-crystal occurs, as they were not strained at high strain ratio or above 95°C. With this in mind creating α-crystals by strain-inducing seems challenging, as 95°C is very close to the T_{cc} temperature of these PLLA tubes. Supposedly the α'-crystal has a looser chain packaging, and the disordered structure will result in a lower modulus and higher ϵ_b[89]. None of the tubes, in this project, were produced at a temperature which could give rise to α-crystals. The impact of the α'-crystal could not be confirmed, as straining above T_{cc} was not possible, and the tubes contain only α'-crystal.

Annealing, heat treatment, and sterilization There are many ways to improve the properties of PLLA. The material must remain free of additives and particles and consists only of material, which is commercially available and approved in combination by the regulatory authorities, and thereby limits the material options. Annealing is one way to overcome this and improve the mechanical properties. Annealing was done to investigate the possibility and influence of heat treatment on already crystalline tubes. The effect of annealing was different for the amorphous extruded tubes compared to the sequential biaxially strained. As expected the closer the annealing was to T_{cc} the faster the crystallization rate. Already highly crystalline tubes, whether just axially strained or biaxially strained tubes, showed no crystallization peak during heating in a DSC scan. It indicates that further crystallization is not possible. It was possible to anneal the biaxially strained tubes at 110°C and above for 30 min and thereby increase the crystallinity further. Such annealing leads to improved stiffness and strength, and a lowering in ϵ_b as described in the literature. It is likely due to

a reduction in the orientation of chains in both the crystal and amorphous domains. This occurs even if further crystallization is not happening during annealing. The rate of crystallization is not indifferent to the previous crystallization within the material. It was possible to establish a linearity in crystallinity growth as a function of temperature for the sequential biaxially strained tubes. The crystallinity growth rate for the extruded tubes was non-linear as a function of time and faster. It means that it takes more energy to overcome the mobility barrier for PLLA which has previously been subjected to strain-induced crystallization. Either the crystals do not grow, or the amorphous chains are aligned and cannot rearrange and create more crystals.

Because a low to moderate crystallinity is preferable, annealing was not considered a viable way to improve the mechanical properties further. The heat treatment is essentially a short form of isothermal annealing. From the annealing experiment, it was safe to use heat treatment at 93°C without further increasing the crystallinity. Annealing at 90°C compromise both the crystal orientation as well as the amorphous orientation and thereby also the mechanical properties. Unfortunately, this also occurs during heat treatment even at short periods of time. During EO sterilization, it was expected that mechanical properties would be compromised due to the presence of both water and temperatures close to T_g. When heat treated first, the amorphous chains relax and due to rapid cooling after heat treatment at 93°C the crystallinity is reduced to 27%. It means that some of the imperfect crystals have melted at that point, which could explain the lower modulus. In retrospect, it was seen that rapid cooling using freeze spray reduces the stiffness and strength, more than slow cooling at room temperature, and rapid cooling is not suggested after heat treatment.

When sterilizing the polymer with EO, the standard sterilization process usually takes 7-8 hours, in which the material is subjected to both heat and moisture. The closer the temperature is to T_g the more aligned the chains become, which is seen by an increase in stiffness and strength, while crystallinity remains constant. The presence of moisture has no impact on the stiffness or strength, and it is expected that the heat close to T_g softens the material, but no changes in mechanical properties or thermal properties are detected. Cold sterilization limits the chain mobility, and they do not align after heat treatment. The mechanical properties do not improve from the sterilization as seen at higher temperatures. Therefore the standard EO sterilization at 53°C is preferred.

Processing concerns In general, the process of biaxially strained tubes was at a point unpredictable and create tubes with larger thickness variations along the tube. The extruded did not seem to have a difference in wall thickness along the tube. At times the supplied extruded tubes were not straight and possibly adding to an uneven distribution of material along the tube. The tube will expand where least resistance is found, which leaves more material on one side of the mold than the other. As the air is injected through the distal end, the end is likely to expand slightly before the proximal end. The material would have to move from the distal to proximal end as the expansion propagates along the tube, leaving the proximal end thicker. The higher the processing temperature, the more difficult it is to evenly distribute the material along the tube. At the highest possible straining temperature (T_p=93°C) tubes with the same strain parameter as tubes processing at lower temperatures, proved to be very thin (0.1 mm) compared to the former (0.2 mm). It was previously seen that despite thickness differences along the tube, there was no difference in T_g, T_m or X_c[13]. It is believed that the biaxial straining is successfully happening all along the tube. The thickness variation was indeed apparent for the tubes with an initial large wall thickness. It appeared that a larger initial axial strain, the less variation was detected along the length of the tube. The expansion process is easier to control for the smaller length (50 mm) rather than, the longer length (100 mm) as used for prototypes in the animal study.

In vivo The size of the vena cava just above the hepatic vein ranged from 13.8 mm to 27.4 mm for 95% of the patients in a study of cava sizes[112]. The animals used in the animal study in this project were in that range of those diameters, but on average in the lower range of the spectra. Despite the failure of the device integrity after 2 weeks implantation, the stent-base showed a positive outcome with no migration and limited inflammatory response to PLLA in the vein. Overall it did no harm to any of the animals. One of the major concerns of an IVC filter is the risk of migration[39]. The stent-base exerted a radial force of approximately 2.3 N on the vessel (15 mm). It is significantly higher than for the Cook Celect filter, which has a radial force of 0.3 N when compressed to 14 mm [113]. The radial force of the PLLA stent-base was considered adequate, as no migration was detected within 2 weeks. During a simple ex vivo test, the stent-base was delivered in an explanted swine IVC but did not give sufficient information on whether or not the stent would migrate. It gave an indication of the friction between the device and the caval wall. It was seen from in vitro testing that over time the PLLA stent-base becomes permanently deformed during

cyclic flat-plate compression. This is partly due to the degree of deformation as well as the physiological environment which weakens the polymer. As it becomes soft, the radial force of stent-base is reduced. In vivo the vein most likely collapses over the stent-base and as a result the individual cells fracture. The animal study was unable to confirm or validate if the stent-base underwent permanent deformation before fracturing.

The FEA showed where the stent was most likely to fracture, and it did fracture in those places. It was not expected that the stent-base would fracture in multiple places, as the stent lost its device integrity and strength after the first few fractures. It cannot be explained why additional fractures were seen. It is possible that the tissue coverage is extensive, and the cells of the stent-base are unable to be compressed. They are held in place by the tissue and as the vein collapses the stent fractures. This is a plausible explanation because the main part of the fractured pieces are still held in place by the tissue despite the fractures. Less tissue was present on the fractured ends compared to along the sides. This indicates that tissue coverage happened after and not necessarily just as the stent-base fractured. Therefore fractures must have occurred after the tissue covered the stent-bases.

The traditional histology paraffin embedding proved not to be suitable for the stented vein. As slices were made, the PLLA was pulled from the tissue, which was damaged in the process. By clearing the explanted tissue in stead, it was possible to visualize the fractures and the underlying tissue better. Additionally, the fluorescent antibody has the great advantage over standard slicing of paraffin-embedded explants by leaving the explant (tissue and implant) intact, while getting the histology information needed. It is possible that the slicing of paraffin could be optimized so that the tissue and PLLA struts were not disrupted upon slicing.

In vitro Testing the device under physiological conditions could not predict the outcome of a device implanted in vivo. The radial force surprisingly showed that a braided stent from oriented PLLA would exhibit a radial force half of the stent-base from stained tubing used in the in vivo study. When braiding it is possible to align the filament in the circumferential direction giving it radial strength. The diamond shape stent design does not benefit from a circumferential strength and stiffness. It is possible that the braided stent would have been able to withstand the cyclic compression in vivo, but it is unknown if the radial force would be adequate. Another bioabsorbable polymer might have performed better. PDS has lower mechanical properties than the oriented PLLA, and the radial force would be less for a PDS

stent. Based on the results presented by Eggers et al. [37] the PDS stent, with presumably less radial force, did not migrate. The oriented braided PLLA stent might have had enough radial force to withstand migration.

Regarding design considerations, it was seen that a wider stent cell from a laser cut tube results in the greatest compression force. A high $\dot{\epsilon_p}$ was previously seen to optimize both the circumferential stiffness and strength of the biaxially strained tubes and the radial force of an equivalent stent. The optimized stiffness and strength were also portrayed by a larger compressional force of a single stent cell. The single stent cells fractured in the same place as the stent did. An interesting observation was that water appears to have a larger effect on the single stent cells compared to biaxially strained tubes during aging. In a static load compression setup, the single stent cells, deform if kept under ambient conditions, but only fractured when kept in water. It was expected that the polymer softened, and relaxed over time due to penetration of water molecules, but in stead of relaxing fractures are observed. This is a very good indication of why the stent-base fractured to a large extend in vivo.

Previously it was discussed that a stent-base processed with a low degree of axial strain, benefits from a high T_p. This is true to the extend where the higher T_p and thereby the greatest stiffness and strength circumferentially, also results in the largest force needed to crimp the stent. It did not exert the largest force on the 15 mm vein. From an integrity perspective, the stent-bases with a high axial strain during processing coiled up upon heat treatment, and released the tension of the aligned chains axially. The stents processed at high T_p are permanently deformed to a larger degree under cyclic compression test in vitro. This is despite the larger radial force and circumferential tube stiffness and strength when processed at high T_p than seen for lower T_p. The parameters were therefore not used for stent processing.

As seen from in vitro testing, the PLLA tubing cut into a diamond shaped stent design, was able to be crimped down to 6 mm, multiple times, without fractures. Permanent deformation at this crimping occurred. It reached a plateau, in which the force to crimp as well as the change in stent diameter remained constant. The flexibility of the stent-base was also detected as the stent survived 150.000 cycles when compressed to 30% in a flat-plate design, under physiological conditions. However, the model was inadequate for prediction of the failure mode in vivo.

Aging of the tubes in serum for two weeks (37 °C) did not increase the crystallinity of the tubes. However, an increase in stiffness and strength was observed, while ϵ_b was reduced.

The tube ultimately became more brittle over time at elevated temperature, and not due to degradation of the amorphous domain. The brittleness mean that the polymer is more likely to fracture and a possible explanation for the failure in vivo. In retrospect, a cyclic compression test after 2 weeks at 37 °C, would possibly clarify this issue.

10.2.1 What can be taken from all of this

It will take some tryouts before a 'true' temporary filter made from bioabsorbable materials will reach the market. This study only investigated the presence of a stent-base in the vena cava. Once successful with no device migration, fracture or loss of integrity, no significant inflammatory response to the material or narrowing of the wall, the next step is to test the functionality of the filter. If moving forward with the idea of a fully bioabsorbable convertible filter, further investigation of the filtration struts and the filtration mechanism must be done to ensure that the filter can trap clots. Such test setup was previously done by Eggers et al. [37], where they induced clots in vivo to the vascular system, and their filter was able to trap multiple clots. This could be a way, if found ethical, to test the functionality of the filter. Furthermore, after an appropriate indication period, the filtration struts must open up and move towards the caval wall, without fracturing. The animal study in this project lacked these and had the result from the study been positive, and device integrity remained, the next animal study would include a fully functional filter. It is very important to investigate if the filtration struts indeed can move towards to caval wall after 2-3 months of indication. It is possible that neointima covers the end of the filtration struts connected to the stent-base, and simple flipability of the struts is not possible. Also PLLA (X_c=27%) is known to relax over time[14]. When the struts are pinned together is the center, the polymer might relax and have the limited elasticity to move towards the caval wall.

10.3 Future

10.3.1 An alternative material: bioabsorbable metals

An interesting alternative to bioabsorbable polymers are the less known bioabsorbable metals. Within the last two decades, these material have been of increasing interest[114], with the first patent in 2002[115]. The focus has mainly been on the magnesium stent for vascular use or orthopedic implants They are becoming more and more used in academia, and

several manufacturers can now supply commercial alloys on a large scale. Biotronik (WE-43-Biotronik, Berlin, Germany) developed a bioabsorbable magnesium stent and the first to be clinically testing in 2007[116]. The drawback is the rapid degradation and can within 2-3 month create significant amounts of hydrogen between the tissue and implant[116]. It is therefore not without issues to corrode metals in bulk in the vascular system. The iron-based alloys seem more appropriate for application with high load (vascular stents and orthopedic implants). They have a significantly slower degradation rate compared to the magnesium alloys[117].

What about the degradation product - the ions Cytotoxicity of iron in high concentrations have been a concern, but overall the concentration have proved to be acceptable in vivo. Pure iron has certain drawbacks. It has an insufficient degradation rate for a bioabsorbable implant and it is ferromagnetic, which can be an issue for patients in need of an MRI scan for diagnostic purposes[114]. To overcome this issue alloying to a significant degree with nickel or manganese has been done. Nickel has the drawback of being a strong allergen, but manganese is not and is essential to the body[117][114]. The Fe-Mn becomes antiferromagnetic, and can enhance mechanical properties so that it matched the ones of stainless steel (316L) the reference material for coronary stents[117]. The incorporation of Mn reduces the corrosion potential and the material becomes less noble and increase the degradation rate [114]. An additional increase in degradation rate can be achieved by alloying with palladium or silicon, which also benefits the mechanical properties. It should be noted that an overdose of manganese can toxic[117] and lead to intoxication and neurotoxicity[118].

Several studies have been done on the alloy Fe-Mn with different Mn content [119][114] [117][120][121][122][123][124][125] behavior in vitro, but limited reporting on in vivo studies exists[116]. Anything over 20 wt% does not lower the ferromagnetic properties further. With increased amounts of Mn the σ_y and UTS decrease, while the ϵ_b increase[117]. FeMn20 has an σ_y of 420MPa, UTS of 700MPa, ϵ_b of 8%, whereas Fe35Mn has a σ_y of 230MPa, UTS of 430MPa and ϵ_b of 30%. The latter composition has properties close to stainless steel 316L with a σ_y of 190MPa, UTS of 430MPa and ϵ_b of 40%. Fe35Mn would therefore be a good candidate for a bioabsorbable metal filter.

10.3.1.1 Challenges with bioabsorbable metal

As described above the mechanical properties are superior to the bioabsorbable polymers. They can exhibit a good radial force while exhibiting good fatigue properties, which the brittle polymers lack. The challenge faced upfront, is the limited knowledge of these materials compared to the bioabsorbable polymers, which have been used in medical devices for decades. The journey of bioabsorbable metals is just beginning. One challenge lies in the degradation of the metals. Without going into the specifics, the degradation profile in vitro can be difficult to match the in vivo degradation. The degradation is corrosion through an electrochemical reaction with electrolyte and produces oxides, hydroxides, and hydrogen gas[126]. As the metal degrades the mechanical integrity of the material is gradually lost. Mechanical loads often speed up the degradation due to a phenomenon is known as stress corrosion. The process includes both stress corrosion cracks and fatigue and makes the in vivo degradation difficult to predict.

During corrosion, metal ions are produced (for example $Fe \rightharpoonup Fe^{2+}+2e^{-}$ and $Mn \rightharpoonup Mn^{2+}+2e^{-}$) and the electrons are used in reduction of oxygen dissolved as hydroxide, which then react with the metals ions and creates a hydroxide layer. The hydroxide layer is not uniformly distributed over the surface of the metal and chloride can access the metal to compensate for the increased metal ions is these spots. The reaction by the two become a metal chloride and when it is hydrolyzed become hydroxide, metal ions, and free acid. The pH level in those particular pits decreases, while the bulk is neutral. This autocatalytic reaction leads to wider and deeper pits[117]. The pitting corrosion is a concern as it is not controlled and it is. Therefore, it is difficult to predict the in vivo degradation from in vitro studies. As their degradation is not dependent on hydrolysis, shelf-life and sterilization are easier. On the positive side, their mechanical properties are superior to polymers, less material is required, and the filter profile is much smaller. The latter is a good selling point amongst the physicians. The shape memory of bioabsorbable metals is excellent and eliminates the risk of a permanent set and can be loaded into the delivery system by the manufacturer and not the physician. Furthermore, metals are much less sensitive to temperature than the polymers.

10.3.2 Future investigation of bioabsorbable polymers

Both the bioabsorbable polymer and metals have their strength and drawbacks. At this point, the bioabsorbable polymers are more understood than the metals and should not be discarded due to the failure of the strained PLLA as a bioabsorbable filter. The design and the material used in this project lacked the flexibility. For the polymer to work in a filter, it needs to either be more flexible and have better fatigue properties. Alternatively, it would need to be stiffer and exhibit a great radial force to prevent the vein from collapsing. The latter would not be advisable as disturbances within the blood flow could cause additional DVTs. It is possible that a braided filter would exhibit the appropriate flexibility while still using PLLA. A different loading procedure would have to be investigated to ensure that it expands fully towards the wall. The most important lesson learned from this study is that PLLA fails too easily under cyclic compression both in vitro and in vivo. Also, it proved to be highly sensitive to temperature and handling during the procedure is difficult. In retrospect, a more expensive investigation of the fatigue properties should have been done rather than optimizing the radial force of the stent-base. PLLA might not be as useful in an IVC filter as it is for an arterial stent, where fatigue requirements are different. The ingrowth or degree of tissue coverage over the PLLA stent-base was faster than anticipated and prevented successful compression of the stent-base. Regarding design, the diamond shaped stent design is not ideal. Fatigue testing will occur near the connection points, which is also seen for materials such as nitinol when incorporated in a diamond shape design and undergone cyclic fatigue testing[127]. The fatigue failure is either due to the poor fatigue properties of PLLA or due to the nature of the design. Regardless of material, it is expected that the design will fracture over time near the connection points. At which point in time this occurs depends on the material.

It is unlikely at this stage that it would be possible to process PLLA in a way which would improve the fatigue properties greatly, and that it would undergo continuous cyclic compression without fatigue failure. This might only be achievable with an elastomer, such as PCL. The tissue growth might be different for PCL, as it exhibits less radial force, and does not stimulate the cells to grow in the same way as PLLA did. This could potentially be an issue as incorporation into the wall diminishes the risk of migration. The answer might lie within a composite, where the initial stent-base skeleton is made from a material with great stiffness and thereby radial force with an underlying elastomeric layer. An adequate radial

force would then be achieved initially, and sufficient tissue coverage occurs. As the stiff polymer fractures, the stent-base is kept together by the underlying elastomer.

The main focus of the project became to optimize the radial force of PLLA to avoid the risk of migration. The focus might have been wrong as it was not determined if the radial force of the PLLA stent-base with too high, only that it was adequate. PCL was previously investigated by others[39] and proved not to have enough radial force. The material of interest might have properties which lie between the strained PLLA and PCL as a copolymer or as a composite.

11

Conclusion

Bioabsorbable polymers are today well known as an alternative to permanent implants. Depending on the different applications different requirements are needed to fulfill the intended function. The overall aim of this project was to investigate the possible material candidates for a bioabsorbable vascular implant, the inferior vena cava (IVC) filter. The overall requirement of a bioabsorbable IVC filter was the need to function as a filter for 2-3 months. Furthermore, no fragments of the filter should cause harm to the patient until complete absorption of the filter has occurred. Additionally, the IVC filter must not migrate upstream to the heart, and the radial force should be adequate until the IVC filter is sufficiently embedded into the caval wall. A challenge with the vena cava is that the blood pressure is low and the vein therefore easily collapses during respiratory movements. The device must, therefore, be able to either withstand the continuous cyclic compressions of the vein (good fatigue properties are required) and have enough radial force to prevent migration. It was found that no polymer seemed to fulfill the requirements of both having adequate flexibility while maintaining a high radial force. It was learned that a monofilament with a great stiffness but low flexibility would provide a braided stent-base for an IVC filter with higher radial force than obtained for monofilament with a lower stiffness. With that in mind, the goal became to improve the stiffness and radial force of a stent-base. This was done by an orientation of chains and crystals through strain-induced crystallization of extruded poly(L-lactide) (PLLA) tubes in a biaxial straining process. It was seen that braiding a filter with the same dimension from highly crystal oriented monofilament would provide only half the radial force of a stent-base from biaxially strained PLLA tubing when placed in a 15 mm vein. Whether or not the radial force is enough to prevent migration was not confirmed in this

study.

Straining of PLLA tubes Biaxial strain of PLLA tubes, induced the tube with improved stiffness and strength in both axial and circumferential direction in correlation with the increase in total area expansion (A_{exp}), despite a constant degree of crystallinity (X_c). The elongation at break (ϵ_b) was also dependent on the degree of A_{exp}. The biaxial strain was done either simultaneously in each direction, or in two steps (sequential) with the axial strain applied first. It was found that certain processing parameters need to be fulfilled to obtain strain-induced crystallization. During the axial processing strain (ϵ_a) the degree of strain must be close to 100% before crystallization occurs. Below this strain the extruded tube remains amorphous. Processing temperatures (T_p) ≥85°C will not induce crystals in the axial direction during strain due to an increase in mobility of the material that prevents permanent alignment of molecular chains and thereby crystal formation. The degree of strain was inadequate at elevated temperature. Unfortunately, the mechanical properties after axial strain were not measured. Applying a transverse strain to the axially strained sample will induce crystals, which in most instances were much larger than the axial strain degree. It is, therefore, possible to induce crystals at elevated temperature, but the degree of strain must be higher than 100%. The crystal orientation is poorer when transverse strain ($\dot{\epsilon_p}$) is imposed at elevated temperatures and the increase in stiffness and strength are dependent on the alignment and elongation of amorphous chains. The strain processing rate also determines if crystals are formed during the axial strain. If the rate is too slow, the chains tend to relax, and crystals are not formed regardless of T_p.

Heat treatment or annealing of the strained tubes reduces the amorphous chain alignment or cause the chains to relax to their initial state before being biaxially strained. Thus heat treatment deteriorates the mechanical properties. The crystal orientation is also reduced, but thought not to be of interest as the improved mechanical properties of the tube did not seem to correlate with the orientation factor previously. The heat treatment was used to expand a laser cut strained tube to a larger diameter (27 mm). It was seen that rapid cooling with freeze spray reduced the mechanical properties even further and cooling in air at room temperature was preferable. The sterilization of the strained tubes proved to be beneficial if sterilized close to the T_g. The improved stiffness and strength were not related to the presence of ethylene oxide (EO) during sterilization, but rather the temperature. During sterilization, it was possible to regain some of the improved stiffness and strength

from the biaxial strain but not to the same level as before heat treatment. Overall the strain-inducing crystallization process was beneficial for improving certain mechanical properties of PLLA, but the process appeared to be reversible through heating.

Evaluation of $\dot{\epsilon_p}$, T_p and sterilization was done on different prototypes and showed the same tendencies as for the biaxially strained tubes. It was concluded that the circumferential properties of the tubes could be correlated to the radial force of a stent-base. Stent-bases processed with a high degree of axial strain or at high T_p were proven not to be ideal and were not chosen for the in vivo study. A braided filter from an oriented PLLA monofilament exhibit about half of the radial force of the biaxially strained laser cut stent-bases in a 15 mm vein. The filter was less prone to permanent deformation and appeared more flexible. Due to the lower radial force, the braided filter was not be considered for an in vivo study. During cyclic compression (120,000) of the laser cut stent-bases under physiological conditions, permanent deformation was seen, but fractures were not detected.

In vivo The biaxially strained PLLA tubes were processed to their optimal abilities and laser-cut into a diamond shape stent cell design. Based on the in vitro findings, the best prototype and processing parameters were chosen. The chosen prototype was implanted in an ovine animal model in vivo. The results were not as promising as anticipated, and the study was terminated after just 3 ½ weeks due to multiple fractures. Despite prediction from the in vitro testing, it was seen that the PLLA stent-base would fracture much sooner than anticipated. It appeared that the caudal stent-base had adequate tissue coverage to prevent to fragmented PLLA pieces from migrating, whereas few pieces of the cranial stent-base remained. It was concluded that the stent-base had shown adequate radial force until fragmentation occurred and prevented migration of the whole stent. The limitation of the stent-base design and material was attributed to poor fatigue properties during compression. The cyclic compression station in vitro, which tested the whole stent-base was not a good model for predicting fractures in vivo. It compressed to the stent-base about 30% which was based on the degree of collapse of the vena cava clinically but was not enough to detect fractures in vitro. PLLA showed poor fatigue properties when used in a diamond shaped stent-base. Therefore it might be better to choose a material with a greater flexibility and better fatigue properties. To ensure both flexibility and appropriate radial force a composite material could be the solution. One layer could contain a stiffer polymer to ensure great radial force until tissue coverage occurred and fragments would stay in the wall. The

second layer could consist of a more flexible polymer with better fatigue properties, and would be able to withstand the compression and hold the stent-base together despite the stiff fragmented layer.

Appendix A

Bioabsorbable materials

A.1 Bioabsorbable stents

Table A.1: Table over bioabsorbable polymeric stents

Name	Company	Application	Configuration	OD(mm)	Material	Study time
Igaki-Tamai	Igaki Medical Planning Company	Coronary Artery Disease	Self-expanding[20]. Zig-zag with straight bridges with gold marker[19]	3	PLLA	10 year clinical, stopped[19]
BVS	Abbott Vascular	Coronary Artery Disease	Out of phase zig zag with straight bridges with platinum markers[19]	3	PLLA back bone with PDLLA coating[128]	Several clinical trials. Upcoming clinical trial for US approval[20]
ReZolve 2 (REVA)	REVA Medical	Coronary Artery Disease	Slide and lock. Iodine impregnated for radio-opacity	2.7-4.0	Tyrosine-derived polycarbonate[20]	Clinical followup expected in 2016[19]
Ideal	Bioabsorbable Therapeutics	Coronary artery disease[128]	Drug eluting poly(anhydride ester) salicylic acid		PLLA, anhydride and saliccyclic acid	Under development[19] [20]
AMS	Biotronik	Coronary artery disease [19]	Sinusoidal in-phase hoops linked by straight bridges	3.0-3.5[129]	Magnesium based	Ongoing clinical trials[19]

Appendix B

Characterization methods

B.1 Mechanical properties definitions

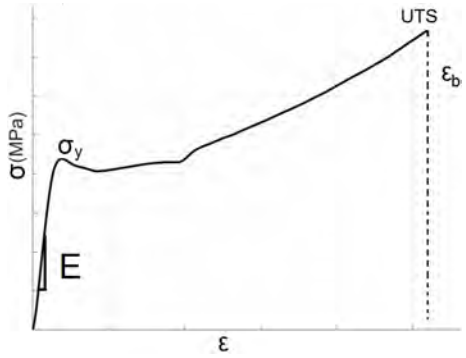

Figure B.1: Stress-strain curve with its mechanical properties defined

B.2 Matlab Scripts

B.2.1 Tensile testing script

```
%% Specify the samples names by sample number. Tube 254, sample 1-3
specimens={'254.1','254.2','254.3'};

%% Import dimensions
run('Importdimension.m')
%Find index for specimens
for i=1:length(specimens);
   for j=1:length(ID)
       if strcmp(ID{j},specimens{i}) == 1
```

```
          index(i)=j;
       end
   end
end
% Find length (L0) and cross-sectional area (A0) for specimens
for k=1:length(index)
    L0(k)=Lmm(index(k));
    A0(k)=A0mm(index(k));
end

%% Import data for each specimen
for i=1:length(specimens)
        % insert correct path
fid = fopen(['Specimen_RawData_' num2str(i) '.csv']);
out = textscan(fid,'%q%q%q%q','delimiter',';');
fclose(fid);
%replace , with .
for     u=1:4
    for j=1:length(out{1,1})
        out{u}{j}=str2double(strrep(out{u}{j},',','.'));
    end
    out{u}=cell2mat(out{u});
end
% Define deflection and load
defl=out{1,3}(5:end);
load=out{1,4}(5:end);

% Calculate stress and strain values
strain254=defl/L0(i);
stress254=load/A0(i);
% Calculate an intersection to move curve to the left going through 0 on the
% x-axis
[Test.flyout,func1]=CalcLinFit(strain254,stress254,2,[5 40]);
Test.a1(i)=func1.p1;Test.b1(i)=func1.p2;
% x-values for which y=0
Xx(i)=func1.p2/func1.p1
h=(ones(1,50)*Xx(i))';
strain254{i}=strain254{i}+h(i)

Test.strain254{i}=strain254;
Test.stress254{i}=stress254;

% Cut off curve after max stress is reaced and stress is dropped to 80% of
% max stress
 maxadd=0.8;
```

```
[imax(i),imaxclip(i)]=CalcMax(Test.stress254{i},maxadd);
Test.strain254{i}=strain254(1:imaxclip(i));
Test.stress254{i}=stress254(1:imaxclip(i));

% Find yield stressat the first local maximum in stran interval [0.02;0.1]
[pks(i),locs(i)]=max(Test.stress254{i}(Test.strain254{i}>=0.02&Test.strain254{i}<=0.1))
Test.stressyield254(i)=pks(i);

% Calculate modulus in a specific stress interval
[Test.Emod254(i),Test.linfitEmod{i}]=
            CalcLinFit(Test.strain254{i},Test.stress254{i},2,[20 40]) ;
%find max stress and max elongation
sigmamax254(i)=max(Test.stress254{i});
elongmax254(i)=max(Test.strain254{i});
end

%% Following functions are written by L. P. Mikkelsen (2009)
% CalcMax
% CalcLinFit
```

B.2.1.1 Import data

```
%% Import dimensions from spreadsheet
[~, ~, raw] = xlsread('dimensions.xls','Ark1');
raw(cellfun(@(x) ~isempty(x) && isnumeric(x) && isnan(x),raw)) = {''};
cellVectors = raw(:,[1,11,12,13,14,15,16,18]);
raw = raw(:,[2,3,4,5,6,7,8,9,10,17,19,20]);

%% Replace non-numeric cells with NaN
R = cellfun(@(x) ~isnumeric(x) && ~islogical(x),raw); % Find non-numeric cells
raw(R) = {NaN}; % Replace non-numeric cells

%% Create output variable
data = reshape([raw{:}],size(raw));

%% Allocate imported array to column variable names
ID = cellVectors(:,1);
A0mm = data(:,6); % Cross-sectional area
Lmm = data(:,7) % Length
```

B.2.1.2 CalcLinFit

The CalcLinFit function was used to calculate a slope of a linear line

```
function [slope,linfit]=CalcLinFit(x1,x2,xn,xnrange,imax)
%% [slope,linfit]=CalcLinFit(x1,x2,xn,xnrange)
% Find a linear fit in the xnrange
%% Inddata:
%  x1: x-vector
%  x2: y-vector
%  xn: =1 or 2 depending on what xnrange is for x or y values
%      =0 istart and iend given in xnrange instead
%      =3 full range, xnrange is not taken into acount
%  xnrange: the range for the fit (x or y values depending on xn)
%  imax(opt.): include large range in CalcRange
%% Outdata:
%  slope: the slope of the linear fit in the plot (e.g. Emod or strainrate)
%  linfit: fit information used in PlotLinFitAdd function
%% Author: L.P. Mikkelsen, AFM-KOM, Risoe-DTU, 2009.
%%
if xn==1
    if nargin>4
        [istart,iend,ierr]=CalcRange(x1,xnrange,imax);
    else
        [istart,iend,ierr]=CalcRange(x1,xnrange);
    end
elseif xn==2
    if nargin>4
        [istart,iend,ierr]=CalcRange(x2,xnrange,imax);
    else
        [istart,iend,ierr]=CalcRange(x2,xnrange);
    end
elseif xn==0
    istart=xnrange(1);iend=xnrange(2);
    ierr=0;
elseif xn==3
    istart=1;iend=length(x1);
    ierr=0;
end
if ierr > 0; % in the case of an error in the range
    disp(['ERROR CalcLinFit range,',num2str(xn),' ',num2str(xnrange)])
    slope=0.0;
    linfit.p1=0.0;
    linfit.p2=0.0;
    linfit.istart=1;
    linfit.iend=length(x1);
    return;
else
    %% Calculate slope for x1range(1)<x1<x1range(2)
```

```
    p=polyfit(x1(istart:iend),x2(istart:iend),1);
    slope=p(1);
    linfit.p1=p(1);
    linfit.p2=p(2);
    linfit.istart=istart;
    linfit.iend=iend;
end
```

B.2.1.3 CalcMax

CalcMax was used to cut the stress curve after UTS.

```
function [imax,imaxclip]=CalcMax(load,maxadd)
%% [imax,imaxclip]=CalcMax(load,maxadd)
% Find the array element with the max value and maybe a later point as well
%% Inddata:
%  load: the vector from where the max value is found
%  maxadd(opt.): a factor < 1 which add some additonal curves to the range and
%  save that array element in imaxclip (used if some part of the curve
%  after the max is wanted in the plots or during the following data
%  analysis
%% Outdata:
%  imax: array element for max value
%  imaxclip: array element for max value or after maxvalue*maxadd
%% Author: L.P. Mikkelsen, AFM-KOM, Risoe-DTU, 2009.
%%
iall=length(load);
maxload=-1.0e99;
for i=1:iall
    if abs(load(i))>maxload
        maxload=abs(load(i));
        imax=i;
    end
end
if nargin>1
    i=imax;
    if maxadd >= 1.0; imaxclip=imax; return; end;
    if maxadd == 0; imaxclip=iall; return; end;
    while i<iall && abs(load(i))>maxload*maxadd
        imaxclip=i;
        i=i+1;
    end
else
```

```
    imaxclip=imax;
end
```

B.3 WAXS package

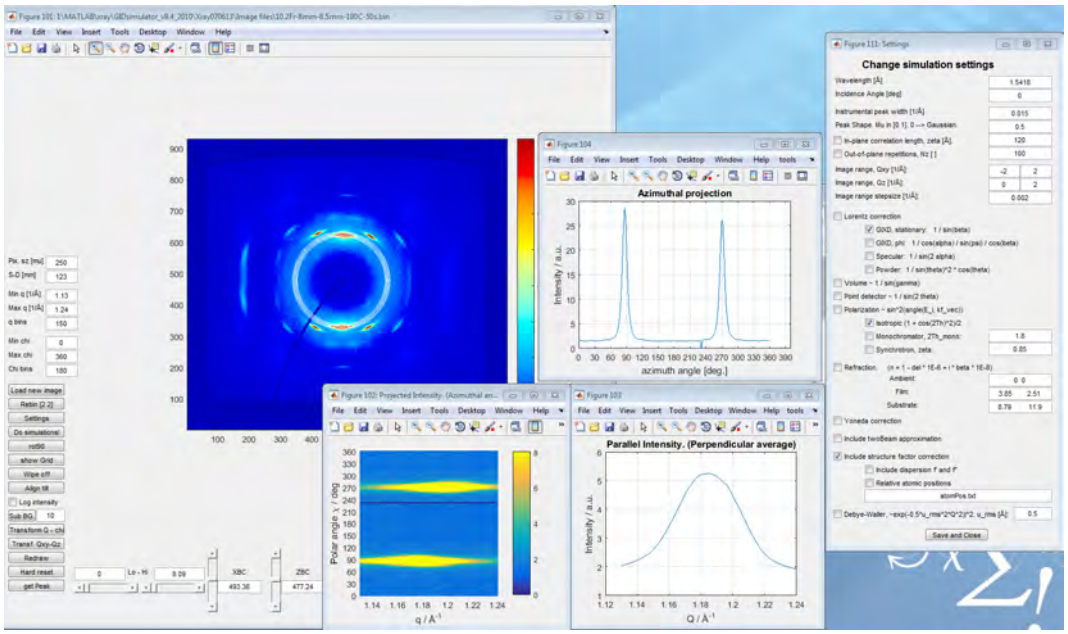

Figure B.2: WAXS package used for analysis for XRD patterns

Appendix C

Materials

C.1 Stereometry

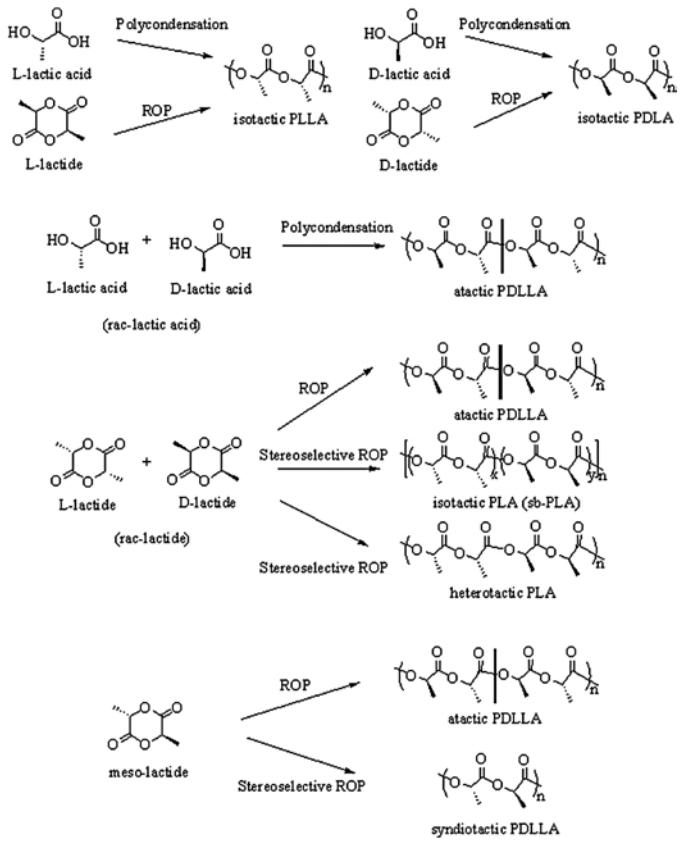

Figure C.1: Stereochemical possibilities observed with polylactide synthesis either through ring opening polymerization (ROP) or polycondensation. Used from [78]

C.2 Specifics on monofilaments from vendors

Table C.1: Composition of the monofilament purchased from Corbion and Zeus

Manufacturer number	Polymer	Processing
Purac Purasorb PL24	PLLA	As extruded Oriented
Purac Purasorb PD24-PL24	PDLA-PLLA blend	As extruded Oriented
Purac Purasorb PLC7015B	70:30 PLLA-PCL blocky	Elongated As extruded
Zeus Absorv 85L/15G PLGA	85:15 PLGA	Oriented
Purac Purasorb PLC8516B	85:15 PLGA	As extruded

Appendix D

Additional results

D.1 Radial force of braided stents during the 1st cycle

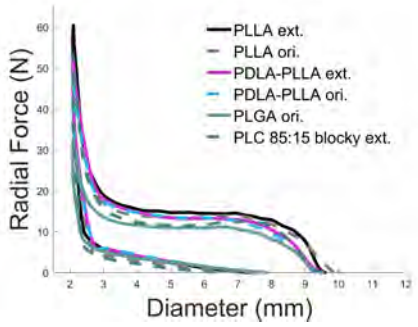

Figure D.1: Radial force of braided stent after 1 compression cycle from 10mm to 2.1mm

D.2 Analysis of tubes from Zeus and BVS from Abbott Vascular

D.2.1 Mechanical properties

Table D.1: Mechanical properties of Zeus extruded and oriented PLLA tube

	E_{axial} (MPa)	$\sigma_{max,ax}$ (MPa)	$\sigma_{y,ax}$ (MPa)	$\epsilon_{f,ax}$ (%)	E_{circ} (MPa)	$\sigma_{y,circ}$ (MPa)	$\sigma_{max,circ}$ (MPa)	$\epsilon_{f,circ}$ (%)
PLLA ext.	1076±56	532±	47±2	368±100	585±107	39±2	44±2	73±23
PLLA 1196	700±24	66±1	71±3	341±41	922±156	78±0	112±1	124±5

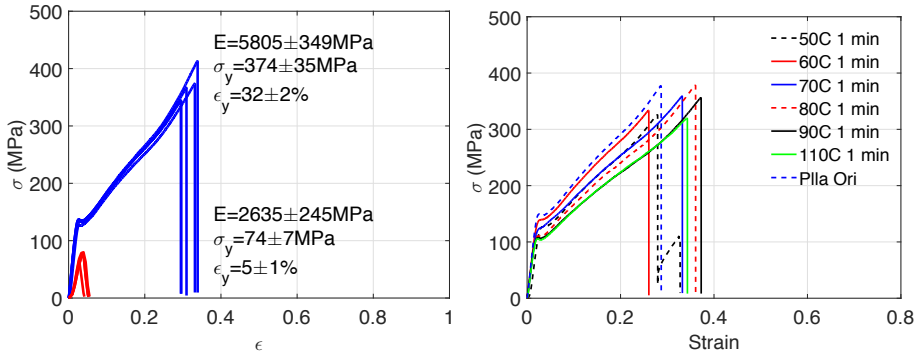

(a) (b)

Figure D.2: Stress-strain curves for PLLA non-oriented and oriented monofilament before and after annealing

D.2.2 Thermal properties and WAXS analysis

Table D.2: Thermal properties and scattering data of Zeus oriented PLLA tube (1196) and PLLA BVS from Abbott

	T_g (°C)	T_m (°C)	X_c%	F2	D_{ax}	D_{circ}
PLLA 1196	63	179	47	0.6	176	74
Abbott BVS	68	178	52	0.02	148	50

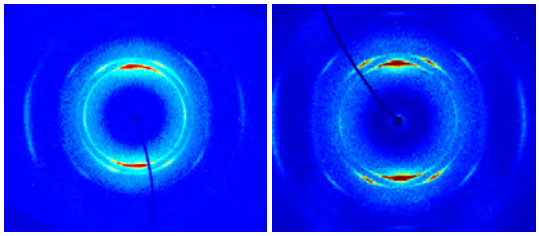

(a) (b)

Figure D.3: WAXS images of BVS from Abbott Vascular and the oriented PLLA tube from Zeus

D.3 Differential scanning calorimetry scans

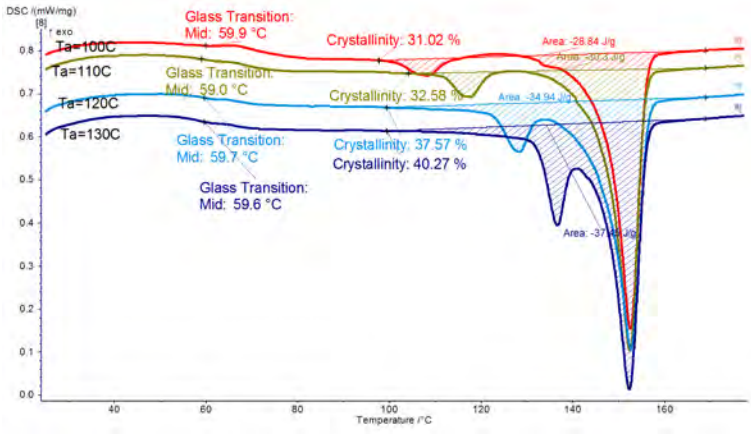

Figure D.4: DSC scan for isothermal annealing of sequential biaxially strained for 30 min at temperatures between 100 and 130°

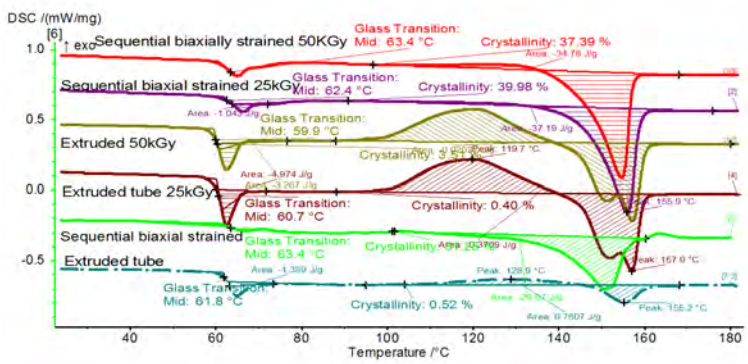

Figure D.5: DSC scan for isothermal annealing of sequential biaxially strained for 30 min at temperatures between 100 and 130°

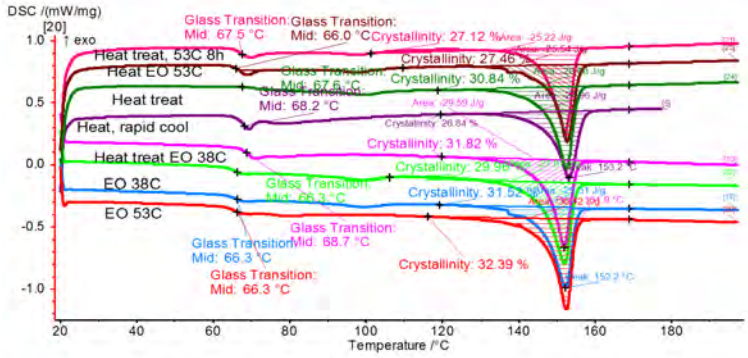

Figure D.6: DSC scan for isothermal annealing of sequential biaxially strained for 30 min at temperatures between 100 and 130°

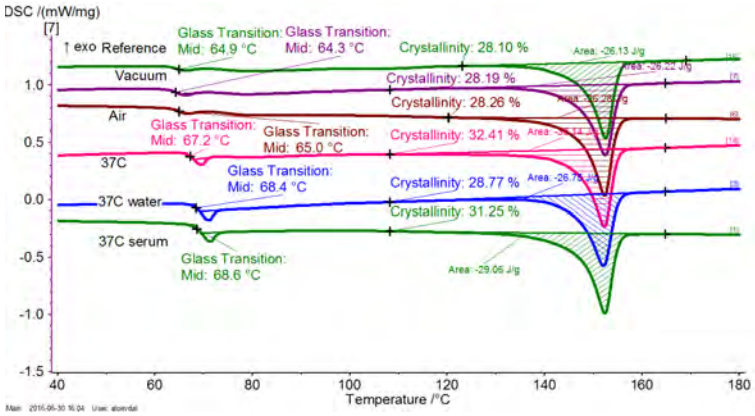

Figure D.7: DSC scan for sequential biaxially strained tubes, which have undergone aging for 2 weeks in air, 37°C serum and water and at ambient conditions

D.4 Gel permeation chromatography measurement

Table D.3: Molecular weight (M_n, M_w), polydispercity index (Pd) and refractive (RI) index area for extruded and sequential biaxially strained tubes under different treatment

Type	Fr size	Lot#	Mass /mg	Mn (kg/mol)	Mw (kg/mol)	Pd	RI area
Concept 0706, heat treated, rapid cool	16.5		17	94.9	193.6	2.04	65.5
				85.9	195.4	2.28	65.5
Concept 0706, heat treated, rapid cool	16.5		18.3	100.1	188.3	1.88	65.8
				94.5	192.7	2.04	67.10
Sequential (1.2;3.2) (2x25kGy)	10.2		21.6	31.9	67.7	2.12	63.7
				35	67.60	1.93	62.1
Concept0608	16.5		26.9	93.3	187.9	2.10	66.5
				97.3	192.1	1.97	66.5
Extruded tube	13.2	JP237396	24.1	94.3	186	1.97	70.00
				106.8	190	1.78	68.50
Extruded tube	10.2	JP253453	25	102.9	195.9	1.90	66.33
				112.7	195	1.73	64.14
Extruded tube	16.5	JP241546	24.9	107.9	194.6	1.804	65.19
				113.3	198.2	1.75	65.10
Extruded tube	16.5	JP241546	25.2	97.8	192.3	1.966	66.72
				115	199.5	1.74	65.95
Extruded tube	10.2	JP246909	23.7	105.9	197.4	1.86	65.67
				102.5	194.8	1.9	65.60
Sequential (1.2;3.2) 60min at 90C	10.2		25.3	98.9	191.7	1.94	68.40
				102.6	190.6	1.86	67.83

D.5 Thickness after sterilization

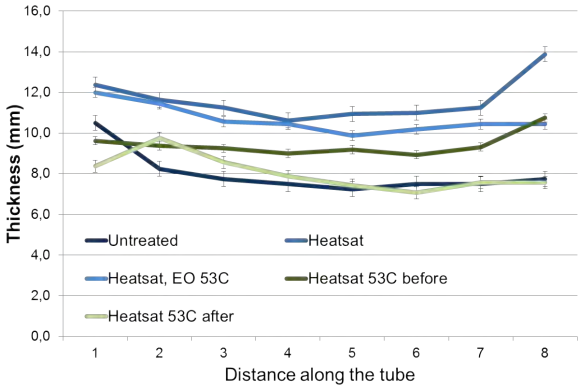

Figure D.8: Thickness of sequential biaixally strained tubes before and heat treatment and sterilization at 53°C from one end to another

D.6 Cylic testing

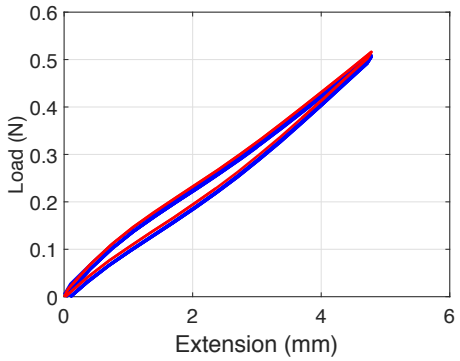

Figure D.9: Load-extension curve for a single stent cell tested under cyclic compression. The cell was strained at T_p=73°C and cut into cells based on the Concept0708 design. It was further heat treated 93°C for 5 min. During testing the cell was crimped to 50% of its initial height.

Appendix E

Tube parameter for in vivo study

Table E.1: Processing parameters for tubes used in the animal study

Process parameters							
Tube size (Fr)	Axial elongation (mm)	Radial expansion (mm)	Form diameter (mm)	Form length (mm)	T(°C)	time(s)	Pressure (bar)
16.5Fr	28	5	10.5	120	73	150	20
Tube parameters							
ϵ_{ax} (mm)	ϵ_r (mm)	A_{exp}	Thickness (mm)				
128%	52%	216%	0.46-0.79				

References

[1] J. Hervey. Neoplasia. In T. J. Nowak and A. Gordon Handford, editors, *Pathophysiology*, chapter 6, pages 130–166. McGraw-Hill, 1221 Avenue of the Americans, New York, NY 10020, 2004. xvii

[2] J. Hervey. Neoplasia. In *Anatomy & Physiology*, chapter 21, pages 723–783. McGraw-Hill, 1221 Avenue of the Americans, New York, NY 10020, 2006. xvii

[3] M. M. Kiguchi and E. D. Dillavou. IVC Filters: Challenges and Future Directions. *Adv Vasc Med*, 2014:1–6, 2014. 1, 2, 3

[4] T. Young, H. Tang, and R. Hughes. Vena caval filters for the prevention of pulmonary embolism(Review). *Cochrane Database Syst Rev*, 2:1–24, 2010. 1, 3, 9, 10

[5] M. Eggers and C. A. Reitman. In vitro analysis of polymer candidates for the development of absorbable vascular filters. *J Vasc Interv Radiol*, 23:1023–1030, 2012. 1, 21

[6] J. A. Kaufman, T. B. Kinney, M. B. Streiff, R. F. Sing, M. C. Proctor, D. Becker, M. Cipolle, A. J. Comerota, S. F. Millward, F. B. Rogers, D. Sacks, and A. C. Venbrux. Guidelines for the Use of Retrievable and Convertible Vena Cava Filters: Report from theSociety of Interventional Radiology Multidisciplinary Consensus Conference. *J Vasc Interv Radiol*, 17:449–459, 2006. 1, 13

[7] D. Imberti, W. Ageno, F. Dentali, M. Donadini, R. Manfredini, and M. Gallerani. Retrievable vena cava filters: a clinical review. *J Thromb Thrombolysis*, 33:258–266, 2012. 1, 2, 3

[8] J. M. Merrigan, G. Piazza, C. Lynm, and E. H Livington. Pulmonary Embolism. *JAMA*, 309:504, 2013. 2

[9] Cardiovascular and Interventional Radiological Society of Europe. Inferior vena cava (IVC) filters placement and retrieval, jul 2016. http://cirse.org/index.php?pid=1051. 2

[10] A. N. Keeling, T. B. Kinney, and M. J. Lee. Optional inferior vena caval filters: where are we now? *Eur Radiol*, 18:1556–1568, 2008. 2, 10

[11] U.S. Food and Drug Administration. Removing Retrievable Inferior Vena Cava Filters: FDA Safety Communication, May 2016. http://www.fda.gov/MedicalDevices/Safety/AlertsandNotices/ucm396377.htm. 3

[12] S. L. Wang and A. J. Lloyd. Clinical review: Inferior vena cava filters in the age of patient-centered outcomes. *Annals of Medicine*, 45:474–481, 2013. 4

[13] M. M. Madsen. Thermal and Mechanical Characterization of Bioabsobable Polymers for Implantation use. Master's thesis, Technical University of Denmark, Anker Engelundsvej 101, 2800 Kgs. Lyngby, 2014. 5, 82, 85, 103, 104, 116, 117, 177

[14] M. Iwersen. Investigation of Biosorbable Polymers under Static and Cyclic Stress. Master's thesis, Technical University of Denmark, Anker Engelundsvej 101, 2800 Kgs. Lyngby, 2015. 5, 136, 137, 180

[15] T. Noorzae. Time dependent properties of medical implants made of Poly(L-lactic acid). Master's thesis, Technical University of Denmark, Anker Engelundsvej 101, 2800 Kgs. Lyngby, 2016. 5, 117, 137, 138

[16] I. Weinberg, J. Kaufman, and M. R. Jaff. Inferior Vena Cava Filters. *JACC Cardiovasc Interv*, 6:539–547, 2013. 9

[17] M. Lessne, M. J. Rinaldi, and R. F Sing. Vena cava filter options: what's on the horizon? *Expert Rev Cardiovasc Ther*, 14:415–421, 2016. 10, 11

[18] J. L. Antevil, M. J. Sise, D.I Sack, K.J. Sasadeusz, S. M Swanson, L. Rivera, B. R Lome, and K. E. Weingarten. Retrievable Vena Cava Filters for Preventing Pulmonary Embolism in Trauma Patients: A Cautionary Tale. *J Trauma*, 60:35–40, 2006. 11

[19] P. Divya, N. Rama, S. Prashanth, N. S. Kumar, and J. V. Sagar. Bioabsorbable stents: Has the concept really translated to clinical benefits? - Concept to clinical - Update: 2012. *JJICC*, 2:156–159, 2012. 11, 189

[20] N. S. van Ditzhuijzen, A. Karanasos, J. N. van der Sijde, G. van Soest, and E. Regar. Bioabsorbable Stent. In I. Jang, editor, *Cardiovascular OCT Imaging*, chapter 13, pages 179–193. Springer International Publishing Switzerland, Harvard Medical School, Boston MA USA, 2015. 11, 189

[21] Medscape. Optional Vena Cava Filters: What, Why, and When, May 2016. `http://www.medscape.com/viewarticle/567034`. 11, 12

[22] Interventional news. First patient enrolled in US study of Novate's Sentry IVC filter, March 2016. `http://www.cxvascular.com/in-latest-news/interventional-news---latest-news/first-patient-enrolled-in-us-study-of-novates-sentry-ivc-filter`. 11

[23] X. Gao, J. Zhang, B. Chen, H. Yu, J. Li, S. Zhang, Z. Feng, L. Ye, and J. Han. A new self-contible inferior vena cava filter: experimental in vitro and in vivo evaluation . *J Vasc Interv Radiol*, 22:829–834, 2011. 12

[24] R. F. Sing, S. M. Camp, B. T. Heniford, E. J. Rutherford, S. Dix, P. M. Reilly, J. H. Holmes, E. Hautt, and A. Hayanga. Timing of Pulmonary Emboli after Trauma: Implications for Retrievable Vena Cava Filters. *J Trauma*, 60:732–735, 2006. 15

[25] N. Patel and A. P. Banning. Bioabsorbable scaffolds for the treatment of obstructive coronary artery disease: the next revolution in coronary intervention? *Heart*, 99:1236–1243, 2013. 16, 18

[26] R. Plonsey. Physiologic Systems. In B. Palsson, J. A. Hubbell, Robert Plonsey, and J. D. Bronzino, editors, *Tissue Engineering*, chapter 1, pages 1–12. CRC Press Taylor & Francis Group, 6000 Broken Sound Parkway NW, Suite 300, Boca Raton, FL, USA, 2003. 16

[27] D. J. Wallace, M. Allison, and M. B. Stone. Inferior Vena Cava Percentage Collapse During Respiration Is Affected by the Sampling Location: An Ultrasound Study in Healthy Volunteers. *Acad Emerg Med*, 17:96–99, 2010. 17, 134

[28] W. Xiao-ping, X. Yue-yong, and Z. Xiao. Inferior Vena Cava Filter based on biodegradable materials. *CRTER*, 15:2133–2137, 2011. 18, 22, 23

[29] R. Samuel, E. Girard, G. Chagnon, S. Dejean, D. Favier, J. Coudane, and B. Nottelet. Radiopaque poly(ϵ-caprolactone) as additive for X-ray imaging of temporary implantable medical devices. *RSC Adv*, 5:84125–84133, 2015. 19, 20

[30] S. Y. Choi, W. Hur, B. K. Kim, C. Shasteen M. H. Kim, L. M. Choi, S. H. Lee, C. G. Park, M. Park, H. S. Min, S. Kim, T. H. Choi, and Y. B. Choy. Bioabsorbable bone fixation plates for X-ray imaging diagnosis by a radiopaque layer of barium sulfate and poly(lactic-co-glycolic acid). *J Biomed Mater Res Part B*, 103B:596–607, 2015. 20

[31] J. Nuutinen, C. Clerc, and P. Törmälä. Mechanical properties and in vitro degradation of self-reinforced radiopaque bioresorbable polylactide ÂŐ bres. *J Biomater Sci Polym Ed*, 7:665–676, 2003. 20

[32] T. Lämsä, H. Jin, J. Mikkonen, J. Laukkarinen, J. Sand, and I. Nordback. Biocompatibility of a New Bioabsorbable Radiopaque Stent Material ($BaSO_4$ Containing Poly-L,D -Lactide) in the Rat Pancreas. *Pancreatology*, 6:301–305, 2006. 20

[33] K. Lei, W. Shen, L. Cao, L. Yu, and J. Ding. An injectable thermogel with high radiopacity. *Chem Commun*, 51:6080–6083, 2015. 20

[34] C. Shasteen, S. M. Kwon, K. Y Park, S. Y. Jung, S. H. Lee, C. G. Park, M. H. Kim, S. Kim, W. Son, T. H. Choi, and Y. B. Choy. Biodegradable internal fixation plates enabled with X-ray visibility by a radiopaque layer of β-tricalcium phosphate and poly (lactic-co-glycolic acid). *J Biomed Mater Res Part B*, 101B:320–329, 2013. 20

[35] K. Miyazaki, T. Nishibe, H. Manase, H. Ohkashiwa, T. Takahashi, S. Watanabe, H. Katoh, and Y. Morita. J Biomater Sci Polym Ed. *Jpn J Surg*, 28:396–400, 1998. 20, 21

[36] J. Nuutinen, C. Clerc, R. Reinikainen, and P. Törmälä. Mechanical properties and in vitro degradation of bioabsorbable self-expanding braided stents . *J Biomater Sci Polym Ed*, 14:255–266, 2003. 21

[37] M. Eggers and C. A. Reitman. Pilot in vivo study of an absorbable polydioxanone vena cava filter. *J Vasc Surg Venous Lymphat Disord*, 3:409–420, 2015. 21, 169, 170, 179, 180

[38] A. Thors and P. Muck. Resorbable inferior vena cava filters: trial in an in-vivo porcine model. *J Vasc Interv Radiol*, 22:330–335, 2011. 21, 22, 169

[39] F. Zhang, H. Li, G. Liang, and H. Zhang. Development and evaluation of a new biodegradable vena cava filter in a canine model. *Asian J Surg*, X:1–5, 2015. 21, 22, 169, 170, 177, 184

[40] D. Y. Kwon, J. I Kim, D. Y. Kim, H. J. Kang, B. Lee, K. W. Lee, and M. S. Kim. Biodegradable stent. *J Biomed Sci Eng*, 5:208–216, 2012. 23, 44

[41] N. Grabow, M. Schlun, K. Sternberg, N. Hakansson, S. Kramer, and KP Schmitz. Mechanical properties of laser cut poly(L-lactide) micro-specimens: Implications for stent design, manufacture, and sterilization. *J Biomech Eng*, 127:25–31, 2005. 23, 24, 107, 121

[42] C. M. Bünger, N. Grabow, K. Sternberg, C. Krøger, L. Ketner, K. Schmitz, H. J. Kreutzer, H. Ince, C. A. Nienaber, E. Klar, and W. Schareck. Sirolimus-Eluting Biodegradable Poly-L-Lactide Stent for Peripheral Vascular Application: A Preliminary Study in Porcine Carotid Arteries. *J Surg Res*, 139:77–82, 2007. 24

[43] J. D. Menczel, L. Judovits, R. B. Prime, H. E. Bair, M. Reading, and S. Swier. Differential Scanning Calorimetry (DSC) . In J. D. Menczel and R. B. Prime, editors, *Thermal Analysis of Polymers: Fundamentals and Applications*, chapter 2, pages 7–239. A John Wiley & Sons, Inc. Publication, 111 River Street, Hoboken, NJ 07030, USA, 2009. 29

[44] A. L. V. Løvdal, K. Agersted, J. W. Andreasen, and L. P. Mikkelsen K. Almdal. Characterization Of Biaxial Strain Of Poly(L-Lactide) Tubes. *Polm Int*, 65:133–141, 2015. 29, 67, 69, 106

[45] W. Zhai, Y. Ko, W. Zhu, A. Wong, and C. B. Park. A Study of the Crystallization, Melting, and Foaming Behaviors of Polylactic Acid in Compressed CO_2 . *Int J Mol Sci*, 10:5381–5397, 2009. 29, 57

[46] L. C. Sawyer, D. T. Grubb, and G. F. Meyers. Problem Solving Summary. In L. C. Sawyer, D. T. Grubb, and G. F. Meyers, editors, *Polymer Microscopy*, chapter 7, pages 479–504. Springer Science & Business Media, 233 Spring Street, New York, NY 10013, USA, 2008. 30

[47] M. Birkholz. Principles of X-ray Diffraction. In *Thin Film Analysis by X-Ray Scattering*, chapter 1, pages 1–42. Wiley-VCH Verlag GmbH & Co. KGaA, Weinheim, Germany, 2006. 30

[48] S. Skou, R. E. Gillilan, and N. Ando. Synchrotron-based small-angle X-ray scattering of proteins in solution. *Nature Protocols*, 9:1727–1739, 2014. 30

[49] R. Gudavarthy and E. A. Kulp. Epitaxial electrodeposition of Chiral Films Using Chiral Precursors. In Jason B. Benedict, editor, *Recent Advances in Crystallograpy*, chapter 8, pages 169–190. Intech, http://www.intechopen.com/books/recent-advances-in-crystallography, 2012. 30

[50] S. Sakurai, S. Aida, S. Okamoto, T. Ono, K. Imaizumi, and S. Nomura. Preferential Orientation of Lamellar Microdomains Induced by Uniaxial Stretching of Cross-Linked Polystyrene-block-polybutadiene-block-polystyrene Triblock Copolymer. *Macromolecules*, 34:3672–3678, 2001. 31

[51] X. Zhang, K. Schneider, G. Liu, J. Chen, K. Brüning, D. Wang, and M. Stamm. Structure variation of tensile-deformed amorphous poly(L-lactic acid): Effects of deformation rate and strain. *Polymer*, 52:4141–4149, 2011. 31

[52] A. W. Rogers. The techniques available. In *Cells and Tissues: An Introduction to Histology and Cell Biology*, chapter 2, pages 3–21. Academic Press Inc., 24/28 Oval Road, London, NW1 7DX, 1983. 32

[53] Abcam. Anti-Fibrinogen gamma chain antibody [5A6] (ab119948), July 2015. http://www.abcam.com/fibrinogen-gamma-chain-antibody-5a6-ab119948.html. 33

[54] BD Bioscience. Purified Rat Anti-Mouse CD31, July 2015. http://www.bdbiosciences.com/us/applications/research/stem-cell-research/cancer-research/mouse/purified-rat-anti-mouse-cd31-mec-133/p/550274. 33

[55] Abcam. 33

[56] Thermo Fisher. DAPI (4',6-Diamidino-2-Phenylindole, Dihydrochloride), July 2015. https://www.thermofisher.com/order/catalog/product/D1306. 34

[57] Thermo Fisher. Wheat germ agglutinin, alexa fluor 488 conjugate, July 2015. https://www.thermofisher.com/order/catalog/product/W11261. 34

[58] Thermo Fisher. Alexa Fluor 488 Phalloidin, July 2015. https://www.thermofisher.com/order/catalog/product/A12379. 34

[59] Thermo Fisher. Alexa Fluor 555 dye, July 2015. https://www.thermofisher.com/dk/en/home/life-science/cell-analysis/fluorophores/alexa-fluor-555.html. 34

[60] Thermo Fisher. Alexa Fluor 647 dye, July 2015. https://www.thermofisher.com/dk/en/home/life-science/cell-analysis/fluorophores/alexa-fluor-647.html. 34

[61] B. D. Ulery, L. S. Nair, and C. T. Laurencin. Biomedical applications of biodegradable polymers. *J Polym Sci B Polym Phys*, 49:832–864, 2011. 37, 38, 39, 40, 42

[62] A. L. Sisson, M. Schroeter, and A. Lendlein. Polyesters. In A. Lendlein and A. Sisson, editors, *Handbook of Biodegradable Polymers: Isolation, Synthesis, Characterization and Applications*, chapter 1, pages 1–21. Wiley-VCH Verlag & Co. KGaA, Boschstr. 12, 69469 Weinheim, Germany, 2011. 37, 38, 39, 43, 44, 45, 47

[63] J. C. Middleton and A. J. Tipton. Synthetic biodegradable polymers as orthopedic devices. *Biomaterials*, 21:2335–2346, 2000. 38, 41, 44, 47, 48

[64] A. C. Vieira, R M. Guedes, and V. Tita. Considerations for the design of polymeric biodegradable products. *J Polym Eng*, 33:293–302, 2013. 38, 42, 44, 46, 47, 108

[65] L. S. Nair and C. T. Laurencin. Biodegradable polymers as biomaterials. *Prog Polym Sci*, 32(8-9):762–798, 2007. 38, 39, 40, 41, 42, 43, 44, 46, 47

[66] S. Grund, M. Bauer, and D. Fischer. Polymers in Drug Delivery - State of the Art and Future Trends. *Adv Eng Mater*, 13:B61–B87, 20111. 39, 40

[67] C. R. Gajjar and M. W. King. Degradation Process. In *Resorbable Fiber-Forming Polymers for Biotextile Applications*, chapter 2, pages 7–10. Springer International Publishing, 233 Spring Street, New York, NY 10013, USA, 2014. 40

[68] M. A. Woodruff and D. W. Hutmacher. The return of a forgotten polymer - Polycaprolactone in the 21st century. *Prog Polym Sci*, 35:1217–1256, 2010. 42

[69] L. F. Boesel and R. L. Reis. Injectable Biodegradables System. In R. L. Reis and J. S. Román, editors, *Biodegradable Systems in Tissue Engineering and Regenerative Medicine*, chapter 2, pages 13–25. CRC Press Taylor & Francis Group, 6000 Broken Sound Parkway NW, Suite 300, Boca Raton, FL, USA, 2005. 42

[70] E. Bat, J. A Plantinga, M. C Harmsen adn M. J. A. Van Luyn, Z. Zhang, D. W. Grijpma, and J. Feijen. Trimethylene Carbonate and ϵ-Caprolactone Based (co)Polymer Networks: Mechanical Properties and Enzymatic Degradation. *Biomacromolecules*, 9:3208–3215, 2008. 42

[71] J. Zuidema, B. van Minnen, C. E. Hissink, M. M. Span, T. G. van Kooten, and R. R. M. Bos. In vitro degradation of a biodegradable polyurethanefoam, based on 1,4-butanediisocyanate: A three-yearstudy at physiological and elevated temperature. *J Biomed Mater Res A*, 90:920–930, 2009. 42

[72] H. Tian, Z. Tang, X. Zhuang, X. Chen, and X. Jing. Biodegradable synthetic polymers: Preparation, functionalization and biomedical application. *Prog Polym Sci*, 37:237–280, 2013. 40, 41, 42, 43

[73] M. Deng, L. S. Nair, N. R. Krogman, H. R. Allock, and C. T. Laurencin. Biodegradable Polyphosphazene Blends for Biomedical Applications. In A. K. Andrianov, editor, *Polyphosphazenes for Biomedical Applications*, chapter 9, pages 139–154. John Wiley & Sons, Inc, 111 River Street, Hoboken, NJ, USA, 2009. 42, 46

[74] M. Deng, C. T Laurencin, H. R Allcock, and S. G. Kumbar. Polyphosphazenes as Biomaterials. In S. Dumitriu and V. I. Popa, editors, *Polymeric Biomaterials: Structure and function, Bind 1*, chapter 4, pages 84–127. CRC Press Taylor & Francis Group, 6000 Broken Sound Parkway NW, Suite 300, Boca Raton, FL, USA, 2013. 42

[75] S. Deb. Biodegradable Systems in Tissue Engineering and Regenerative Medicine. In P. K. Chu and X. Liu, editors, *Biomaterials Fabrication and Processing Handbook*, chapter 15, pages 457–477. CRC Press Taylor & Francis Group, 6000 Broken Sound Parkway NW, Suite 300, Boca Raton, FL, USA, 2008. 44, 45, 46, 47, 63

[76] M. Suzuki and Y. Ikada. Biodegradable Polymers in Medicine. In R. L. Reis and J. S. Román, editors, *Biodegradable Systems in Tissue Engineering and Regenerative*

Medicine, chapter 1, pages 3–11. CRC Press Taylor & Francis Group, 6000 Broken Sound Parkway NW, Suite 300, Boca Raton, FL, USA, 2005. 44

[77] A. L. V. Løvdal, T. L. Andersen, B. Madsen, and L. P. Mikkelsen. Influence of temperature on mechanical properties of Jute/Biopolymer Composites. *J Appl Polym*, 128:2038–2045, 2013. 43

[78] K. Masutani and Y. Kimura. PLA Synthesis. From the Monomer to the Polymer. In A. Jiménez, M. Peltzer, and R. Ruseckaite, editors, *Poly(lactic acid) Science and Technology: Processing, Properties, Additives and Applications*, chapter 1, pages 1–36. The Royal Society of Chemistry, Thomas Graham House, Science Park, Milton Road, Cambridge CB4 0WF, UK, 2014. 45, 197

[79] M. J. Stanford and A. P. Dove. Stereocontrolled ring-opening polymerisation of lactide. *Chem Soc Rev*, 39:486–494, 2010. 45

[80] L. Fambri and C. Migliaresi. Crystallization and Thermal Properties. In R. Auras, L. Lim, S. E. M. Selke, and H. Tsuji, editors, *Poly(Lactic Acid) Synthesis, Structures, Properties, Processing, and Applications*, chapter 9, pages 113–124. John Wiley & Sons, Inc., Publication, 111 River Street, Hoboken, NJ 07030, USA, 2010. 45, 46, 56, 57, 58

[81] H. Tsuji. Poly(lactide) Stereocomplexes: Formation, Structure, Properties, Degradation, and Applications. *Macromol Biosci*, 5:569–597, 2005. 45

[82] X. Jiang, Y. Luo, X. Tian, D. Huang, N. Reddy, and Y. Yang. Chemical Structure of Poly(lactic acid). In R. Auras, L. Lim, S. E. M. Selke, and H. Tsuji, editors, *Poly(Lactic Acid) Synthesis, Structures, Properties, Processing, and Applications*, chapter 6, pages 69–82. John Wiley & Sons, Inc., Publication, 111 River Street, Hoboken, NJ 07030, 2010. 47

[83] C. Chen, J. Chueh, H. Tseng, H. Huang, and S. Lee. Preparation and characterization of biodegradable PLA polymeric blends. *Biomaterials*, 24:1167–1173, 2003. 47

[84] N. A. Dotson, R. Galvan, R. L. Laurence, and M. Tirrell. Copolymerization. In *Polymerization Process Modeling*, chapter 4, pages 163–204. John Wiley & Sons, Inc., Publication, 605 Third Avenue, New York, NY 10158-0012, 1996. 48

[85] L. Mandelkern. Oriented crystallization and contractility. In *Crystallization of Polymers Volume 1, Equilibrium Concepts*, chapter 8, pages 357–409. Cambridge University Press, Edinburgh Building, Cambridge, CB2 2RU, UK, 2002. 50, 56, 60

[86] M. L. Di Lorenzo, M. Cocca, and M. Malinconico. Crystal polymorphism of poly(l-lactic acid) and its influence on thermal properties. *Thermochim Acta*, 522:110–117, 2011. 56

[87] X. Zhang, K. Schneider, G. Liu, J. Chen, K. Brüning, D. Wang, and M. Stamm. Deformation-mediated superstructures and cavitation of poly(L-lactide): In-situ small-angle X-ray scattering study. *Polymer*, 53:648–656, 2012. 56, 66, 85

[88] X. Chen, J. Kalish, and S. L. Hsu. Structure Evolution of α'-Phase Poly(lactic acid). *J Polym Sci Part B Polym Phys*, 49:1446–1454, 2011. 56, 59, 66

[89] S. Saeidlou, M. A. Huneaulta, H. Li, and C. B. Park. Poly(lactic acid) crystallization. *Prog Polym Sci*, 37(12):1657–1677, 2012. 56, 175

[90] P. U. Dhanvijay and V. V. Shertukde. Review: Crystallization of Biodegradable Polymers. *Polym-Plast Technol*, 50(13):1289–1304, 2011. 56, 57, 117

[91] A. Pawlak. Plastic deformation and cavitation in semicrystalline polymers studied by X-ray methods. *Polimery*, 59:533–541, 2014. 57, 62, 68, 85, 99

[92] X. Ou and M. Cakmak. Influence of biaxial stretching mode on the crystalline texture in polylactic acid films. *Polymer*, 49:5344–5352, 2008. 58, 60, 61, 62, 66, 173

[93] X. Ou and M. Cakmak. Comparative study on development of structural hierarchy in constrained annealed simultaneous and sequential biaxially stretched polylactic acid films. *Polymer*, 51:783âĂŞ792, 2010. 58, 66

[94] G. M. Bohlmann. General characteristics, Processability, Industrial applications and Market evolution of biodegradable polymers. In C. Bastioli, editor, *Handbook of Biodegradable Polymers*, chapter 6, pages 183–218. Rapra Technology„ Shawbury, Shrewsbury, Shrosphire, SY4 4NR, UK, 2005. 59

[95] G. Perego and G. D. Cella. Mechanical Properties. In R. Auras, L. Lim, S. E. M. Selke, and H. Tsuji, editors, *Poly(Lactic Acid) Synthesis, Structures, Properties, Processing,*

and Applications, chapter 11, pages 141–153. Wiley& Sons, Inc., 605 Third Avenue, New York, NY 10158-0012, 2010. 59, 63, 115

[96] P. B. Maurus and C. C. Kaeding. Bioabsorbable Implant Material Review. *Oper Tech Sports Med*, 12:158–160, 2004. 63

[97] F. Carrasco, P. Pagàs, J. Gámez-Pérez, O.O. Santana, and M.L. Maspoch. Processing of poly(lactic acid): Characterization of chemical structure, thermal stability and mechanical properties. *Polym Degrad Stab.*, 95:116–125, 2010. 66

[98] G. Stoclet, R. Seguela, J. M. Lefebvre, S. Elkoun, and C. Vanmansart. Strain-Induced Molecular Ordering in Polylactide upon Uniaxial Stretching. *Macromolecules*, 43:1488–1498, 2010. 66

[99] M. Yasuniwa, S. Tsubakihara, Y. Sugimoto, and C. Nakafuku. Thermal Analysis of the Double-Melting Behavior of Poly(L-lactic acid). *J Polym Sci Part B Polym Phys*, 42:25–32, 2004. 82

[100] Y. Shieh and G. Liu. Temperature-Modulated Differential Scanning Calorimetry Studies on the Origin of Double Melting Peaks in Isothermally Melt-Crystallized Poly(L-lactic acid). *J Polym Sci Part B Polym Phys*, 45:466–474, 2007. 82

[101] Y. Choi, S.Y. Kim, M.H. Moon, S.H. Kim, K.S. Lee, and Y. Byun. Poly(ethylene glycol)-poly(L-lactide) diblock copolymer prevents aggregation of poly(L-lactide) microspheres during ethylene oxide gas sterilization. *Biomaterials*, 22(9):995–1004, 2001. 107, 108

[102] J. Nuutinen, C. Clerc, T. Virta, and P. Törmölö. Effect of gamma, ethylene oxide, electron beam, and plasma sterilization on the behaviour of SR-PLLA fibres in vitro. *J Biomater Sci Polym Ed*, 13,:1325–1336, 2002. 108, 111

[103] D. Milicevic, D. Milivojevic, and E. Suljovrujic. The influence of the initial preparation and crystallinity on the free radical evolution in gamma irradiated PLLA. *Radiat Phys and Chem*, 81:1361–1365, 2012. 108

[104] ITW Spraytec Nordic. Kema FS-35A - Frostspray, June 2016. `http://itw-scan.com/datasheets/download/clp/4/FS-35A%20FROSTSPRAY`. 112

[105] ITW Spraytec Nordic. FS-35A - Frostspray, June 2016. http://itw-scan.com/datasheets/download/tds/4/FS-35A%20FROSTSPRAY. 112

[106] P. Pan, B. Zhu, and Y. Inoue. Enthalpy Relaxation and Embrittlement of Poly(L-lactide) during Physical Aging. *Macromolecules*, 40:9664–9671, 2007. 115

[107] R. Waksman. Update on Bioabsorbable Stents: From Bench to Clinical. *J Interv Cardiol*, 19:414–421, 2006. 170

[108] N. Gonzola and C. Macaya. Absorbable stent: focus on clinical applications and benefits. *Vasc Health Risk Manag*, 8:125–132, 2012. 170

[109] S. Venkatraman, K. Keith, Y. Rosen, Y. Huang, T. W. J. Steele, and F. Alexis. Drug Delivery Systems for Vascular Disease Therapy. In S. W. Shalaby, K. J. Burg, and W. Shalaby, editors, *Polymers for Vascular and Urogenital Applications*, chapter 2, pages 5–38. CRC Press Taylor & Francis Group, 6000 Broken Sound Parkway NW, Suite 300, Boca Raton, FL, USA, 2012. 170

[110] R. Dargazany, V. N. Khiêm, E. A. Poshtab, and M. Itskov. Constitutive modeling of strain-induced crystallization in filled rubbers. *Phys Rev E*, 89:0226041–12, 2014. 171

[111] A. Mahendrasingam, D. J. Blundell, M. Parton, A. K. Wright, J. Rasburn, T. Narayanan, and W. Fuller. Time resolved study of oriented crystallisation of poly(lactic acid) during rapid tensile deformation. *Polymer*, 46:6009–6015, 2005. 171

[112] D. J. Blehar, D. Resop, B. Chin, M. Dayno, and R. Gaspari. Inferior vena cava displacement during respirophasic ultrasound imaging. *Crit Ultrasound J*, 4:1–5, 2012. 177

[113] J. Eli Robins, I. Ragai, F. Parker C. S Powell, and D. Yamagushi. Differences in Radial Expansion Force Amongst IVC Filter Models Support Documented Perforation Rates. In *The Society for Clinical Vascular Surgery 2016*, Las Vegas, Nevada, Mar. 12-16 2016. 177

[114] J. Čapek, J. Kubásek, D. Vojě, E. Jablonská, J. Lipov, and T. Ruml. Microstructural, mechanical, corrosion and cytotoxicity characterization of the hot forged FeMn30(wt.%) alloy. *Mater Sci Eng C Mater Biol Appl*, 58:900–908, 2016. 180, 181

[115] H. Hermawan, D. Dubé, and D. Mantovani. Developments in metallic biodegradable stents. *Acta Biomater*, 6:1693–1697, 2010. 180

[116] A. Francis, Y. Yang, S. Virtanen, and A. R. Boccacini. Iron and iron-based alloys for temporary cardiovascular applications. *J Mater Sci: Mater Med*, 26:1–16, 2015. 181

[117] H. Hermawan, A. Purnama, D. Dubé, J. Couet, and D. Mantovani. Fe-Mn alloys for metallic biodegradable stents: Degradation and cell viability studies. *Acta Biomater*, 6:1852–1860, 2010. 181, 182

[118] M. Aschner, J. S. Schneider T.R Guilarte, and W. Zheng. Manganese: recent advances in understanding its transport and neurotoxicity. *Toxicol Appl Pharmacol*, 221:131–147, 2007. 181

[119] Q. Zhang, X. G. Wang, P. Gao, and W. Gao. Degradation behavior of biodegradable Fe-Mn alloy produced by powder sintering. *Int J Mod Phys Conf Ser*, 6:774–779, 2012. 181

[120] S. Harjanto, Y. Pratesa, B. Suharno, and J. Syariff. Corrosion Behavior of Fe-Mn-C Alloy as Degradable Materials Candidate Fabricated via Powder Metallurgy Process. *Adv Mat Res*, 576:386–389, 2012. 181

[121] H. Hermawan and D. Mantovani. Susceptibility to stress corrosion cracking of Fe-35Mn alloy under a pseudo-physiological condition. *App Mech and Mater*, 284-387:216–219, 2013. 181

[122] M. Heiden, E. Walker, E. Nauman, and L. Stanciu. Evolution of novel bioresorbable ironâĂŞmanganese implant surfaces and their degradation behaviors in vitro. *J Biomed Mater Res Part A*, 103A:185–193, 2015. 181

[123] M. Heiden, A. Kustas, K. Chaput, E. Nauman, D. Johnson, and L. Stanciu. Effect of microstructure and strain on the degradation behavior of novel bioresorbable iron-manganese alloy implants. *J Biomed Mater Res Part A*, 103A:738–745, 2015. 181

[124] J. E. Schaffer, E. A. Nauman, and L. A. Stanciu. Cold drawn bioabsorbable ferrous and ferrous composite wires: An evaluation of in vitro vascular cytocompatibility. *Acta Biomater*, 9:8574–8584, 2013. 181

[125] N. B. Sing, A. Mostavan, E. Hamzah, D. Mantovani, and H. Hermawan. Degradation behavior of biodegradable Fe35Mn alloy stents. *J Biomed Mater Res Part B*, 103B:572–577, 2015. 181

[126] Y. F. Zheng, X. N. Gu, and F. Witte. Biodegradable metals. *Mater Sci Eng R-Rep*, 77:1–34, 2014. 182

[127] A. Zipse, M. Schlun, G. Dreher, J. Zum Gahr, , and N. Rebelo. Accelerated Fatigue Testing of Stent-Like Diamond Specimens. *JMEPEG*, 20:579–583, 2011. 183

[128] J. A. Ormiston and P. W. S. Serruys. Bioabsorbable Coronary Stents. *Circ Cardiovasc Intervent*, 2:255–260, 2009. 189

[129] C. D. Mario and F. Borgia. Assimilating the current clinical data of fully bioabsorbable stents. *EuroIntervention Supplement*, 5:F103–F108, 2009. 189

Declaration

I herewith declare that I solely have written this thesis. Third party contributions from any source, which have been used to clarify my findings and hypotheses in my work in either directly or indirectly form have been specified accordingly. This paper has not previously been presented in identical or similar form.

The thesis work was conducted from 1st of November 2013 to 1st August 2016 under the supervision of Kristoffer Almdal at Department of Micro- and Nanotechnology, Technical University of Denmark.

Kgs. Lyngby

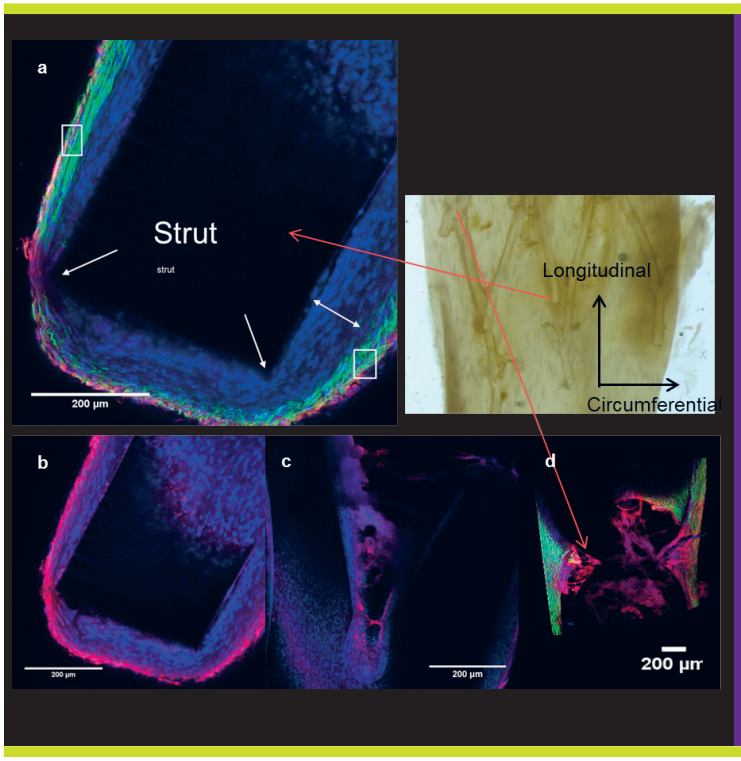

Published by:
DTU Nanotech
Department of Micro- and Nanotechnology
Technical University of Denmark
Ørsteds Plads, building 345C
DK-2800 Kgs. Lyngby